JRC Scientific and Technical Reports

EFNUDAT Fast Neutrons

Proceedings of the Scientific Workshop on Neutron Measurements, Theory and Applications
Nuclear Data for Sustainable Nuclear Energy
28 – 30 April, 2009
Geel, Belgium

Edited by F.-J. Hambsch

EUR 23883 EN - 2010

JRC
EUROPEAN COMMISSION

irmm
Institute for Reference Materials and Measurements

The mission of the JRC-IRMM is to promote a common and reliable European measurement system in support of EU policies.

European Commission
Joint Research Centre
Institute for Reference Materials and Measurements

Contact information
F.-J. Hambsch
European Commission
Joint Research Centre
Institute for Reference Materials and Measurements
Retieseweg 111
B - 2440 Geel
Belgium

E-mail: Franz-Josef.Hambsch@ec.europa.eu
Tel.: +32 (0) 14 571351
Fax: +32 (0) 14 571376

http://irmm.jrc.ec.europa.eu/
http://www.jrc.ec.europa.eu/

JRC 56548

EUR 23883 EN
ISBN 978-92-79-11705-3
ISSN 1018-5593
DOI 10.2787/23116

Luxembourg: Publications Office of the European Union

Printed in Belgium

EFNUDAT Fast Neutrons

Proceedings of the Scientific Workshop on Neutron Measurements, Theory and Applications

Nuclear Data for sustainable nuclear energy

28 – 30 April, 2009

Geel, Belgium

Edited by F.-J. Hambsch

Foreword

On April 28 – 30, 2009 the first EFNUDAT (European Facility for Nuclear Data Measurements) scientific workshop on Neutron Measurements, Theory and Applications, EFNUDAT – Fast Neutrons was held at the JRC-IRMM. The workshop was organized by the Neutron Physics Unit of JRC-IRMM. The organisers were assisted by a Programme Advisory Committee consisting of G. Barreau (CNRS/IN2P3 Bordeaux, France), F. Gunsing (CEA Saclay, France), R. Jacqmin (CEA Cadarache, France), A. Koning (NRG Petten, The Netherlands), J.P. Meulders, UCL Louvain-la-Neuve, Belgium) and A. Mengoni (IAEA, Vienna, Austria).

The purpose of the workshop was to provide a comprehensive overview of nuclear data measurements with fast neutrons, their influence on theoretical models and final applications with potential economic impact. The contributions have highlighted the state of the art and the new developments relevant for advanced reactor systems. Users of data have presented comprehensive views on their data requirements.
Both invited presentations as well as normal contributions have been given. The success of the workshop must be attributed to the 33 contributions and more than 50 participants, many of which were post-doctoral fellows and PhD students.

The workshop was organised within the EFNUDAT project, which is an Integrated Infrastructure Initiative funded under the 6th Framework Programme of the European Community. The aim of the initiative is to integrate all infrastructure-related aspects of nuclear data measurements and to provide trans-national access to key facilities.
More details can be found on the EFNUDAT website: www.efnudat.eu

I would like to express my gratitude to the program advisory committee, G, Barreau of CENBG Bordeaux, France, F. Gunsing of CEA Saclay, France, R. Jacqmin of CEA Cadarache, France, A. Koning of NRG Petten, The Netherlands, J.P. Meulders of UCL, Louvain-la-Neuve, Belgium and A. Mengoni of IAEA, Vienna, Austria. A special thank you goes to the local organisational support of C. Cabanillas Platero and S. Roulette.

Franz-Josef Hambsch
December 2009

Group photo of the participants

CONTENTS

Measurement of the ratio between the capture and the fission cross sections of ^{233}U

M. Aïche[1)], G. Barreau[1)], B. Jurado[1)], S. Czajkowski[1)], D. Dassié[1)], B. Hass[1)], G. Boutoux[1)], P. Schillebeeckx[2)], F. Gunsing[3)], A. Bidaud[4)], A. Billebaud[4)], S. Chabot[4)], D. Heuer[4)], G. Kessedjian[4)]

1) CENBG, Université Bordeaux 1, F-33175 Gradignan, France
2) European Commission, Joint Research Centre, Institute for Reference Materials and Measurements, Retieseweg 111, 2440 Geel, Belgium
3) CEA Saclay, DSM/DAPNIA/SPhN, 91191 Gif-sur-Yvette cedex, France
4) LPSC, Université Joseph Fourier, F-38026 Grenoble, France
aiche@cenbg.in2p3.fr

Abstract: Recent sensitivity studies of the impact of the cross section uncertainties on the breeding capability of the thorium cycle have shown that fissile regeneration is dominated by the uncertainty in the α ratio between the capture and fission cross section of ^{233}U. The most critical region is the resolved resonances in connection with the epithermal spectrum proposed for some moderated Molten Salt Reactors, typically from 1 eV to 100 eV neutron energy range. A test experiment has been done with the electron linear accelerator facility at IRMM (GELINA) as a neutron source. A fission fragments chamber containing six ^{233}U samples (Φ=2cm, thickness=0.4mg/cm²) has been installed at the 10 meters flight path basis of Geel. Very satisfactory results have been obtained with the fission fragments ionization chamber. Moreover tests with 4 C6D6 γ array surrounding the fission chamber showed us that some efforts has to be done in order to reduce the parasitic γ rays associated with the background.

Introduction

The public concerns about nuclear waste from nuclear power plants are related primarily to the long term toxicity of the spent nuclear fuels; in the current 'once-through' fuel cycle, this is dominated by plutonium and other minor actinides. The actinides play a dominant role both in terms of total radioactivity and potential dose to the public. As an alternative solution, in $^{232}Th/^{233}U$ fuel cycle, much lesser quantity of plutonium and long-lived Minor Actinides (MA: Np, Am and Cm) are formed as compared to the $^{238}U/^{239}Pu$ fuel cycle, thereby minimizing toxicity and decay heat.
Several thorium-based fuel design options investigated in recent years, have demonstrated the basic feasibility of Th–based fuel cycles of current and next generation technology. Activities have focused on examining the $^{232}Th/^{233}U$ cycle as a replacement for conventional uranium-based fuels in existing reactors, as well as a way to manage the growth of plutonium stockpiles by burning plutonium. Water moderated reactors burn ^{235}U, which is the only naturally occurring fissile isotope. The Thorium cycle can ensure breeding of fissile fuel. This breeding is possible in both thermal and fast neutron spectrum, whereas the ^{238}U cycle can only be a breeder in the fast spectrum.
Over the years, efforts have been made to improve the quality of basic nuclear data in the thorium cycle. Thermal reactor designs and applications have been the driving force for new data evaluations in the low energy range. Recently, data evaluations in the high-energy region have been accomplished primarily in support of transmutation or incineration applications and GEN IV fast reactor design. Although the accuracy of the nuclear data such as neutron interaction cross sections, has been significantly improved. Recent sensitivity studies [1] of the impact of the cross section uncertainties on the breeding capability of the thorium cycle have shown that fissile regeneration is dominated by the uncertainty in the ratio (called α ratio) between the capture and fission cross section of ^{233}U. Indeed, the available data for this ratio [2-6] present a dispersion of 25%. Moreover, the calculated uncertainty for the breeding capability of thorium reactors is about 4%, whereas the breeding potential itself is expected to be of the same order. Therefore, it is not yet possible to ensure that this cycle is self-sufficient in the regeneration of the fissile element. The sensitivity results are relatively

independent of the neutron energy. However, the most critical region is the resolved resonances in connection with the epithermal spectrum proposed for some moderated Molten Salt Reactors [7], typically from 1 eV to 100 eV neutron energy range.
In order to obtain accurate α ratio in the context of the Generation IV nuclear energy systems, the neutron time of flight facility GELINA of IRMM at Geel is one of the most appropriate installations.

Experiment

The aim of the experiment presented above is to improve our knowledge on the (n,γ) reaction capture in the resolved resonance region for the Th/U fuel cycle. The main difficulty in the measurement of the ^{233}U α ratio as compared to ^{235}U is the separation of γ rays associated with the capture reaction (average multiplicity 4 to 5) from the ones that come from fission fragments (average multiplicity 7 to 8), The latter represent parasitic radiation which has to be rejected. Indeed, the capture cross section at thermal neutron energy of ^{233}U is smaller by a factor two than the corresponding one for the ^{235}U.
The electron linear accelerator facility at IRMM (GELINA) was used as a neutron source [8]. The neutron energy distribution emitted by the target ranges from sub thermal to about 20 MeV, with a peak at 1-2 MeV. To have a significant number of neutrons in the energy range below 100 keV, a hydrogen-rich moderator is added. The neutron energy was measured by its time of flight over 10m from moderator to detector. The neutron beam was collimated to 8cm diameter by a series of collimators installed along the neutron drift tube. The neutron beam impinged on the ^{233}U fission chamber located at the 10m flight station and surrounded by the 4 C_6D_6 multi-detector gamma array of the IRMM.
The fission chamber is detailed in Fig. 1 it contained a total of 8.5 mg of ^{233}U fabricated at Geel.

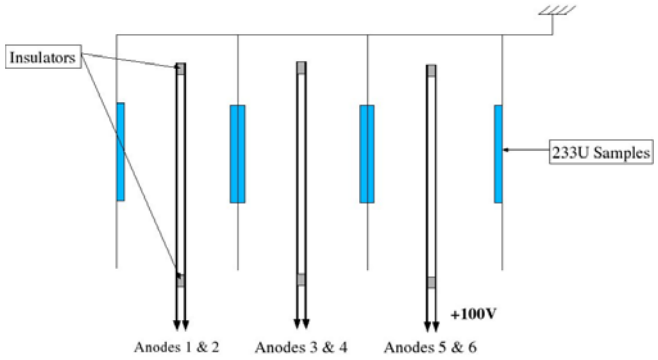

Figure 1. *Plates arrangement and anode signals from fission fragments.*

The chamber consisted of 6 plates of 0.6 mm dural coated on one side with 450 µg/cm² of ^{233}U to a diameter of 2 cm. The plates were assembled as six independent and high-efficiency multi ionization chambers that would allow to separate fission fragments and alpha's generated by the very high decay rate of ^{233}U. In this configuration, the fission fragment ionization chamber will be used to tag the γ rays originating from fission fragments.

Preliminary results

The detection efficiency (96 $\pm$ 0.5) % for fission fragments has been measured at CENBG using a ^{252}Cf layer fission source in the same geometry as one of the ^{233}U deposits. Very satisfactory results have been obtained at GELINA with the fission fragments ionisation chamber as shown in Fig. 2. The overlap between fission fragments and ^{233}U alpha decay distributions is quite small (less than 1%).

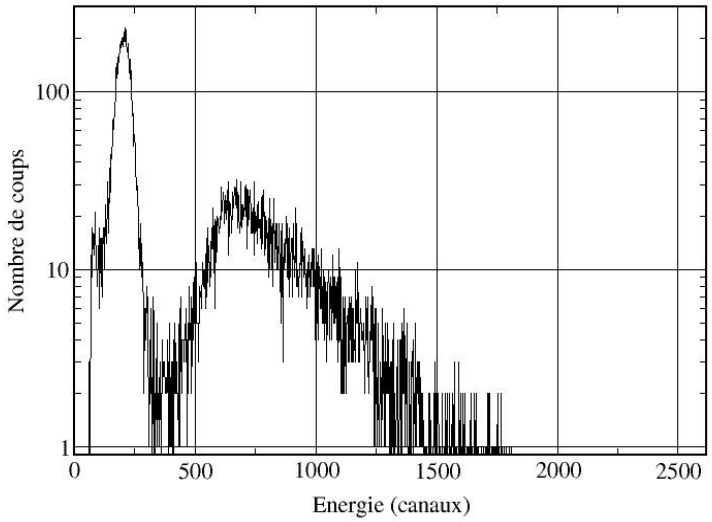

***Figure 2**. Fission Fragments and alpha decay of ^{233}U obtained with the ionization chamber.*

The time resolution of the setup (see Fig. 3) is 3 ns FWHM. It was also measured at CENBG with the ^{252}Cf source, using the coincidence technique between the ionization chamber and C_6D_6 detector. A time of flight of about 40 cm was used to separate the neutrons and prompt γ rays coming from fission fragments.

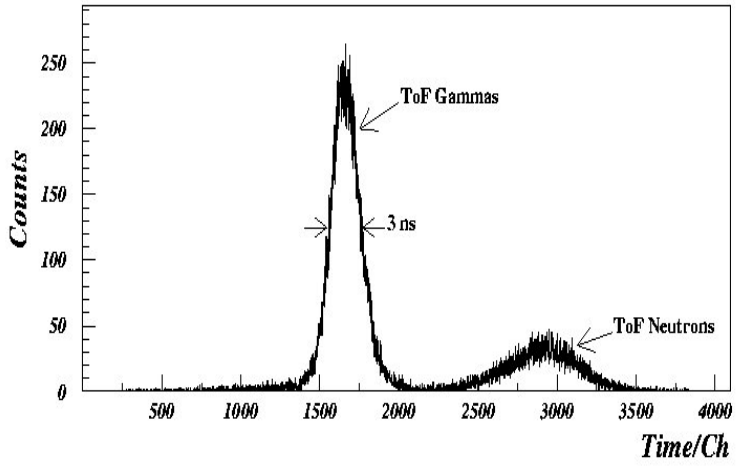

***Figure 3**. Time resolution of the setup measured with a ^{252}Cf spontaneous fission source.*

The measurements performed at the neutron source facility (GELINA) using the time-of-flight discrimination of neutron-induced fission events, allow us to obtain the resolved resonances spectrum of the reaction $^{233}U(n,f)$ as shown in Fig.4a). Coincidence with prompt γ rays emitted by the fission fragments, decreases the total number of counts due to the C_6D_6 efficiency as shown in Fig.4b).

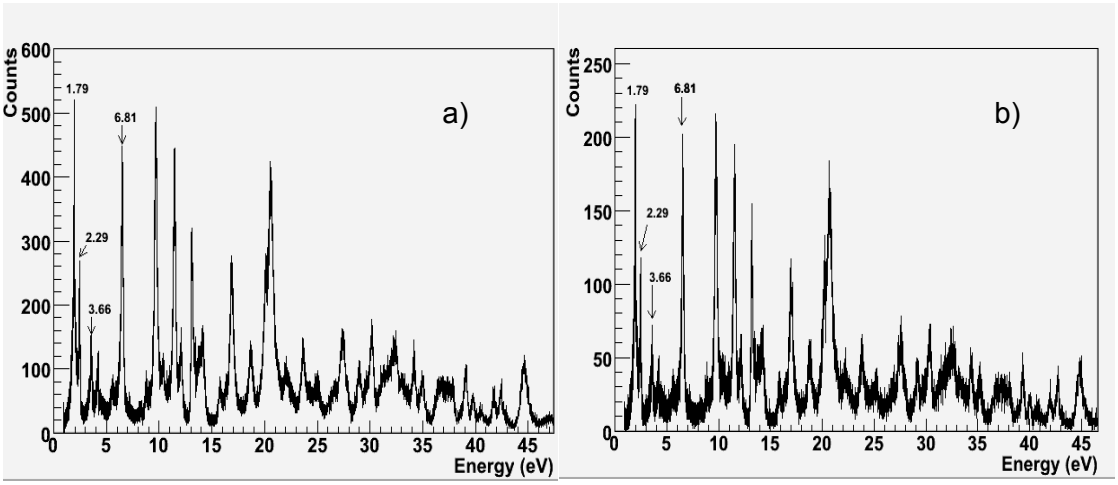

Figure 4. *Resolved resonances spectra of the ^{233}U observed with the fission fragments only a) and b) with γ-prompt coincidence too.*

Conclusion

The test experiment described above has been done within the NUDAME project in 2008. The fission fragments ionization chamber installed at the 10 meters flight path basis of Geel allow us to obtain very satisfactory results. In addition, the strong γ flash of GELINA which precede the neutron burst did not induce significant signal in the ionization chamber. Moreover the spectra obtained with the 4 C_6D_6 array showed us that some efforts has to be done in order to reduce the parasitic γ rays associated with the background. Therefore, the new ionization chamber will contain a total of 110 mg of ^{233}U (thirteen times more than in the former chamber) distributed over 10 layers (6 cm in diameter) deposited on 10 high purity Al plates (30 µm-thick). The chamber will be surrounded by 10 C_6D_6 γ detectors in order to increase the γ detection efficiency. The neutron beam will be also collimated and reduced to a 60 mm diameter.

Acknowledgements

This work has been supported by the CNRS programme PACE/GEDEPEON and the EURATOM Transnational Access Program NUDAME. We thank warmly the radio chemists at Geel to make available the ^{233}U Targets. The authors thank also the GELINA staff of the IRMM at Geel for their great support during the experiment.

References

[1] A. Bidaud, et al., Nuclear Data for science and Technology, (2007), Nice, France, pp 241.
[2] J. Halperin et al., Nuclear Science and Engineering 16 (1963) 245.
[3] J.C. Hopkins et al., Nuclear Science and Engineering 12 (1962) 169.
[4] M.S. Moore et al., Phys. Rev. 18 (1959) 714.
[5] O.D. Simpson et al., Nuclear Science and Engineering 7 (1960) 187.
[6] L.W. Weston, et al., USAEC Report ORNL-TM-1751, Oak Ridge National Laboratory, 1967.
[7] L. Mathieu, PhD Thesis, INPG, 2005.
[8] http://www.irmm.jrc.be/html/about_IRMM/laboratories/gelina_neutron_flux.htm.

Measurements of elastic neutron scattering at high energies with SCANDAL at TSL

P. Andersson[1)], R. Bevilacqua[1)], J. Blomgren[1)], C. Gustavsson[1)], A. Kolozhvari[2)], F.R. Lecolley[3)], N. Marie[3)], Y. Naitou[4)], L. Nilsson[1)], M. Österlund[1)], S. Pomp[1)], A. Prokofiev[5)], V. Simutkin[1)], M. Tesinsky[1,6)], U. Tippawan[7)], Y. Watanabe[4)]

1) Department of physics and astronomy, Division of applied nuclear physics, Uppsala University, Box 516, 751 20 Uppsala, Sweden
2) St. Petersburg State University, Russia
3) Laboratoire de Physique Corpusculaire, Caen, France
4) Department of Advanced Energy Engineering Science, Kyushu University, Japan
5) The Svedberg Laboratory, Uppsala University, Sweden
6) Department of reactor physics, Kungl. Tekniska Högskola, Sweden
7) Fast Neutron Research Facility, Chiang Mai University, Thailand
Pernilla.Andersson@fysast.uu.se

Abstract: The Scattered Nucleon Detection AssembLy SCANDAL, located at the neutron beam facility of The Svedberg Laboratory (TSL), Sweden, measures elastic neutron scattering at high energies. The obtained data are of highest relevance for the development of nuclear reaction codes since they provide information on the base ingredient in such codes, the optical model potential. Thus, measuring elastic neutron scattering provides needed data for applications involving fast neutrons. Such applications can be found in so widespread areas as medicine (dosimetry), electronics (single event effects), and energy production (accelerator-driven systems).
After several experimental campaigns on H, D, C, O, Fe, Y, Pb at 96 MeV (see, e.g., Ref. [1]), SCANDAL has recently been upgraded to be able to measure at 175 MeV, the highest energy available at TSL. An extensive run, financed by the EFNUDAT project, with Fe and Bi as targets was performed over a period of three weeks in January and February this year.
Using the experimental data on elastic scattering, a recent analysis showed that also inelastic cross sections down to about 40 MeV can be extracted. A publication with data for C, Fe, Y and Pb is currently in preparation.
We will discuss the motivation for measuring elastic neutron scattering, the used experimental and analysis method and present an overview of the results obtained thus far.

Introduction

Several different fields of applications motivate measurements of neutron scattering at high energies. But there are also purely theoretical reasons. It helps us understand the basic physics of nucleon-nuclei interactions. The data is needed in fields such as nuclear power technologies, medicine involving radiation therapy of cancer tumors and dosimetry, and electronics failure due to radiation damage, so called single event effects. The data libraries today mainly contain information on cross sections at energies up to 20 MeV. Measurements at higher energies are needed to improve the theoretical models of nuclear reactions, in particular the optical model potential (OMP). The OMP is a key ingredient in nuclear reaction codes. Measurements at higher energies are also directly applicable in the development of future nuclear reactor concepts, e.g. accelerator driven systems.
Cross sections of elastic nuclear scattering at 96 MeV on H, D, C, O, Fe, Y and Pb have previously been measured at the The Svedberg Laboratory (TSL) in Uppsala, using the experimental setup SCANDAL (SCAttered Neutron Detection AssembLy), e.g. [1], [2]. The results show good agreement with theoretical predictions. From some of these data sets, information on inelastic scattering has been extracted, and a publication with data for C, Fe, Y and Pb is currently in preparation [3].
SCANDAL has recently been upgraded with new thicker CsI detectors in order to measure elastic, and possibly inelastic, neutron scattering at the maximum energy provided by TSL, 175 MeV. The experimental campaign was carried out during three weeks in January and February this year. Fe and Bi were chosen as target nuclei. Natural Fe was chosen because it is a very common construction material and therefore very abundant in almost all nuclear technology applications. ^{209}Bi was chosen because it is by nature isotopically pure, and because data on Bi

is of highest interest for future bismuth/lead cooled reactor concepts. Another reason to choose ^{209}Bi is that data on nuclei with mass numbers close to the doubly magical nuclei, i.e. ^{208}Pb, is very valuable for the development of theoretical models of nuclear reactions. It is possible to run measurements with SCANDAL on a wide range of other nuclei. However, the cross sections are very low in this energy range, which makes experiments costly because it takes a lot of time to gather enough data to get good statistics.

The SCANDAL setup

SCANDAL detects recoil protons from hydrogen in a plastic scintillator, rather than the original scattered neutrons. The use of an active converter, which measures the energy loss of the recoil proton in the converter material, means that a thicker converter can be used since the energy loss is compensated for. This gives a more efficient conversion without loss of energy resolution. Figure 1 shows the two SCANDAL arms. Each arm covers about 45 degrees of scattering angle. The right arm is placed as close to the beam as possible without the beam hitting the detectors, while the left arm is placed in such a way that is has a slight overlap with the angular range of the right arm. This cross check of the data gives a good control over any systematical differences between the two arms.
The neutron beam enters the setup from the bottom of the picture, as seen in figure 1. Neutrons are scattered in the target, which is placed on a table at the pivot point of SCANDAL. The first detector on both the SCANDAL arms is a 2 mm thick plastic scintillator that works as a veto for charged particles. The second detector is the active converter, a 20 mm thick plastic scintillator. Because the angle at which the particle travels may change in the conversion from neutron to proton, the converter is followed by two drift chambers. The particle track can be reconstructed from the two positions registered in the drift chambers and the calculated conversion point in the converter scintillator defines the scattering angle. But in order to create a trigger for the data acquisition, a 2 mm thick plastic scintillator is placed between the converter and the drift chambers, and an identical scintillator is placed after the drift chambers. A coincidence between these two scintillators defines an event for the read out system. The very last detector on SCANDAL is an array of CsI crystals. They measure the full energy of the protons, which means that we can distinguish between protons originating from elastically scattered neutrons, and protons originating from inelastically scattered neutrons.
Thanks to the veto scintillator and the trigger criteria employed in the data acquisition, SCANDAL can be run in both proton mode and neutron mode by excluding or including the veto signals in the trigger.

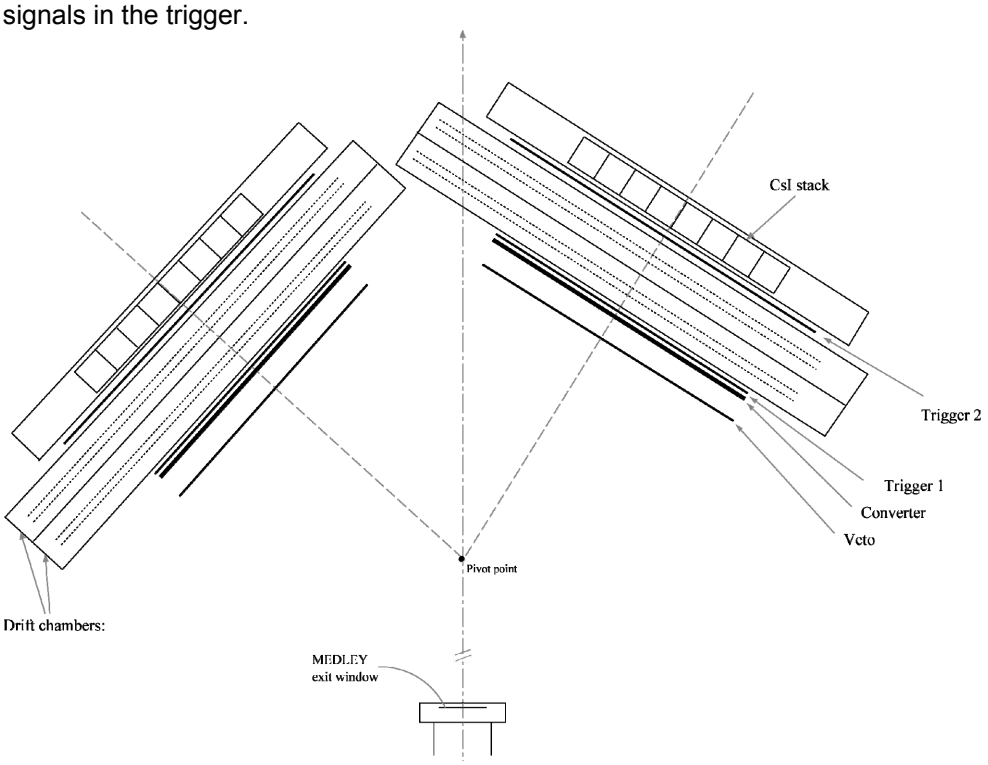

Figure 1. *The SCANDAL setup consists of two arms, each covering 45° of scattering angle.*

SCANDAL upgrades

As mentioned above, the SCANDAL setup has recently been upgraded with new Na-doped CsI detectors. To fully stop 175 MeV protons in the detector material, and thereby measure their full energy, a detector depth of about 8 cm is required. The new SCANDAL is equipped with 16 CsI scintillating detectors, eight on each arm, with an individual surface area of 8 cm $\times$ 22 cm and a depth of 9 cm, together covering a solid angle of approximately 0.4 steradians. The CsI crystals are fitted with one PM-tube each, collecting the light via a 5 mm thick silica light guide. To improve the reflectivity of the walls, the crystals are wrapped in white silicon tape. But because of the hygroscopic properties of Na-doped CsI, they are also wrapped in aluminum foil to keep any moist out.
Details on the metal frame holding the CsI crystals has also been changed so that the detectors can be placed closer to the beam than what was possible in the old set up. This means that we can measure neutrons scattered at smaller angles, which is important for the absolute normalization. The smallest achievable angle will partially depend on geometrical cuts introduced in the analysis, but it is so far estimated to be around 5°.
Recent changes in the experimental hall at TSL, made to improve the background conditions, have forced SCANDAL 87 cm further downstream compared to the position of the old SCANDAL setup. This might have implications on the beam size and the neutron yield at the target position, but it has not caused any problems.

The The Svedberg Laboratory and the neutron beam

The neutron beam facility at TSL has been described in great detail before, e.g. in ref [2], [4], and only a brief summary will be given here. Protons from the cyclotron hit a ^{7}Li target, and produce a quasi mono energetic neutron beam, via the ^{7}Li (p,n) ^{7}Be reaction. A 24 mm thick Li-target was used for this experiment. The proton beam is then bent into a well-shielded beam dump after the neutron production target.
The neutron beam enters the experimental hall via a set of conical iron collimators and the vacuum chamber of the experimental setup Medley. Medley measures light ion production and was operating parallel to SCANDAL during the beam time. The targets for the Medley experiment were Fe and Bi. The exit window of Medley is a 0.1 mm thick stainless steel foil. A new feature in the experimental hall at TSL is the 1.5 m thick iron wall built upstream of Medley to reduce the background noise. Between Medley and SCANDAL there was an ionization chamber monitor and a thin film breakdown counter for beam monitoring during the run. The total amount of material in the beam; the Medley target, the Medley exit window and the beam monitors, is considered to be negligible. After passing the SCANDAL setup, the neutron beam ends up in the beam dump about ten meters down the line.
The neutron beam at TSL is well characterized. It has a peak at an energy slightly lower than the initial proton energy, in this case about 175 MeV, and a low-energy tail. But about 40 % of the neutrons are found within the full energy peak. The low energy neutrons can be suppressed in the analysis using time-of-flight techniques.

Experimental procedure

The experiment was carried out during three weeks in January and February this year. The beam time, in total 120 hours of data collection, was shared between the two targets, Fe and Bi, and background measurements. During the first days of the campaign a few runs in proton mode devoted to calibration were carried out as well. During the calibration runs, a multi target box was placed in the beam, containing five plastic targets of a total thickness of 4.85 mm, and one carbon target of 1 mm thickness. The reaction we are interested in for calibration purposes is (n,p) scattering on H. Multiwire proportional counters separate the targets in the multi target box, so the scattering plane for each event can be identified, and H data can be extracted by subtracting a carbon background form the plastic data.
A total of 6 hours of beam time were spent on calibration. During that time the SCANDAL arms were successively placed at the most forward angle, in order to calibrate each CsI at the highest possible energy.
The multitarget box was left empty for the rest of the experimental campaign, acting as a veto for charged particles in the neutron beam. SCANDAL was switched into neutron mode and the scattering target was placed on the table downstream of the multitarget box, at the pivot point. To reduce the background consisting of particles scattered in the Medley setup, an iron wall was built on each side of the neutron beam between the multitarget box and the scattering target.

The beam time was spent alternating between the two targets, Fe and Bi, and background measurements. In total 36 hours were spent on Fe, 53 on Bi and 24 on background. This means that we got good statistics in all three cases. The Fe target is a solid cylinder with a diameter of 11.6 cm and a height of 16.0 cm and a mass of 12.15 kg. The dimensions of the Bi target are not as well defined, because Bi has the peculiar property of expanding as it cools off in the casting process. But the target is approximately a 13 cm high solid cylinder with a diameter of 11 cm. Its mass is 11.80 kg.

Data analysis

The data analysis that will be carried out during the coming years is done on an event-by-event basis. The first step in the analysis is the energy calibration of the plastic scintillators and the CsI scintillators. This is done by finding the pedestal channel, corresponding to zero energy, and the H (n,p) peak in the pulse height spectra, see figure 2, from the calibration runs in proton mode. The following steps involve data reduction by applying a number of cuts on the neutron mode data. Time-of-flight information will be used to reject low energy neutrons in the beam. A criterion on the maximum conversion angle allowed in the converter will be applied, to ensure that we can distinguish between conversion on hydrogen and carbon. Geometrical cuts on the hit position in the CsI crystals are also used to make sure that the proton deposits its full energy in one single crystal.
The drift chamber information defines the scattering angle of the neutrons, and the cross section is found by integrating the peak corresponding to elastic scattering for each angular bin.

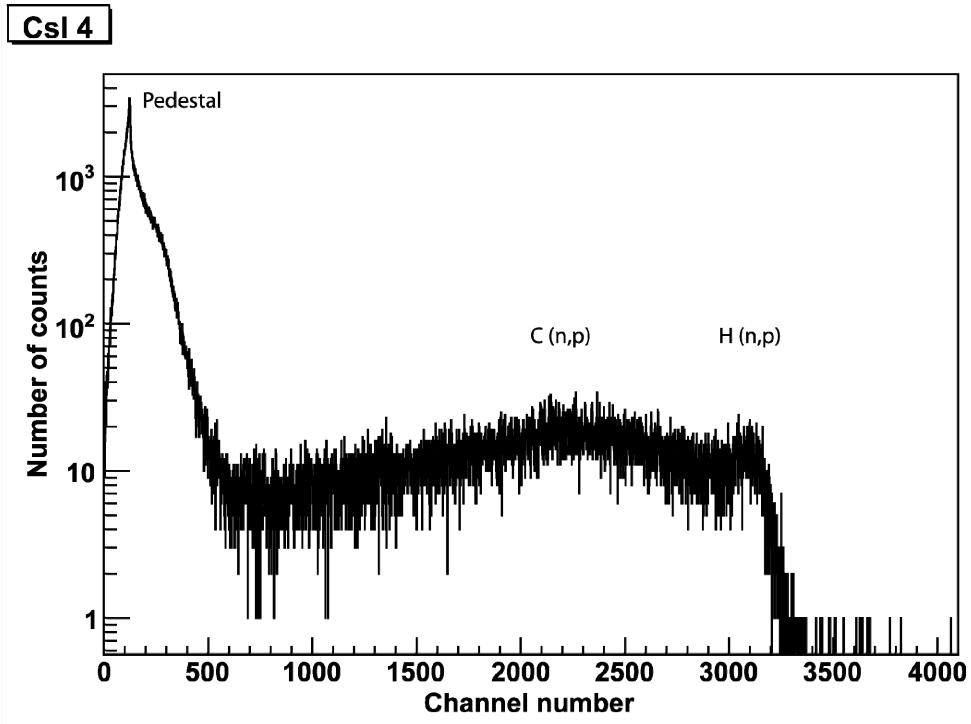

Figure 2. *The pulse height spectra from a CsI scintillator at 30°, from a calibration run in proton mode, shows that the hydrogen peak is clearly visible.*

Outlook

Our first task is to analyze the recently collected data and produce cross sections for elastic neutron scattering on Fe and Bi. Previous work [3] has shown that it is also possible to extract cross sections for inelastic neutron scattering from SCANDAL data. This will be our second objective. However, many other target nuclei are suitable for measurements with SCANDAL at the neutron beam energy 175 MeV. Si, O, C and Y are easy to handle as solid or liquid targets and would be interesting from an applications and theoretical point of view.

Acknowledgements
We would like to thank the EFNUDAT collaboration for making these experiments possible. We would also like to thank the staff at TSL for all their help, and the members of the NEXT project; SKB, SSM and Ringhals.

References
[1] A. Öhrn et al., Phys. Rev. C 77 (2008) 024605.
[2] J. Klug et al., Phys. Rev. C 68 (2003) 064605.
[3] A. Öhrn et al., Inelastic neutron scattering cross sections at 96 MeV for iron, in manuscript.
[4] S. Pomp et al., Proceedings of International Conference on Nuclear Data for Science and Technology, Santa Fé, NM, September 26 - October 1 2004, AIP Conference Proceedings No. 769 (Melville, New York, 2005), pp. 780-783.

On consistent analysis of ^{50,52,53,54}Cr fast-neutron activation

V. Avrigeanu

'Horia Hulubei' National Institute for Physics and Nuclear Engineering, P.O. Box MG-6, 77125 Bucharest-Magurele, Romania
vavrig@ifin.nipne.ro

Abstract: An overview of the calculated fast-neutron activation cross sections of the Cr stable isotopes shows that an analysis based on a consistent local parameter set is necessary in order to explain some large differences between the experimental and global calculated cross sections especially around 20 MeV. Still open questions of nuclear-reaction model parameters, established or checked by means of various independent experimental data are discussed in this respect.

Introduction

The Cr stable isotopes are known for the model inconsistency found by JRC/ANL/FZJ scientists within a trial [1] to describe unitary the corresponding (n,p) and (n,2n) reaction cross sections up to the incident energy of 20 MeV. This lack of consistency remains also within the more recent work of Han [2] which stops at the incident energy of 20 MeV while more data are known up to 40 MeV. Actually the case of ^{52}Cr activation cross sections is used within the well-known code EMPIRE-II manual [3] as a sample of nuclear model-calculation difficultness. Similar features have been revealed by a most recent high-resolution cross section measurement for inelastic scattering and (n,2nγ) reaction on the ^{52}Cr isotope [4], whose comparison with TALYS defaults model calculations [5] was considered however by authors only as a starting point for the future improvements in the theoretical models. On the other hand, the latest results obtained in activation experiments on Cr by using both a white-spectrum neutron field [6]and a quasi-monoenergetic neutrons below 35 MeV [7], led to only half of the calculated to experimental activation (C/E) ratio values proving a reasonable agreement with the library EAF-2005 [8] while large discrepancies were found for the others. The need of an updated evaluation being thus pointed out, the present work has used in this respect both global [3,5] and local [9] approaches for a consistent analysis of all activation data for the Cr isotopes, available up to 40 MeV, in line with similar studies of nearby elements [10] as well as still open questions of nuclear-reaction models and linked parameterizations.

Model parameters

The neutron optical model potential (OMP) of Koning and Delaroche [11], used by default in both TALYS and EMPIRE codes, does not fully reproduce the minimum around the neutron energy of 1-2 MeV for the total neutron cross sections of the mass A~60 nuclei. Following also their comment of the constant geometry parameters which may be responsible for this point, we have applied the SPRT method [12] by using the recent RIPL-2 recommendations [13] as well as most recent results [14] for the low-energy neutron scattering properties (S_0, S_1, R'), and the available measured neutron total cross sections [15] including the latest measurements [16] of the neutron total cross sections for ^{50,52,53,54}Cr stable isotopes beyond the neutron energy of even 60 MeV. A particular feature concerns the measured neutron strength functions within an energy range where their energy dependence is not linear (Fig. 1). A realistic comparison of them should be not done in this case with respect to model prediction calculated in the middle of this energy range but through a proper averaging over this range. Unfortunately the variance of the averaged S_0 values is even larger than the values themselves (Fig. 1, bottom), so that the availability of experimental data over smaller energy ranges would be useful. Actually this point was earlier proved also with respect to the measured s-wave resonance spacings on ^{52,54}Cr isotopes [17]. Finally, a decrease of ~7% for the neutron total cross section has thus resulted around the incident energy of 1 MeV, corresponding to the average energy of the statistically emitted neutrons. Next, this potential has been involved in the calculation of the corresponding collective inelastic scattering cross sections by means of the direct-interaction distorted-wave Born approximation (DWBA) method, fractions of the direct inelastic scattering to compound-nucleus cross section being obtained as large as ~11% for ^{50}Cr and ~7% for ^{52}Cr at low energies and decreasing by ~50% up to 60 MeV.

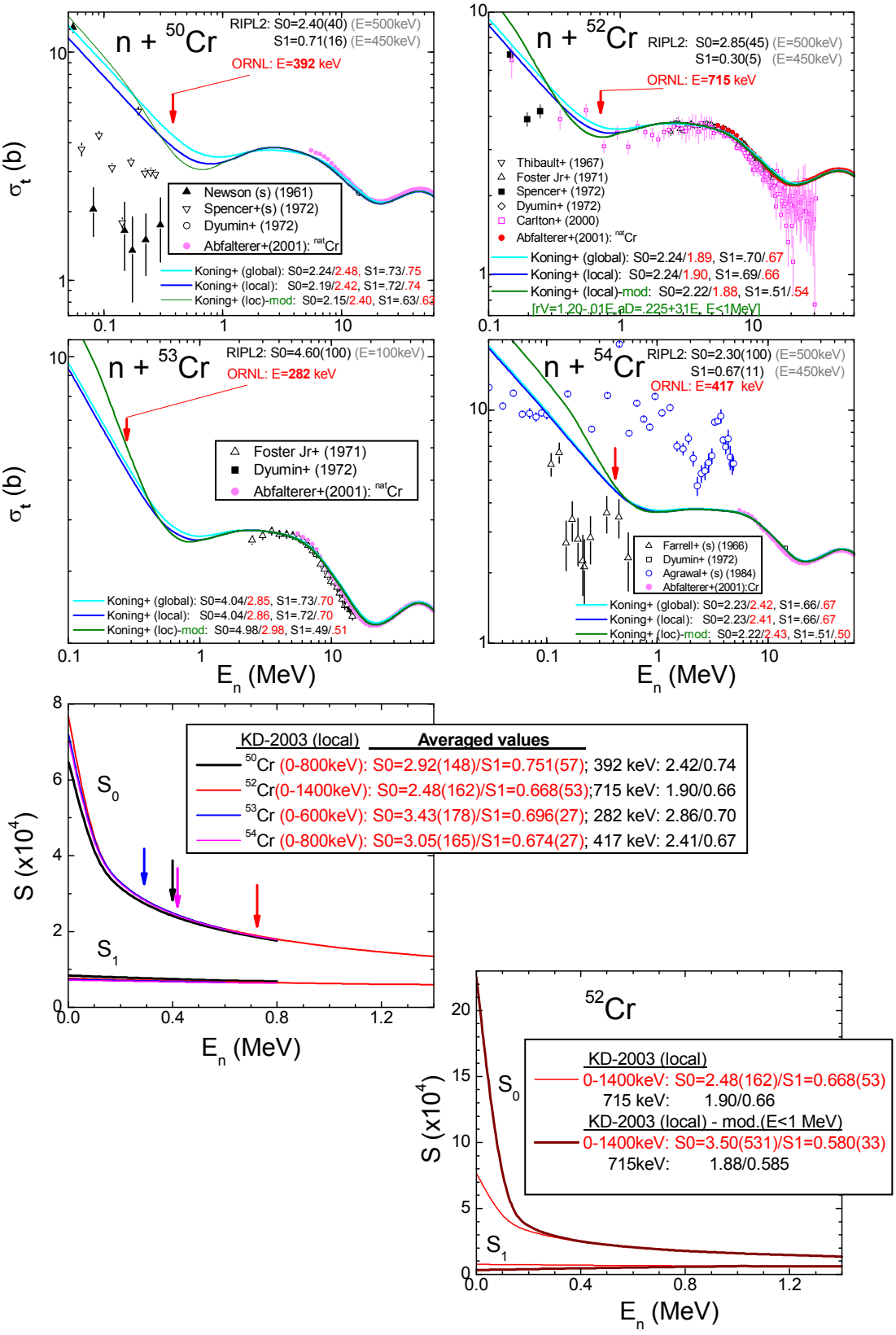

Figure 1. *Comparison of calculated and measured [15,16] neutron total cross sections for all stable Cr isotopes by using the local neutron optical potential of Koning and Delaroche for ^{52}Cr target nucleus [11] as well as modified geometry parameters bellow the energy of 1 MeV.*

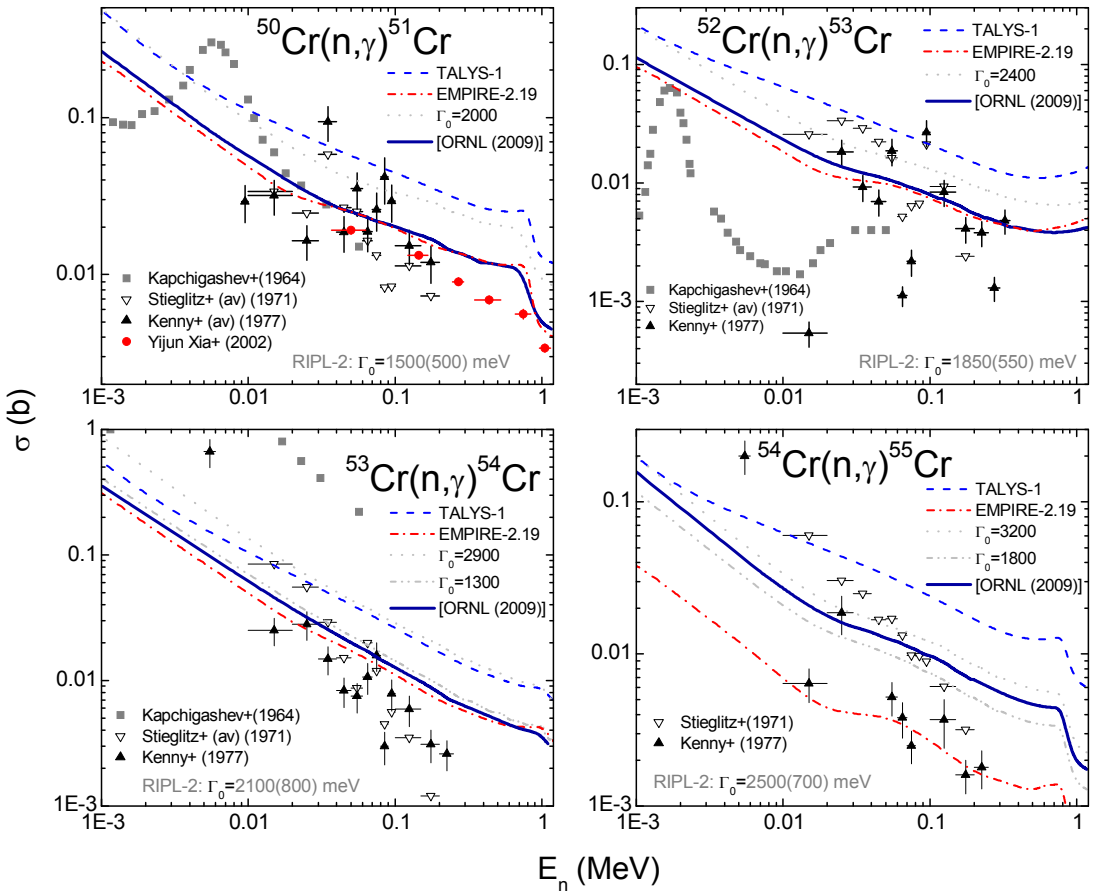

Figure 2. *Comparison of measured [15] and calculated (n,γ) reaction cross sections on ^{50,52,53,54}Cr stable isotopes by using the EMPIRE-II [3] and TALYS-1.0 [5] codes and the EDBW-model electric dipole γ-ray strength functions $f_{E1}(E_\gamma)$ corresponding to the recent experimental average radiative widths [14], within the local approach [9].*

The electric dipole γ-ray strength functions $f_{E1}(E_\gamma)$ which have to be used for the calculation of the γ-ray transmission coefficients, have been obtained within the framework of a modified energy-dependent Breit-Wigner (EDBW) model [18]. Moreover, systematic EDBW correction factors F_{SR} were obtained by using the experimental average radiative widths $\Gamma_{\gamma 0}^{exp}$ of the *s*-wave neutron resonances, and assuming that $F_{SR}=\Gamma_{\gamma 0}^{exp}/\Gamma_{\gamma 0}^{EDBW}$. Next, the calculated $f_{E1}(E_\gamma)$ have been checked within an analysis of capture cross sections for all ^{50,52,53,54}Cr stable isotopes in the neutron energy range from keV to 2-3 MeV (Fig. 2). The RIPL values for $\Gamma_{\gamma 0}^{exp}$ lead to $f_{E1}(E_\gamma)$ strength functions which are too large, so that more appropriate values have been established on the basis of this capture cross-section analysis and the recent ORNL $\Gamma_{\gamma 0}^{exp}$ values. At the same time the capture cross sections thus calculated are rather close to the same results provided by EMPIRE-II code [3] and smaller by a factor of even 5 than the TALYS-1.0 [5] results. Unfortunately the measured neutron-capture cross section are either too scarce or less consistent in order to make possible certain proofs of the electric dipole γ-ray strength functions finally used in the activation cross-section calculations. The need of additional measured cross section is thus obvious.

The proton optical potential of Koning and Delaroche [11] has also been involved within the analysis of the available measured cross sections of (p,n) as well as the (p,γ) reactions on ^{51}V target nucleus, to check the adopted proton OMP and γ-ray strength functions $f_{E1}(E_\gamma)$. Another change of the geometry parameters of this potential, corresponding to a decrease of ~20% for the (p,n) reaction cross sections in the energy range of the statistically emitted protons has thus been found necessary for the proton energies below 20 MeV (Fig. 3). At the same time, the electric dipole γ-ray strength functions $f_{E1}(E_\gamma)$, obtained through the above-mentioned analysis of the neutron-capture cross sections, have to be decreased by around 25% (Fig. 3, the right-bottom corner). Fortunately, former studies of Zyskind et al. [19] showed that the isospin effects, not included in the present basic Hauser-Feshbach model calculations, play

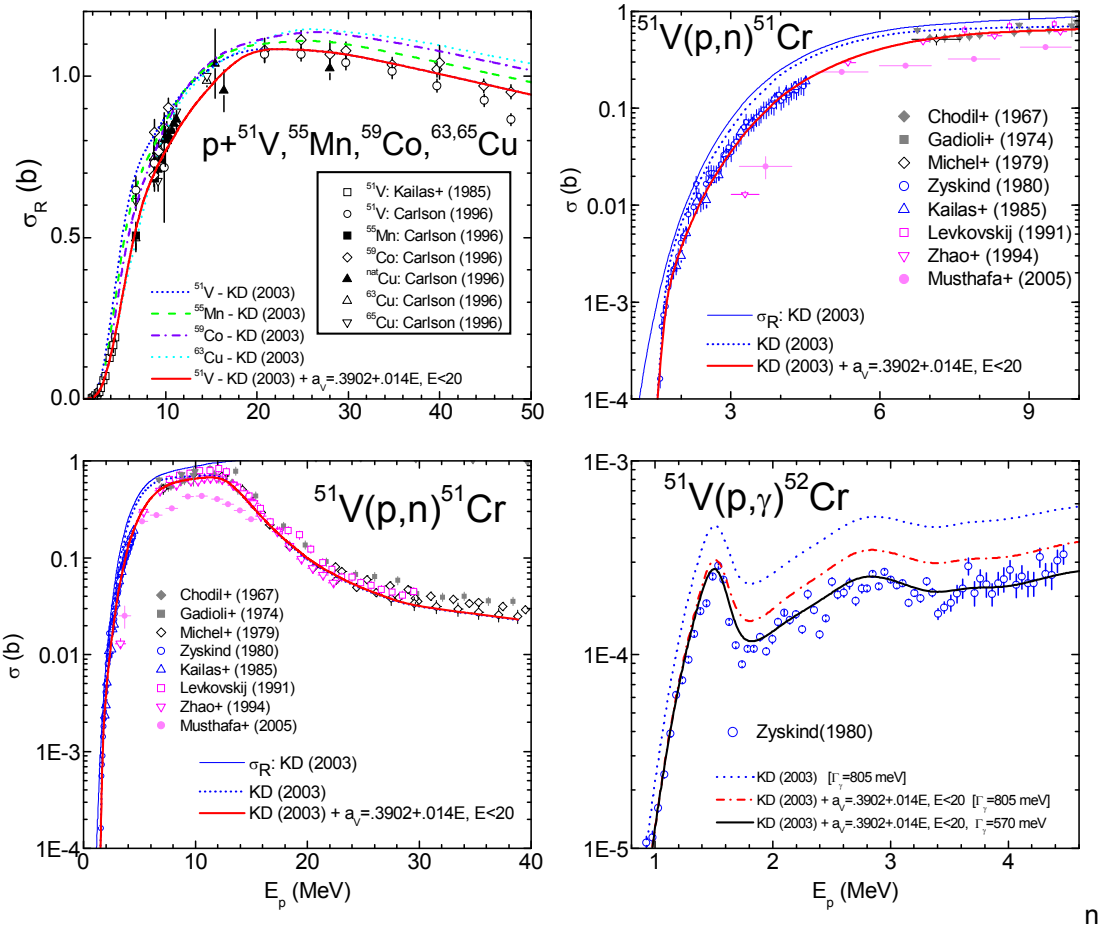

Figure 3. *Comparison of measured [15] and calculated total reaction cross sections of protons on ^{51}V and adjacent similar odd-Z nuclei, and (p,γ) and (p,n) reaction cross sections also on ^{51}V, within the local approach [9].*

no role in the case of $^{51}V(p,\gamma)^{52}Cr$ reaction. Thus they found the value μ=1 for the isospin mixing parameter, corresponding to the complete isospin mixing, when the cross-section model expression reduces to the usual Hauser-Feshbach form and the present results remain valid.

The pre-equilibrium emission (PE) local approach [9] within the Geometry-Dependent Hybrid (GDH) model [20] has moreover been proved by the good agreement of the calculated (p,n) reaction cross sections with the recent data between ~20 and 45 MeV (Fig. 3, left-bottom corner). While no free parameter has been involved, the basic point in this respect has been the use of an advanced particle-hole state density [21] within the PE description which has recently been described elsewhere [22,23]. These data description is obviously improved with reference to previous PE related analysis [24], providing confidence in the present results obtained without using of adjustable PE parameters.

The nuclear level densities were derived on the basis of the back-shifted Fermi gas (BSFG) formula [25], for the excitation energies below the neutron-binding energy, with small adjustments of the parameters *a* and Δ [26] obtained by a fit of more recent experimental low-lying discrete levels and *s*-wave nucleon resonance spacings D_0 [13]. Above the neutron binding we took into account the washing out of shell effects within the approach of Junghans et al. [27], with an asymptotic value $A/9$ for the level density parameter, and using the method of Koning and Chadwick [28] for fixing the appropriate shell correction energy. A transition range from the BSFG formula description to the higher energy approach has been chosen between the excitation energies of 15 and 25 MeV, respectively, in agreement with former shell model level densities [29]. On the other hand, the spin distribution has been determined by a variable ratio I/I_r of the nuclear moment of inertia to its rigid-body value, between 0.5 for ground states, 0.75 at the neutron binding energies, and 1 around the excitation energy of 15 MeV [26].

Results and discussion

The careful former assessment of the consistent model parameters involved finally within the local analysis of the Cr isotopes' fast-neutron activation cross sections has however been followed by a surprising disagreement of the calculated and even most recent and precise measured data. An illustration of this feature is shown in Fig. 4, for the (n,p) and (n,2n) reactions on the ^{52}Cr target nucleus. The proton OMP modified according to the analysis results shown in the previous section leads is significantly underestimate the experimental (n,p) reaction data below the neutron energies of 13-14 MeV, the calculated excitation function coming close to the measured data only beyond them. At the same time a large overestimation of the (n,2n) reaction cross sections around its maximum corresponds to the same model parameters. The latter excitation function is however well described by the proton OMP of Koning and Delaroche [11] as well as the (n,p) reaction cross sections below the neutron energy of ~9 MeV. Then again this proton OMP parameter set, formerly disproved by the above-mentioned (p,n) reaction discussion, has also provided too large (n,p) reaction cross section around the maximum of the corresponding excitation function (Fig. 4, left side).

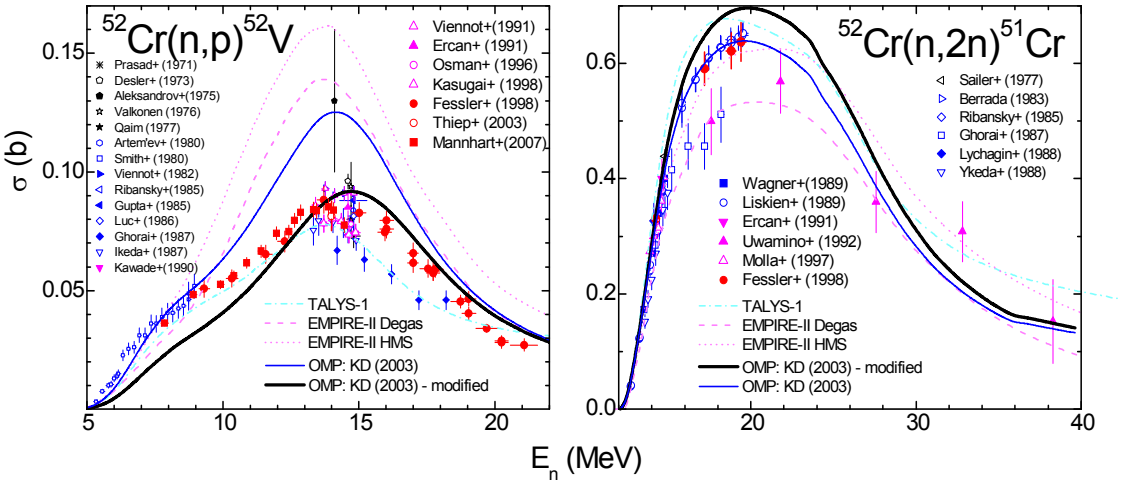

Figure 4. *Comparison of measured [15] and calculated activation cross sections for the ^{52}Cr target nucleus by using the TALYS and EMPIRE-II codes' global approach and the modified model parameters within the local approach [9].*

This model calculation breakdown for reaction cross sections at even lower incident energies, where the PE effects are small, has been rather unexpected. One may note especially that a similar parameter set was successfully used in the same mass region for the account of many reaction data around the Coulomb barrier of incident α-particles [30]. In this circumstances it seems that becomes important a question of the nuclear level density which is still open to discussion concerning its account within nuclear model calculations, namely the related parity distribution. While the parity equipartition is still assumed to be a quite good approximation at energies of a few MeV and higher [31], there is a simple model based on a combinatorial approach in the framework of the shell model [32] showing that the equipartition of parity is realized at an excitation energy close to 15 MeV. These results are also supported by recent advanced models, e.g. Ref. [33], pointing out a large effect especially at the nucleon binding energy where the parity equipartition has usually been assumed in order to obtain the level density parameters by the fit of the *s*-wave nucleon resonance spacings. This point will be considered in the continuation of the present work.
On the other hand, the (n,2n) reaction cross-section analysis shown in Fig. 4 points out the considerable data errors above the incident energies of ~20 MeV, close or even larger than the global and local model calculations. Therefore, in order to make possible a deeper view on the model status and development, more accurate experimental data are needed at least up to 40 MeV. The presently developing projects NFS@SPIRAL2 [34] and n_TOF-Ph2 [35] could be most helpful in this respect.

Acknowledgements
Work carried out within the CNCSIS-Bucharest project ID-PCE-43/2008. The EFNUDAT project support for the attendance of the Workshop on Fast Neutrons, 28-30 April 2009, at EC/JRC/IRMM in Geel is gratefully acknowledged.

References

[1] A. Fessler, E. Wattecamps, D. L. Smith, and S. M. Qaim, Phys. Rev. C 58, 996 (1998).
[2] Y. Han, Nucl. Phys. A 748, 75 (2005).
[3] M. Herman et al., in: Proc. Int. Conf. on Nucl. Data for Science and Technology, Nice, 2007, O. Bersillon et al. (Eds.), EDP Sciences, Paris, 2008; EMPIRE-2.19 Manual, p. 171, http://www-nds.iaea.org/empire/.
[4] L.C. Mihailescu, C. Borcea, A.J. Koning, and A.J.M. Plompen, Nucl. Phys. A 786, 1 (2007).
[5] A.J. Koning, S. Hilaire, and M.C. Duijvestijn, as Ref.3, p. 211; TALYS-1.0 User Manual, Dec. 21, 2007, www.talys.eu.
[6] E. Simeckova et al., in: A. Plompen (Ed.), Proc. 4th NEMEA-4 Workshop on Neutron Measurements, Evaluations and Applications, Prague, Czech Republic (2007), European Commission Report EUR 23235 EN, Belgium, 2008, p. 35; www.irmm.jrc.be/html/publications/.
[7] M. Honusek et al., as Ref. [6], p. 39.
[8] R.A. Forrest et al., Validation of EASY-2005 using integral measurements, Report UKAEA FUS 526 (2006)
[9] M. Avrigeanu and V. Avrigeanu, STAPRE-H95 Computer Code, News NEA Data Bank 17, 22 (1995), and Refs. cited therein; updated version (2008).
[10] P. Reimer et al, Phys. Rev. C 65, 014604 (2001); M. Avrigeanu et al., Nucl. Phys. A 806, 15 (2008); V. Semkova et al., Nucl. Phys. A 730, 255 (2004).
[11] A.J. Koning and J.P. Delaroche, Nucl. Phys. A 713, 231 (2003).
[12] J.P. Delaroche, Ch. Lagrange, and J. Salvy, IAEA-190 (IAEA, Vienna, 1976), vol. 1, p. 251.
[13] A.V. Ignatyuk, http://www-nds.iaea.or.at/RIPL-2/resonances/ .
[14] L. Leal, Report EFFDOC-1055, OECD/NEA Data Bank, Nov. 2008.
[15] EXFOR Nuclear reaction data, http://www-nds.iaea.or.at/exfor/ .
[16] W.P. Abfalterer et al., Phys. Rev. C 63, 044608 (2001).
[17] H.M. Agrawal, J.B. Garg, and J.A. Harvey, Phys Rev. C 30, 1880 (1984).
[18] M. Avrigeanu, V. Avrigeanu, G. Cata, and M. Ivascu, Rev. Roum. Phys. 32, 837 (1987).
[19] J.L. Zyskind, C.A. Barnes, J.M. Davidson, W.A. Fowler, R.E. Marrs, and M.H. Shapiro, Nucl. Phys. A343, 295 (1980).
[20] M. Blann and H. K. Vonach, Phys. Rev. C 28, 1475 (1983), and Refs. cited therein.
[21] M. Avrigeanu and V. Avrigeanu, Comp. Phys. Comm. 112, 191 (1998); A. Harangozo, I. Stetcu, M. Avrigeanu, and V. Avrigeanu, Phys. Rev. C 58, 295 (1998).
[22] M. Avrigeanu , S. Chuvaev, A. A. Filatenkov, R. A. Forrest, M. Herman, A. J. Koning, A. J. M. Plompen, F. L. Roman, and V. Avrigeanu, Nucl. Phys. A806, 15 (2008).
[23] P. Bém, E. Šimečková, M. Honusek, U. Fischer, S.P. Simakov, R.A. Forrest, M. Avrigeanu, A.C. Obreja, F.L. Roman, and V. Avrigeanu, Phys. Rev. C 79, 044610 (2009).
[24] M.M. Mustafa, Manoj Kumar Sharma, B.P. Singh, and R. Prasad, Appl. Rad. Isotopes 62, 419 (2005).
[25] H. Vonach, M. Uhl, B. Strohmaier, B.W. Smith, and E.G. Bilpuch, G.E. Mitchell, Phys. Rev. C 38, 2541 (1988).
[26] V. Avrigeanu, T. Glodariu, A.J. M. Plompen, and H. Weigmann, J. Nucl. Sci. Tech. S2, 746 (2002).
[27] A.R. Junghans, M. de Jong, H.-G. Clerc, A.V. Ignatyuk, G.A. Kudyaev, and K.-H. Schmidt, Nucl. Phys. A629, 635 (1998) , and Refs. cited therein.
[28] A.J. Koning and M.B. Chadwick, Phys. Rev. C 56, 970 (1997).
[29] M.J. Canty, P.A. Gottschalk, and F. Pühlhofer, Nucl. Phys. A317, 495 (1979).
[30] M. Avrigeanu, A.C. Obreja, F.L. Roman, V. Avrigeanu, and W. von Oertzen, At. Data Nucl. Data Tables (in press), doi: 10.1016/j.adt.2009.02.001.
[31] A.J. Koning, S. Hilaire, and S. Goriely, Nucl. Phys. A810, 13 (2008).
[32] B. Pichon, Nucl. Phys. A568, 553 (1994).
[33] D. Mocelj, T. Rauscher, G. Martínez Pinedo, K. Langanke, L. Pacearescu, A. Faessler, F. K. Thielemann, and Y. Alhassid, Phys. Rev. C 75, 045805 (2007).
[34] X. Ledoux, S. Simakov, in The SPIRAL2 Project. Neutrons For Science (GANIL, Caen, 2006), http://www.ganil.fr/research/developments/spiral2/ .
[35] A. Mengoni, F. Käppeler, E. González Romero et al. (The n_TOF Collaboration), n_TOF-Ph2 Activities at the neutron time of flight facility at CERN (CERN, Geneva, 2005), http://www.cern.ch/ntof/Documents/LoI_2005/.

CACAO: a project for a laboratory for the production and characterization of thin radioactive layers

C.-O. Bacri

Institut de Physique Nucléaire d'Orsay, 91406 Orsay Cedex, France, CNRS/IN2P3, UMR8608, Université Paris-Sud.
bacri@ipno.in2p3.fr

Abstract: The CACAO project, Chimie des Actinides et Cibles radioactive à Orsay, consists on the installation of a hot laboratory dedicated to the production and the characterization of thin radioactive layers. One of its goals is to be able to coordinate, at least for the French community, the different activities related to radioactive target preparation and characterization. For this end, it will be complementary to already existing international installations, and could be considered as the first step of a kind of network of laboratories, each of them specialized in some techniques and/or isotopes.
After a brief description of the motivations, in term of physics programs, the foreseen installations will be presented, and the different collaborations in which we are involved will be briefly described. To conclude, the status of the project, which has obtained the approval of the French institutions and a part of the budget, will be presented.

Introduction and motivations

The CACAO project, Chimie des Actinides et Cibles radioActives à Orsay [1], is still under construction. It consists on the installation of a hot laboratory dedicated to the production and the characterization of thin radioactive layers. The starting point of the project is of course the numerous experimental programs which need radioactive targets, associated to the big difficulties encountered by physicists to obtain these targets. Two of these programs will be introduced in the following.
One of these programs is related to the nuclear fuel cycle and reactor physics. The nuclear cycle is based on the capability of the ^{235}U to fission under the impact of slow neutrons. However, nuclear fuel is mainly composed of ^{238}U, which is a fertile isotope: it produces a fissile isotope, the ^{239}Pu through n-capture and beta-decays. Transuranium isotopes are then formed through successive neutron captures and beta minus decays, starting from ^{235}U or ^{238}U. These isotopes are mainly isotopes of Np, Am and Cm, and they constitute the most radiotoxic radioactive waste. One of the main issues of the future management of nuclear waste consists to try to incinerate them through reactors, either dedicated ones or not. The design of these reactors for nuclear waste incineration requires high quality nuclear data. Not only neutron induced fission and capture cross section are needed, but also elastic and inelastic neutron scattering on all these actinides.
Another possibility consists to minimize their production in reactors. For this purpose, the study of the thorium/uranium cycle is promising. ^{232}Th is indeed another fertile nucleus which plays the same role than ^{238}U in the current cycle: under the impact of neutron, it produces a fissile isotope, the ^{233}U, which fission under the impact of another neutron. The interest of this cycle, besides the fact that thorium resources are important, is also the relatively low Z of the thorium: it then becomes more difficult to produce transuranium elements through n-capture. This leads to less radiotoxic waste. In order to master this cycle, high quality nuclear data on U, Pa, and Np isotopes are needed.
For these studies on nuclear fuel cycle, radioactive targets are then needed. They concern nuclei with half-lives going from few days up to millions years; some of them are beta-emitters, most of them are alpha emitters, and some can fission under neutron impact; of course, gamma and X-rays can also be emitted. At last, some of these nuclei can spontaneously fission and emits neutrons. This great variety leads to real difficulties in the production of these targets because numerous techniques are needed to be used, depending on the isotope of interest.
Another program which needs radioactive targets is related to the production and the study of super-heavy elements. The question of the existence of an island of stability for Z higher than 100 raise the question of the evolution of nuclear forces and of the existence of magic

numbers far from the stability. Moreover, chemistry of super-heavy elements is also an open question. Of course, one of the main issues of such a physics is to be able to produce these super-heavy elements[1]. Fusion mechanism has shown to produce at least up to Z=112, but production cross sections falls of a factor 10 when increasing Z by 1. Nevertheless, recent studies showed that hot fusion between beams such as ^{48}Ca on actinide targets, leads to a plateau on the curve of production, giving hope in the possibility to produce super-heavy elements with not too low cross-sections. Development of radioactive targets which can support strong deposits of power is then needed.
Both programs are included in the physics program of the future facility SPIRAL2 at Ganil, Caen [3]. The NFS (Neutron For Science) installation will provide high flux neutron beam, in the 100 keV-40 MeV energy range and part of its beam will be used for studies related to nuclear fuel cycle. It was designed for the use of actinide targets. On another hand, the S3 spectrometer will provide the opportunity to develop a program on super-heavy elements at the Ganil facility.

CACAO, a tool for coordination of the acquisition of radioactive targets

The main difficulties to obtain radioactive targets concern the different steps of the process of production, but also the fact that the needed knowledge to make thin radioactive layers is nearly lost. Moreover, difficulties related to manpower and to the cost of “nuclear installations” lead to limit investments to maintain this activity.
These difficulties become nowadays a real obstacle to the realization of some programs: obtain the radioactive isotope of interest with the needed purity, find the laboratory able to make the target and that possesses the techniques and the manpower, find installations able to make a precise characterization of the target (homogeneity, chemical and isotopic contaminant determinations), obtain the safety authorization and make transport of the target is more and more difficult, and very time consuming task, especially for physicist who is not specialist neither of radiochemistry nor of thin layers production.
The aim of the CACAO project is first to be able to coordinate all these different steps, going from the finding of isotope, to the characterisation of the target, through its production. This installation will be then complementary to other existing laboratories, in order to be able to supply all the physicist needs, thanks to collaborations, each time it will be not possible to directly make the targets. An important work to develop a kind of network of “target makers” is then needed, and is yet in progress. This is partly why European program EFNUDAT [4] has dedicated a JRA (Joint Research Activity) to reactions targets. Interactions between EFNUDAT and the CACAO project will be discussed further.

Constraints related to thin radioactive layers fabrication

One of the main constraints is of course related to the handling of the activity of the isotope of interest. Nevertheless, it should be reminded that targets are supposed to be used with an accelerator and then to be able to be handled in a beam line. This leads to dimension the CACAO facility as gloves boxes in controlled zone. The first consequence is then the limited activities of the produced target. Another constraint comes from the fact that thin layers are usually not self-supported and then, a backing is necessary. This backing is an “as thin as possible layer”, made with a stable isotope. The possibility to realize a stable thin layer is then necessary to get a radioactive target ! Finally, it is of course to master radiochemistry first to make the good chemical form of the necessary isotope, and then to be able to develop the adequate technique considering the needs of the physicist.
Thanks to our radiochemical group [5] and our target manufacturing department [6], IPN Orsay is well equipped to overcome these difficulties. However, even if our radiochemical group has expertises in the chemistry of actinides, allowing manufacturing actinide targets, it is a research group and it cannot produce targets for a large community. Taking into account the current forces, the transfer of knowledge to CACAO cannot be done with constant personnel. This, amongst other things, is why we have obtained from the EFNUDAT European I3 the recruitment of a person for one year in preparation of a possible longer term engagement, in order to carry out this transfer of expertise.
The training of this EFNUDAT contractor will be assured by our radiochemistry group which has already realized targets, but also via collaborations with the other laboratories which possess the know-how.

Current and forthcoming collaboration for the target fabrication

Two main techniques allow making deposit of an isotope onto a backing: evaporation and electrodeposition. The implementation of the first one is relatively simple and high purity layers can be built up, but its efficiency is small, due to the fact that solid angle of the backing is usually a small fraction of 4π. Moreover, in order to minimise cross contamination between different isotopes, it is necessary to have as many vacuum chambers as isotopes, which becomes quickly very expensive.
The other technique requires, for each isotope, finding the good chemical solution allowing its electrodeposition. Radiochemistry techniques are then necessary to master, not only to develop these solutions, but also in order to have the good chemical form of the isotope of interest allowing the development of the target. This technique has two big advantages: it is not expensive to develop, and its efficiency is nearly 100%, allowing then the use of very expensive isotopes.
The radiochemistry group of IPN Orsay has already manufacture target by electrodeposition for the program of the IPNO's group related to measurements of fission cross sections at the n_TOF facility at CERN: a deposit of 8 cm diameter of 300 µg/cm^2 ^{233,234,235,238}U, ^{232}Th, and ^{237}Np, on a support of 2 µm thick Al. This group contribute now to transfer his knowledge to the EFNUDAT contractor, who is present at Orsay since September 2008
Besides this collaboration, another one has been established with the Berkeley University Wadworth center [7]. Its purpose is to develop techniques to electrodeposit thin layers (300 μg/cm^2) of actinides, onto an "as thin as possible" backing. This technique is needed for fission studies, for which the two fission fragments have to get out of the target. A backing of metalized Mylar is foreseen because of its relatively low stopping power. Up to now, some work has still to be done, especially because the metallic layer tends to be extracted during the process of electrodeposition. This technique is also developed onto a polyimide layer, thanks to collaboration with the IRMM/Geel target laboratory and the French CEA/DAM/IdF laboratory. All these collaborations, which can be considered as the support of the training of the EFNUDAT fixed-term contract, are financed thanks to the French research grouping GEDEPEON, of the research program PACEN [8].
Moreover, different laboratories, such as GSI, Mainz or Munich are already able to provide radioactive targets, under some "restrictive" conditions. In order to be able to play the role of coordination in the different steps of the production of radioactive targets, CACAO is working to establish close links with these laboratories.

Target characterization

A precise characterization of the targets is an important demand of the users. The thickness, the homogeneity, and the chemical and isotopic purity of a target are indeed very important not only for the quality of the data obtained with the target, but also for the interpretation of these data.
CACO will be able to provide an α cartography of the target. Thanks to the expertise on Ge detector of the IPNO's detector service [9], a γ spectrometry will be possible. Our Tandem facility [10], which can deliver protons down to 3 MeV, can be used to perform RBS (Rutherford BackScattering), measurements. For very active targets, the proximity of the Pierre Süe laboratory (LPS,[11]), located at Saclay, can be very useful. Indeed, the LPS has a 3.75 MV Van de Graaff which accelerates $^1H^+$, $^2H^+$, $^3He^+$, $^4He^+$. This electrostatic accelerator is equipped with a dedicated shielded hot line allowing the analysis of very radioactive samples by ions beams; PIXE (Proton Induced X-ray Emission), RBS (Rutherford BackScattering), and NRA (Nuclear Reaction Analysis). Moreover, experimental areas related to the OSIRIS and ORPHEE reactors allow for sample irradiation and neutron activation analysis. Work has started between CACAO and the Pierre Süe laboratory, in order to establish collaborations.
Finally, CACAO will benefits from the proximity of the CEA/Saclay site, where the French Henri Becquerel laboratory [12] (CEA/LNHB) is located. Within the framework of its mission of metrology, CEA/LNHB has the necessary equipment for characterizations with α and β autoradiographs. Moreover, they have an expertise in metrology measurements that will be very important for target characterization. In order to fully benefit of their know-how, IPNO has signed a collaboration agreement with the LNHB, allowing an "easy access" to their installations, if needed.

Status of the project / Conclusion

The CACAO project is an ambitious project for a French national laboratory for the production and characterization of radioactive thin layers. Its main goal is to be a national point of coordination for the different activities related to radioactive target preparation and characterization. For this purpose, CACAO will be complementary to other existing laboratories, and collaborations with them are in progress. These collaborations will allow CACAO to become a kind of node of a network of hot labs dedicated to radioactive target manufacturing.
The project was approved by the scientific council of CNRS/IN2P3, and benefit of a strong support of the PACEN program [8]. A detailed study of the needed installations has been done and has allowed giving a precise estimation of the cost of the project. Part of the financing is already obtained, and 3 years of fixed term contract has been obtained, in order to start the project and renew the engagement of the EFNUDAT contractor.
The construction of an agreement with the CEA is in progress and the final political approval of the project is waited before July 2009. First targets are foreseen at the beginning 2010.

Acknowledgements
One of the authors wants to thank all the CACAO group without which the project would not exist, and especially Y. Ades, J.F. Le Du, V. Petitbon and N. Vigot of IPNO. Part of this work took benefit of the European EFNUDAT consortium of the 6th PCRD and of the financing of the PACEN/GEDEPEON program.

References

[1] C.O. Bacri, proceedings of the 24th World Conference of the International Nuclear Target Development Society developing techniques for target preparation and applications. September 2008. To be published in NIM A.
[2] P.H. Heenen et al., Europhysics News (2002) vol.33 N°1.
[3] Physics case of SPIRAL2 at GANIL; http://www.ganil-spiral2.eu/spiral2-us.
[4] http://www.efnudat.eu.
[5] http://ipnweb.in2p3.fr/~rad/index_E.html.
[6] V. Petitbon, these proceedings. http://ipnweb.in2p3.fr/~cibles/index_E.html.
[7] Lawrence Berkeley National Laboratory, Berkeley, USA, and Wadsworth Center, Laboratory of Inorganic and Nuclear Chemistry, Albany, New York, USA.
[8] GEDEPEON (waste management and energy production with innovative option) is a national research group, inside the national PACEN (Backend nuclear fuel cycle and energy production) which coordinate in CNRS all studies related to nuclear fuel cycle.
[9] http://ipnweb.in2p3.fr/~detsemi/.
[10] http://ipnweb.in2p3.fr/tandem-alto/index_E.html.
[11] http://iramis.cea.fr/lps/.
[12] http://www.nucleide.org.index.htm.
[13] V. Petitbon, these proceedings. http://ipnweb.in2p3.fr/~cibles/.

Target preparation for in-beam thermal neutron capture experiments

T. Belgya

Institute of Isotopes Hungarian Academy of Sciences (II HAS or IKI), H-1525 POB 77, Budapest, Hungary
belgya@iki.kfki.hu

Abstract: Target preparation is an important technique at facilities where the samples are irradiated with particle beams. The cold neutron-beam at the PGAA-NIPS facilities of the Budapest reactor requires special attention to certain preparation requirements in order to obtain the highest quality scientific results. These special requirements are summarized and explained.

Introduction

Prompt Gamma Activation Analysis (PGAA) is a relatively new method for chemical element analysis and there are only a handful of facilities in the world which are using it for routine sample analysis [1, 2]. At the Budapest Research Reactor we irradiate samples with beams of cold neutrons. The neutrons excite the target nuclei which then emit γ-rays. These γ-rays are detected and their full energy peaks in the spectra are used in the quantitative analysis. The facility has been described on many occasions [1, 2]. A detailed description of standardization was presented in Ref. [3], which gave a number of examples of the form and quantity of samples, but sample preparation was not described in detail. Besides the analytical work, the facility can also be used to determine cross sections of nuclei at low neutron energies, which are important in the EFNUDAT project. The purpose of this paper is to describe a variety of the sample preparations we have already used. Before this description, we provide some information on the beam characteristics at the PGAA and at the Neutron Induced Prompt-gamma Spectrometry (NIPS) facilities of II HAS. The facility as a whole is called PGAA-NIPS.
Sample size effects on the counting rate has been already studied by Copely and Stone, and are important in the absolute measurements [4]. Due to this effect we prefer homogeneous samples in a comparator arrangement. Based on some simplifying assumptions for the neutron transport, we present the best sample preparation practice for high precision PGAA-NIPS experiments.

Beam characteristics at the PGAA and NIPS facilities

In 2001, a liquid-hydrogen-containing cold neutron source was installed in the 10-MW Budapest Research Reactor. The neutron guide system was also reconstructed at the same time. Due to these modifications the neutron flux increased more than an order of magnitude [5]. A further improvement of the beam guide with 2-theta super-mirror sections in the last 12.5 meter section was finished in 2007, which yielded a thermal-equivalent flux of 1.2×10^8 $n \cdot cm^{-2} \cdot s^{-1}$ at the PGAA sample position with the sample chamber at atmospheric pressure and 1.5×10^8 $n \cdot cm^{-2} \cdot s^{-1}$ in an evacuated sample chamber. The neutrons at the end of the guide are collimated into two beams which serves the two facilities.
The PGAA facility is dedicated to chemical analysis. It is equipped with a well calibrated, BGO-guarded, HPGe spectrometer. The efficiency of the spectrometer is 27% and the resolution is 2.2 keV at the 1332 keV γ-ray energy of a ^{60}Co source. The efficiency of the detector is regularly measured over the 50 keV to 10 MeV range with a precision of 1 %.
The NIPS facility is used for all other nuclear spectroscopic measurements involving the detection of prompt gamma radiation from materials activated in neutron beam. At this latter facility, the flux is 4.7×10^7 $n \cdot cm^{-2} \cdot s^{-1}$, which is somewhat smaller than at the PGAA facility. The station is equipped with three HPGe detectors, including a high resolution LeGe detector.
Figure 1 shows the PGAA-NIPS facilities, the PGAA sample holder and the way that the sample is placed in the target chamber. The usually flat samples are set at an angle of 30° relative to the neutron beam in order to share the amount of absorption between the neutron beam and the gamma rays. The beam just before the PGAA sample holder is collimated to

the maximum beam size of 2 × 2 cm^2. This can be decreased to a 5 mm^2 hole by insertable collimators. The beam profile is rather inhomogeneous and is shown in Figure 2, which was taken with a radiograph.

Figure 1. *The PGAA and NIPS beam tubes. The two neutron beams are indicated by the two black arrows. They are inside the aluminium tube which is lined with Li-6 polymer neutron-absorbent sheets to decrease the flux of escaping scattered neutrons. The upper (PGAA) beam is stopped by Li-6 polymer sheets at the end of the upper section (indicated by 1). The lower beam continues to the NIPS station indicated by a circle. The sample holder and the placing of a sample in the target chamber are shown in the lower-left insert.*

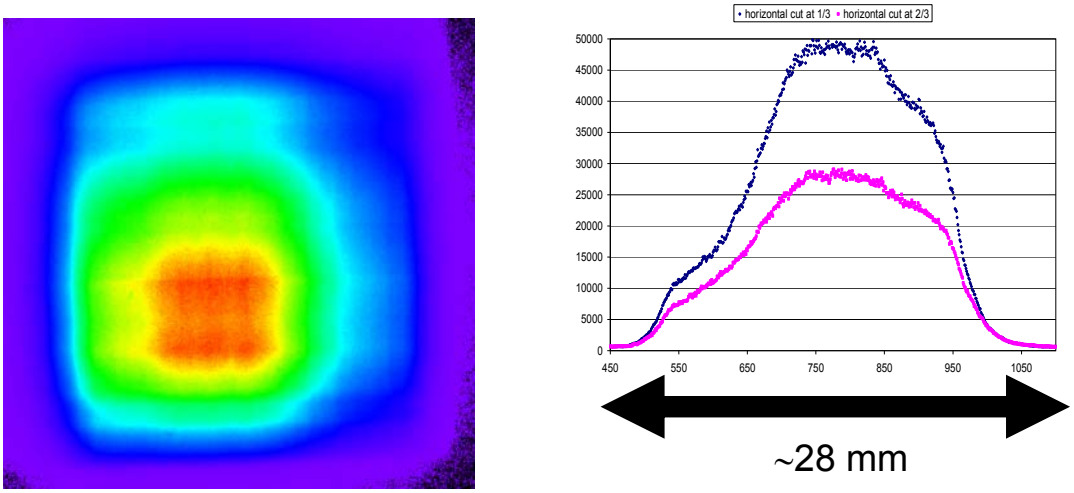

Figure 2. *The picture is the intensity map of the beam as seen by a radiograph at the NIPS station. The graph on the right shows the beam intensities at the upper 1/3 of the red area (higher value curve) while the lower value curve is at the lower 1/3 of the red area.*

The beam inhomogeneity is quite obvious from Fig. 2, which puts a rather strong constraint on the sample geometrical distribution in order to be able to measure quantities in a way that is independent of these local flux variations. This will be discussed later at the sample preparation section.

The experimental procedure is the following. The sample with mass *m* is placed in the neutron beam. The nuclei of the target are left in an excited state by neutron capture and then

they release their energy by gamma radiation. The radiation is detected by a Compton-suppressed HPGe detector and the energies of the γ-rays deposited in the detector are analyzed with standard nuclear electronics. The measured γ-ray spectra usually contain a large number of peaks. The energy E_γ of a peak is a characteristic of the emitting nucleus and the peak count rate A is proportional to the number of nuclei n or the mass m of these nuclei in the target. Thus the measurement is able to provide the composition of the target or if the composition is known, other quantities can be determined.

Considerations for sample preparation for the PGAA-NISP facilities

The measured γ-ray-peak count rate A depends on the characteristic quantities of the experimental setup. It can be described using the following improved equation presented in Ref. [1, 4]

$$A_{X\gamma} = P_{X\gamma} \int_V d\underline{r}^3 \varepsilon(E_\gamma, \underline{r}) n_X(\underline{r}) g(E_\gamma, \underline{r}) \int_0^\infty d\nu \int_\Omega d\Omega \cdot \sigma_X(\nu) \Phi(\nu, \underline{\Omega}, \underline{r}, t), \quad (1)$$

where P_γ is the absolute decay probability (for one neutron capture) of the de-exciting γ-ray, $\varepsilon(E_\gamma,\underline{r})$ is the detector efficiency at gamma energy E_γ, t is the irradiation and measurement time, V is the volume of the target, ν is the neutron velocity, $\underline{\Omega}$ is the unit length direction vector at point $\underline{r}$ in the sample through which the neutron is propagating, $n_X(\underline{r})$ is the number of atoms of type X at point $\underline{r}$ in the unit volume, $\sigma_X(\nu)$ is the capture cross section of atom type X, $\Phi(\nu,\underline{\Omega},\underline{r},t)$ is the scalar neutron flux density, $d\Omega$ is the differential solid angle around $\underline{\Omega}$ and $g(E_\gamma,\underline{r})$ is the gamma absorption in the target.
For highest accuracy the equation has to be calculated using the solution of the neutron transport in the target, which gives the flux distribution throughout the volume of the sample. An analytical solution is rather difficult for a general sample and in practice it is a very lengthy procedure and thus it is not practical. In our case even using Monte Carlo simulation is difficult due to the complicated spatial dependence of the flux (see Figure 2). With the following assumptions we can avoid all of these complications that are posed by the need to solve the neutron transport inside the sample.

1./ The cross section of the sample materials are of $1/\nu$ behavior. This means that the cross section can be expressed with the thermal (th) values

$$\sigma(\nu) = \sigma(\nu_{th}) \frac{\nu_{th}}{\nu}. \quad (2)$$

2./ The number density of atoms does not depend on the position in the sample (homogeneous sample). Thus $n_X(\underline{r})=n_X/V$ so the constant can be moved out from the integral.
3./ The flux does not change in time (this is almost always true for reactors, if unexpected events do not happen).
4./ Gamma absorption of the target is negligible i.e. g=1.
5./ The variation of the detection efficiency is small throughout the target volume

With the above assumptions Eq. (1) can be written as

$$A_{X\gamma} = P_{X\gamma} \varepsilon(E_\gamma) n_X \sigma_X(\nu_{th}) \nu_{th} \frac{1}{V} \int_V d\underline{r}^3 \int_\Omega d\Omega \int_0^\infty d\nu N(\nu, \underline{\Omega}, \underline{r}). \quad (3)$$

In this equation the neutron density $N(\nu,\underline{\Omega},\underline{r})$ in phase space is introduced. The triple integral over the phase space provides the number of neutrons N in the target volume V. The final equation using $\sigma_{X\gamma} = P_{X\gamma}\sigma_X(\nu_{th})$ and $\phi_{th} = \frac{\nu_{th} N}{V}$ notations is

$$A_{X\gamma} = \varepsilon(E_{X\gamma}) n_X \sigma_{X\gamma} \phi_{th}. \quad (4)$$

This corresponds to a case of a very thin, homogeneous sample. If the cross section is low and if the sample contains a homogeneous mixture of an unknown X and a well known comparator C, then dividing Eq. (4) with a similar equation for the comparator we arrive to the equation from which the cross section of the unknown can be determined [6]

$$\sigma_{X\gamma} = \sigma_{C\gamma} \frac{A_{X\gamma}}{A_{C\gamma}} \frac{n_C}{n_X} \frac{\varepsilon(E_{C\gamma})}{\varepsilon(E_{X\gamma})} \frac{f(E_{C\gamma})}{f(E_{X\gamma})} . \quad (5)$$

Here we have relaxed assumption 4./ and let γ-ray and neutron absorptions be taken into account with the appropriate correction factors $f(E_\gamma)$. We call any experiment which uses Eq. (5) a comparison or standardization experiment. Note that the ratio of number of atoms for the comparator and the unknown has to be known with high precision in order that the experiment can yield a high precision cross section. This requirement is easy to satisfy with stable chemical compounds which contain both *X* and *C*. In any cases of mixtures of compounds or elements, the relative masses of unknown and comparator must be known with high precision. This is also true for the stack type of experiments where the thickness of the stack sheets should be known because in this case only the thickness can be used to calculate the ratio. If the shapes of the unknown sheet and the comparator are the same, and they are positioned identically in the neutron beam, then the total masses can be used to calculate the ratio. In all other cases the integral must be performed and the flux distribution throughout the sample volumes must be known. To determine the spatial distribution of the flux is not a trivial job. Using the mass or thickness for the calculation of the number of atoms assumes that the composition of the target is known with high precision. Hygroscopic compounds can cause problems, as well as other absorbing materials.

Best sample forms

From the above considerations the best sample form for the PGAA-NIPS facility is a self supported pressed disk with a maximum diameter of 2 cm and a thickness which does not absorb more than a few percent of the neutrons and γ-rays. The second is a rectangular shape of $2\times2\times Z$ cm^3 form used when powder samples are packed in FEP foil (Fluorinated Ethylene Propylene foil of 10 μm thickness). The thickness *Z* of the sample should be adjusted so that the absorption for both neutrons and γ-rays should be less then a few percent. In the case of a small amount and/or large cross section, a smaller sample size is also acceptable at the price of a possibly smaller yield. For radioactive materials, the best choice is usually a sealed aluminum container of disc shape, but it depends on the experiment.

To determine the suitability of a target for experiments at our PGAA-NIPS facilities we give some hints below. The decrease of the initial neutron flux ϕ_0 in a brick shaped sample can be calculated from the macroscopic cross section.

$$\Sigma_{tot} = (\sigma_{absorption} + \sigma_{scattering}) \cdot n_X / V \quad (7)$$

The corresponding formula in the first approximation is

$$\phi = \phi_0 \exp(-\Sigma_{tot} \cdot z) \quad (8)$$

where *z* is the distance the neutron travels in the target along the beam direction. The combined neutron and γ-absorption $f(E_\gamma)$ in a brick shaped sample with thickness of *a* , which is set at an angle of θ relative to the neutron beam is a simple integral along the neutron direction of the neutron and the corresponding γ-attenuation. The formula for large detector distance and neglecting multiple scattering of neutrons in the sample is

$$f(E_\gamma) = \frac{\sin(\theta)}{a} \int_0^{a/\sin(\theta)} \exp(-\Sigma_{tot} \cdot z) \exp(-\mu(E_\gamma) \cdot z \cdot \mathrm{tg}(\theta)) dz \quad (9)$$

where $\mu(E_\gamma)$ is the linear attenuation coefficient of a γ-ray with an energy of E_γ. To calculate the linear attenuation coefficient of γ-rays in a given composite material we use the XMuDat program [7].

The detector counting rate can be estimated from the following equation.

$$A = \varepsilon_{tot} n_X \sigma_X(\nu_{th}) \phi_{th} . \quad (4)$$

The total efficiency ε_{tot} of our fixed configuration PGAA detector is approximately 0.001 at practically any γ-ray energy [8]. The counting-rate increase due to the sample should exceed the no-sample counting rate with beam-on which is about 10 cps, but should not be higher than a few thousand cps. At higher count rates the full-energy peak shape will be deformed so much that the analysis becomes difficult.

For the comparator experiments it is best to select a compound such that the yields from the comparator and the unknown have similar values. This is true for both prompt and decay comparisons. In the case of decay comparisons, the half-lives should also be similar.

Examples for samples

In his section we show a few examples of samples that we have already used for experiments. Below, there are five pictures showing various samples and our standard sample holder. In each picture, the objects rest on millimeter graph paper to show the sample sizes.

In Picture 1 we can see three powder samples of various sizes. The sample to the left is a geological powder sample containing mainly low cross section silicon and other metallic compounds characteristic of rocks. The two rightmost contains mixture of NaCl and carbon powder (black, see enlarged in Picture 4), and NaCl and Cu powder (red, see enlarged in Picture 4). They are for standardization of sodium relative to carbon and copper. In the middle, the two white cylindrical containers are for liquid samples. They are made of FEP which is almost invisible in capture experiments. The coin like sample, wrapped in FEP foil (see enlarged in Picture 4), was used in an activation experiment within the EFNUDAT project proposed by Anton Wallner. The sample is a mixture of natural U_3O_8 and Au powder. The latter is for neutron fluence determination during the irradiation. The pressed mixture is enclosed with two thin Au-foil discs and assembled in an Al ring.

In Picture 2 the Al frame to the left is our regular sample holder with thin Teflon monofilaments that holds the sample firmly in the beam position. It also helps to form flat rectangular shape for the powder samples. Next to the frame on the right there is an 8 cm diameter and 1 mm thick Zr disc for which we determined its composition also within the EFNUDAT project. The disc is used at IRMM in transmission experiments and is connected to the Zr-96 cross section experiments in CERN (proposer Giuseppe Tagliente). The white vial to the right is the same as in Picture 1. Quartz vials in the glass beaker are also good for holding liquids since quartz is almost invisible in our experiments.

In Picture 3 we can see two pressurized gas containers. The larger with 8 cm diameter is made of aluminum and hold gases up to 20 bar pressure. It was used to measure the ^{22}Ne cross section using the invisible container concept [9]. The smaller one is able to hold up to 200 bar and contained a mixture of ^{22}Ne and methane (CH_4) as comparator. The rightmost is a roll of FEP monofilament which is used in our sample holder frame.

Picture 1

Picture 2

Picture 3

Picture 4

Picture 5

In Picture 5 we can see enriched metal samples of ^{57}Fe and ^{60}Ni which are ideal for PGAA experiments. These targets will be used in another experiment within EFNUDAT which was proposed by Frank Gunsing. The purpose of the experiments is to characterize the targets and if possible to determine their thermal capture cross sections. Study of these and other iron and Ni isotopes will be performed at the n-TOF facility of CERN.

Our last example is an ultra thin ^{235}U target (see Picture to the left, middle of third plate from the bottom) that was used in a fission chamber to measure the thermal-neutron-capture induced fission-neutron angular distribution at the NIPS facility [10] (proposer Franz-Josef Hambsch). The motivation for this investigation was to verify recent results measured at IRMM using 0.5-MeV incident neutron energy and the literature data measured during the past 20 years, which contradict the Los Alamos model as well as integral and benchmark experiments.

In summary, the author hopes that the information provided in this short article helps to design targets for experiments at the Budapest PGAA-NIPS facilities for users arriving within the EFNUDAT or other projects.

Acknowledgements

The support of EURATOM FP6 EFNUDAT project (Contract No. 036434) is acknowledged. Thank to Jesse L. Weil for revising the manuscript.

References

[1] H.D. Choi, R.B. Firestone, R.M. Lindstrom, G.L. Molnár, S.F. Mughabghab, R. Paviotti-Corcuera, Z. Révay, A. Trkov, V. Zerkin, and C. Zhou, Database of prompt gamma rays from slow neutron capture for elemental analysis 2007: International Atomic Energy Agency, Vienna, 2007. 1-251.

[2] G.L. Molnár, ed. Handbook of Prompt Gamma Activation Analysis with Neutron Beams. 2004, Kluwer Academic Publisher Dordrecht, Boston, London: Budapest. 1-423.

[3] Z. Révay, and G.L. Molnár, Standardisation of the prompt gamma activation analysis method. Radiochim. Acta, 2003. 91(6): p. 361-369.

[4] J.R.D. Copley and C.A. Stone, Neutron scattering and its effect on reaction rates in neutron absorption experiments. Nuclear Instruments & Methods in Physics Research Section A, 1989. 281: p. 593-604.

[5] Z. Révay, T. Belgya, Z. Kasztovszky, J.L. Weil, and G.L. Molnár, Cold neutron PGAA facility at Budapest. Nucl. Instrum. Methods Phys. Res. Sect. B-Beam Interact. Mater. Atoms, 2004. 213: p. 385-388.

[6] T. Belgya, P. Schillebeeckx and A. Plompen. Thermal neutron capture cross section measurements using a cold neutron beam. in Neutron Measurements, Evaluations and Applications. 2008. Prague, Czech Republic, 16-18 October 2007: (European Communities, 2008), 31-34.

[7] R. Novotny, XMuDat: Photon attenuation data. 1998, IAEA, http://www-nds.iaea.org/reports/nds-195.htm Vienna, Austria.

[8] T. Belgya and Z. Révay, Gamma-Ray Spectrometry, in Handbook of Prompt Gamma Activation Analysis with Neutron Beams, G.L. Molnár, Editor. 2004, Kluwer Academic Publishers, Dordrecht, Boston, London. p. 71-111.

[9] T. Belgya, E. Uberseder, D. Petrich, and F. Kaeppeler. Thermal neutron capture cross section of 22Ne. in 13th Int. Symposium on Capture Gamma-ray Spectroscopy and related Topics. 2009. Köln, Germany: (AIP 1090), 367-371.

[10] N. Kornilov, F.-J. Hambsch, I. Fabry, S. Oberstedt, T. Belgya, Z. Kis, L. Szentmiklosi, and S. Simakov, The 235U(n,f) prompt fission neutron spectrum at 100oK input neutron energy. Nucl. Science and Eng., 2009: p. Submitted.

First measurements of inelastic neutron scattering at nELBE

R. Beyer[1)], E. Birgersson[1)], E. Grosse[1,2)], R. Hannaske[1)], A. R. Junghans[1)], A. Matic[1)], M. Mosconi[3)], R. Nolte[3)], K.-D. Schilling[1)], R. Schwengner[1)], A. Wagner[1)]

1) Forschungszentrum Dresden-Rossendorf, Institute of Radiation Physics, Bautzner Landstr. 400, 01314 Dresden, Germany
2) Technische Universität Dresden, 01062 Dresden, Germany
3) Physikalisch-Technische Bundesanstalt Braunschweig, Bundesallee 100, 38116 Braunschweig, Germany

Roland.Beyer@fzd.de

Abstract: At the nELBE facility at Forschungszentrum Dresden-Rossendorf fast neutrons with kinetic energies of 0.1 to 10 MeV will be used to deliver nuclear data on neutron induced reactions.
First experiments on inelastic neutron scattering on ^{56}Fe were performed using a double time-of-flight detector setup. This setup is based on proton recoil detectors and an array of 42 BaF_2 crystals. The emitted photons and neutrons can be detected in coincidence. First results will be presented.

Introduction

Fast neutron induced reactions are important for the design and construction of future types of nuclear power plants and transmutation facilities. One of these reactions is inelastic neutron scattering, where an impinging neutron excites a target to a certain nuclear level by the transfer of a defined amount of energy. The neutron itself flies away under a certain angle with an accordingly lower kinetic energy $E_{n,out}$. The excited nucleus decays within typically pico seconds back to the ground state via the emission of one or more γ-rays. To undergo this type of reaction the incoming neutron has to have a kinetic energy $E_{n,in}$ above the excitation energy E_x of the level to be excited.
The inelastic scattering cross section is usually measured by bombarding of target nuclei with neutrons of known energy and by detection of the emitted γ-ray. The energy of the γ-ray can be assigned to the excited level and its frequency of occurrence delivers the cross section. The difficulty of this method is on the one side to have detectors which have a good energy resolution to identify the γ-ray energy and at the same time good time resolution to measure the energy of the incoming neutron. On the other side one gets ambiguities if one wants to measure the cross section of a single state above the threshold of the next higher level.
For example, neutrons of $E_{n,in}$ = 2700 keV impinging on the nucleus ^{56}Fe can excite the first, second and third level at 846.8, 2085.1 and 2657.6 keV, respectively. If one wants to measure the inelastic scattering cross section of the first excited level one would determine the intensity of the 846.8 keV γ-ray. But this transition contains also contributions from the second and the third excited level which decay to 100 and 97 %, respectively, to the first level before they reach the ground state. That means, one first has to know the cross sections for the higher levels, before one can determine the cross section of the lowest one.
A way to avoid this procedure could be to detect not only the γ-ray but also the scattered neutron. This is what was investigated at the neutron time of flight setup nELBE at the electron accelerator ELBE at Forschungszentrum Dresden-Rossendorf.

The experimental setup

At the nELBE source fast neutrons are produced by using the electron beam of the superconducting **E**lectron **L**inac for beams with high **B**rilliance and low **E**mittance ELBE [1]. The electrons are shot onto a liquid lead target, where they produce bremsstrahlung, which in turn produces the neutrons via photonuclear reactions on the lead again. The energy distribution can be seen in Figure 1. It is similar to the energy distribution of neutrons stemming from nuclear fission, which show a Maxwellian energy spectrum like is indicated in Figure 1.

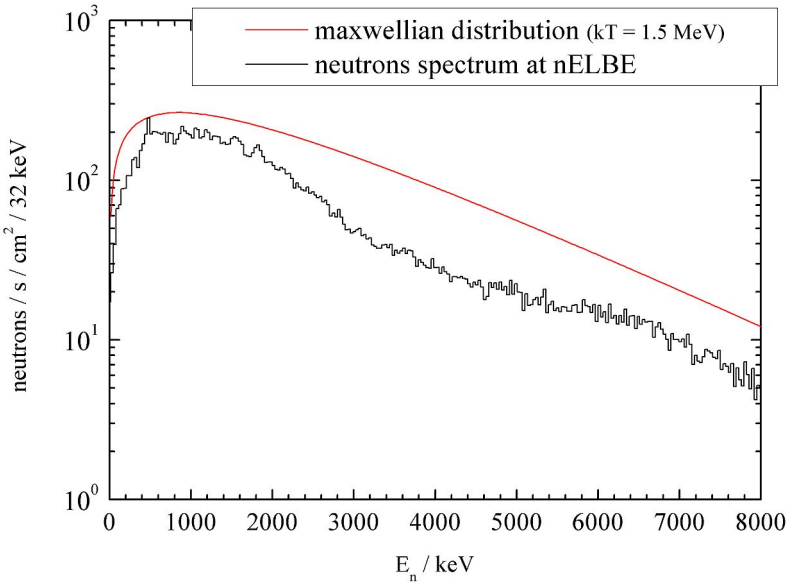

Figure 1. *Neutron energy distribution of the nELBE neutron source measured with a ^{235}U fission chamber after a flight path of 430 cm in comparison to the energy spectrum of fission neutron from ^{235}U. The shape of the nELBE spectrum is modified by 6 cm Pb absorber in front of a 2.4 m long collimator.*

The neutrons are emitted isotropical around the production target. A conical shaped collimator with an entrance diameter of 2 cm and an exit diameter of 3 cm is used to let a defined beam of neutrons pass through the 2.4 m thick wall to the adjacent room, where the detector setup is placed. Different absorbers in front the collimator can be used to reduce the bremsstrahlung intensity entering the collimator (or to perform transmission measurements).
The detector setup is sketched in Figure 2 and consists of a ^{235}U fission chamber [2,3] borrowed by the PTB Braunschweig to measure the primary neutron flux, an array of up to 42 BaF_2 detectors to detect the de-excitation γ-rays and several plastic scintillation detectors [4] to detect the scattered neutrons. Inside the BaF_2 array a sample to be investigated can be mounted.
For the data acquisition a dedicated VME based electronics setup was build up to measure the signals timing relative to the accelerator pulse structure. All detectors have time resolutions of about 600 ps to perform time of flight with good energy resolutions even at short flight paths of several meters.

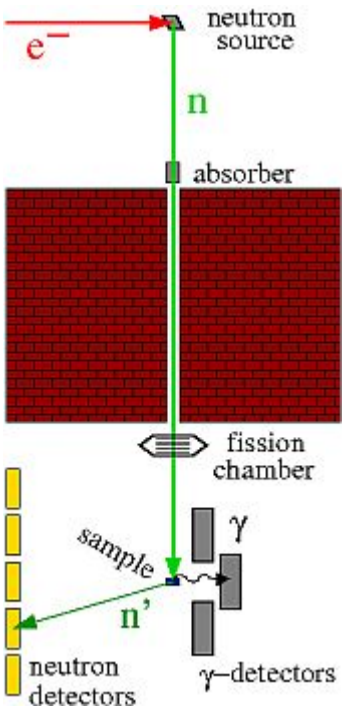

Figure 2. *Sketch of the nELBE neutron time of flight setup for the measurement of inelastic neutron scattering cross sections. The ELBE electron beam produces fast neutrons in a liquid lead target. A neutron collimator forms the neutron beam that enters the detector setup. The detector setup consists of a ^{235}U fission chamber to measure the incoming neutron flux, an array of BaF_2 scintillation detector to measure the de-excitation γ-rays and a set of plastic scintillation detectors to detect the scattered neutrons.*

The BaF_2 detectors will detect the γ-rays from the decay of the excited nucleus. By knowing the distance of the crystal from the sample, the point in time of the γ detection gives the time when the inelastic scattering reaction took place and by knowing the flight path from the neutron production target to the sample one can determine the energy $E_{n,in}$ of the incoming neutron. The plastic scintillators will detect the scattered neutron. The time difference between the detection of the neutron and the γ detection will give the energy $E_{n,out}$ of the scattered neutron. In Figure 3 the distributions of detected events in an experiment on the inelastic scattering on ^{56}Fe are shown in dependence of $E_{n,in}$ *and* $E_{n,out}$. The left panel shows the result from the measurement without a sample in place and the right panel shows the distribution obtained with a 20 g sample. One can clearly see the diagonal signatures of the inelastic scattering to the different excited levels, at least of the first three to four. Unfortunately these signatures are lying on top of a huge background of uncorrelated events. From the comparison of both graphs one can see, that a lot of these uncorrelated events moreover stem from the sample itself. This is more visual in Figure 4, which shows a vertical cut through the graphs of Figure 3 at $E_{n,in}$ = 1600 keV. Here one can see the signature of the inelastic scattering to the first excited level as a peak at about 700 keV in the sample-in-histogram in black. The shape of spectrum beside the peak can be approximated by $E^{-3/2}$ distribution.

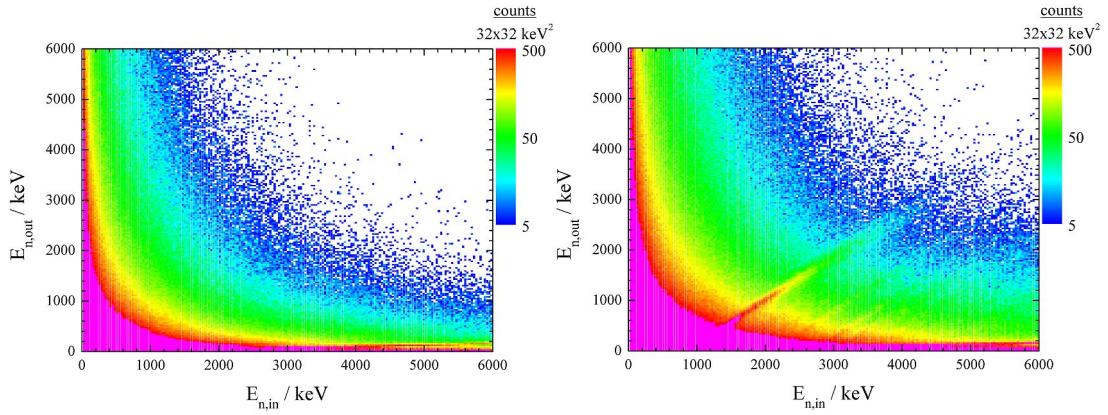

Figure 3. *$E_{n,out}$ vs. $E_{n,in}$ distribution of events detected while a measurement of inelastic neutron scattering on ^{56}Fe without (left) and with (right) sample in beam. The measurement without sample is normalized to the same time of measurement of the measurement with sample. In the right panel one can clearly see the diagonal structures stemming from the inelastic scattering to the first three excited levels.*

This distribution stems apperently from a constant background in the time-of-flight histograms $\frac{dN}{dt}$, which is converted to the energy histograms $\frac{dN}{dE}$ via the relation $\frac{dN}{dE} = \frac{dt}{dE} \cdot \frac{dN}{dt}$. In a classical approximation it is $E = \frac{mc^2}{2}\left(\frac{s}{t \cdot c}\right)^2$ and it follows $\frac{dt}{dE} = \sqrt{\frac{mc^2}{2}} \cdot \frac{s}{c} \cdot E^{-3/2}$.

The same is the case for the sample-out measurement. But there the height of the count rate is by a factor of about 2 lower, which indicates a quite high level of sample induced background. To determine the source of this background Monte-Carlo simulations are in progress [5].

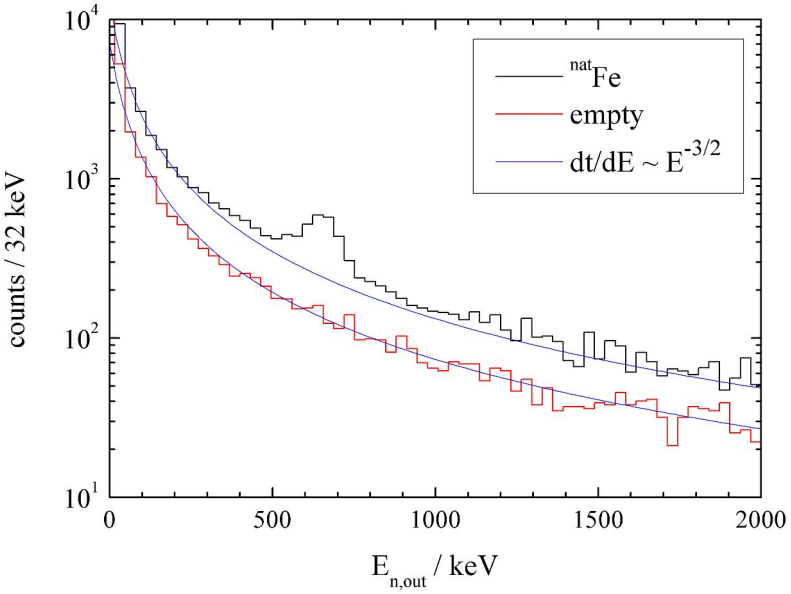

Figure 4. *Cut through the graphs of Figure 3 at $E_{n,in}$ = 1600 keV. The shape of the background indicated by the blue lines stemms apparently from radomly distributed events in the time-of-flight histograms which convert in first order of approximation to an $E^{-3/2}$ distribution in the energy histogram.*

The determination of the inelastic neutron scattering cross section

As a first order of analysis to determine the inelastic neutron scattering cross section, the sample-out measurement was normalized to the same count rate like in the sample-in measurement, at energies higher than the inelastic scattering signature. Then the normalized sample-out measurement was subtracted from the sample-in measurement. From the resulting distribution, the incoming neutron flux measured by the ^{235}U fission chamber and the efficiencies of the different detectors one can calculate the cross section wanted. The result of this procedure is shown in Figure 5.
The comparison to the values from ENDF/B-VII.0 [6] and from the measurement of Perey et al. [6] shows good agreement for the absolute scale as well as the structural features. It can also be seen, that, in contrast to the method used by Perey, where only the γ-ray was measured, the double-time-of-flight method used in this work can easily access the energy region above the second excited state of ^{56}Fe at 2085.1 keV without knowing anything about this state.

Summary and Outlook

The inelastic neutron scattering cross section to the first excited state of ^{56}Fe was determined by means of a double-time-of-flight method. The results show good agreement to evaluated and previously measured data and extent the dataset to the energy region above the threshold of the second excited level.
Beside the promissing results of the first analysis, a lot of work has still to be done to determine and reduce the sources of background and to deliver final results. Additionally the angular dependence of the cross section could be investigated.

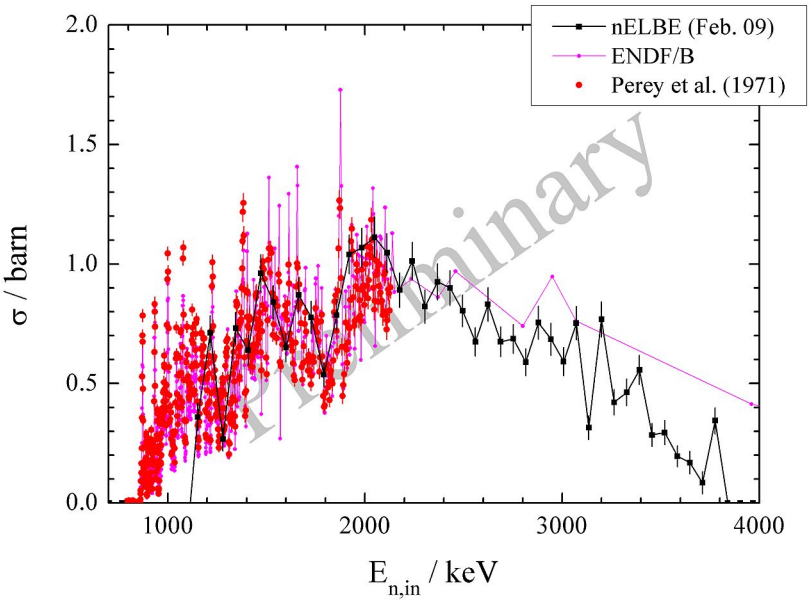

Figure 5. *The inelastic neutron scattering cross section to the first excited level of ^{56}Fe. In black the preliminary result of this work is shown. The error bars contain the statistical uncertainties only. In pink and red the values of the ENDF/B-VII.0 data base and the measurement of Perey et al. (both taken from [6]) are plotted for comparison. Good agreement in shape and absolute scale can be seen.*

Acknowledgements
This work was supported by the EURATOM 6. FRAMEWORK PROGRAMME "European Facilities for Nuclear Data Measurements" (EFNUDAT) contract number FP6-036434.

References
[1] J. Klug et al., NIMA 577 (2007) 641.
[2] D.B. Gayther, Metrologia 27 (1990) 221.
[3] R. Nolte et al., Nucl.Sci.Engin. 159 (2007) 197.
[4] R. Beyer et al., NIMA 575 (2007) 449.
[5] E. Birgersson, this proceedings.
[6] Janis, Version 3.0-Build 5.4.636 (June 2007), www.nea.fr.

Investigation of the experimental conditions at nELBE

E. Birgersson[1)], E. Altstadt[2)], C. Beckert[2)], R. Beyer[1)], H. Freiesleben[3)], V. Galindo[2)], E. Grosse[1,3)], R. Hannaske[1)], A. R. Junghans[1)], J. Klug[1)], A. Matic[1)], M. Mosconi[4)], R. Nolte[4)], B. Naumann[3)], K.-D. Schilling[1)], R. Schlenk[2)], S. Schneider[2)], R. Schwengner[1)], A. Wagner[1], F.-P. Weiss[2)]

1) Institut für Strahlenphysik, Forschungszentrum Dresden-Rossendorf, 01314 Dresden, Germany
2) Institut für Sicherheitsforschung, Forschungszentrum Dresden-Rossendorf, 01314 Dresden, Germany
3) Technische Universität Dresden, 01062 Dresden, Germany
4) Physikalisch-Technische Bundesanstalt, Bundesallee 100, 38116 Braunschweig, Germany

e.birgersson@fzd.de

Abstract: The neutron time-of-flight facility nELBE at the radiation source ELBE (Electron Linear accelerator with high Brilliance and low Emittance) of the Forschungszentrum Dresden-Rossendorf produces neutrons by bremsstrahlung photons through (γ, n)-reactions when electron pulses are impinging on a liquid lead target.
The liquid lead is circulated by an electromagnetic pump and cooled by a heat exchanger far from the neutron source, thus reducing the amount of material close to the neutron source leading to less scattering of neutrons. The nELBE has been in operation for 1.5 years. The neutrons from the lead are going through a 2.4 m thick concrete wall to the measuring room via a collimator. The measurements of energy resolved neutron cross sections by a time-of-flight arrangement are performed with a flight path of only 6 meters. This is possible since the electron beam has a pulse width less than 10 ps and the volume of the irradiated lead is only 1 cm^3 resulting in a sharp temporal distribution without moderation of the neutrons. MCNP simulation of the beam profile compare well to the experimental beam profile scans, however more scattered neutrons and gamma rays in the beam halo are observed then simulated. The amount of neutrons which are scattered inside of the collimator was studied using an extra scattering shielding wall.

Introduction

In order to reduce the radiotoxicity of the nuclear waste, future nuclear reactors are investigated. Accelerator driven systems and generation IV nuclear reactors will reduce the radiotoxicity to a level below natural uranium in less than thousand years compared to the current waste which takes some million years to reach this level. The future reactors have to be economical and safe in operation as well as producing less nuclear waste.
Six nuclear energy systems have been selected for further study by the Generation IV International Forum (GIF) [1], where most reactor types are fast reactors. Research has to be done in many areas, such as materials, reactor design, and of course improvement of nuclear data. The average neutron energy in a fast reactor is very sensitive to the inelastic scattering and neutron capture on structure material and coolant. The fission and neutron capture cross of the minor actinide are important for the transmutation of the waste. This requires higher demands on the accuracy of the involved cross sections, which have been listed for each of the 6 reactor types by the working party on evaluation cooperation WPEC of the OECD Nuclear agency [2].
At the ELBE accelerator a neutron time-of-flight facility called nELBE exists. The neutrons are coming from (γ,n)-reactions induced by the bremsstrahlung, which is created when the electrons hit a liquid lead target. The neutron energy spectrum is similar to a neutron energy spectrum of a fast reactor. In this energy region (0.1 to 10 MeV), nuclear data for transmutation is needed.

Neutrons at nELBE

The ELBE radiation source can accelerate electrons up to about 40 MeV, The beam intensity can be as high as 1 mA when the frequency of the source is 26 MHz. For neutron production the frequency is reduced to between 100 to 500 kHz with a corresponding reduction of the average current. After the summer 2009 a new superconducting radio frequency photo electron injector (SRF gun) will be installed, which will allow an unreduced beam current of 1 mA at 500 kHz repetition rate.

The neutrons are created by (γ,n)-reactions in lead. The electrons create bremsstrahlung as they slow down in the lead. Because of the very high energy deposition, a solid lead target would melt. A liquid lead target was designed and simulations in order to optimize the design of the thermal stress and necessary lead flow has been performed [4]. The liquid lead is circulating in a molybdenum channel inside a stainless steel housing. In order for the electrons to reach the lead, they have to leave the electron beam line via a beryllium window, then they travel in a nitrogen atmosphere before entering the evacuated stainless steel housing through another beryllium window. Investigation of the effect of the beam size was simulated [4] concerning heat and stress in the molybdenum channel. Approximately half of the energy of electrons will not be deposited in the lead but in a water cooled aluminium beam dump.

The neutron source strength is 1.9 $\times 10^{13}$ neutrons/s for 30 MeV electrons when the electron current is 1 mA [3]. The neutrons are isotropically emitted and a conical segmented collimator was designed [3] for the effective reduction of neutrons and gamma rays in the adjacent room outside of the neutron beam. In Figure 1, simulations of the neutron and gamma spectrum at the entrance of the collimator are shown. The neutron spectrum has a maximum intensity around 1-2 MeV, similar to the neutron energy spectrum in a fast reactor and is ideal for measuring cross sections important for such reactors. The two spectra in Figure 1 were used in the MCNP simulation later described in this work. From PTB, a parallel plate ionization chamber was on loan [5]. It has 10 well defined ^{235}U layers with a total mass of 201.6 mg. The diameter of the uranium discs are 7.2 cm. It is used for measurement of the absolute neutron flux. A comparison of the simulated and measured neutron spectra is shown in Figure 1. The simulated flux has been scaled a factor of 1/2.3. The higher simulated neutron flux depends on three things. Firstly, the measurement of the electron current has a large uncertainty. Secondly, the electron beam has to hit the lead at the right position in order for the neutron to go through the collimator. Thirdly, loss of the electron beam might happen before it hits the lead. This loss of the beam intensity was larger during the initial experiments at nELBE, but with better beam tuning this loss has decreased. In order to suppress the gamma to neutron yield ratio which is approximately 1300 in the direction of the collimator, different lead absorbers are used at the entrance of the collimator. For a 10 cm lead absorber the neutron intensity has decreased almost 1 order or magnitude. However, the gamma to neutron yield ratio is then only 20.

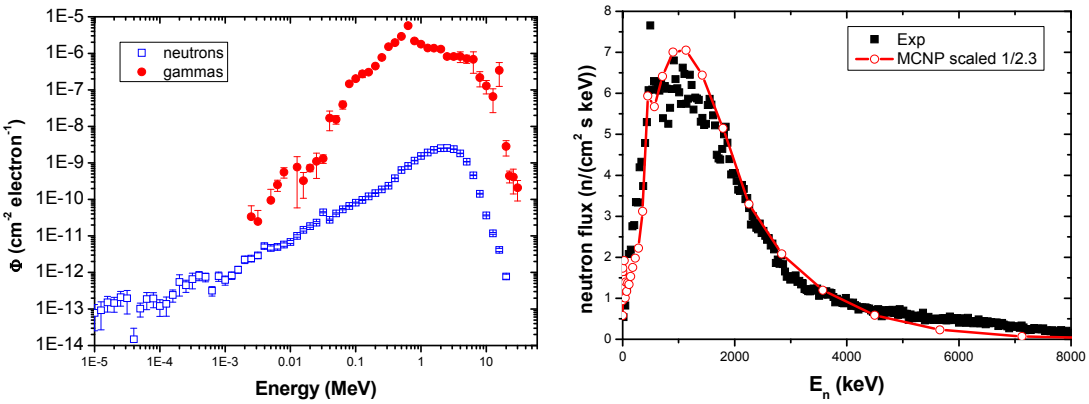

Figure 1. *Neutron and gamma spectra at the entrance of the collimator. The flux is plotted per incident electron and the width of energy bins are equally distributed on logarithmic scale (left). After scaling the simulated spectrum a factor 1/2.3, the shapes of the measured and simulated neutron energy spectrum 430 cm from the neutron source are nicely corresponding (right).*

Simulation and experiments

The simulation of the neutron and photon intensities in different part of the nElbe facility as well as their ToF was performed with the MCNP code [7]. The nElbe facility has already been simulated concerning neutron and gamma ray production, design of the collimator and beam dumps [3]. However the first experiments showed more background neutrons than expected and more effort has been put into understanding the neutron source. The MCNP simulations described here are using a few variance reductions techniques existing in the program. The neutrons are isotropically emitted but more neutrons with a reduced weight are started in the direction of the collimator. This avoids tracking particles in the neutron hall which anyway have negligible probability to enter the measurement room. In addition to this angle biasing a so called weight window was used to enhance the transport of particles through the wall and the collimator. In many of the simulations, so called point detectors were used. A point detector in MCNP can be used to estimate the particle flux at a location using only a fraction of the computer time compared to using the standard techniques. The reason is that after each interaction in the simulation, the probability that the particle then goes in the direction of the point detector as well as that it would actually reach the point detector is calculated and is added to estimate the total flux in this point. The experiments at nElbe so far has included a few total cross section measurements, which also gave a confirmation of the energy resolution when compared to well known results [8]. The main beam time has been dedicated to measure the inelastic cross section on ^{56}Fe. During this experiment the time of flight (ToF) of the incident neutron is used to determine its energy by detecting the gamma rays from the excited iron relative to the time zero signal from the ELBE accelerator. An array of BaF_2 detectors are used for the gamma ray detection. The energy of the inelastically scattered neutron is determined by its second time of flight from the iron to one of four plastic scintillators which are positioned approximately one meter on the side of the neutron beam. The 20 g iron sample is put in the beam approximately 6 m from the liquid lead target. Detailed explanation and results from this experiment is described elsewhere in these proceedings [9].
Simulations and dedicated experiments were performed to characterize the beam profile. In order to fully understand the background of scattered neutrons, a series of simulations with mono energetic neutrons were performed The effect of introducing an extra scattering shield wall could clearly be seen both in simulations and experiments.

Beam profile

If the electrons hit the liquid lead target too low or high, the collimator will not be in the direction of the neutron source, which will affect the beam profile as well as the total number of neutrons which pass the collimator. In order to investigate a possible misalignment of the electron beam one plastic scintillator was put on a movable stand. In Figure 2 the result of such beam scan in vertical direction is shown together with a MCNP simulation. The simulation is performed by starting neutrons and gamma rays and their respective flux is determined in boxes with equal size as the real detector. In Figure 2 it can be seen that the simulation of the main beam profile is well reproduced by the experimental beam scan. However, the beam halo is different. There are considerably less scattered particles in the results from the simulation compared to the experiment. The are several possible explanation for this. The accuracy of a MCNP simulation depends on how well the geometry and the cross sections involved in the problem are described. Another explanation for the discrepancy could be that the geometry of the neutron source is not a cylinder. If additional neutrons and gamma rays are created in the neutron hall at another position then the liquid lead, they can not pass the collimator without scattering. As a consequence this contribution would then mainly be seen in the beam halo.

Simulation of scattered neutrons using mono-energetic neutrons

Since the neutron source at nELBE is a white source, the result from a simulation with mono energetic neutrons can not be compared directly with experimental results. However such simulations can give great insight on how the neutron background is generated. When the inelastic scattering cross section of ^{56}Fe is measured at nELBE [9], measurements with and without the iron sample in the beam are performed. The scattered neutrons are detected by 100 cm long plastic scintillators, placed in a vertical alignment 1 m from the beam at 90 degrees relative to the beam line. In the MCNP simulation instead of a similar large detector a point detector was put at the detector position.

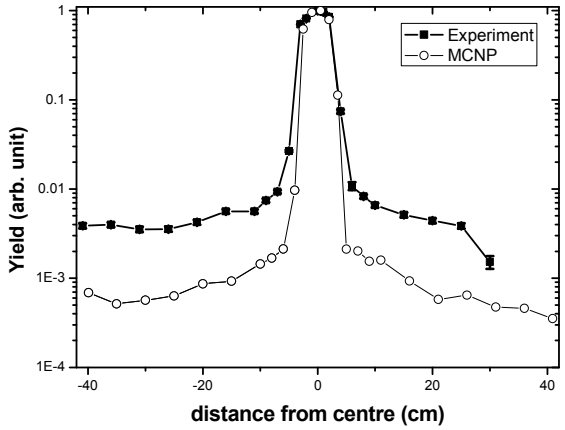

Figure 2. *Neutron and gamma beam profile of a vertical beam scan. The experiment is performed with a movable plastic scintillator, and a similar geometry was used in the simulation. The main beam is in good agreement, but the beam halo shows larger yield for the experiment. Both curves have been given the value 1 at their maximum intensity.*

A series of such simulations were performed where the first simulation was without any materials in the measurement room. One by one the materials were added in the other simulations. The result of the 2 MeV MCNP simulations with and without an iron sample is shown in Figure 3. The collimator and the wall between the room with the neutron source and the measurement room are of course always present. Since 2 MeV neutrons were simulated the effect of scattering in the collimator is clearly seen in the simulated ToF spectra. This peak is present regardless of if iron is present in the main beam. When the iron is put in the beam peaks from elastically and inelastically scattered neutrons appear in the ToF spectrum. The difference in the simulated ToF spectrum when introducing more materials can mainly be seen on the peaks from neutron scattered on the iron. Now the peaks are followed by an additional background. A background which is not present in the simulation without iron. The explanation to this background is that the neutrons which are scatted on iron then undergo a second scattering and after this one they continue in the direction of the detector. By the many simulations introducing materials one by one the effect of the walls, floor and ceiling in the room contribute add to this effect, but the major contributor is scattering on the BaF_2 gamma detector array. This tail in the ToF spectrum is also seen in the experimental data [9].

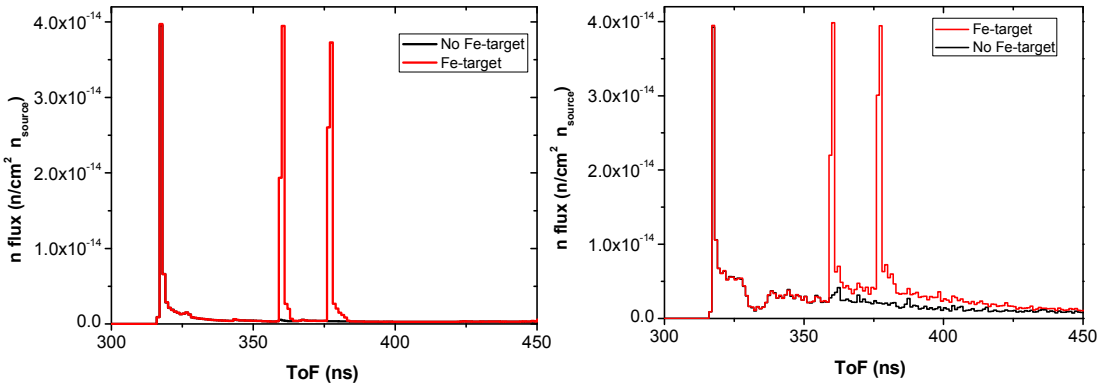

Figure 3. *Simulated neutron ToF spectra from 2 MeV source neutrons, with and without iron in the beam. The flux is given per cm2 and source neutron, the time bin width are 1 ns. The iron is put 6 m from the neutron source and the spectra is determined 1 m from the 20 g iron at 90 degrees relative to the neutron beam. When no material except the collimator is put in the simulation, three distinct peaks are seen: scattering in the collimator as well as inelastic and elastic scattering on iron (left) . When more the materials are added in the simulation, such as air, walls, floor, ceiling, and BaF_2 gamma detector array the probability that scattered neutron undergoes another scattering has increased (right).*

Effect of an additional scattering protective wall

The undesired scattering of neutron (and gamma rays) in the collimator increases the background at the position where the neutron from scattering on iron is measured. In order to prevent this an additional scattering protective wall (S-wall) was introduced. It was put between the exit of the collimator and the position where the scattered neutrons are measured. It consists of threes layers, 8 cm borated polyethylene, 15 cm lead, and then another layer of 25 cm borated polyethylene. In Figure 4 simulations with and without the S-wall are shown. The S-wall effectively reduces the scattering of the neutron and gamma rays. The neutron simulations were performed by starting 2 MeV mono energetic neutrons and the gamma ray simulation was performed by starting gamma rays according to an energy spectrum, which has previously been determined for the nELBE facility [3]. These gamma rays also create additional neutrons by (γ,n)-reaction in the collimator. However, this contribution is 100 times lower than the contribution from the scattered neutrons. When looking at the experimental ToF spectra in Figure 5 the difference between with and without iron is larger when the wall is present. The same effect is qualitatively seen for the gamma rays. Unfortunately there is another gamma peak in the experimental ToF spectra before the gamma flash. These gamma rays are created before the electron beam hits the liquid lead target, and they have to go through a thick concrete door in order to enter the measuring room. This contribution depends on the electron beam tuning, and varies from experiment to

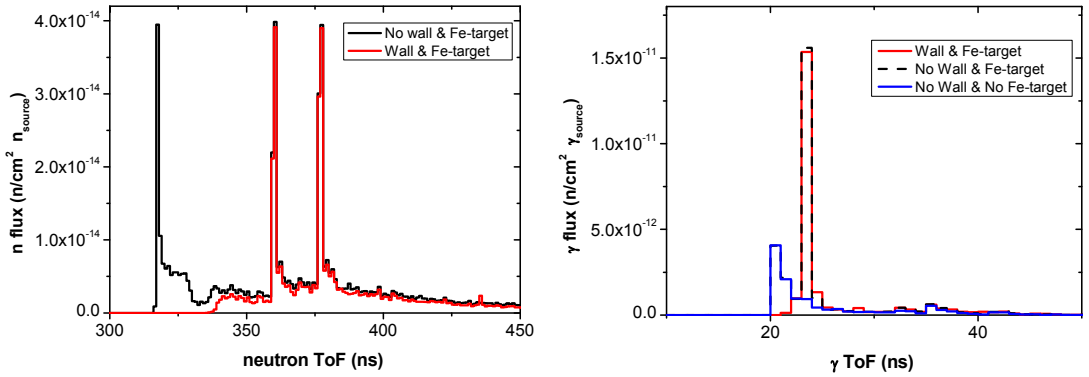

Figure 4. *Simulated neutron ToF spectra from 2 MeV source neutrons ,with and without the scattering protective wall with iron in the beam (left) .The wall also shields from the scattered gamma rays in the collimator (right).*

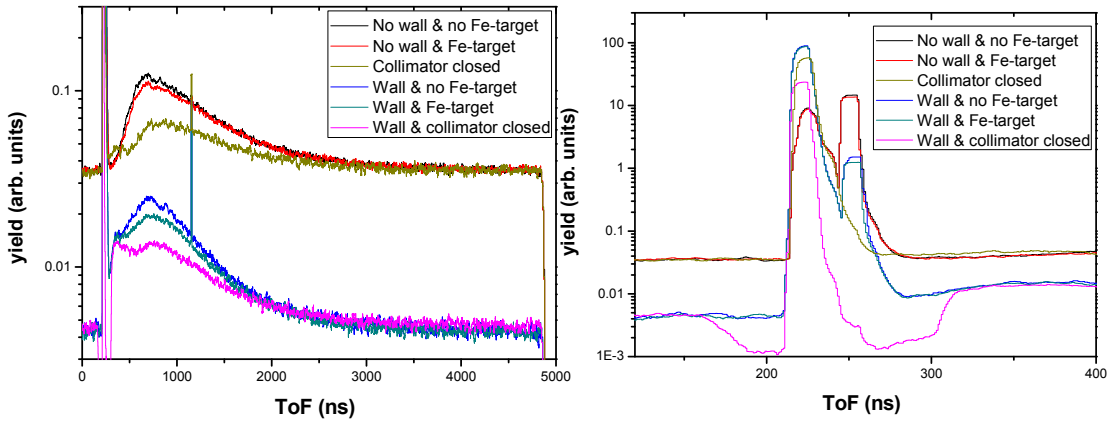

Figure 5. *Measured ToF spectra with and without the scattering protective wall and with and without iron in the beam. Measurements with the collimator closed are also shown in which only the gamma rays from the adjacent room are detected. The yield is normalised to the background level before the gamma flashes and arbitrary scaled for better visibility. The difference between with and without iron is larger when the S-wall is in place for the neutrons (left). A similar difference is seen for the gamma flash (right). During the measurement with closed collimator and the S-wall present a gamma veto was used, this is the reason for the reduced intensity in this region. After-pulsing triggers the data acquisition, which reduces the efficiency of the gamma veto, but makes the peak visible. The sharp peak at 1200 ns is due to cross talk in the cables.*

experiment. In Figure 4 a small additional contribution of neutrons are created due to the S-wall. A more clever design of the S-wall is needed if the gamma rays through the door can not be avoided.

Summary

The nELBE neutron beam facility has been in operation for 1.5 years. The need for more MCNP simulations in order to understand the experimental conditions has been performed. These simulations showed that the contribution of scattered neutrons from the collimator is of the same order as the scattering from a 20 g iron target in the beam at the position where the scattered neutrons are measured. The effect of a scattering protective wall was both simulated and studied with experiment. The wall did shield from the scattered neutrons but also seems to increase the background due to the unexpected scattered gamma rays created before the electron beam hit the liquid lead, which also reach the measurement room.

Acknowledgements
This work was supported by the EURATOM 6. Framework Programme “European Facilities for Nuclear Data Measurements” (EFNUDAT), contract number FP6-036434.

References

[1] A technology roadmap for generation IV nuclear energy systems, GIF-002-00, US Department of Energy (2002).
[2] M. Salvatores (Co-ordinator), Uncertainty and target accuracy assessment for innovative systems using recent covariance data evaluations, Nuclear Science ISBN 978-92-64-99053-1 NEA/WPEC-26 (2008).
[3] J. Klug, E. Altstadt, C. Beckert, R. Beyer, H. Freiesleben, V. Galindo, E. Grosse, A.R. Junghans, D. Légrády, B. Naumann, K. Noack, G. Rusev, K.D. Schilling, R. Schlenk, S. Schneider, A. Wagner, F.-P. Weissb, Development of a neutron time-of-flight source at the ELBE accelerator, NIM A 577 (2007) 641–653.
[4] E. Altstadt, C. Beckert, H. Freiesleben, V. Galindo, E. Grosse, A.R. Junghans, J. Klug, B. Naumann, S. Schneider, R. Schlenk, A. Wagner, F.-P. Weiss, A photo-neutron source for time-of-flight measurements at the radiation source ELBE, Ann. Nucl. Energy 34 (2007) 36–50.
[5] R. Nolte, M. S. Allie, D. Brooks, A. Buffler, V. Dangendorf, J. P. Meulders, H. Schuhmacher, F. D. Smit, and M. Weierganz, Cross Sections for Neutron-Induced Fission of 235U, 238U, 209Bi, and natPb in the Energy Range from 33 to 200 MeV Measured Relative to n-p scattering, Nucl. Sci. Eng. 156 (2007), 197-210.
[6] R. Beyer, E. Grosse, K. Heidel, J. Hutsch, A.R. Junghans, J. Klug, D. Légrády, R. Nolte, S. Röttger, M. Sobiella, A. Wagner, Proton-recoil detectors for time-of-flight measurements of neutrons with kinetic energies from some tens of keV to a few MeV, NIM A 575 (2007) 449–455.
[7] X-5 Monte Carlo team, MCNP-A General Monte Carlo N-Particle Transport Code, version 5, Volume I-III, LA-UR-03-1987,LA-CP-03-0245 and LA-CP-03-0284, April, (2003).
[8] A. R. Junghans, E. Altstadt, C. Beckert, R. Beyer, V. Galindo, E. Grosse, R. Hannaske, A. Matic, M. Mosconi, B. Naumann, R. Nolte, S. Röttger, k. D. Schilling, R. Schlenk, S. Schneider, R. Schwengner, A. Wagner, F.-P. Weiss, The nElbe neutron time-of-flight facility, IEEE Nuclear Science Symposium Conference Record (2008).
[9] R. Beyer et al., Contribution to this Workshop (2009).

Fission studies with fast neutrons: overview of the latest experimental results

N. Colonna[1)], M. Calviani[15)], U. Abbondanno[26)], G. Aerts[17)], H. Álvarez[3)], F. Álvarez-Velarde[4)], S. Andriamonje[17)], J. Andrzejewski[5)], P. Assimakopoulos[6)], L. Audouin[7)], G. Badurek[8)], P. Baumann[9)], F. Becvar[10)], F. Belloni[26)], E. Berthoumieux[17)], F. Calviño[11)], D. Cano-Ott[4)], R. Capote[12,13)], A. Carrillo de Albornoz[14)], P. Cennini[15)], V. Chepel[16)], E. Chiaveri[15)], G. Cortes[18)], A. Couture[19)], J. Cox[19)], M. Dahlfors[15)], S. David[7)], I. Dillman[20)], R. Dolfini[21)], C. Domingo-Pardo[22)], W. Dridi[17)], I. Duran[3)], C. Eleftheriadis[23)], L. Ferrant[7)], A. Ferrari[15)], R. Ferreira-Marques[16)], H. Frais-Koelbl[12)], K. Fujii[26)], W. Furman[24)], I. Goncalves[16)], E. González Romero[4)], A. Goverdovski[25)], F. Gramegna[2)], E. Griesmayer[12)], C. Guerrero[4)], F. Gunsing[17)], B. Haas[27)], R. Haight[28)], M. Heil[20)], A. Herrera Martínez[15)], M. Igashira[29)], S. Isaev[7)], E. Jericha[8)], F. Käppeler[20)], Y. Kadi[15)], D. Karadimos[6)], D. Karamanis[6)], M. Kerveno[9)], V. Ketlerov[25)], P. Koehler[30)], V. Konovalov[24)], E. Kossionides[31)], M. Krticka[10)], C. Lampoudis[23),17)], H. Leeb[8)], A. Lindote[16)], I. Lopes[16)], M. Lozano[13)], S. Lukic[9)], J. Marganiec[5)], L. Marques[14)], S. Marrone[1)], T. Martínez[4)], C. Massimi[32)], P. Mastinu[2)], A. Mengoni[12),15)], P.M. Milazzo[26)], C. Moreau[2)], M. Mosconi[20)], F. Neves[16)], H. Oberhummer[8)], S. O'Brien[19)], M. Oshima[33)], J. Pancin[17)], C. Papachristodoulou[6)], C. Papadopoulos[34)], C. Paradela[3)], N. Patronis[6)], A. Pavlik[35)], P. Pavlopoulos[36)], L. Perrot[17)], M.T. Pigni[8)], R. Plag[20)], A. Plompen[37)], A. Plukis[17)], A. Poch[18)], C. Pretel[18)], J. Praena[1)], J. Quesada[13)], T. Rauscher[38)], R. Reifarth[28)], M. Rosetti[39)], C. Rubbia[21)], G. Rudolf[9)], P. Rullhusen[37)], J. Salgado[14)], L. Sarchiapone[15)], I. Savvidis[23)], C. Stephan[7)], G. Tagliente[1)], J.L. Tain[22)], L. Tassan Got[7)], L. Tavora[14)], R. Terlizzi[1)], G. Vannini[32)], V. Variale[1)], P. Vaz[14)], A. Ventura[39)], D. Villamarin[4)], M.C. Vicente[4)], V. Vlachoudis[15)], R. Vlastou[34)], F. Voss[20)], S. Walter[20)], H. Wendler[15)], M. Wiescher[19)], K. Wisshak[20)]

The n_TOF Collaboration

1) Istituto Nazionale di Fisica Nucleare (INFN), V. Orabona 4, 70126 Bari, Italy
2) Istituto Nazionale di Fisica Nucleare (INFN), Laboratori Nazionali di Legnaro, Italy
3) Universidade de Santiago de Compostela, Spain
4) Centro de Investigaciones Energéticas Medioambientales y Technológicas CIEMAT, Madrid, Spain
5) University of Lodz, Lodz, Poland
6) University of Ioannina, Greece
7) Centre National de la Recherche Scientifique/IN2P3 - IPN, Orsay, France
8) Atominstitut der Österreichischen Universitäten,Techn. Universität Wien, Austria
9) Centre National de la Recherche Scientifique/IN2P3 - IReS, Strasbourg, France
10) Charles University, Prague, Czech Republic
11) Universidad Politécnica de Madrid, Spain
12) International Atomic Energy Agency (IAEA), Nuclear Data Sect., Vienna, Austria
13) Universidad de Sevilla, Spain
14) Instituto Tecnologico e Nuclear(ITN), Lisbon, Portugal
15) CERN, Geneva, Switzerland
16) LIP - Coimbra & Departamento de Fisica da Universidade de Coimbra, Portugal
17) CEA/Saclay - DSM/DAPNIA, Gif-sur-Yvette, France
18) Universitat Politècnica de Catalunya, Barcelona, Spain

19) University of Notre Dame, Notre Dame, USA
20) Forschungszentrum Karlsruhe GmbH (FZK), Institut für Kernphysik, Germany
21) Università degli Studi Pavia, Pavia, Italy
22) Instituto de Física Corpuscular, CSIC-Universidad de Valencia, Spain
23) Aristotle University of Thessaloniki, Greece
24) Joint Institute for Nuclear Research, Frank Lab. Neutron Physics, Dubna, Russia
25) Institute of Physics and Power Engineering, Kaluga region, Obninsk, Russia
26) Istituto Nazionale di Fisica Nucleare (INFN), Trieste, Italy
27) Centre National de la Recherche Scientifique/IN2P3 - CENBG, Bordeaux, France
28) Los Alamos National Laboratory, New Mexico, USA
29) Tokyo Institute of Technology, Tokyo, Japan
30) Oak Ridge National Laboratory, Physics Division, Oak Ridge, USA
31) NCSR, Athens, Greece
32) Dipartimento di Fisica, Università di Bologna, and Sezione INFN di Bologna, Italy
33) Japan Atomic Energy Research Institute, Tokai-mura, Japan
34) National Technical University of Athens, Greece
35) Institut für Isotopenforschung und Kernphysik, Universität Wien, Austria
36) Póle Universitaire Léonard de Vinci, Paris La Défense, France
37) CEC-JRC-IRMM, Geel, Belgium
38) Department of Physics and Astronomy - University of Basel, Basel, Switzerland
39) ENEA, Bologna, Italy
nicola.colonna@ba.infn.it

Abstract: The development of advanced nuclear systems for energy production and nuclear waste transmutation has triggered in the past few years a vast experimental activity around the world aiming at collecting new and accurate data on neutron-induced fission cross-sections. Fission studies with fast neutrons are being carried out at various neutron facilities for several long-lived Pu isotopes and Minor Actinides, while isotopes with short half-lives are subject of investigation with the surrogate technique, employing charge particle beams.
As part of the world-wide effort on fission studies with fast neutrons, measurements have been performed at the n_TOF facility at CERN, Geneva. Results have been obtained on several isotopes involved in the Th/U fuel cycle, as well as on Minor Actinides involved in Generation IV reactors. The measurements have been performed with a Fast Ionization Chamber (FIC) and with Parallel Plate Avalanche Counter, relative to the standard cross-section of the ^{235}U(n,f) reaction. The main results obtained at n_TOF are reported.

Introduction

It is now commonly believed that an increasingly important role in the mix of energy sources of the future could be played by nuclear energy, which has the advantage of a low emission of greenhouse gases and could help reducing the dependence on fossil fuels. The use of current generation nuclear reactors is however limited by two major issues: the inefficient use of the Uranium resources, and the problem of nuclear waste disposal. In particular, it is estimated that availability of fuel may start to become a problem within the end of the century, if once-through reactors continue to be used. On the contrary, fast breeder reactors, characterized by a burn-up efficiency much higher than current thermal reactors, would guarantee availability of U resources for a much longer period. The second, even more important problem is nuclear waste treatment and storage. A significant fraction of the spent fuel is constituted by long-lived fission fragments and transuranic elements built up as a result of multiple neutron captures and radioactive decays. While fission products loose most of their radiotoxicity in a few hundred years, Pu and minor actinides, i.e. Np, Am and Cm, maintain a high radiotoxicity level for thousands of years. At present, the only viable solution for the management of this high-level nuclear waste is the disposal in geological repositories. A much better solution to the problem of nuclear waste disposal could come from transmutation, via neutron induced fission of TRU's, in subcritical systems, such as an Accelerator Driven System (ADS), or in critical systems, such as future Gen-IV fast nuclear reactors [1]. Another possibility currently being considered is the development of lighter fuel

cycles, such as the Thorium/Uranium Fuel Cycle, characterized by a much lower production of minor actinides.
In order to reduce calculation uncertainties in the design and operation of advanced nuclear systems, high precision data on neutron-induced reaction cross-sections are required for a variety of transuranic elements. Various sensitivity studies indicate that the development of innovative systems for energy production and/or nuclear waste transmutation requires data on several reactions, with precisions of a few percent (see for example ref. [2]). A pressing need exists in particular for new data on fission induced by fast neutrons on various U and Pu isotopes, as well as on the long-lived Np, Am and Cm isotopes, mostly in the energy region corresponding to the neutron spectrum of fast reactors, i.e. between a few keV and several MeV.
With the aim of fulfilling the request of new and accurate nuclear data for advanced nuclear reactors, a large experimental and theoretical work is being performed worldwide. Within the ongoing efforts, an important contribution is being provided by the n_TOF project. Measurements of neutron-induced fission cross-sections have been performed on several isotopes involved in the Th/U fuel cycle, and in the design of ADS and Gen IV fast reactors. In this talk, the recent results on fission cross-sections measured at n_TOF are shown.

The neutron beam and experimental apparatus

The CERN n_TOF facility is a spallation neutron source for time-of-flight measurements. Neutrons are produced by 20 GeV/c protons from the CERN Proton Synchrotron accelerator, impinging onto a lead block, surrounded by a water layer acting as coolant and moderator of the neutron spectrum. The main features of the facility are the wide energy range, spanning over nine orders of magnitude, from thermal energy to 1 GeV, the very high instantaneous neutron flux, which results in a good signal-to-background ratio even for isotopes with high specific activity, and the low repetition rate (0.4 Hz), which eliminates the need of corrections for wrap-around bunches. Finally, at the measuring station located at 187.5 m from the spallation target, the neutron beam presents a very high resolution in energy (1.1×10^{-3} at 30 keV), while a series of beam shaping collimators and thick shielding walls made of iron and concrete result in a very low ambient background [3]. These basic characteristics make n_TOF a suitable source for high-accuracy measurements of fission cross-sections.

The fission setup

Fission measurements at n_TOF have been performed with two different detector setups: a Fission Ionization Chamber, for single-fragment detection, and Parallel Plate Avalanche Counters, used to detect both fission fragments in coincidence. The Fission Ionization Chamber (FIC) is based on parallel-plate chambers with 5 mm spacing between electrodes, operated with argon/tetrafluormethane (90% Ar+10% CF_4) at 720 mbar, with no gas circulation [4]. The whole detector is made of a stack of 17 ionization chambers, accommodating a total of 16 samples that can be measured simultaneously. The diameter of the samples is 8 cm, their thickness range from 4 to 450 $\mu g/cm^2$, and the mass uncertainty is between 1 and 2% for most samples. Different chambers have been used in the n_TOF measurements: one of them, dedicated to measurements of highly radioactive species, was qualified as a "sealed source" compliant with the ISO 2919 norm. The samples measured with the Fission Ionization Chamber were: ^{233}U, ^{234}U, ^{236}U, ^{237}Np, ^{241}Am, ^{243}Am, ^{245}Cm, as well as ^{235}U and ^{238}U used as reference or for monitoring of the neutron beam.
Another method used at n_TOF for fission cross-section measurements is based on the coincident detection of both fission fragments. Relative to the single-fragment method, the coincidence technique is more efficient for discriminating fission events from the α-particle background associated with the natural radioactivity of the sample, as well as from competing reactions, occurring at energies above a few MeV. The main drawback of the coincidence system is related to a smaller angular coverage, since one of the fragments has to cross the backing before being detected. This has the consequence of a smaller efficiency and a larger correction for possible angular anisotropies.
The setup used for measurements with the coincidence method is based on Parallel Plate Avalanche Counters (PPAC). These detectors have the advantage of being transparent to neutrons and γ-rays, since they can be designed with thin windows and electrodes and are operated at low gas pressure (7 mbar). Furthermore, they are characterized by good timing properties. In addition, the low-pressure of the gas and the small material of the detectors results is a very small prompt flash, thus allowing one to extend the fission cross-section data

up to around 1 GeV. The setup used at n_TOF is made of a stack of 10 PPAC and 9 samples inserted between two detectors. The following radioactive isotopes were measured with the PPAC system: ^{232}Th, ^{233}U, ^{234}U, and ^{237}Np (as well as ^{235}U and ^{238}U, used as reference). In all cases, the thickness of the deposits was 200-300 μg/cm^2. The fission cross-sections of ^{nat}Pb and ^{209}Bi were also measured with this apparatus.
For both detection systems, the detector signals were acquired with a set of 8 bit Acqiris Flash Analog to Digital Converters (FADC) modules. For the FIC detector data were recorded for flight times up to 80 ms, corresponding to neutrons in the thermal energy region. A detailed off-line analysis of the digitized signal allows one to extract relevant information on the neutron time-of-flight and energy deposited by the fission fragments in the detectors.

New data for the Th/U fuel cycle

The results of the ^{233}U(n,f) reaction measured with the FIC detector are here discussed [5]. As for all other isotopes, the cross-section is determined relative to the ^{235}U(n,f) data, standard at thermal energy and from 0.15 eV to 200 MeV. Therefore, as a first step of the analysis, the fission yield for the ^{235}U reference sample was extracted. A relatively low threshold is employed on the amplitude distribution of the signals, to reject electronic noise and α-particle background while keeping the detection efficiency close to 100 %. A resonance analysis, performed with SAMMY (including the n_TOF resolution function), is used to calibrate the neutron energy.
In the Unresolved Resonance Region (E_n>10 keV) the cross-section for all isotopes are extracted directly from the ratio to ^{235}U(n,f). A different procedure is instead used at lower energy, to avoid artificial fluctuations related to small differences between n_TOF data and evaluated cross-sections in the valleys of the ^{235}U(n,f) resonances. In particular, between 0.15 and 250 eV the cross-sections are determined using the smooth flux obtained from the ^{6}Li(n,α) reaction, normalized to the average value extracted from the ^{235}U(n,f) data.
The ^{233}U(n,f) cross-section is shown in Figure 1 and 2. In the analysis of this isotope, the same threshold used for ^{235}U was applied on the signal amplitude distributions. Nevertheless, since the thickness of the $^{233}U_3O_8$ samples is approximately half of the one of the $^{235}U_3O_8$ deposit, a slight difference is expected for the detection efficiency and for the dead-time of the two samples, which has to be accounted for in the ratio method. The efficiency was estimated by means of realistic Monte Carlo simulations of the energy deposited by the fission fragments in the sample and in the gas volume, while the loss of counts due to dead-time was calculated with the usual non-paralyzable model. The efficiency and dead-time corrections were found to be of the order of a few percent, with a corresponding uncertainty of less than 1 %. The overall systematic uncertainty in extracted cross-section is ~3%, mostly due to the uncertainty in the sample mass.

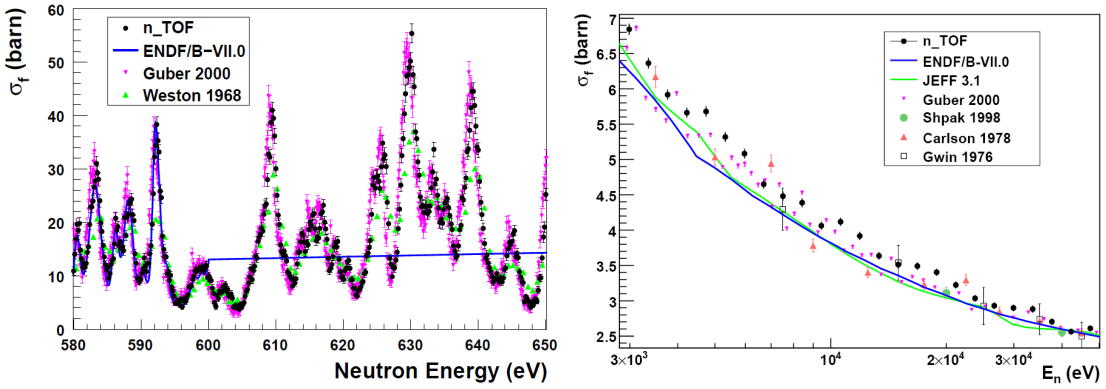

Figure 1. *Left: The results of the ^{233}U(n,f) reaction at few hundreds eV show that resonance structures are still clearly observed above the limit of the Resolved Resonance Region in current evaluations. Right: The n_TOF cross-section compared with previous data and evaluations in the keV region.*

The reliability of the results is demonstrated by the results obtained for the thermal cross-section, where a value of 534±0.2 b is extracted from the n_TOF data, less than 1 % different from the recommended value of 530.7 b. The results in different energy regions, compared to previous measurements and to various evaluated libraries, are shown in Figures 1 and 2. From the plots, the following conclusions can be drawn:

- The n_TOF data are characterized by an accuracy and resolution higher than previous data, except for the recent results of Guber *et al.*, [6], which have a resolution and accuracy similar to the present data, although in a smaller energy region. Resonance-like structures are identified at higher energies than before, providing the basis for more accurate estimates of self-shielding effects in reactor simulations.
- The n_TOF data agree within systematic uncertainty with the recent data from Guber *et al.* [6], while important discrepancies are observed with earlier measurements and, especially, with evaluated cross-sections, in particular in the keV region.

A synoptic view of the differences between n_TOF results and previous data or evaluations is shown in the right panel of Figure 2, which shows the cross-section averaged over a decade in neutron energy. The plot calls for a new evaluation of the ^{233}U(n,f) cross-section, with a major revision needed in particular between 100 eV and 10 keV. It is worth mentioning that an evaluation was recently performed for ENDF/B-VII by Leal *et al.* [7], in which Guber's data were taken into account. However, the final evaluated cross-sections were lowered by 8% to account for the results of an integral measurement. In light of the present results, such a choice does not seem justified. The FIC results are confirmed by the analysis of another measurement performed at n_TOF with the coincidence method (PPAC detectors).
The cross-section for the ^{233}U(n,f) reaction has been also determined above a few MeV. In the case of the FIC detector, due to the presence of a strong γ-flash, a more complicated analysis is necessary, in which a software compensation technique [8] is used to suppress the large oscillations induced by the γ-flash. A comparison between the FIC and PPAC data indicates that the compensation procedure gives reliable results up to a few tens of MeV, with uncertainties still within 3%. Above 30 MeV, a discrepancy of 10% is observed between the two data sets, which can be attributed to a residual contribution of the γ-flash oscillations in the FIC data. The right panel of Figure 2 shows the results of the FIC measurement from 500 keV to 200 MeV, compared with previous data. A reasonable agreement is observed also with evaluated cross-sections, although below 1 MeV ENDF/B-VI.8 reproduces the n_TOF data better than the latest ENDF/B-VII.0 version.

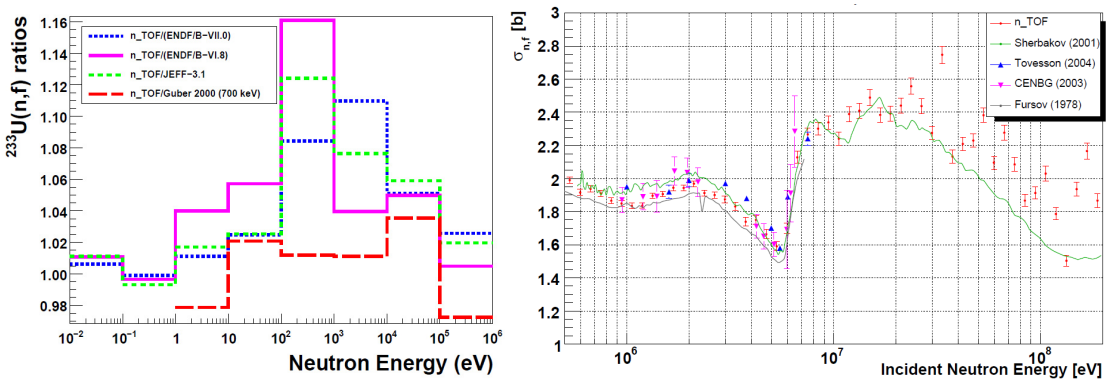

Figure 2. *Left: Ratio of the n_TOF cross-section to previous data and various evaluations, averaged over a decade in neutron energy. Right: The ^{233}U(n,f) cross-section at high energy. The n_TOF data (red symbols) are compared with previous results.*

Together with ^{233}U, new fission data have been obtained at n_TOF for other isotopes involved in the Th/U fuel cycle. In particular, data taken with both FIC and PPAC detectors will soon be available on ^{234}U(n,f) [9]. They indicate the need for a revision of the resonance parameters below the fission threshold, and provide accurate data for reducing the uncertainty in the threshold region. Finally, results of a measurement performed on ^{236}U(n,f) will soon be

released both for the sub-threshold region, where the high resolution of the n_TOF beam allows to clearly identify the main resonances, and in the threshold region, where the shape of the cross-section may allow to better characterize the fission barrier.

Isotopes relevant for Gen IV and ADS

Accurate new data on fission cross-section are required for several minor actinides, as well as for all Pu isotopes, since the present uncertainties, in particular above a few hundred keV, are too high compared to the accuracy required for the design of Gen IV reactors. In this respect, new results are being released from major facilities around the world. In the case of ^{237}Np, the new data from LANSCE [10] have clarified most of the issues still pending on this isotope just below and above the fission threshold, while new high-resolution results from n_TOF [9] provide additional information on sub-threshold resonances. Similarly, new results have been recently reported from LANL on ^{240}Pu and ^{242}Pu in the threshold region, while some issues still remain to be solved at lower energy.

At n_TOF, measurements of the ^{241,243}Am(n,f) and ^{245}Cm(n,f) cross-sections have been performed in the wide energy range from thermal to several tens of MeV. The measurements were performed at n_TOF with the FIC chamber. Above 500 keV neutron energy, a software compensation technique was applied in order to suppress the oscillations in the baseline of the signal produced by the strong γ-flash. Similarly to the ^{233}U case, the cross-section was extracted relative to the ^{235}U(n,f) standard. A correction for the differences in efficiency and dead-time between the measured isotope and the reference ^{235}U sample was considered.

An important result was obtained for the ^{243}Am(n,f) cross-section, for which new data are needed to clarify a long-standing 15% discrepancy between different earlier measurements. Figure 3 shows the cross-section for the ^{243}Am(n,f) reaction, compared with previous results and to evaluated data from ENDF/B-VII.0 [11]. The final overall uncertainty was estimated to be ~4% up to 20 MeV, while at higher energy the residual effect of the γ-flash currently prevents from obtaining reliable results. The new n_TOF data clearly indicate that the recent data from Laptev [12] overestimate the cross-section, and confirm the current evaluations of ENDF/B-VII.0. A similar conclusion was reached by Aiche *et al.* in a quasi-absolute measurement performed at JRC-IRMM and CEN-Bordeaux [13]. A combination of the two most recent datasets now provide definite evidence for the validity of the current evaluated data, thus settling an important and disturbing issue on the cross-section data for this isotope.

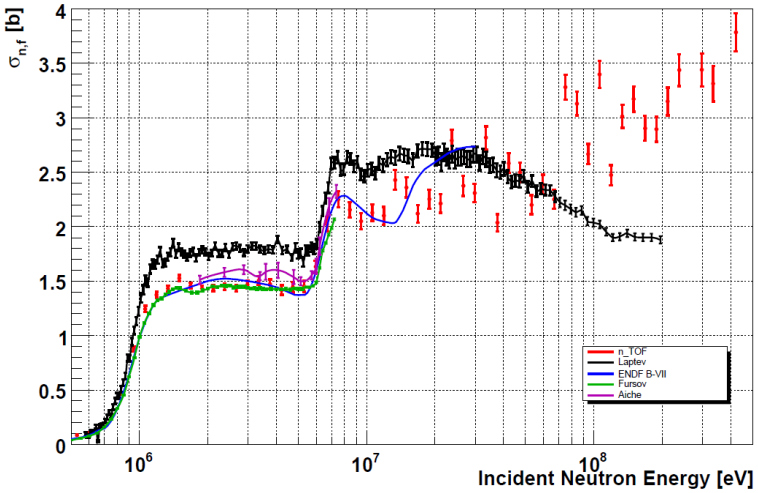

Figure 3. *The ^{243}Am(n,f) cross-section measured at n_TOF (red symbols), compared with ENDF/B-VII.8 (blue line) and with previous evaluations. Above 20 MeV, the residual background related to the γ-flash is responsible for large fluctuations and for a possible overestimation of the cross-section.*

The fission cross section of ^{241}Am is difficult to measure because of the extremely high α-particle activity of this nuclide. For this reason, although several measurements have been performed in the past, large uncertainties still persist. At n_TOF, the signal/background ratio is improved by a large factor, thanks to the very high instantaneous neutron flux. New results on the cross-section of the ^{241}Am(n,f) reaction were obtained in the energy range from thermal to 2 MeV [14]. In this case, the analysis was complicated by a large background due to α-particles and, in particular, to their pile-up. A large fraction of the background was suppressed by a high threshold on the amplitude spectrum, which however results in an increased uncertainty of the efficiency correction. The residual α-particle background was estimated from runs without neutron beam and subtracted. A small unexpected presence of Pu was also asserted from two resonances at 7.8 eV and 75 eV. The contribution of the Pu impurity, which was estimated from the two resonances to be of 0.2 %, was subtracted from the fission yield. With the aim of reducing the uncertainty, the background- and Pu-subtracted yield was renormalized to the data of Dabbs *et al.* [15] in the energy region of the third resonance (which is not affected by the Pu contamination), whose cross-section is known with reasonable accuracy. Overall, a systematic uncertainty of the order of ~10% is estimated for the ^{241}Am(n,f) cross-sections, mostly due to the normalization procedure. Figure 4 shows the results in two energy regions, compared with various evaluations and previous data. In the resonance region (left panel), the resolution and accuracy of the n_TOF data may contribute to improve evaluated databases, especially in regions where large discrepancies exist. The new results will also contribute to improve the accuracy of the cross-section around and above fission threshold, where an uncertainty as low as 2% is required for the design of advanced reactor systems. The n_TOF data in that energy region are shown in the right panel of Figure 4, together with previous data and evaluations. The analysis necessary to extend the energy region to several tens of MeV is now in progress. Furthermore, the accuracy of the present data in the whole energy region can be substantially improved if new dedicated measurements are performed for normalization purposes.

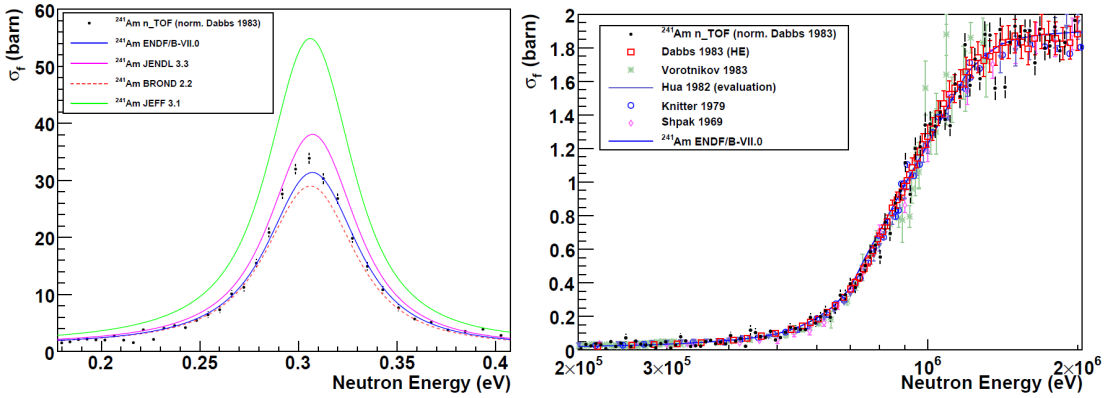

Figure 4. *The ^{241}Am(n,f) cross-section at low energy (left panel) compared with four different evaluations. The n_TOF data in this case confirm the evaluations of ENDF/B-VII.0, while JEFF 3.1 largely overestimates the strength of the resonance. Right: the n_TOF cross-section in the threshold region is compared with previous results and evaluated cross-sections.*

The neutron-induced fission cross-section was also measured for ^{245}Cm, for which only few and discrepant experimental data exist, due to the relatively short half-life of this isotope ($t_{1/2}$ ~8500 yr). As for ^{241}Am, the measurement is affected by a very large α-background and by the pile-up of α-particles. A further complication is related to a 6.6% impurity of ^{244}Cm, which has a much higher rate of spontaneous fission. To minimize the background related to the natural radioactivity of the sample, a high amplitude threshold was used. The residual background was estimated from runs with no-beam and subtracted from the fission yield. Due to a large uncertainty in the efficiency correction, the n_TOF data have been normalized to the ENDF/B-VII.0 cross-section at 0.03 eV. However, the adopted value of the thermal cross-section is still affected by large discrepancies (of the order of 30%) between various results. New measurements at low energy are therefore mandatory for normalization purposes, in

order to reduce the systematic uncertainty to the required value of a few percent. The results of the n_TOF measurement in different energy regions are shown in Figure 5.
The energy range of the n_TOF data is wider than in any previous measurement, covering the whole region from 0.03 eV to 2 MeV (the extension to even higher energies is currently under way). A previous measurement for this isotope with a resolution comparable to that of n_TOF from Moore *et al.* [16] was obtained with the intense single neutron pulse of a nuclear explosion, but only for neutron energies above 10 eV. The left panel in Figure 5 shows the ^{245}Cm(n,f) cross-sections for the first two resonances in the few eV region. The n_TOF data show a higher cross-section in the right tail of these resonances than the evaluated data. In this case as well, the problem seems to be associated to the data libraries, since good agreement is observed between the n_TOF and previous data. Similar problems are observed for other resonances. Finally, the right panel in Figure 5 shows the high resolution of the n_TOF data, which could be useful to improve current databases for reactor applications.

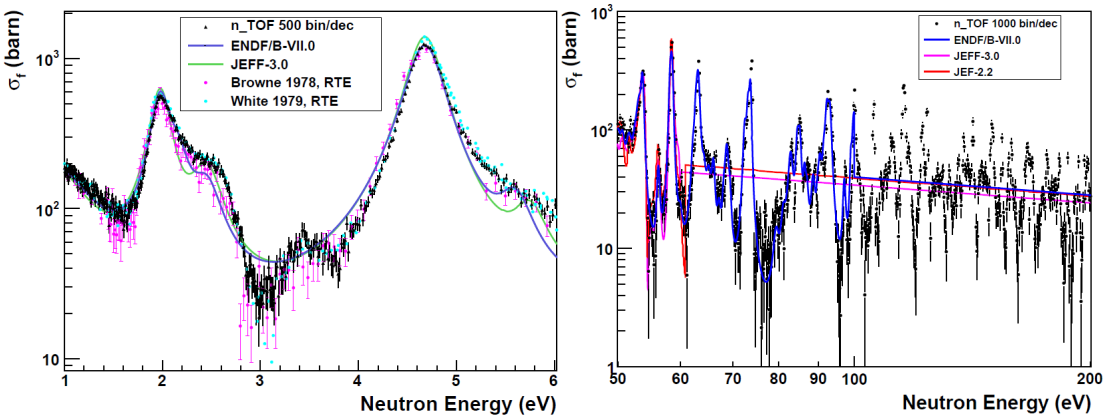

Figure 5. *The ^{245}Cm(n,f) cross-section determined at n_TOF. The shapes and strengths of the resonances in evaluated libraries do not adequately reproduce the new data. Furthermore, resonance-like structures are observed above the limit of the Resolved Resonance Region in current evaluations.*

Conclusions

Neutron-induced fission cross-section measurements of several isotopes relevant for the Th/U fuel cycle and for Gen IV fast reactors have been performed at n_TOF with two detection systems. The new data are part of a worldwide effort aimed at improving the current knowledge of basic nuclear data for the development of advanced reactors. Two systems have been used at n_TOF: a Fast Ionization Chamber and Parallel Plate Avalanche Counters. The results for the ^{233}U(n,f) reaction, characterized by a 3% uncertainty, indicate that a substantial revision of the databases in the fast neutron region is in order. New high-accuracy results have been obtained around and above threshold for the ^{243}Am(n,f) cross-section, which confirm the current evaluations and rule-out the recent indication of a higher cross-section. For ^{241}Am and ^{245}Cm, results in the whole energy region from thermal to 20 MeV (and possibly higher) are now being finalized, although an absolute normalization can not be performed, due to the large α-background affecting the measured data for these samples. Nevertheless, the n_TOF measurements provide important new data, with a typical uncertainty of 10%, which can help to reduce current uncertainties substantially. New data at thermal energy are necessary for reducing the remaining uncertainties towards the level requested by the design studies of advanced reactor concepts.

References

[1] NEA-OECD, *ed.,* Accelerator Driven Systems (ADS) and Fast Reactors (FR) in Advanced Nuclear Cycles (NEA-OECD, 2002).
[2] NEA/WPEC 26, OECD 2008, ISBN 978-92-64-99053-1.
[3] U. Abbondanno et al., (The n_TOF Collaboration), n_TOF Performance Report, CERN/INTC-O-011, INTC-2002-037 (2002).
[4] M. Calviani et al., (The n_TOF Collaboration), Nucl. Instr. and Meth. A 594, 220 (2008).

[5] M. Calviani et al., (The n_TOF Collaboration), submitted to Phys. Rev. C (April 2009).
[6] K.H. Guber et al., Nucl. Sci. Eng., 135, 141 (2000).
[7] L.C. Leal et al., Report ORNL/TM-2000/372, Oak Ridge National Laboratory, 2001.
[8] N. Colonna et al., (The n_TOF Collaboration), Nucl. Instr. and Meth. A, in preparation.
[9] C. Paradela et al., (The n_TOF Collaboration), Phys. Rev. C, in preparation.
[10] F. Tovesson and T.S. Hill, Phys. Rev C 75, 034610 (2007).
[11] F. Belloni et al., (The n_TOF Collaboration), Nucl. Sci. Eng., in preparation.
[12] A. Laptev et al., Conf. on Nucl. Data for Sci. and Techn., p. 865 (Santa Fe, USA, 2004).
[13] M. Aiche et al., Proceedings of the International Conference on Nuclear Data for Science and Technology 2007, CEA 2008, DOI: 10.1051/ndata:07473.
[14] M. Calviani, PhD thesis, University of Padova, 2009.
[15] J.W.T. Dabbs et al., Nucl. Sci. Eng., 83, 22 (1983).
[16] M.S. Moore et al., Phys. Rev. C 3, 1656 (1971).

Neutron-induced cross sections of short-lived nuclei via the surrogate reaction method

S. Czajkowski[1)], M. Aiche[1)], G. Barreau[1)], A. Bidaud[1)], D. Dassie[1)], B. Haas[1)], B. Jurado[1)], G. Kessedjian[1)], L. Mathieu[1)], L. Audouin[2)], N. Capellán[2)], L.Tassan-Got[2)], J.N. Wilson[2)], E. Berthoumieux[3)], F. Gunsing[3)], Ch. Theisen[3)], O. Serot[4)], E. Bauge[5)], V. Méot[5)], O. Roig[5)], I. Ahmad[6)], J.P. Greene[6)], R.V.F. Janssens[6)], F.-J. Hambsch[7)], S. Oberstedt[7)], P. Schillebeeckx[7)]

1) CENBG, CNRS/IN2P3, Univ. Bordeaux I, BP120, 33175 Gradignan, France
2) IPN, CNRS/IN2P3, Univ. Paris-Sud, 91405 Orsay, France
3) CEA Saclay, DSM/DAPNIA/SPhN, 91191 Gif-sur-Yvette cedex, France
4) CEA-Cadarache, DEN/DER/SPRC/LEPh, 13108 Saint Paul lez Durance, France
5) CEA, SPN, BP12, 91680 Bruyères-le-Châtel, France
6) Physics Division, Argonne National Laboratory, IL 60439, USA
7) EC-JRC-IRMM, Retieseweg 111, 2440 Geel, Belgium
czajkows@cenbg.in2p3.fr

Abstract: Neutron-induced cross sections of short-lived nuclei are crucial for nuclear reactor physics. However, the high radioactivity of the samples makes the direct measurement of these cross sections extremely difficult. The surrogate reaction method is an indirect way of determining cross sections for nuclear reactions that proceed through a compound nucleus. This method presents the advantage that the target needed is stable or less radioactive than the target required for the neutron-induced measurement. After explaining the surrogate method and discussing its validity, the results of an experiment performed by the CENBG to determine the neutron-induced fission cross sections of various highly radioactive minor actinides are presented. These data are of great importance for the incineration of nuclear reactor waste. Currently we work on the application of this powerful technique to the determination of neutron-induced capture cross sections. We will start by checking the validity of the surrogate method when applied to obtain capture cross sections in the rare-earth region.

Introduction

There is a renewal of interest in nuclear reaction studies of nuclei involved in reactor physics, e.g. these relevant to innovative fuel cycle and nuclear waste transmutation. Minor actinides are the most radiotoxic part of the nuclear waste. Studies to reduce their production (thorium fuel cycle) or to incinerate them in fast neutron reactors or ADS need a more complete and precise knowledge of their neutron induced cross sections, as fission and capture cross sections. There is presently an important lack of precise experimental data for some short lived curium isotopes, due to the difficulties in very active target handling.
For a typical direct neutron measurements with actinide targets using a neutron beam of about 10^6 $cm^{-2}s^{-1}$, the target thickness is about 200 µg/cm^2, i.e. 10^{18} target atoms, leading to reaction rates of approximately 1 s^{-1} for reaction cross section around 1 barn. In the case of short lived nuclides, the very intense alpha activity (e.g. MBq for ^{243}Am, several GBq for $^{242-244}$Cm isotopes, up to 300 GBq for ^{233}Pa) induce detector damage, background and contamination, and last but not least very hard safety constraints. The surrogate reaction technique allows one to overcome these difficulties.

The surrogate method

This indirect method was developed in the 70's by Cramer and Britt [1]. It consists in measuring the decay probability of a compound nucleus produced via an alternative reaction (e.g. transfer reaction) chosen in a way that the compound nucleus produced in this surrogate reaction has the same A and Z that the one obtained in the considered direct neutron reaction. The neutron induced cross section for the given target nucleus ^{A}Z is thus obtained by multiplying the measured partial decay probability of the compound nucleus ^{A+1}Z by the compound nucleus cross section for the neutron induced reaction obtained from optical model

calculations. This method has been more recently used to determine the fission cross section ^{233}Pa(n,f) by means of the ^{232}Th(^{3}He,pf) surrogate reaction [2].

Fission cross section of Am and Cm isotopes

For this experiment, we have used a ^{243}Am target ($T_{1/2}$: 7370y) and a ^{3}He beam to study the fission cross section of Am and Cm isotopes. Transfer reactions produce ^{242}Am and $^{243-245}$Cm compound nuclei associated to α and t,d,p emitted particles. These compound nuclei are the same as the ones produced by direct neutron reaction on ^{241}Am and $^{242-244}$Cm targets (see Figure 1). Note that the surrogate method allows to study simultaneously the four reaction channels in a wide range of excitation energy.

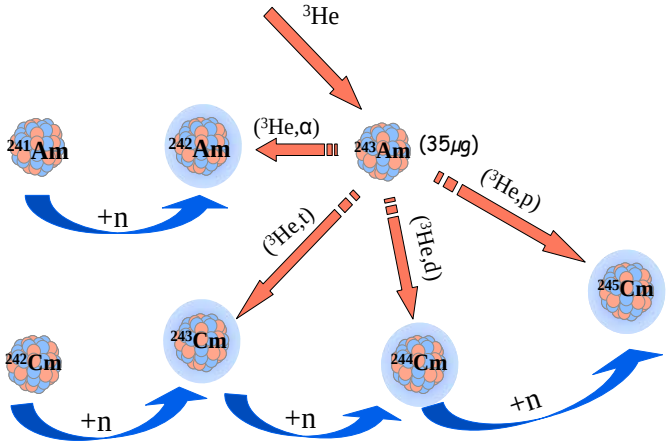

Figure 1. *Schematic representation of the surrogate method for minor actinide studies. Using a ^{243}Am target, transfer reactions from a ^{3}He beam lead to the formation of ^{242}Am and $^{243-245}$Cm compound nuclei associated to α and t,d,p particles, the same compound nuclei can be obtained from direct neutron absorption by ^{241}Am and $^{242-244}$Cm targets.*

Thus, the detection and identification of the emitted particles and the measurement of their kinetic energy allows the identification of the associated compound nucleus and the determination of its excitation energy. The fission probability is obtained by dividing the number of coincident fission events by the number of emitted particles for the corresponding channel (α,p,d,t), taking in account the detector efficiency and the reaction kinematics.

Experimental set-up

The fission experiment has been performed at the Tandem accelerator at IPN Orsay, using the 30Mev ^{3}He beam. The active target (250 kBq) was made of a 35μg ^{243}Am layer of 0.6cm diameter on a 50μg/cm^{2} carbon film. The target was provided by Argonne National Laboratory. Two sets of two Si telescope each were placed at 90° and 130° backward angle relative to the beam direction, at each side of the horizontal plane. Each of four telescope comprise a 300μm detector for energy loss and a 5mm detector for residual energy measurement of the emitted particles. Fission detector consists in five sets of 3 photovoltaic cells (2x4cm^{2} each) all covering almost half of the angular distribution of the fission fragments. A schematic view and a picture of the detectors are shown in Figure 2.

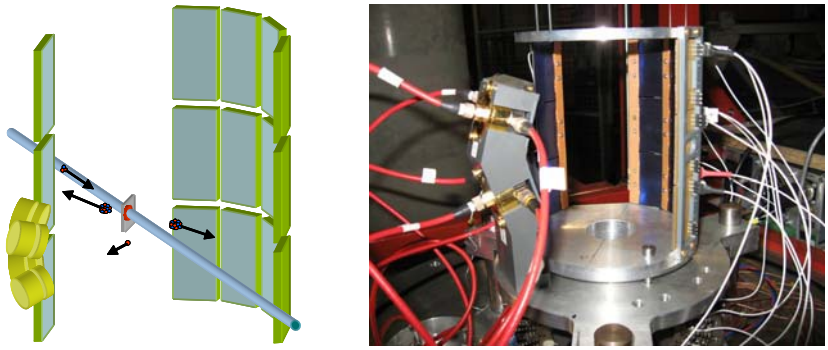

Figure 2. *Experimental set-up for fission probability measurements. The target is 45° to the beam direction. Emitted particles (α, p, d, t) are detected in four ΔE-E silicon telescopes located at 90° and 130° to the beam axis. The fission detector consists in 5 walls of 3 photovoltaic cells covering almost half of the solid angle.*

The emitted particles are identified by means of their ΔE-E measurement. The left part of Figure 3 shows the identification pattern for particles. The energy spectra are calibrated using the excited states of ^{207}Pb and ^{209}Bi produced in the ^{208}Pb(^{3}He,d) and ^{208}Pb(^{3}He,α) reactions. Background contribution from reactions with the carbon film is measured and subtracted. The right part of Figure 3 shows the total energy spectrum of the tritons emitted at 130°. The particle energy has been converted to the excitation energy of the associated compound nucleus (^{243}Cm). Residual background from reactions with light element contamination occurs at high excitation energy and can be subtracted by extrapolating the shape of the excitation function. The events in coincidence with a fission event have been superposed on the same figure.

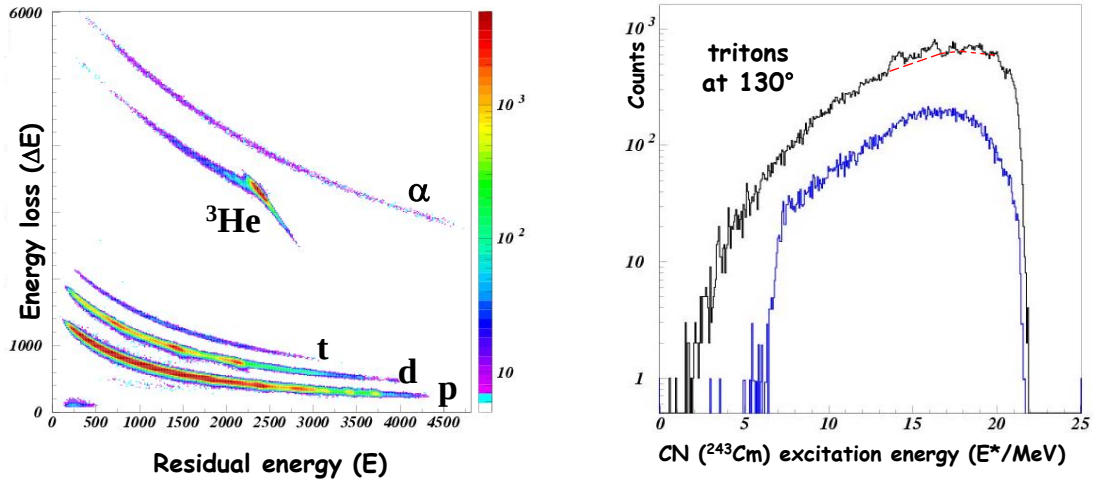

Figure 3. *Left: Energy loss versus residual energy in one of the Si telescopes. Right: Number of tritons as a function of the ^{243}Cm excitation energy: all events (black) and with a fission event detected in coincidence (blue). The extrapolation of the singles spectrum under the ^{19}F contaminant peaks is represented by the red dotted line (see text for details).*

The ratio of the two spectra, corrected by the efficiency of the fission detection setup, gives the fission probability as a function of the compound nucleus excitation energy. To obtain the neutron induced fission cross section ^{242}Cm(n,f) this fission probability is then multiplied by the cross section for the ^{243}Cm* compound nucleus formation in direct neutron reaction. The latter has been obtained with a semi-microscopic optical model calculation [3].

Validation with ^{241}Am

The fission probability of 242Am compound nucleus in 243Am(3He,α) reaction is shown in Figure 4 (left). One can see on the right part of Figure 4 that the neutron induced fission cross section of ^{241}Am obtained in this experiment using the surrogate method is in very good agreement with all the evaluations and the experimental data by Dabbs et al. [4].

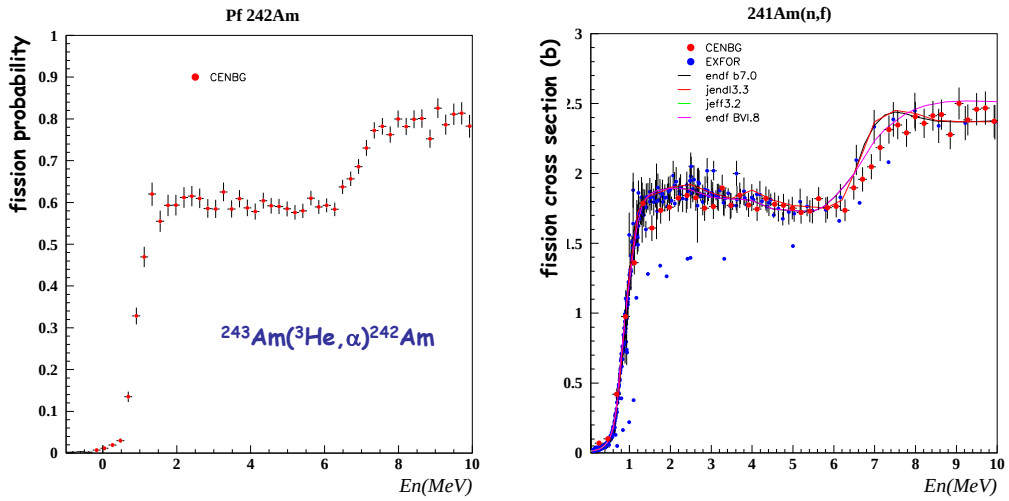

Figure 4. *(left) Fission probability measured in the ^{243}Am(^{3}He,α)^{242}Am reaction and (right) ^{241}Am(n,f) fission cross section determined with the surrogate method as a function of neutron energy compared with available data and evaluations.*

Cm isotopes

The fission cross section of ^{242}Cm is shown in Figure 5. Our data are compared with the ones from Vorotnikov et al. [5] and the various international libraries. There is a good agreement between both sets of experimental data under 1.4 MeV neutron energy. Note that there is no other experimental data from direct neutron reaction above 1.4 MeV where the evaluations present important discrepancies. JEFF and JENDL libraries present the best overall agreement with our data.

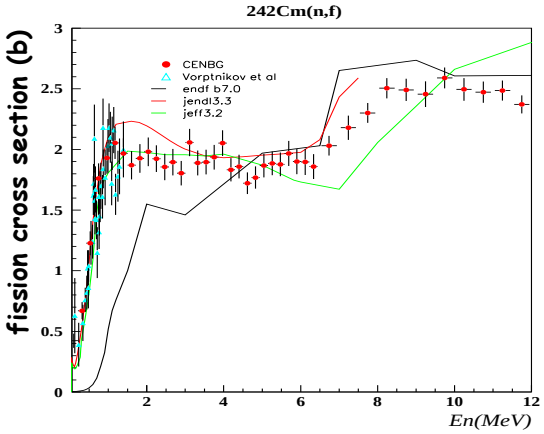

Figure 5. *^{242}Cm(n,f) fission cross section determined with the surrogate method as a function of neutron energy compared with available data and evaluations.*

The case of ^{243}Cm is more complex. The results obtained in these experiments are shown on the right part of Figure 6, together with the most recent measurement by Fomushkin et al. [6] and by Fursov et al.[7] and the ENDF, JENDL and JEFF libraries. The agreement between the three experimental data sets is satisfactory at lowest neutron energies. Above 0.7 MeV, our data from surrogate method follow those by Fomushkin but clearly disagree with Fursov's data. Fursov's cross section in the 1-3 MeV range is significantly higher than the experimental values of neighbouring fissile isotopes of curium ^{245}Cm [8,9] and ^{247}Cm [7] shown in Figure 6. Optical model calculations [3] predict a total compound nucleus cross section of 3 b, including the neutron inelastic scattering cross section of ^{243}Cm which can be reasonably assumed to range from 1 to 1.5 b at these neutron energies. All these considerations suggest that Fursov's data, and thus JENDL evaluation, overestimate the ^{243}Cm(n,f) cross section in the 0.7-3 MeV range.

The excellent accord observed at the lowest neutron energies between our results and the neutron-induced fission data for even-even ^{242}Cm and odd-even ^{243}Cm indicates that the angular momentum population generated by the transfer reactions used in this work sample a similar angular momentum distribution as the neutron-induced reactions. This clearly

illustrates the potential of the surrogate reaction method to extract neutron-induced cross sections of short-lived nuclei.

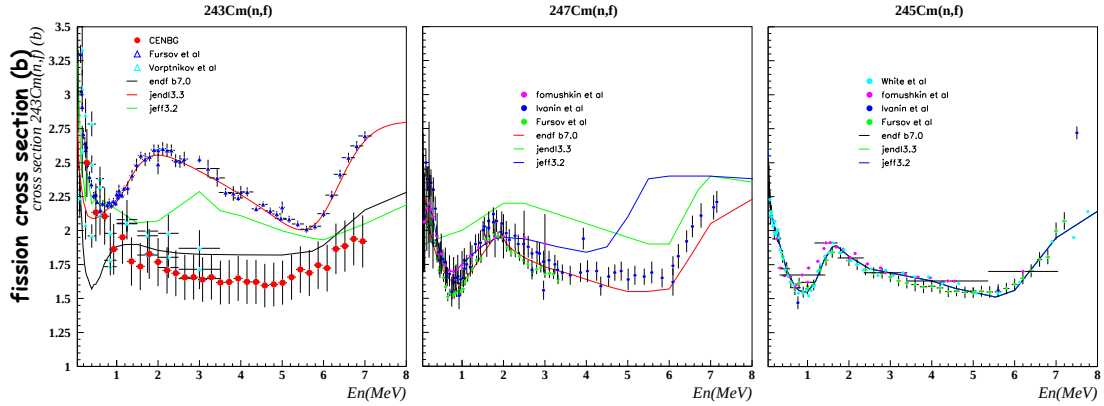

Figure 6. *^{243}Cm(n,f) fission cross section determined with the surrogate method as a function of neutron energy compared with available data and evaluations (right), and fission cross sections of the fissile Cm isotopes ^{247}Cm(n,f) and ^{245}Cm(n,f).*

Extending the surrogate method to capture cross section measurements

The surrogate technique can be extended to radiative capture cross section measurements. In this case, the more compact reaction chamber only contains the target and the particle telescopes, and is surrounded by dedicated gamma detectors. For capture events, the compound nuclei decay by a gamma cascade the multiplicity of which is about 4-5. The detection efficiency is low (a few %) and energy dependant. To infer the capture probability, gamma rays are detected in coincidence with the ejectile in a set of C_6D_6 liquid scintillators using the total energy detection principle in combination with the pulse height weighting technique [10]. Our group has performed such an experiment to determine the capture cross section ^{233}Pa(n,γ) using the ^{232}Th(^{3}He,p)^{234}Pa* surrogate reaction [11]. These results are shown in Figure 7.

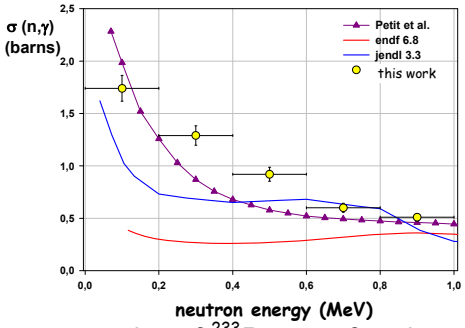

Figure 7. *Neutron capture cross section of ^{233}Pa as a function of neutron energy, obtained from ^{232}Th(^{3}He,p)^{234}Pa surrogate reaction. Our data are compared with JENDL and ENDF evaluations, and a calculation from M. Petit et al.*

The range of excitation energy investigated is very narrow, between neutron emission threshold and fission threshold, and the obtained raw gamma probability must be corrected due to (n,n'γ) contribution that has to be estimated.

An important issue to be investigated in the context of surrogate reactions is the difference between the distributions of the J^{π} states populated in the compound nucleus produced in the desired and surrogate reactions. This is referred in the literature [12] as the J^{π} population entrance channel mismatch. Since the J^{π} population influences the decay probabilities of the compound nucleus, one could expect differences between the decay probabilities measured in surrogate and in neutron-induced experiments. The validation of the surrogate method when applied to (n,γ) reactions remains to be done. In the future we to use the ^{237}Np(n,γ), ^{238}U(n,γ) and ^{232}Th(n,γ) cross sections to validate the ^{236}U(^{3}He,p)^{238}Np, ^{238}U(d,p)^{239}U and ^{232}Th(d,p)^{233}Th surrogate reactions. Unfortunately, the latter surrogate reactions require thin actinide targets which are not yet available.

We started by checking the validity of the surrogate method in the rare earth region. The ^{175}Lu(n, γ) cross section is one of the best known capture cross sections [13,14]. Moreover, a program using the 4π DANCE [15] detector array at Los Alamos has been started to expand the available databases for ^{175,176}Lu(n, γ). This allows to validate several surrogate reactions with stable targets: ^{174}Yb(^{3}He,pγ)^{176}Lu, ^{176}Yb(^{3}He,tγ)^{176}Lu and ^{175}Lu(d,pγ)^{176}Lu. Lu isotopes have also attracted interest in astrophysics due to their importance to s-process studies [14]. For this experiment, Ge detectors are used in addition to C_6D_6 to select discrete low-lying γ-rays emitted by the residual nucleus to infer the calculated level spin distribution and to constraint the reaction models. For example, ***Figure 8*** shows the intensity ratio for a $6^-\rightarrow7^-$ transition over a $1^-\rightarrow1^-$ transition (left) and a $6^+\rightarrow4^+$ transition (right) as a function of the neutron energy, obtained from Hauser-Feshbach calculations using the TALYS code [16].

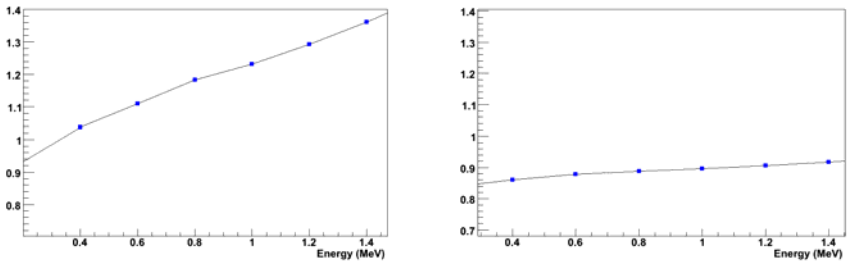

Figure 8. *Gamma transition ratio for the $6^-\rightarrow7^-$ transition at 563.9 keV to the $1^-\rightarrow1^-$ transition at 263.7 keV (left), and the ratio of the $6^-\rightarrow7^-$ transition to the $6^+\rightarrow4^+$ transition at 219.3 keV (right) for the ^{175}Lu(n,γ) reaction versus incident neutron energy.*

The behaviour of such sensitive ratios in both direct neutron capture and surrogate experiments should be a test of the validity of the surrogate method when applied to capture cross section measurements. In a first test experiment in winter 2009 at the Tandem facility of IPN Orsay, a new large area telescope has been tested comprising a large position sensitive silicon detector (300μm) associated to a 5mm Si(Li) for residual energy. The main experiment is planned for spring 2010.

Conclusion and outlook

The surrogate reaction method has been successfully used to measure the neutron induced fission cross section of ^{241}Am and ^{242,243}Cm short lived minor actinides. The experimental data set has been extended to neutron energies above the second chance fission. The main limitation remains the availability of thin targets of very high purity. We have started to check the validity of the extension of the surrogate method to extract radiative capture cross section.

Acknowledgements
We thank the ALTO-Tandem accelerator staff and the target laboratory of the IPN Orsay for their great support during the experiment. This work was partly supported by the CNRS program PACEN/GEDEPEON, the Conseil Régional d'Aquitaine, the U.S. Department of Energy, Office of Nuclear Physics, under contract DE-AC02-06CHII357.

References

[1] J. Cramer and H. Britt, Nucl. Sci. Eng. 41, 177 (1970).
[2] M. Petit et al., Nucl. Phys. A 735, 345 (2004).
[3] E. Bauge, private communication.
[4] J.W.T. Dabbs et al., Nucl. Sci. Eng. 83, 2 (1983).
[5] P. E. Vorotnikov et al., Yadern. Fiz. 40, 1141 (1984).
[6] E.F. Fomushkin et al., At. Energ. 69, 258 (1990).
[7] B.I. Fursov et al., Conf. Nucl. Data for Sci. and Techn., Trieste 1997, p.448.
[8] E. F. Fomushkin et al., At. Energ. 63, 242 (1987).
[9] R.M. White et al., Conf. Nucl. Data for Sci. and Techn., Antwerp 1982, p.218.
[10] J.N. Wilson et al., Nucl. Instr. Meth. A 511, 388 (2003).
[11] S. Boyer et al., Nucl. Phys. A 775, 175 (2006).
[12] J.E. Escher et al., Nucl. Instr. Meth. B 261, 1075 (2007).
[13] R.L. Macklin et al., Nucl. Sci. Eng. 95, 189 (1987).
[14] K. Wisshak et al., Phys. Rev. C 73, 015807 (2006).
[15] M. Heil et al., Nucl. Instr. Meth. A 459, 229 (2001).
[16] A.J. Koning et al., NRG Report 21297/04.62741/P FAI/AK/AK, Dec 5 (2004).

KADoNiS v0.3 – The third update of the "Karlsruhe Astrophysical Database of Nucleosynthesis in Stars"

I. Dillmann[1)], R. Plag[2)], F. Käppeler[3)], T. Rauscher[4)]

1) Physik Department E12 and Excellence Cluster 'Universe', Technische Universität München, James-Franck-Strasse, D-85748 Garching
2) GSI Helmholtzzentrum für Schwerionenforschung GmbH, Plankstrasse 1, D-64291 Darmstadt
3) Institut für Kernphysik, Forschungszentrum Karlsruhe, Postfach 3640, D-76021 Karlsruhe
4) Departement Physik, Universität Basel, Klingelbergstrasse 82, CH-4056 Basel
iris.dillmann@ph.tum.de

Abstract: The "Karlsruhe Astrophysical Database of Nucleosynthesis in Stars" (KADoNiS) project is an online database for experimental cross sections relevant to the s process and p process. It is available under http://www.kadonis.org and consists of two parts. Part 1 is an updated sequel to the previous Bao et al. compilations for stellar (n,γ) cross sections relevant to nucleosynthesis in the Big Bang and in the s process. The second part is a collection of experimental data within the Gamow window of the p process and still under construction. Part 1 of the KADoNiS project was launched in April 2005, and the third update (v0.3) was released recently.

History of stellar neutron capture compilations

The pioneering work for stellar neutron capture cross sections was published in 1971 by Allen and co-workers [1]. This paper reviewed the role of neutron capture reactions in the nucleosynthesis of heavy elements and presented also of a list of recommended (experimental or semi-empirical) Maxwellian averaged cross sections at kT= 30 keV (MACS30) for nuclei between carbon and plutonium.
The idea of an experimental and theoretical stellar neutron cross section database was picked up again by Bao and Käppeler [2] in 1987 for s-process studies. This compilation included cross sections for (n,γ) reactions between ^{12}C and ^{209}Bi, some (n,p) and (n,α) reactions for isotopes between ^{33}S and ^{59}Ni, and also (n,γ) and (n,f) reactions for long-lived actinides. A follow-up compilation was published by Beer, Voss and Winters in 1992 [3].
In the update of 2000 the Bao et al. compilation [4] was extended to Big Bang nucleosynthesis. It now included a collection of recommended MACS30 for isotopes between ^{1}H and ^{209}Bi, and − like the original Allen paper − also semi-empirical recommended values for nuclides without experimental cross section information. These estimated values are normalized cross sections derived with the Hauser-Feshbach code NON-SMOKER [5], which account for known systematic deficiencies in the nuclear physics input of the calculation. Additionally, the database provided stellar enhancement factors and energy-dependent MACS for energies between kT= 5 keV and 100 keV.

KADoNiS

The KADoNiS project [6] is based on these previous compilations and aims to be a regularly updated database with online access via www.kadonis.org. It was launched in April 2005 as online version of the Bao et al. compilation [4]. The current version is already the third update (KADoNiS v0.3), and a paper version is planned for 2010 (KADoNiS v1.0).
In total, data sets are available for 356 isotopes, including 77 radioactive nuclei (22%) on or close to the s-process path. For 13 of these radioactive nuclei experimental data is available: ^{14}C, ^{60}Fe, ^{93}Zr, ^{99}Tc, ^{107}Pd, ^{129}I, ^{135}Cs, ^{147}Pm, ^{151}Sm, ^{154}Eu, ^{163}Ho, ^{182}Hf, and ^{185}W. The remaining 64 radioactive nuclei are not yet measured in the stellar energy range and are represented only by semi-empirical cross section estimates with typical uncertainties of 25% to 30%. Almost all stellar (n,γ) cross sections of the 279 stable isotopes have been measured until now. The few exceptions are ^{17}O, ^{36,38}Ar, ^{40}K, ^{50}V, ^{70}Zn, ^{72,73}Ge, ^{77,82}Se, ^{98,99}Ru, ^{131}Xe, ^{138}La, ^{158}Dy and ^{195}Pt. Most of these cross sections are difficult to determine because they are

not accessible by activation measurements or samples are not available in sufficient amounts and/or enrichment for time-of-flight measurements.

KADoNiS v0.3

The third update of the s-process database was released in August 2009. In this version the stellar enhancement factors were updated [7], and a dataset for the long-lived isotope ^{60}Fe added. The semi-empirical estimates for the p-process isotopes ^{168}Yb, ^{184}Os, and ^{196}Hg were replaced by values from activation measurements [13].

Figure 1 gives an overview of the changes between the present version and the Bao 2000 compilation [4]. The isotopes with the largest changes are labelled. Whereas most of these changes are due to remeasurements with up-to-date techniques and remove previous uncertainties, some of these nuclei were measured for the first time and thus replace semi-empirical estimates, e.g. for ^{78}Se, ^{129}Xe, ^{147}Pm, and ^{196}Hg.

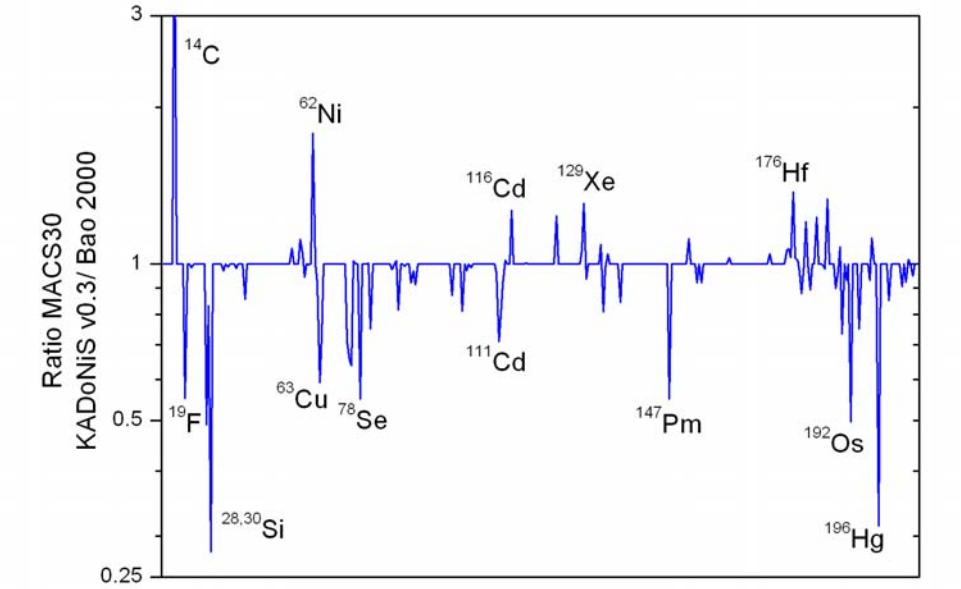

Figure 1. *Comparison of Maxwellian cross sections at kT=30 keV (MACS30) from the present update and the Bao compilation [4].*

The present average uncertainty of the recommended experimental values at kT=30 keV is ±6.5% (Figure 2). Most recommendations were derived from weighted averages of two or more measurements, which reduced the uncertainty of the recommended value below the uncertainties of the single measurements. One prominent example is the ^{62}Ni(n,γ)^{63}Ni cross section with a recommended MACS30 of 22.3±1.6 mb, which was derived from four measurements [8,9,10,11] with single uncertainties between 10% and 20%. All four measurements were performed by independent methods with different systematic uncertainties, two time-of-flight measurements [8,10] and two activation measurements with subsequent Accelerator Mass Spectrometry (AMS) at different facilities [9,11]. The experimental value with the obviously smallest uncertainty [12] from another TOF measurement was neglected since it lies far out of the range of the other four “agreeing” measurements. As can be seen in Figure 2 some isotopes of chromium and platinum still have rather large uncertainties.

One feature of the KADoNiS database is also the presentation of so-called “isotopic mass chain” plots with the recommended MACS30 for all isotopes of one element. From these plots the tendency of smaller cross sections when approaching a neutron shell closure is clearly visible, as well as the even-odd staggering. Figure 3 shows these plots for osmium and mercury in comparison to values of the Bao et al. compilation [4]. The semi-empirical estimates for the p-process isotopes ^{184}Os and ^{196}Hg were replaced by activation measurements, as well as the cross section of ^{192}Os [13]. The decrease towards the N=126 shell closure can now be clearly seen in Fig. 3.

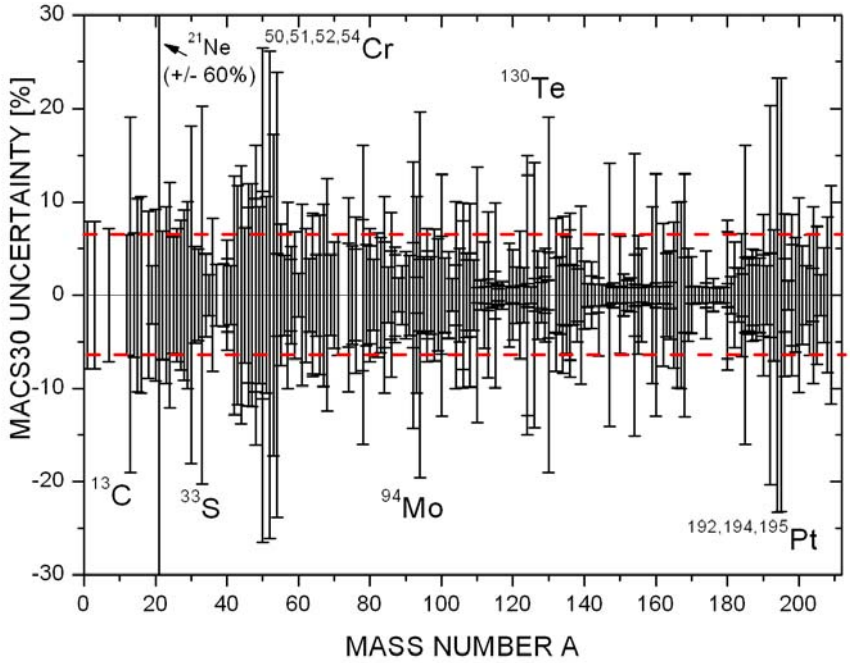

Figure 2. *Uncertainties (in %) of the experimental MACS30 in KADoNiS v0.3. The red dashed line indicates the average uncertainty of ±6.5%.*

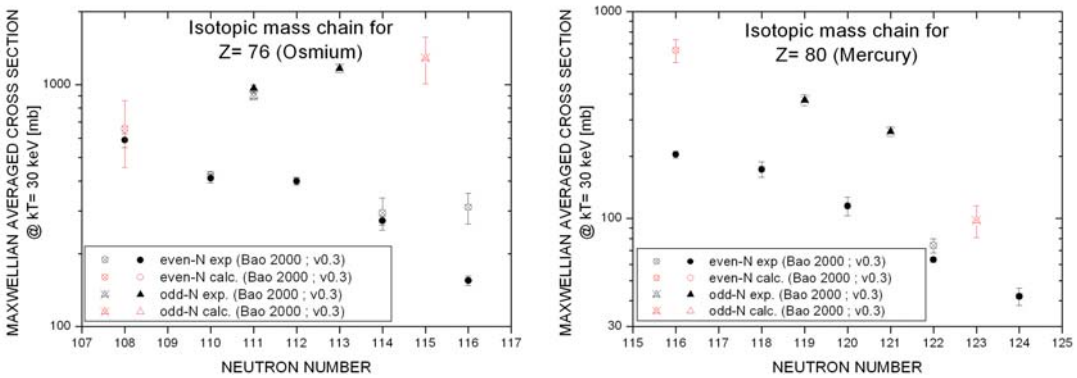

Figure 3. *Comparison of MACS30 in the isotopic mass chains of osmium (left) and mercury (right). Red symbols indicate semi-empirical values.*

Astrophysical impact of the updated cross sections

The largest astrophysical impact of changes in recommended cross sections comes from ^{62}Ni (+78%) [9] and ^{63}Cu (-41%) [14]. A larger (smaller) cross section means more (less) reaction flow towards higher masses. Because the reaction flow of the weak s-process is not equilibrated, it is very sensitive to the bottle neck isotopes ^{62}Ni and ^{63}Cu. Changes in these cross sections affect the abundances of all isotopes up to the next shell closure at A~90 (N=50). For plots of the effect of the single changes, see Refs. [9,14]. Figure 4 shows the combined propagation effect [15] for the changes of the cross sections of the iron-group elements ^{54,58}Fe, ^{59}Co, ^{60,62,64}Ni, and ^{63,65}Cu. Since the changes in ^{62}Ni and ^{63}Cu point in different directions, they almost cancel each other and the combined influence is not as strong as the single effects in Refs. [9,14].

Outlook: Extensions

Several extensions are planned for the neutron capture compilation. The s-process library will be complemented in the near future by some (n,p) and (n,α) cross sections of light isotopes measured at kT=30 keV, as it was already done in [2]. Additionally some "gaps" in the list of stable isotopes will be filled. For different reasons the datasets for ^{2}H, ^{6}Li, ^{9}Be, ^{10,11}B, ^{17}O, and ^{138}La were missing in previous compilations.

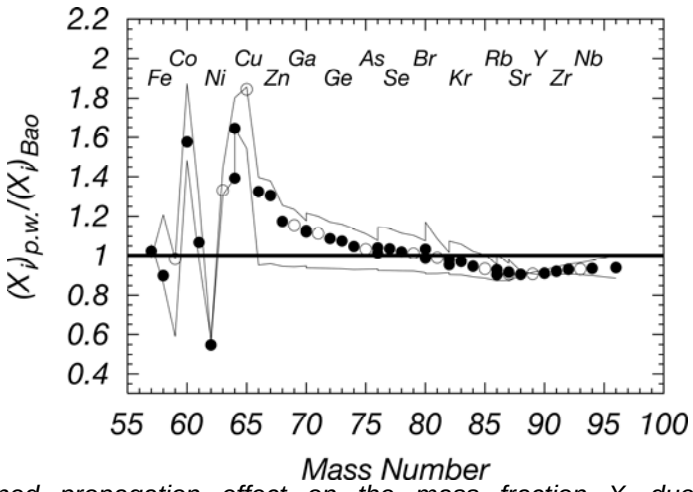

Figure 4. *Combined propagation effect on the mass fraction X_i due to changes of recommended cross sections between the present work ("p.w.") and the Bao compilation [4] for the weak s-process. Full circles indicate even-Z isotopes, open circles odd-Z isotopes.*

Furthermore it is planned to include more radioactive isotopes, which are relevant for s-process nucleosynthesis at higher neutron densities (up to 10^{11} cm^{-3}). These isotopes are more than one unit away from the "classical" s-process path on the neutron-rich side of stability, and their stellar (n,γ) cross sections have to be extrapolated from known cross sections with support from Hauser-Feshbach predictions. The present list covers 73 new isotopes, including long-lived isomers like ^{108m}Ag, and is available on the KADoNiS homepage. However, only a few of these radioactive isotopes can be or have already been measured with present techniques (e.g. ^{60}Fe). Future cross section studies on unstable isotopes will benefit from sample production at radioactive beam facilities and from new or improved intense neutron sources.
Once all available datasets are implemented in the s-process database, a re-calculation of semi-empirical estimates based on the latest experimental results of neighboring nuclides will be performed. A paper version of KADoNiS will then be published in 2010.

Acknowledgements
I.D. is supported by the DFG cluster of excellence "Origin and Structure of the Universe".

References
[1] B.J. Allen et al., Adv. Nucl. Phys. 4 (1971) 205.
[2] Z.Y. Bao and F. Käppeler, At. Data Nucl. Data Tables 36 (1987) 411.
[3] H. Beer, F. Voss, and R.R. Winters, Astrophys. J. Suppl. 80 (1992) 403.
[4] Z.Y. Bao et al., At. Data Nucl. Data Tables 76 (2000) 70.
[5] T. Rauscher and F.-K. Thielemann, At. Data Nucl. Data Tables 75 (2000) 1.
[6] I. Dillmann et al., AIP Conf. Proc. 819, 123; online at http://www.kadonis.org.
[7] T. Rauscher, priv. comm. (2009).
[8] H. Beer and R. Spencer, Nucl. Phys. A 240, 29 (1975).
[9] H. Nassar et al., Phys. Rev. Lett. 94, 092504 (2005).
[10] A.M. Alpizar-Vicente et al., Phys. Rev. C 77, (2008) 015806.
[11] S. Walter, Ph.D. Thesis, Universität Karlsruhe (2008); Forschungszentrum Karlsruhe Report FZKA-7411.
[12] A. Tomyo et al., Astrophys. J. 623, (2005) L153.
[13] J. Marganiec, Ph. D. Thesis, University of Lodz/ Poland (2008).
[14] M. Heil et al., Phys. Rev. C 77, 015808 (2008).
[15] M. Pignatari, private communication (2009).

A new measurement of the prompt fission neutron emission spectrum of ^{235}U(n,f)

I. Fabry [1], N. Kornilov[1,2], F.-J. Hambsch[1], S. Oberstedt[1], T. Belgya[3], Z. Kis[3], L. Szentmiklosi[3], S. Simakov[4]

1) European Commission, Joint Research Centre, Institute for Reference Materials and Measurements, Retieseweg 111, 2440 Geel, Belgium
2) Accelerator Lab, Physics and Astronomy Department, Ohio Un., Athens, OH 45701, USA
3) Institute of Isotopes HAS, Dept. of Nuclear Research, Budapest, Hungary
4) Forschungszentrum Karlsruhe, Institut für Reaktorsicherheit, D-76344 Eggenstein-Leopoldshafen, Germany

Imrich.Fabry@ec.europa.eu

Abstract: The prompt fission neutron emission spectrum (PFNS) of ^{235}U(n,f) at 100 ^{o}K incident neutron energy was measured at the Budapest Reactor. The work was motivated by the discrepancy between literature data and the fact that the measured PFNS at thermal incident neutron energy can not be reproduced by theory. The PFNS was measured by the time-of-flight method with three neutron detectors at different angles, at a flight path length ~3m and a time resolution of 1.7 ns (FWHM). The ^{235}U spectrum was measured simultaneously relative to the ^{252}Cf standard spectrum to avoid systematic errors. Neutron scattering corrections were calculated by the Monte Carlo method. The spectra measured by three neutron detectors are in the excellent agreement with each other. The neutron detector efficiencies were calculated by Monte Carlo simulations and compared to the measured ones and show very good agreement. Finally, the resulting average neutron spectrum is in excellent agreement with literature data in the energy range of 0.7 - 10 MeV. Nevertheless, the present PFNS shape cannot predict integral experimental data. These results suggest that the disagreement between microscopic and macroscopic data is not due to a systematic experimental error of the PFNS at low incident neutron energy.

Introduction

As ^{235}U is the most important isotope for nuclear energy production, it is essential for a safe and economic use of nuclear power to understand the prompt fission neutron emission spectrum (PFNS) of ^{235}U(n,f). The PFNS has been investigated in several experiments at different incident neutron energies from thermal to the fast region. These efforts were motivated by a persistent discrepancy between microscopic and macroscopic (integral average cross section and K_{eff} experiments) data which still exists today, see e.g. Ref. [1]. Calculated spectra from differential measurements or based on model calculations cannot reproduce the integral measurements and differential data simultaneously.

The Working Party on Evaluation Cooperation (WPEC) of the OECD/NEA established a subgroup, which gave as recommendation that a new and highly accurate measurement of the prompt fission neutron spectrum for the reaction n(thermal)+^{235}U should be undertaken as soon as possible [2]. Based on this recommendation the JRC-IRMM started to measure the PFNS of ^{235}U(n,f). Three experiments were performed during 2006 to 2008. Eight PFN spectra have been measured at 0.5 MeV incident neutron energy at various emission angles [3]. Very good agreement was found of one of our spectra with at least one of the old experimental results. First results were presented at the Nuclear Data conference in Nice [4]. To investigate the thermal region and to answer the main question as to what is the “real” PFNS needed to describe both integral data and benchmark experiments motivated the present investigation in the frame of the EFNUDAT project [5].

Experimental setup and procedure

The PFNS was measured using the time-of-flight technique at the cold-neutron PGAA facility of the Budapest Nuclear Research Reactor [6] at 100 K incident neutron energy. The experimental setup is show in Fig. 1. The neutron flux was ~ $5 \cdot 10^7$ 1/cm^2·s, with a beam dimension at the measuring station of 2 x 2.5 cm^2. The experimental procedure is described in Ref. [7].

Three LSI301 (NE213-equivalent) organic liquid scintillator neutron detectors of the same size (Ø = 101.6 mm, h = 50.8 mm) were placed at different angles θ relative to the neutron beam, and at slightly different flight paths L (Det 1, θ = 72°, L = 298.1 cm, Det 2, θ = 102°, L = 282.8 cm, Det 3, θ= 132°, L = 301.1 cm). The uncertainties in flight path length and angle were ± 0.5 cm, and ± 1°, respectively. All detectors were coupled to XP4312 photomultiplier tubes and placed in massive shielding collimators.

The target consisted of a 112 μg/cm^2 thick, 97.7% enriched $^{235}UF_4$ target evaporated onto a thin polyimide foil (24 μg/cm^2) coated with gold (40 μg/cm^2). It was placed in the centre of the ionisation chamber (IC), see Fig. 2. The fission count rate was $5 \cdot 10^4$ 1/s. The fast current signal at the cathode (C_u) was used as the start signal. A ^{252}Cf layer (Ø = 10 mm) was placed in the same chamber but shifted out of the neutron beam by 5cm relative to the U layer. The fission fragment count rate was $2 \cdot 10^4$ 1/s. The fission fragment counting efficiency was 98% for both neutron sources and was measured as described in Ref. [7]. The Ionization chamber was used with a constant flow of P10 (90% Ar and 10% CH_4) counting gas at atmospheric pressure.

The electronic setup is shown in Fig. 3. For each neutron detector, the pulse height and pulse shape were recorded using a fast MPD-4 pulse shape discriminator module. The anode signal of the photomultiplier tube was used for the pulse height as well as for pulse shape analysis for the neutron-gamma discrimination. For the time-of-flight measurement the dynode signals were used and each of the neutron detectors could provide the start of the TAC. The fast cathode current signal from the ionization chamber for both sources were used as "neutron tagger" via a fast current preamplifier, TFA, and CFD as stop signal for the TAC module. The signals were delayed with a long cable for about 500 ns to detect "parent" pulses created by fission fragments for any of the neutron detector pulse. The data acquisition system allowed identifying fission fragment events either from the ^{235}U or ^{252}Cf cathode.

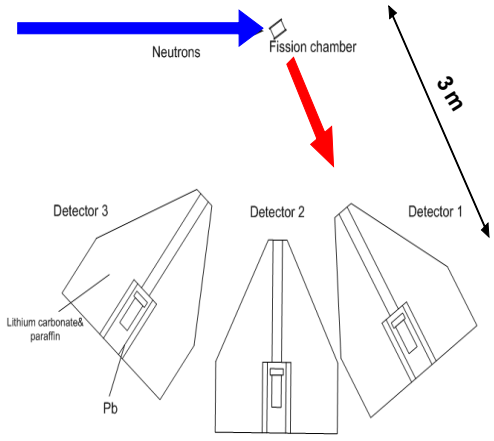

Figure 1. *Experimental setup together with the three n-detectors located in their heavy shielding.*

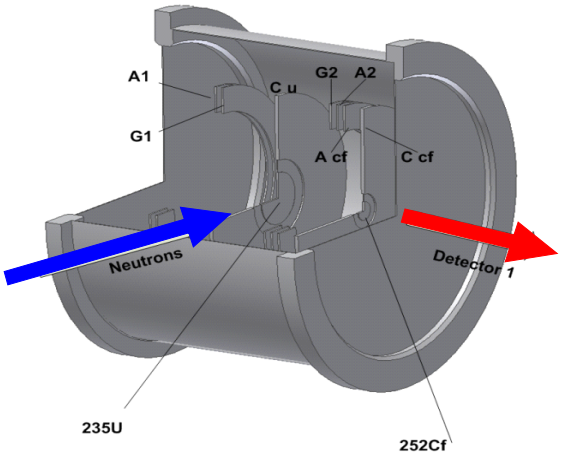

Figure 2. *Schematical view of the double Frisch grid ionisation chamber with both U and Cf sources.*

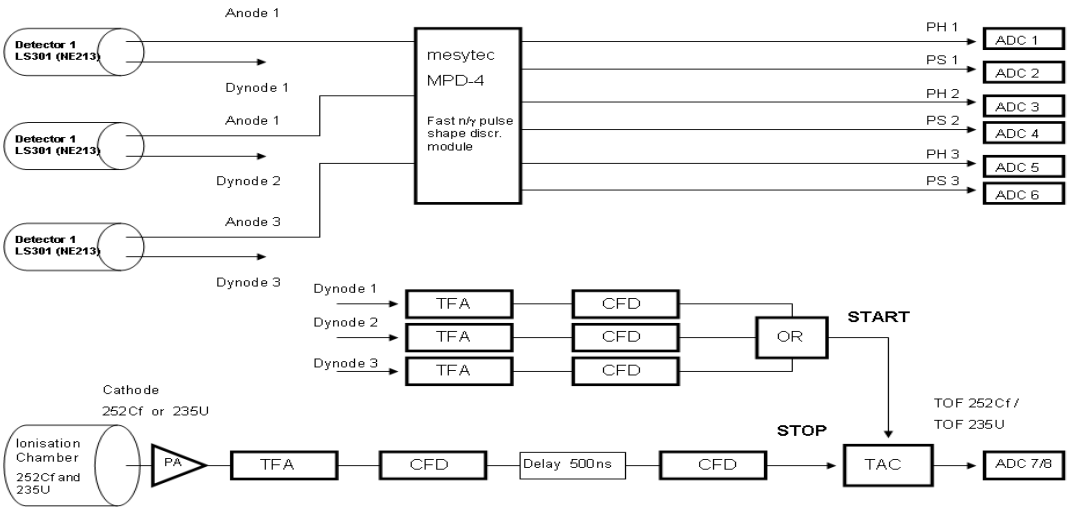

Figure 3. *The electronics setup used in the experiment.*

Data Analysis

The data analysis was performed as described in Ref. [7]. The data were stored in list mode using the data acquisition software GENDARC [8]. An event was stored when one of the neutron detectors had fired. The calibration of the pulse height scale was done using gamma sources. After proper selection between neutron and gamma events a γ-ray suppression factor of 200 was achieved. The time shift (time walk) as a function of the pulse height was corrected. The channel width for each TAC (together with the corresponding ADC) was measured with an accuracy of < 0.1 % to 0.1178 ns and 0.1150 ns for the U- and Cf-channels, respectively. The detector thresholds were ~ 0.6 MeV. The total count rate from all detectors was about 5000 1/s mainly due to γ-rays from neutron capture in the stainless steel of the ionization chamber.

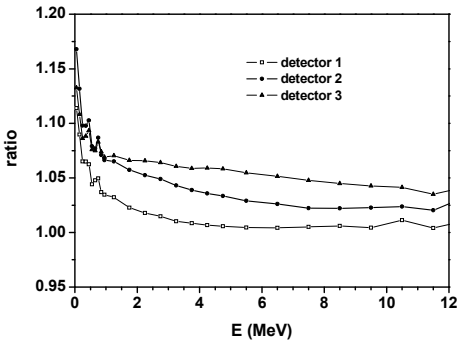

Figure 4. *Ratio of multiple scattering corrections for Cf- and U- sources.*

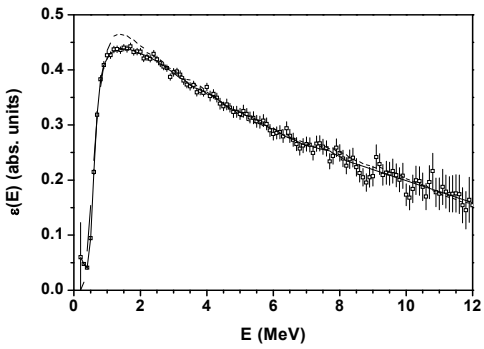

Figure 5. *Efficiency of neutron detector. Line trend and Monte Carlo result are shown by solid and dashed lines.*

A total of about 10^6 neutron events for each detector were collected during ~ 50 hours. In a first stage the stability of the electronic units and the neutron detectors was tested. In the final stage all list mode data were analyzed as one single file. The TOF spectra were corrected for time independent and time correlated background which was subtracted [7].
Monte Carlo simulations using MCNP were performed to calculate correction factors for the U and Cf sources for multiple scattering and attenuation as a ratio of a neutron spectrum emitted from the source surrounded by the real chamber to a spectrum calculated without chamber materials. The ratio of the correction factors of Cf to U is shown in Fig. 3 for the three detectors.
The efficiency for detector 1 is shown in Fig. 4. The error bars include statistical error and systematic uncertainties of the ^{252}Cf standard. The trend line used for the U energy spectrum calculation is also in good agreement with Monte-Carlo simulations of the neutron detectors [7, 9, 10]. A small difference of 6 % at low energy may be explained due to imperfect neutron-gamma discrimination.
A timing resolution of 1.7 ns (^{252}Cf) and 2.1 ns (^{235}U) was achieved. The different timing resolutions are due to a smaller capacitance and larger cathode signal since both fission fragments are detected in the U- chamber. As the timing resolution is similar in both cases no correction was incorporated.

Comparison to literature data

The experimental PFNS was normalized to unity and the average secondary neutron energy was calculated. A Maxwellian spectrum was fitted in the energy range of 0.7 - 1.5 MeV and 9 - 11 MeV to the measured spectrum and an extrapolation to zero and to 20 MeV was performed. Since the fission count rate is known, also the multiplicity of the prompt fission neutrons may be calculated. The average energy <*E*> and the number of prompt neutrons per fission (ν-prompt) for each detector are shown in Table 1. The average multiplicity for all detectors is <ν> = 2.47 ± 0.08. This value is in reasonable agreement with evaluated data (<ν> = 2.421; ENDF/B-VII). The ~3.5% spread may be a result of uncertainties in the chamber and detector orientations.

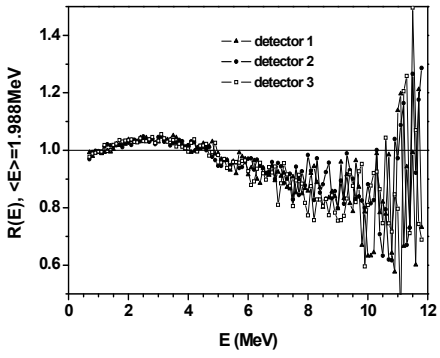

Figure 6. *The PFNS measured by three neutron detectors as a ratio to a Maxwellian spectrum with average energy <E> = 1.988MeV.*

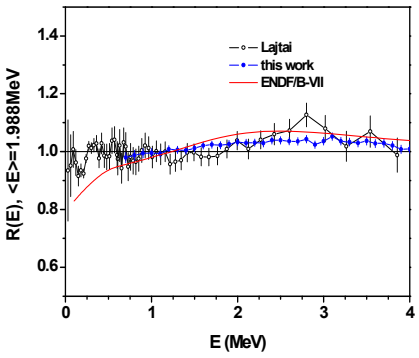

Figure 7. *Comparison between our results, averaged over all detectors, and Ref. [13]. All data are shown as a ratio to a Maxwellian spectrum.*

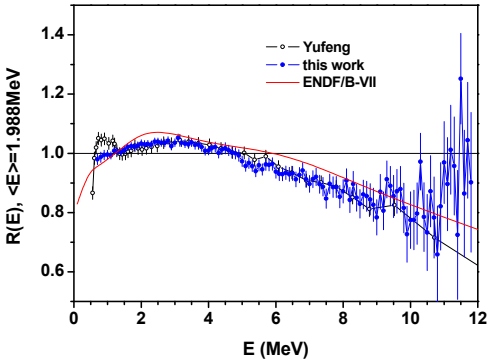

Figure 8. *Comparison between our results, averaged over all detectors, and Ref. [12].*

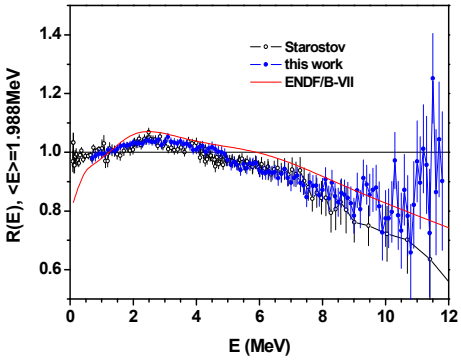

Figure 9. *Comparison between our results and Ref. [11].*

The spectra measured with the three detectors are in excellent agreement and do not exhibit any angular dependence (see Fig. 6). The average spectrum of the three detectors (<*E*> = 1.988 ± 0.010 MeV) agrees inside error bars with data from Ref. [12] in the energy range 0.7 - 11 MeV (see Fig. 8), with data of Ref. [13] in the energy range 1.5 - 12 MeV, and Ref. [13] in the energy range 0.7 - 4 MeV (Fig. 7). At the same time all the results mentioned above contradict the ENDF/B-VII evaluation and the Los Alamos model (full line in above Figures).

Table 1. *Average parameters of the PFNS for the reaction 235U(nth,f)*

Detector No.	Angle, degree	<*E*>, MeV	v-prompt
1	72	1.987	2.491
2	102	1.990	2.548
3	132	1.987	2.378

New Model for PFNS Calculation

So far PFNS modelling is based on the assumption of neutron emission from fully accelerated fragments. We have shown in Fig. 6 that the presently measured PFNS can not be described by the Los Alamos model. Hence, a new approach is proposed which also includes scission neutron emission (SCN). This leads to a model with three neutron sources: emission from the compound nucleus, emission from the nucleus after scission neutron emission and scission neutron emission. The information about scission neutron emission is very scarce. In Ref. [14] an estimation is given that the probability of fission with scission neutron emission is about 40 %, and that the scission neutron spectrum consists of a low (~ 0.8 MeV) and a high (~ 2.5 MeV) energy component. In Ref. [14] evidence was given that scission neutrons are emitted by a compact fissile system (fission fragments with high total kinetic energy). If SCN emission is considered, the resulting spectrum is therefore composed of three sources:

$$N(E) = N_{A+1}(E) + N_A(E) + N_{SCN}(E) \qquad (1)$$

The different terms of eq. (1) are given as follows:

1. Neutrons from fragments after fission of the compound nucleus A+1

$$N_{A+1}(E) = (1-\alpha)\cdot W_{A+1}(E) \qquad (2)$$

where α is the share of scission neutrons and W_{A+1} is the spectrum which describes the neutron emission from accelerated fragments;

2. Neutrons from accelerated fragments after fission of the nucleus A, which is formed due to the emission of one SCN:

$$N_A(E) = \alpha\cdot(\nu-1)\cdot W_A(E)/\nu\,. \qquad (3)$$

3. Scission neutrons themselves:

$$N_{scn}(E) = \frac{\alpha}{\nu}\cdot E\cdot\left(\frac{\varsigma}{T_1^2}\exp\left(-\frac{E}{T_1}\right)+\frac{1-\varsigma}{T_2^2}\exp\left(-\frac{E}{T_2}\right)\right), \qquad (4)$$

where ζ is the share of the low energy component and □ is the neutron multiplicity.
The spectrum W_{A+1} was taken from the ENDF/B-VII library for thermal energy. The spectrum W_A was found by extrapolation of the ENDF/B-VII data to the energy a fissile system has after emission of one SCN E_o-B_n-$<E_{scn}>$ = -8.5 MeV. So, these spectra were calculated on the basis of the Los Alamos model [16]. The equation for $N_{scn}(E)$, and the corresponding parameters α, T_1, T_2 were taken from Ref. [14] introducing minor corrections: α = 0.41, T_1 = 0.34 MeV, T_2 = 1.31 MeV, ζ=0.26.
The model spectra according to eqs. (1-4), are shown together with the data of the present experiment in Fig. 7. The average energy is $<E_{cal}>$ = 1.986 MeV. The residual chi-square is χ^2 = 0.64. The calculated spectrum describes the total set of the experimental data from 0.1 MeV to 12 MeV within the error bars.

Comparison to integral Data

The data of the IRDF-2002 dosimetry library and experimental average cross sections [17] were used for the validation of the measured PFNS. We used only those threshold reactions which provide a good agreement between calculated and experimental data for ^{252}Cf. Together with the average cross sections the average energies of the reaction response were calculated. We compared the ratio of calculated and experimental cross sections R=C/E for different PFNS. 17 threshold reactions with three PFNS were checked. The average ratios are: ^{252}Cf (Ref.18) <R>=0.995±0.004, ^{235}U (ENDF/B-VII), <R>=0.998±0.009, ^{235}U(this work, eqs 1-4), <R>=0.938±0.010.
The ratio R = C/E versus average energy of the reaction response for ^{235}U for both the present experimental spectrum as well as for the ENDF/B-VII spectrum is shown in Fig. 11. It is obvious that the measured PFNS of ^{235}U which is in excellent agreement with literature data is not able to describe the integral experiments.

Possible source of discrepancies between microscopic and macroscopic data

For the ENDF/B-VII [19] data library significant systematic uncertainties for the PFNS at thermal energy have been assumed, although it was proclaimed that experimental fission neutron spectra above 2 MeV and integral experiments at the thermal point do not contain systematic errors and may be used for neutron data library preparation. This has lead to the incorporation of an unphysical dependence (Fig. 9 from Ref. [19]) for the average energy of the PFNS of ^{235}U, to describe successfully the majority of benchmark experiments (K_{eff}). This strange dependence can not be explained in the frame of existing models for PFNS calculation and, as a consequence, can not be applied for other fissile isotopes.
Different experimental setups were developed for the creation of the ^{235}U fission neutron field used in integral experiments. In Ref. [20] a big plate of ^{235}U (1.1 cm thick and 31.3 cm in diameter) exposed to thermal neutrons was used as a source of prompt fission neutrons. The authors simulated the experimental set up with the MCNP code. The ^{27}Al(n,α) reaction was used as a neutron flux monitor.
In Ref. [21] the source configuration Makr IIA was used. The activated samples were placed inside a ^{235}U (89.66% enrichment) cylinder with a height of 79.6 mm and a wall thickness of

0.18 mm. The perturbation effect was calculated on the basis of the ENDF/B-IV neutron data library and the 171 group structure VITAMIN-C. The corrections were in the order of (4-9%) depending on the reaction threshold.
It is very difficult to find systematic uncertainties which may increase the average energy of the neutron spectrum measured with integral experiments relative to microscopic ones. Multiple scattering of fission neutrons inside a large sample may reduce the average energy but not increase it. The results of different integral experiments are also in good agreement. This leads to the conclusion that probably integral experimental results are correct, too. In addition, the PFNS that describes the integral data is able to calculate K_{eff} in benchmark experiments. An obvious conclusion could be that we do not understand the mechanism of neutron emission in fission and the fission process itself.
Incorporation of SCN emission into the theoretical model is not enough. We should assume that PFNS formation (SCN emission) and interaction of the neutrons depend both on the same parameter *p*. The large amount of fissile material which is involved in the process may provide an additional selection of the *p* parameter and as a result may change the PFNS in large samples. This effect may explain the difference between microscopic and macroscopic results for PFNS estimation.

Summary and conclusions

The ^{235}U(n,f) prompt fission neutron spectrum was measured using the time-of-flight technique at the cold-neutron PGAA facility of the Budapest Nuclear Research Reactor at 100 K incident neutron energy. We would like to highlight the following points:

1. The PFNS was measured simultaneously relative to ^{252}Cf, which minimized systematic errors.
2. The measurements with three independent neutron detectors are in excellent agreement. With each other. No angular effect has been observed.
3. The measured thermal microscopic PFNS doesn't agree with the integral experiments nor the benchmark results (K_{eff}).
4. Our new results are in very good- excellent agreement with literature data. The PFNS at thermal energy does not confirm the model calculations based on the assumption that fission neutrons are emitted from fully accelerated fragments alone.
5. An improved model using scission neutron emission describes all experimental data at thermal energy within the error bars in the energy range from 0.1 - 12 MeV.

Acknowledgements
This experiment was supported by the European Commission within the Sixth Framework Programme of EURATOM through the Integrated Infrastructure Initiative EFNUDAT ("European Facilities for Nuclear Data Measurements" Contract No. FP6-036434).

References
[1] P.I. Johansson, B. Holmqvist, Nucl. Sci. Eng. 62 (1977) 695.
[2] D.G. Madland, ISBN-92-64-02134-5, NEA/WPEC-9, 2003.
[3] N.V. Kornilov, F.-J. Hambsch, I. Fabry, S. Oberstedt, JRC-IRMM, Neutron Physics Unit, Scientific report 2007 (2008), p. 27.
[4] N.V. Kornilov, F.-J. Hambsch, I. Fabry et al., Proc. of the Int. Conf on Nucl. Data for Sci. and Tech. (ND2007), Nice, France, Apr. 22-27, 2007, EDP Sciences (2008), p. 387.
[5] EFNUDAT-2008, www.efnudat.eu.
[6] Z. Révay, T. Belgya, Z. Kasztovszky, J.L. Weil, and G.L. Molnár, NIM B213 (2004) 385-388.
[7] N.V. Kornilov, I. Fabry, S. Oberstedt, F.-J. Hambsch, NIM A599 (2009) 226.
[8] I. Fabry, JRC Technical Notes GE/NP/01/2008/01/13, JRC-IRMM, 2008.
[9] I. Fabry, Diploma thesis, Bonn University, 1998, unpublished.

[10] G. Dietze, H. Klein, PTB-ND-22 Report (1982).
[11] B.I. Starostov et al., Nejtronnaja Fizika (6-th Conf. for Neutron Phys., Kiev. 1983), 1984. v2. p 285, 290, 294, EXFOR 40871, 40872, 40873.
[12] W. Yufeng et al., Chin. J. Nucl. Phys. 11(1989) 47, EXFOR 32587.
[13] A. Lajtai, IAEA-TECDOC-335, 1985, 312, EXFOR 30704.
[14] N.V. Kornilov, A.B. Kagalenko, F.-J. Hambsch et al., Nucl. Phys. A686, 2001, 187., Phys. of Atomic Nuclei 64, 2001, 1372.
[15] N.V. Kornilov, F.-J. Hambsch, A.S. Vorobyev, Nucl. Phys. A789, 2007, 55.
[16] D.G. Madland, J.R. Nix, Nucl. Sci. Eng. 81 (1982) 213.
[17] K.I. Zolatorev, INDC(NDC)-448, 2003, 25.
[18] W. Mannhart, Proc. Advisory Group Meeting on Properties of Neutron Sources, Leningrad, June 1986, report IAEA-TECDOC-410, Ed. K. Okamoto.
[19] M.B. Chadwick et. al. Nuclear Data Sheets 107 (2006) 2931.
[20] K. Kobayashi, T. Kobayashi, Progress Report NEANDC(J)-155/U, p.52, 1990.
[21] W. Mannhart Proc. 5-th ASTM-EURATOM Symp. on Reactor Dosimetry. Geesthacht, Sep.24-28, 1984, Vol.2, p.813, 1985.

Measurement of the $^{16}O(n,\alpha_0)^{13}C$ cross section

G. Giorginis[1)], V. Khryachkov[1,2)], M. Kievets[1)], V. Corcalciuc[1,3)]

1) European Commission, Joint Research Centre, Institute for Reference Materials and Measurements (IRMM), Retieseweg 111, 2440 Geel, Belgium
2) Institute for Physics and Power Engineering (IPPE), Obninsk, 249020, Russia
3) Institute for Physics and Nuclear Engineering, PO BOX MG6, Bucharest, Romania
georgios.giorginis@ec.europa.eu

Abstract: A TPC (time projection chamber) was developed and used at IRMM to measure the $^{16}O(n,\alpha_0)^{13}C$ cross section for neutron energies between 3.9 and 9 MeV. The basic components of this novel charged particle spectrometer are a gridded ionisation chamber with signal digitisation and a krypton/carbon dioxide mixture as detector gas. The oxygen of the carbon dioxide was used as target for the $^{16}O(n,\alpha_0)^{13}C$ the reaction. The amplitude and time information of the digitised signals were used to determine the energy of the alpha particles and effectively suppress interfering background, respectively. Two measurements of low energy resolution were performed in the energy intervals 3.9-5.2 MeV and 6-9 MeV with T(p,n) and D(d,n) neutrons by using thick TiT and deuterium gas targets, respectively. The measured cross sections corrected for energy resolution by indirect deconvolution are in very good agreement with the ENDF/B-VII.0 evaluation below 5.2 MeV but the agreement is good with ENDF/B-VI.8 above 6 MeV. Two additional measurements with high energy resolution by using thin TiT targets for neutron production confirmed the scale and the shape of the ENDF/B-VII.0 excitation function in the 3.9-5.2 MeV range.

Introduction

Accurate neutron data for oxygen are of prime importance in nuclear applications. A request for the measurement and evaluation of the $^{16}O(n,\alpha)^{13}C$ cross section in the range 2.5-10 MeV was submitted in 2005 to the High Priority Request List (HPRL), which is maintained by the Nuclear Energy Agency (NEA) [1]. A 5% accuracy instead of currently 30% is needed in order to improve predictions of the effective multiplication factor k_{eff} and helium production for thermal and fast reactors, as well as to achieve a higher precision in the calibration of neutron sources using the manganese sulfate bath technique. The ENDF/B-VI.8 (2001) and ENDF/B-VII.0 (2006) evaluations of the $^{16}O(n,\alpha)^{13}C$ cross section are based on measurements of the inverse reaction $^{13}C(\alpha,n)^{16}O$ by Bair and Haas [2] and Harissopulos et al. [3], respectively. In the latter case a comparison is reported showing that the $^{13}C(\alpha,n)^{16}O$ cross section is in the mean 32% lower than in the former case for α particle energies 2.3-5.0 MeV. Although this corresponds to 4.2-6.4 MeV neutron energy for the direct ground state reaction $^{16}O(n,\alpha_0)^{13}C$ the 32% reduction was applied in the extended 2.4-8.9 MeV range in order to produce ENDF/B-VII.0 from ENDF/B-VI.8 [4]. In the range 3-8 MeV neutron energy the $^{16}O(n,\alpha)^{13}C$ cross section in JENDL-3.3 (2002) is 10%-50 % lower than in ENDF/B-VI.8. A novel experimental technique was developed and used at IRMM in order to produce data with the requested accuracy (5%) and resolve the large discrepancies between existing measurements and evaluations. The principles of the experimental technique and the status of the measurements at IRMM are presented in this paper.

Charged particle spectrometer

A 1D-TPC (one-dimensional time projection chamber) was used for the spectrometry of charged particles. The main components of the new instrument are a gridded ionisation chamber (GIC) and signal digitisation, as is schematically shown in Fig. 1. The oxygen content of the detector gas, a $Kr(97\%)CO_2(3\%)$ mixture, was used as target in cross section measurements of the $^{16}O(n,\alpha)^{13}C$ reaction. A thin ^{238}U standard mounted on the reverse side of the GIC cathode in a back-to-back geometry was used as monitor of the incident neutron beam. The fission fragments were detected by an ionisation chamber without grid which had the same cathode with the main chamber. Monoenergetic neutrons below 5.2 MeV and above

4.9 MeV were produced at the 7 MV Van de Graaff accelerator of IRMM by using the T(p,n)^{3}He and D(d,n)^{3}He reactions, respectively. The anode signals of the GIC and the common cathode signals at the exit of the corresponding charge sensitive preamplifiers were linearly amplified (without shaping) and fed to the inputs of a two channel waveform digitiser (WFD, Signatec, model PDA12A, 12 bit). The digitisation rate was 62.5 MHz or equivalently a signal sample was taken every 16 ns.

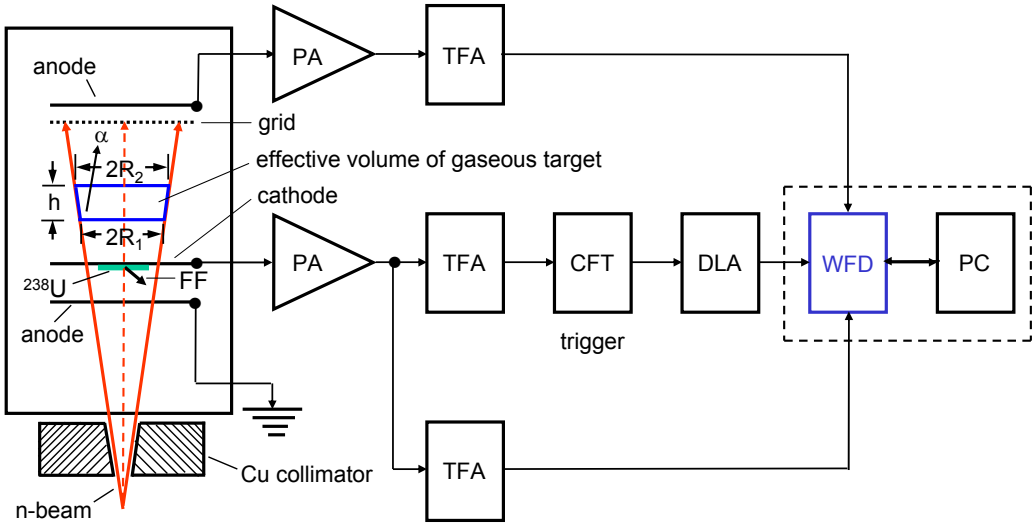

Figure 1. *Block diagramme of the IRMM experimental setup (1D-TPC).*

Typical digitised signals of an α particle and a fission fragment can be seen in Fig. 2. They contain all needed information for the production of clean ^{16}O(n,α)^{13}C and ^{238}U fission signatures, which is a condition for accurate cross section measurements.

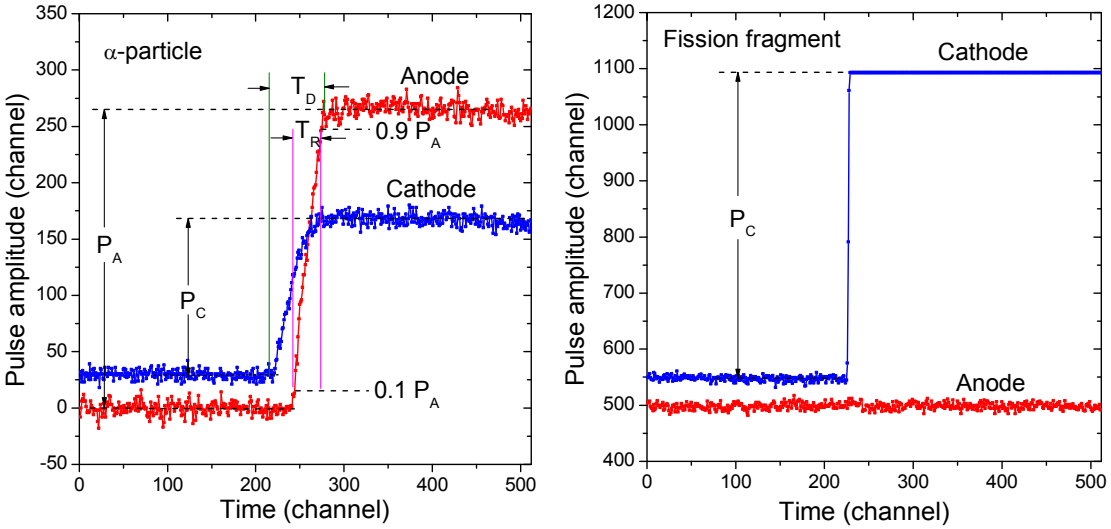

Figure 2. *Digitised signals of an α particle (left) and a fission fragment (right).*

Off-line analysis of digitised signals

The analysis software is composed of a series of algorithms for the reduction and visualisation of digitised data. In comparison to the conventional GIC (gridded ionisation chamber), which only uses pulse heights, the TPC uses in addition the time information of the signals for background reduction. The rise time of the anode signal T_R (see Fig. 2) was used to resolve α particles from protons as illustrated in Fig. 3 (left), which is a two-dimensional

spectrum of the rise time versus the pulse amplitude of the anode signal. The analysis software eliminates the events above the dashed line, keeps the α particle component, and produces a two-dimensional spectrum of the drift time of the origin (or end) of the particle track T_D (see Fig. 2) versus the anode pulse amplitude as shown in Fig. 3 (right). The dashed rectangle defines a region of interest (ROI) containing those α_0 particles with track origin (or end) in the effective target volume and track end (or origin) within the sensitive detection volume between cathode and grid. The drift time window ΔT_D determines the height **h** of the effective volume of the gaseous target (see Fig. 1).

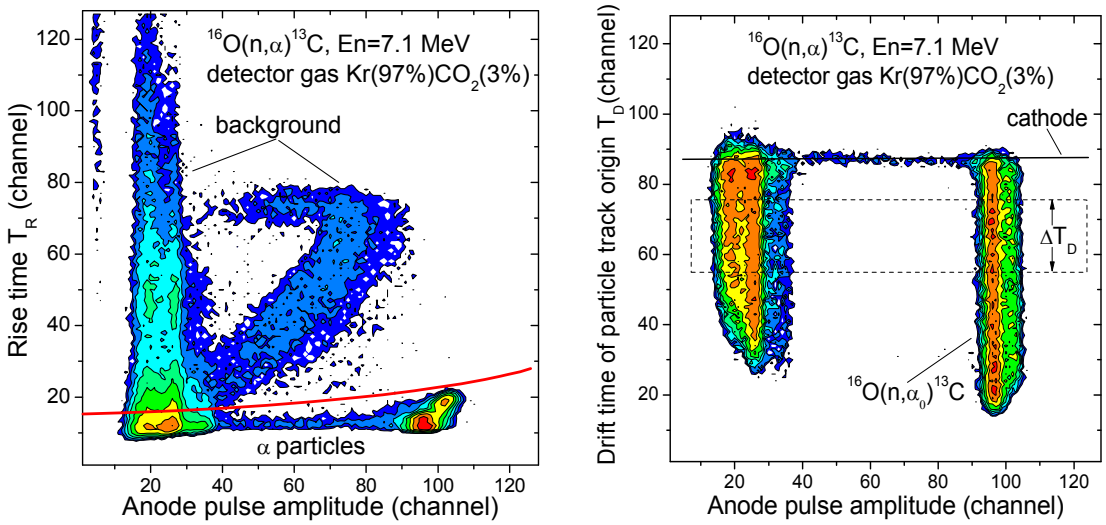

Figure 3. *Two dimensional spectrum of anode pulse amplitude versus rise time of anode signal (left) and drift time of the origin (or end) of the particle track (right), respectively.*

The achieved background suppression can be seen in a comparison between pulse height spectra obtained by using the GIC and TPC modes of operation of the spectrometer as shown in Fig. 4. The pulse height window ΔP_A in mode (3) was used to obtain the number of $^{16}O(n,\alpha_0)^{13}C$ events for the cross section determination.

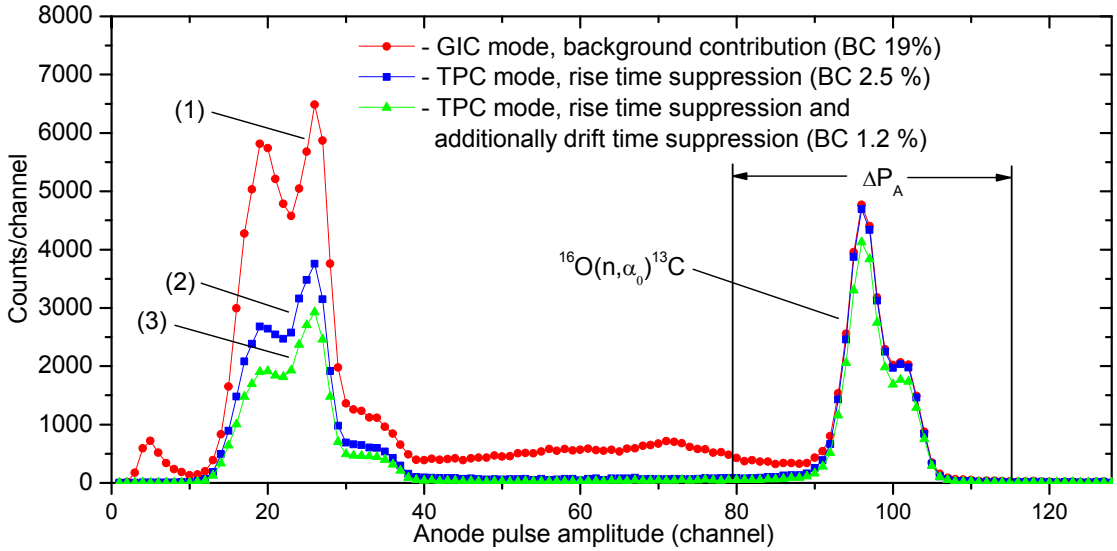

Figure 4. *Pulse height spectrum measured with the charged particle spectrometer in: (1) GIC mode, (2) TPC mode after rise time suppression of background, and (3) TPC mode after rise time and drift time suppression of background. The percentages in brackets show the background contribution (BC) to the α particle line within the pulse height window ΔP_A for the three different operation modes of the spectrometer.*

The FNBP (fast neutron beam profiling) technique

The use of a gaseous reaction target requires the determination of an effective volume in a way that α particles produced in this volume are fully stopped within the detection volume which is determined by the electrodes of the cathode and grid in order to avoid wall effects. Furthermore the dimensions of the effective volume have to be well known for an accurate calculation of the number of target atoms. The effective volume in the present application is a truncated cone. Its height is deduced from the drift time of the origin (or end) of the α particle track T_D (see Fig. 1-3) as discussed above. The radius of the cone at each of the two circular bases was determined by a new FNBP technique, which was developed at IRMM. Two sets of aluminium (Al) and indium (In) rings of equal diameter installed at the exit of the copper collimator along its axis were activated by neutron beams of 7.4 and 2.5 MeV, respectively. The projection of each ring length on the exit radius of the collimator was equal to one mm. The radius of the cone at the collimator exit R_0 was determined by fitting an error function to the gamma ray yields of the activated rings as shown in Fig. 5 (left) for the Al rings. Rotational symmetry was proved by using neutron activation of two sets of 24 aluminium and indium disks installed with their centres on the circle of the collimator exit, so that part of each disk was in the shadow of the collimator and part directly exposed to neutron beams of 7.4 and 2.5 MeV, respectively. A disk at the centre of the collimator was used for normalisation. A beam radius was obtained for each disk using proportionality between the measured gamma ray yield and the disk surface exposed to the neutron beam. A circle fitted to the set of the 24 radii provided the proof for rotational symmetry as shown in Fig. 5 (right) for the Al rings. The disks technique is another method for the determination of the neutron beam radius at the collimator exit. Due to its simplicity it is more accurate than the rings technique. For this reason the R_0 value of 38.64 mm (disks) and not 37.73 (rings) was used to determine the radii R_1 and R_2 of the effective target volume (see Fig. 1). On the other hand the rings technique determines with high resolution the radial shape of the neutron beam profile. The results obtained with indium rings and disks at 2.5 MeV neutron energy were in very good agreement with those measured with aluminium using 7.4 MeV neutrons.

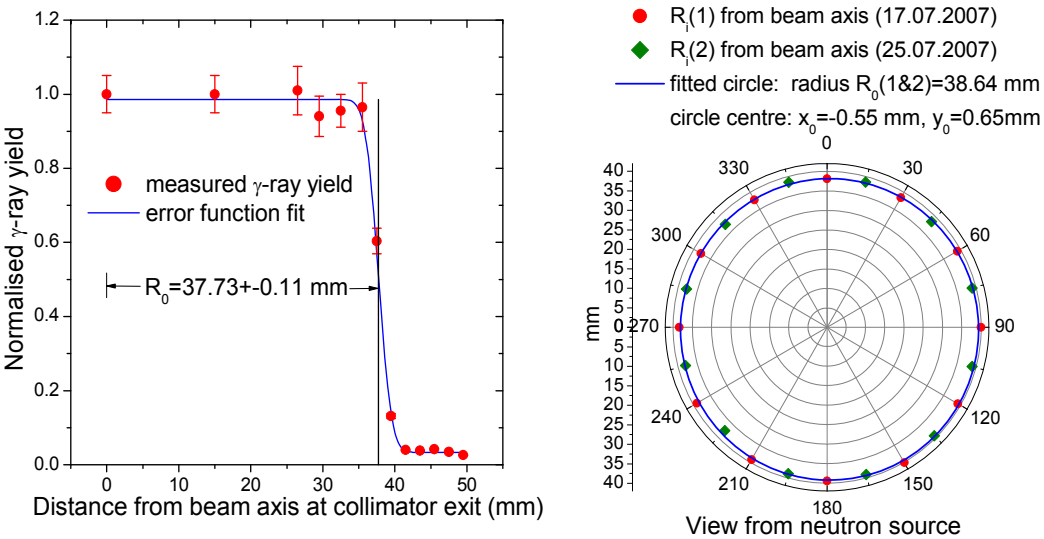

Figure 5. *Fast neutron beam profile (radial) at the exit of the Cu collimator measured by using neutron activation of Al rings (left), shape (rotational symmetric) of the neutron beam at the exit of the Cu collimator obtained by using Al discs (right).*

Cross section

The number of reacting atoms was determined from the effective volume and the atomic density of oxygen. The former is a function of $R_1(\sim R_0)$, $R_2(\sim R_0)$, and $h(\sim \Delta T_D)$, with R_0, and ΔT_D obtained as described above. The latter is a function of the gas pressure, temperature, and composition provided by the gas manufacturer. The number of $^{16}O(n,\alpha_0)$ events was

deduced as discussed in the off-line analysis section. The neutron flux was obtained from the fission yield of the ^{238}U standard measured simultaneously with the ^{16}O(n,α_0) reaction yield. The cross section as function of neutron energy (excitation function) in the 3.9-5.2 MeV range measured at IRMM with a 1941 μg/cm^2 TiT target and the T(p,n)^{3}He reaction as neutron source is shown in Fig. 6. The convolution of the ENDF/B-VII.0 excitation function with the energy resolution (indirect deconvolution) is in very good agreement with the IRMM data.

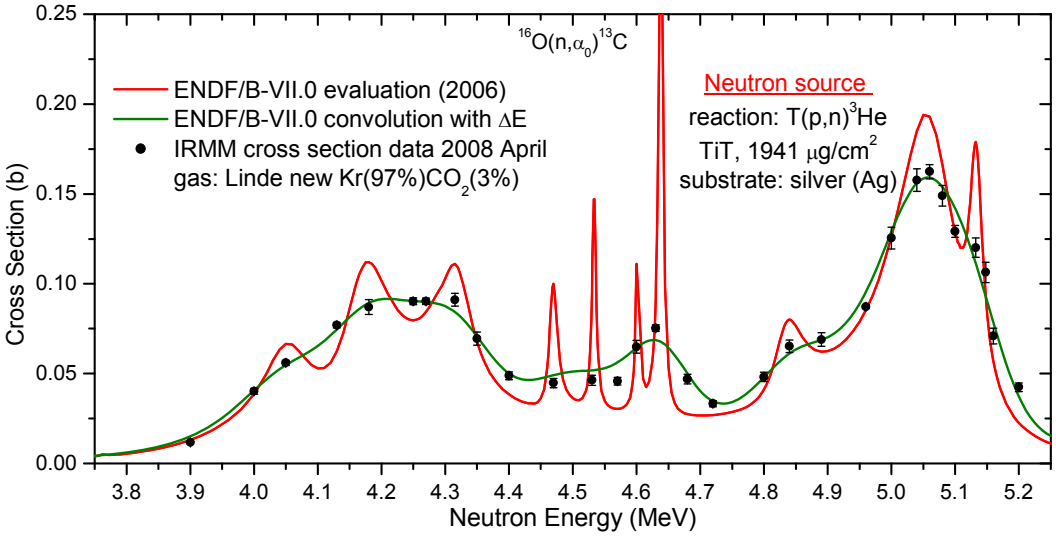

Figure 6. *Excitation function of ^{16}O(n,α_0)^{13}C measured with a low resolution neutron beam (filled black circles) at IRMM compared with ENDF/B-VII.0 (solid red line) and its convolution with the experimental energy resolution (solid olive green line).*

The cross section in the 4.9-9.0 MeV range measured at IRMM with a gas deuterium target and the D(d,n)^{3}He reaction as neutron source is shown in Fig. 7. The convolution of the ENDF/B-VII.0 excitation function with the energy resolution (CONV) is in very good agreement with the IRMM data in the region of the 5.04 MeV resonance. Above 6 MeV CONV had to be height adjusted in order to achieve agreement with the IRMM data.

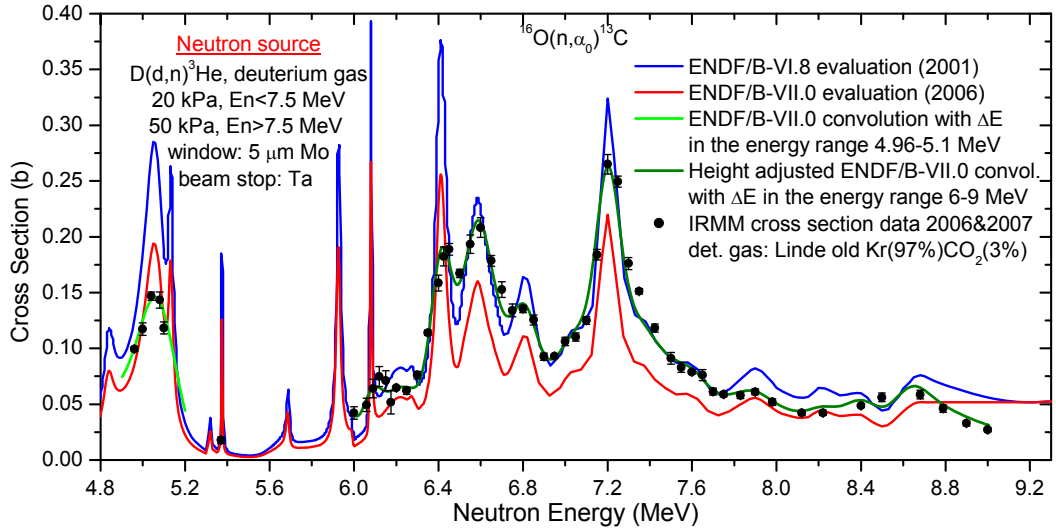

Figure 7. *Excitation function of ^{16}O(n,α_0)^{13}C measured at IRMM with a low resolution neutron beam (filled black circles) compared with ENDF/B-VII.0 (solid red line), ENDF/B-VI.8 (solid blue line), ENDF/B-VII.0 convolution with the experimental energy resolution for 4.9-5.1 MeV (solid green line), and height adjusted ENDF/B-VII.0 convolution with the experimental energy resolution for 6-9 MeV (solid olive green line).*

From the height adjustment of CONV as function of neutron energy a normalisation function NF was obtained. NF is constant with a value of 1 in the 3.9-5.2 MeV range and varies with energy in the 6-9 MeV range with a maximum value of 1.56. A new ENDF normalisation was produced by multiplication of NF with ENDF/B-VII.0. The normalised ENDF/B-VII.0 is identical to the original ENDF/B-VII.0 for energies 3.9-5.2 and is in good general agreement with ENDF/B-VI.8 for energies 6-9 MeV as shown in Fig. 8.

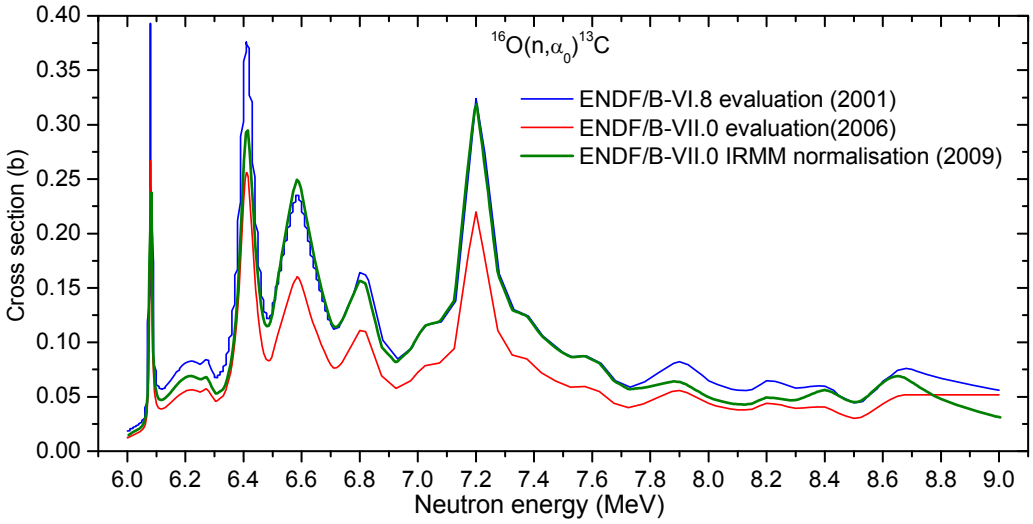

Figure 8. *ENDF/B-VII.0 and ENDF/B-VI.8 in comparison with ENDF/B-VII.IRMM for the $^{16}O(n,\alpha_0)^{13}C$ cross section. ENDF/B-VII.IRMM is the result of the correction of the IRMM data for energy resolution by using the shape of the ENDF/B-VII.0 excitation function and the experimental energy resolution.*

Two additional high resolution cross section measurements at IRMM by using 214 and 493 μg/cm^2 TiT targets and the T(p,n)^{3}He reaction as neutron sources confirmed again the scale and shape of ENDF/B-VII.0 in the 3.9-5.2 MeV range. The overall accuracy of the $^{16}O(n,\alpha_0)^{13}C$ cross section measured at IRMM with the new TPC and FNBP techniques is 6%.

Conclusion

Three measurements of the $^{16}O(n,\alpha_0)^{13}C$ cross section in the lower part (3.9-5.2 MeV) and one in the upper part (4.9-9 MeV) of the requested 2.5-10 MeV energy interval confirmed the shape and scale of the ENDF/B-VII.0 in the 3.9-5.2 MeV range. A new ENDF/B-VII.0 normalisation was obtained for 6-9 Mev energies, which is in good general agreement with ENDF/B-VI.8. The achieved accuracy of 6% is very close to the requested 5% value.

References

[1] http://www.nea.fr/html/dbdata/hprl/hprlview.pl?ID=417.
[2] J.K. Bair and F.X. Haas, Phys. Rev. C, 7 (1973) 1356.
[3] S. Harissopulos, H. W. Becker, J. W. Hammer, A. Lagoyannis, C. Rolfs, and F. Strieder, Phys. Rev. C 72, 062801(R) (2005).
[4] http://www.nndc.bnl.gov/exfor/servlet/E4sGetIntSection?SectID=13857&req=87108.

Operation of the liquid lead loop at nELBE

A. R. Junghans[1)], R. Beyer[1)], E. Birgersson[1)], E. Grosse[1,2)], R. Hannaske[1)], A. Matic[1)], M. Mosconi[3)], R. Nolte[3)], K.-D. Schilling[1)], R. Schwengner[1)], A. Wagner[1)]

1) Forschungszentrum Dresden-Rossendorf, Institute of Radiation Physics, Bautzner Landstr. 400, 01314 Dresden, Germany
2) Technische Universität Dresden, 01062 Dresden, Germany
3) Physikalisch-Technische Bundesanstalt Braunschweig, Bundesallee 100, 38116 Braunschweig, Germany

a.junghans@fzd.de

Abstract: The photoneutron source at Forschungszentrum Dresden-Rossendorf operates a liquid lead circuit as a neutron radiator, which has been operational since November 2007. The electron beam with electron energy up to 40 MeV from the superconducting electron linac with high brilliance and low emittance (ELBE) hits the liquid lead in a small sub-cm^3 volume, where the neutrons are produced in sub-ns pulses. The short beam pulses of ~10 ps provide the basis for an excellent time resolution for neutron time-of-flight experiments, giving an energy resolution of about < 1 % at 1 MeV with a short flight path of ~ 6 m. The neutrons pass to the measurement room through a thick concrete wall via a collimator. The beam profile through the collimator has been investigated by horizontal and vertical scans of the electron beam on the radiator.

Introduction

In the EURATOM FP6 program partitioning of nuclear waste and transmutation of long-lived isotopes to nuclides with shorter lifetime are being investigated. In 2003 EURATOM joined the Generation IV International Forum [1], where six different transmutation schemes have been proposed. The primary goals for generation IV (Gen-IV) nuclear reactors are to improve nuclear safety, improve proliferation resistance, minimize waste and natural resource utilization and to decrease the cost to build and run such nuclear power plants. Besides reactor technology development also cross section measurements on structure materials, coolants and fissile materials with smaller uncertainty are needed to meet the primary goals for the six reactor types. In the report from WPEC group 26 [2] the necessary accuracy of different neutron cross sections for materials present in different reactor types was estimated. The required uncertainty for a particular reaction in one Gen-IV reactor was found by MCNP simulations were the investigated cross section was raised and lowered. The uncertainty limits of the reaction cross section were determined in such way that the uncertainty in integral reactor parameters such as k_{eff}, power distribution, transmutation potential and void coefficient was still within acceptable limits. The results show that many reactions need to be more accurately determined. Even inelastic cross section on Iron and Sodium need to be known better along with the reactions on the minor actinides which will be a part of the fuel for Gen-IV reactors. It is not a surprise that inelastic scattering becomes important for these reactor types since many of the them will operated with a fast neutron spectrum. i.e. un-moderated neutrons. The neutron spectrum should be as hard as possible in order to fission the minor actinides.
ELBE is worldwide the first superconducting electron linac to be used for neutron generation. At the nELBE facility fast neutrons in the energy range from ca. 0.1 to 10 MeV are produced by the pulsed electron beam impinging on a liquid lead. The neutron energy is determined by Time of Flight (ToF). The neutron spectrum of nELBE is similar to the spectrum of a fast neutron reactor, which makes nELBE especially suited for transmutation research.

Photo production

At the radiation source ELBE of the Forschungszentrum Dresden-Rossendorf electrons can be accelerated up to 30 - 40 MeV in cw-mode by superconducting rf-cavities. The maximum average beam current at a micropulse rate of 13 MHz is 1 mA. The frequency can be reduced to f = 13 MHz/2^n, with a corresponding reduction in average beam current. The normal working frequency for nELBE is 100 or 200 kHz. The neutrons are generated by (γ, n) reactions with bremsstrahlung from the high intensity electron beam. A superconducting radio frequency photo electron injector (SRF gun) is being developed for ELBE. The current possible bunch charge is 77 pC and with the SRF gun 2 nC will be possible. This will allow an unreduced beam current of 1 mA at 500 kHz repetition rate.
A sketch of the nELBE photoneutron source is shown in Fig. 1. The electrons leave the electron beam line through a beryllium window. Then they pass through a nitrogen atmosphere before entering a stainless-steel vacuum chamber. Inside the vacuum chamber a molybdenum channel confining the liquid lead exists. The channel has a rhombic cross section with 11 mm side length. The electrons generate bremsstrahlung photons which in secondary (γ, n) reactions on lead release neutrons. The neutrons are almost isotropically emitted, while the electrons and photons are forward-peaked. To reduce the gamma flash, the measurement room is put at approximately 90 relative to the incident electron beam. The neutrons pass to the experimental setup via a collimator. In order to reduce the gamma flash a lead absorber can be put at the entrance of the collimator. At this position a target-ladder is available for different absorbers or transmission measurements.

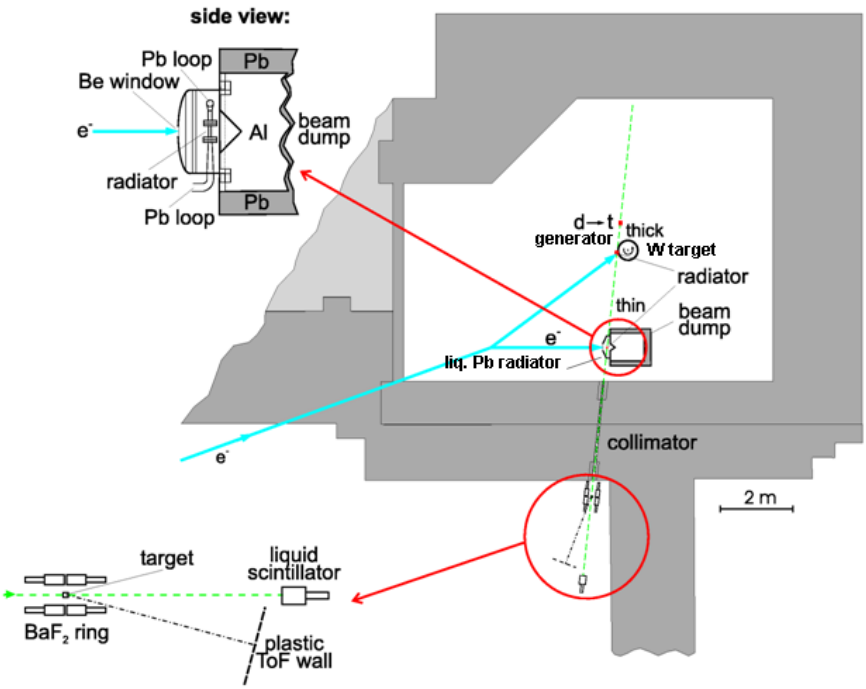

Figure 1. *Floorplan of the nELBE photo neutron source. A cross section of the liquid lead circuit is shown in the upper left part of the picture. The neutrons enter the measurement room via a collimator. The experimental setup is reached after a flight path of ca. 5-6 m.*

The electrons lose approximately half of their energy as they pass the lead. This is means that with the planned SRF-Gun, 20 kW of heat will be deposited in approximately 1 cm^3 and has to be transported away. With the molten lead this heat power can be cooled using a temperature regulated heat exchanger with an InGaSn eutectic has transfer fluid. Because of the large temperature differences in the molybdenum channel, it has to stand a substantial stress. This effect as well as other technical design parameters of the liquid lead radiator and the electron beam dump is discussed in [3].

So far the maximum beam power that has been deposited in the liquid lead is about 500 W. This means that instead of using the cooler to keep the lead in a liquid state, it has to be heated, which is done at several positions around the liquid lead loop. The operation of the liquid lead loop at nELBE is remarkably stable and has now been running smoothly for more than 900 hours.

Research program at nELBE

At nELBE cross sections relevant to Gen-IV and ADS shall be measured. The total cross sections for ^{181}Ta, ^{27}Al, ^{nat}C and polyethylene have been performed and preliminary results are shown for ^{27}Al in Figure 2. The preliminary results are compared to results from Rohr [4], which have been binned with the energy resolution of nELBE in order to demonstrate the energy resolution of nELBE. The total cross section measurements were performed with a reduced beam intensity using a plastic scintillator with low energy threshold. The major part of the available beam time has been devoted to the measurement of the inelastic cross section for ^{56}Fe. At nELBE the inelastic scattering cross section is determined by detecting both the gamma ray and the inelastically scattered neutron. The gamma rays are detected with a BaF_2 array, their ToF compared to the time zero from the accelerator is used to determine the incident neutron energy. The scattered neutrons are detected with 4 plastic scintillators which are 1 m long. They are put approximately 1 m from the iron target and by this second ToF, which is measured relative to the detected gamma ray, the inelastically scattered neutron can be detected. Because of the only 1 m long second flight path, only isotopes which have well separated energy levels can be measured with the current setup for inelastic cross sections at nELBE. Detailed explanation and results from this experiment is described elsewhere in these proceedings [5]. Iron is used as a structure material in reactors and inelastic scattering is very important for the shape of the neutron spectrum in a fast reactor. In a sodium cooled reactor the inelastic cross section of sodium is important for the same reason and at nELBE measurement of the inelastic cross section of sodium is also planned.

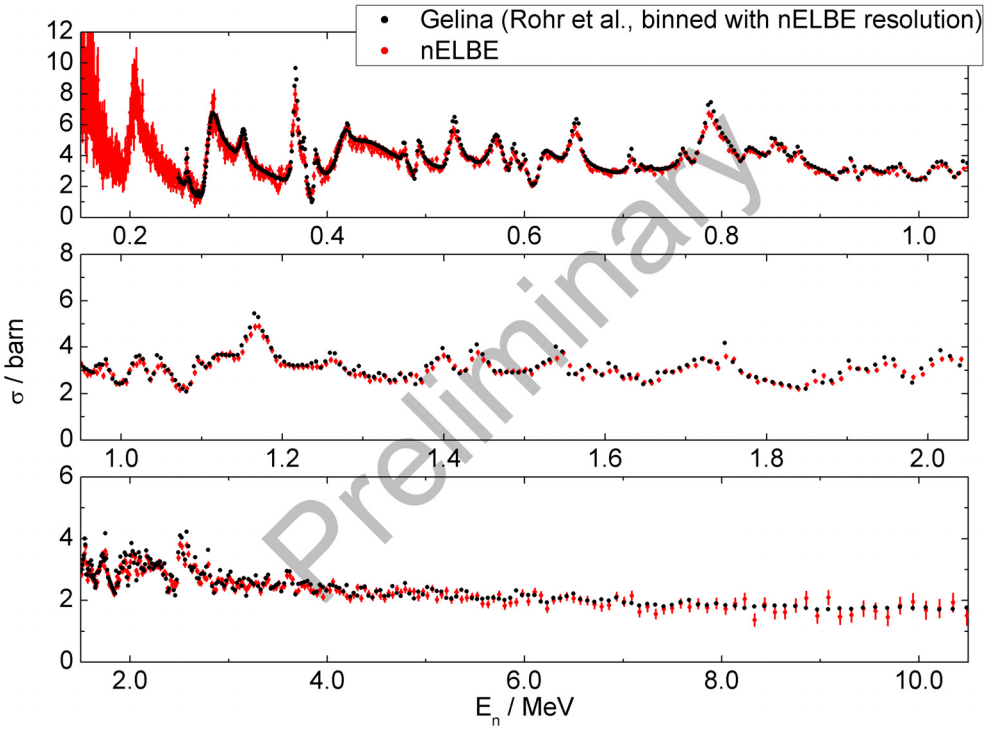

Figure 2. *Total cross section for ^{27}Al. The results from nELBE show good agreement compared to the high resolution results from Rohr [4] which have been binned with the nELBE resolution for comparison.*

Neutron flux monitoring has so far been performed with a fast fission ionization chamber on loan from PTB [6]. It has 10 well defined ^{235}U layers with a total mass of 201.6 mg. A new fission chamber for flux monitoring is being developed.
Since the ELBE accelerator is used for various other purposes not all beam time is devoted to nELBE. Totally 36 days have been devoted to nELBE during the first 1.5 years of operation.

Experiments and Performance of nELBE

From the results of the total cross section, it is clear that the energy resolution of nELBE is according to expectations [7]. However a high background at the position where the scattered neutrons are detected is seen in the inelastic scattering experiments. To further investigate this, the neutron beam profile has been measured with a movable plastic scintillator.
Compared to MCNP simulations of the beam profile, the experiment shows a higher halo of neutrons and gamma ray background outside of the geometrical cross section of the beam. More details and discussion about possible sources of the background can be found elsewhere in these proceedings [8]. Due to electron beam losses the neutron flux is lower than expected. Better electron beam tuning and a recent realignment of the electron beam line close to the liquid lead radiator, increase the neutron flux. Beam losses in an adjacent room lead to the detection of gamma rays before the real gamma flash arrives at the detectors in the measurement room. This increases the dead time. The yield of these gamma rays also depends on how well the electron beam is tuned.

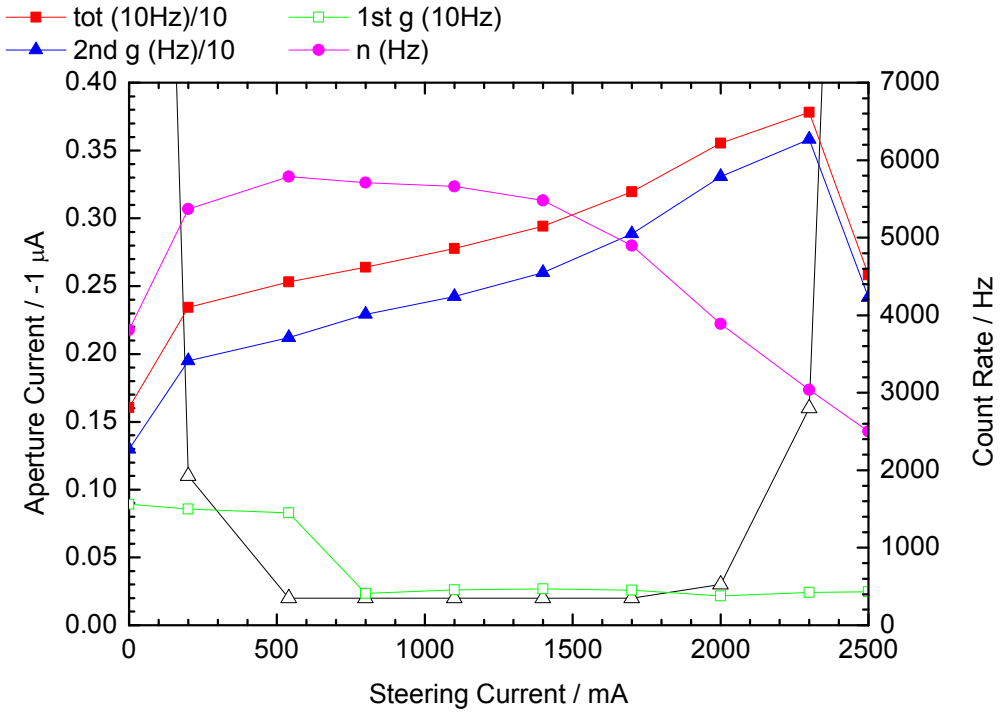

Figure 3. *Vertical electron beam scan. The current on an aperture is shown on the left axis (open triangles) as a function of the vertical steering current. The neutron and gamma ray count rates, detected by a plastic scintillator in the measurement room, are also shown as a function of the vertical steering current (closed circles-neutron, closed triangles-gamma flash, open boxes-gammas from adjacent room, closed boxes the sum of all contributions). When the vertical steering current is increased the neutron yield is decreasing whereas the gamma ray count rate increases. This is probably observed due to the misalignment of the electron beam line at the time of the experiment.*

The maximum neutron yield is achieved when the electrons hit the liquid lead in the correct position on the center of the collimation axis. If the beam is missing the ideal spot the neutrons are not emitted in the direction of the collimator. It is not possible to observe if the

correct position is hit directly. Instead the electron beam can be steered vertically and horizontally and the detected neutron and gamma ray yield can be measured. Results from such an electron beam scan is shown in Figure 3. Because of misalignment of the electron beam line the maximum neutron yield could not be reached before the electron beam hit an aperture. This is probably also the explanation for the observed increasing gamma ray yield when the neutron yield is decreasing.

Summary and outlook

The nELBE neutron beam facility has been in operation since November 2007. During the first 1.5 years, ca. 900 hours of beam time have been used for measurements and investigation of the experimental condition at nELBE. Total cross section measurements have successfully been performed which also confirmed the energy resolution of the facility. More background neutrons than expected are observed in the measurement of the inelastic cross section for ^{56}Fe. However the situation is continuously improving. Improved tuning of the electron beam and realignment of the electron beam line increase the absolute neutron yield in the measurement room. Soon a new superconducting radio frequency photo electron injector will be installed at ELBE and the ion current and corresponding neutron flux will increase considerably for the experiments at nELBE.

Acknowledgements
This work was supported by the EURATOM 6. Framework Programme “European Facilities for Nuclear Data Measurements” (EFNUDAT), contract number FP6-036434.

References

[1] A technology roadmap for generation IV nuclear energy systems, GIF-002-00, US Department of Energy (2002).
[2] M. Salvatores (Co-ordinator), Uncertainty and target accuracy assessment for innovative systems using recent covariance data evaluations, Nuclear Science ISBN 978-92-64-99053-1 NEA/WPEC-26 (2008).
[3] E. Altstadt, C. Beckert, H. Freiesleben, V. Galindo, E. Grosse, A.R. Junghans, J. Klug, B. Naumann, S. Schneider, R. Schlenk, A. Wagner, F.-P. Weiss, A photo-neutron source for time-of-flight measurements at the radiation source ELBE, Ann. Nucl. Energy 34 (2007) 36–50.
[4] Rohr et al., EXFOR Nuclear Data Library.
[5] R. Beyer et al., Contribution to this Workshop (2009).
[6] R. Nolte, M. S. Allie, D. Brooks, A. Buffler, V. Dangendorf, J. P. Meulders, H. Schuhmacher, F. D. Smit, and M. Weierganz, Cross Sections for Neutron-Induced Fission of 235U, 238U, 209Bi, and natPb in the Energy Range from 33 to 200 MeV Measured Relative to n-p scattering, Nucl. Sci. Eng. 156 (2007), 197-210.
[7] J. Klug, E. Altstadt, C. Beckert, R. Beyer, H. Freiesleben, V. Galindo, E. Grosse, A.R. Junghans, D. Légrády, B. Naumann, K. Noack, G. Rusev, K.D. Schilling, R. Schlenk, S. Schneider, A. Wagner, F.-P. Weiss, Development of a neutron time-of-flight source at the ELBE accelerator, NIM A 577 (2007) 641–653.
[8] E. Birgersson et al., Contribution to this Workshop (2009).

^{243}Am fission cross section measurements – variance-covariance analysis

G. Kessedjian[1)], G. Barreau[1)], M. Aïche[1)], B. Jurado[1)], A. Bidaud[1-6)], S. Czajkowski[1)], D. Dassié[1)], B. Haas[1)], L. Mathieu[1)], L. Tassan Got[2)], J. Wilson[2)], F.-J. Hambsch[3)], S. Oberstedt[3)], I. AlMahamid[4)], J. Floyd[5)], W. Lukens[5)], D. Shuh[5)]

1) CENBG, Université de Bordeaux 1, F-33175 Gradignan Cedex, France
2) IPN Orsay, Université Paris-Sud, F-91406 Orsay, France
3) EC-JRC-IRMM, B-2440 Geel, Belgium
4) Laboratory of Inorganic and Nuclear Chemistry, NY 12201, USA
5) LBNL, CA 94720, USA
6) LPSC-IN2P3-CNRS/Université Joseph Fourier/Grenoble-INP, 53 Avenue des Martyrs 38026 Grenoble Cedex
Present address at LPSC kessedjian@lpsc.in2p3.fr

Abstract: ^{243}Am is present in a rather important amount in the waste generated by current PWR nuclear reactors. Nowadays, ^{241}Am and ^{243}Am are the only isotopes that can be fully separated and extracted from spent fuel rods. Therefore, they represent the only nuclei for which fast neutron incineration could be seriously considered in a relatively near future. A reliable design of incineration reactors requires the precise knowledge (around 5% of accuracy) of the neutron-induced fission cross section of ^{243}Am in a fast neutron spectrum. However, the existing evaluations of this cross section have been questioned by recent studies performed at the GNEISS facility. In the neutron energy range between 1MeV and 6 MeV, the GNEISS data present deviations of more than 15% with respect to the evaluations.
In the literature, most of the earlier fission data on ^{243}Am have been measured relative to that of ^{235}U. Thus, their accuracy is necessarily limited by the precision of the ^{235}U fission cross section and these data are not independent. In order to solve this problem, we have performed new measurements of the ^{243}Am neutron-induced fission cross section from the fission threshold up to the onset of second-chance fission with accuracy better than 5%. Our data are completely independent from the rest since we have used the neutron-proton scattering cross section as reference reaction to reconstruct the incident neutron flux. This cross section is known with a precision better than 0.5 % over a wide range of neutron energies (0.1 MeV to 20 MeV). This high precision explains why our measurements are "quasi-absolute" ones. Moreover, we have performed new measurements of the ^{243}Am cross section in reference to the fission cross sections of $^{235,\ 238}$U to verify that systematic parameters have been correctly evaluated. For all measurements of the reaction ^{243}Am(n,f), the analysis of error correlations allowed to interpret the importance of these measurements within the existing data. We will describe the experimental technique and the results will be discussed using a variance-covariance analysis.

Introduction

A reliable design of incineration reactors requires the precise knowledge (better than 5% of accuracy) [1] of the neutron-induced fission cross section of ^{243}Am in a fast neutron spectrum. However, in the 1MeV to 6 MeV neutron-energy range, the existing data show systematic and significant discrepancies, they could be separated into two distinct groups. The experimental data of the first group set by Knitter et al. ref. [2], Fursov et al. [3] and Seeger et al. ref. [4] while the second group of data set including Behrens et al. ref. [5] Goverdovsky et al. ref [6] and more recently Laptev et al. [7] gives systematically higher fission cross section than the first group. Most of these data have been obtained in reference to the fission cross section of ^{235}U, Fursov et al. have used ^{239}Pu(n,f) as reference. The most recent data from Laptev et al. lie in the higher-cross section group which is more than 15% above the current evaluations. As pointed out recently by Talou et al. ref [8], this discrepancy seems to be related to a normalisation problem.
In order to disentangle this controversy, we have performed new measurements in reference to three standard reactions to determine the incident neutron flux. The first one is the neutron-

proton elastic scattering cross section, known with a precision better than 0.5% over a wide range of neutron energy (1 meV to 20 MeV refs. [9,10]). This high precision allowed us to qualify these measurements as “quasi-absolute”. Additional measurements have been realised in reference to the ^{238}U and ^{235}U fission cross sections which are known with an accuracy of 1 to 3% in the fast neutron energy range (0.1 MeV to 10 MeV). These data allowed us to compare the normalization procedures using different standard reactions

Quasi-absolute neutron-induced fission cross section of ^{243}Am

Experiment

The measurements were performed at the 7MV Van-de-Graaff of the IRMM in Belgium and more recently at the 4 MV accelerator facility (AIFIRA) at CENBG [11]. The fast neutrons in the energy range from 1 MeV to 8 MeV were produced with the T(p,n)^{3}He reaction below 4 MeV, the neutron with energies above 4 MeV were produced with the D(d,n)^{3}He reaction. Two layers of ^{243}Am were placed back to back in a vacuum chamber at 39 mm from the neutron source and at 0° with respect to the incident neutron direction. Each layer (diameter 6 mm) has been prepared by electro deposition onto a 0.6 mm thick stainless steel backing; the sample thickness was about 550µg/cm^2. Fission detectors were composed of two sets of photovoltaic cells in a very compact geometry. They were placed on one side of each Am target to obtain a geometrical efficiency of around 70%. These photovoltaic cells allowed a complete separation between alpha particles and fission fragments. Concerning the neutron detector, a polypropylene (PP) foil ($(C_3H_6)_n$) was placed at 80 mm from the neutron source. This foil was placed at 0 degree with respect to the incident neutron beam. It served as a radiator to convert incident neutrons into recoiling protons. Its thickness (10 to 50 µm) has been adjusted according to the neutron energy. Recoiling protons were detected by a silicon ΔE-E telescope located at 75 mm from the foil. The ensemble PP-telescope formed our neutron flux detector. The efficiency of proton detector was around 1%. Monte Carlo simulations of neutrons passing though the experimental setup have been performed in order to determine the neutron spectrum hitting the ^{243}Am targets or the PP foil as well as the efficiencies of proton detector as a function of neutron energies. Thus we have deduced the mean value of (n,p) cross section from which the neutrons flux hitting the PP foil has been deduced [11,12]. Our simulation code has been compared to the MCNPX code and the results (proton spectrum and the efficiency of proton detector) are in a good agreement with this reference code.

Variance-covariance analysis

A few parameters are needed to convert the fission rate into cross section. These parameters represent the quantities of matter (atom numbers of ^{243}Am or hydrogen), detector efficiencies, solid angles of targets (^{243}Am or polypropylene) and mean value of (n,p) cross section. We define the lth measurement of fission cross section as the ratio:

$$\sigma^{l}_{(n,f)}(E_n) = \frac{F_l/\Omega_l}{\Phi_n/\Omega_n}(E_n) \qquad (1)$$

where F_l is the lth normalized (per atom) fission rate, Ω_l and Ω_n are the solid angle of the lth target of ^{243}Am and the solid angle of neutron detector respectively, Φ_n represents the neutron fluence. We have used two targets of ^{243}Am for most of the measurements (l=1,2), therefore, the mean value of fission cross sections at neutron energy E_i and its variance are defined by the relations::

$$\langle\sigma_{(n,f)}\rangle(E_i) = \langle\sigma_{(n,f)}\rangle_i = \frac{\langle F/\Omega\rangle}{\Phi_n/\Omega_n}(E_i)$$

$$\frac{Var(\langle\sigma_{(n,f)}\rangle)}{\langle\sigma_{(n,f)}\rangle^2} = \frac{Var(\langle F/\Omega\rangle)}{(\langle F/\Omega\rangle)^2} + \frac{Var(\Phi_n)}{(\Phi_n)^2} + \frac{Var(\Omega_n)}{(\Omega_n)^2} - \frac{2}{m}\sum_{0<l<l'}^{m}\frac{Cov(\Omega_n;\Omega_l)}{\Omega_n.\Omega_l} \qquad (2)$$

$$\frac{1}{Var(\langle F/\Omega\rangle)} = \sum_{l=1}^{m}\frac{1}{Var(F_l/\Omega_l)} + 2\sum_{0<l<l'}^{m}\frac{F_l/\Omega_l}{Var(F_l/\Omega_l)}.\frac{F_{l'}/\Omega_{l'}}{Var(F_{l'}/\Omega_{l'})}.\frac{Cov(\Omega_l;\Omega_{l'})}{\Omega_n.\Omega_l}$$

In the relations (2), we can probe that all the parameters are independent except the solid angles of Am targets and polypropylene foil [12]. Therefore, in addition to the variance (Var)

of each parameter, the covariances of the solid angles have to be evaluated. For all the measurements using the same set-up, the systematic parameters have not changed. Then the covariance between two measurements at neutron energies E_i and E_j of the ^{243}Am fission cross section is defined as [12]:

$$\frac{Cov(\langle\sigma_{(n,f)}\rangle_i;\langle\sigma_{(n,f)}\rangle_j)}{\langle\sigma_{(n,f)}\rangle_i.\langle\sigma_{(n,f)}\rangle_j}=\left(\frac{Var(\langle F/\Omega\rangle)}{(\langle F/\Omega\rangle)^2}\right)_{syst}+\left(\frac{Var(\Phi_n)}{(\Phi_n)^2}\right)_{syst}+\frac{Var(\Omega_n)}{(\Omega_n)^2}-\frac{2}{m}\sum_{0<l<l'}^{m}\frac{Cov(\Omega_n;\Omega_l)}{\Omega_n.\Omega_l} \quad (3)$$

where the label “syst” indicates that only systematic variances have been considered (without the statistical errors). In our case, three experiments were performed with three different neutron sources at IRMM in Belgium and CENBG at Bordeaux. For two measurements performed at two different facilities, only fission rates and neutron flux errors have to be propagated. The covariance of two measurements is defined by the relation:

$$\frac{Cov(\langle\sigma_{(n,f)}\rangle_i;\langle\sigma_{(n,f)}\rangle_j)}{\langle\sigma_{(n,f)}\rangle_i.\langle\sigma_{(n,f)}\rangle_j}=\left(\frac{Var(\langle F\rangle)}{(\langle F\rangle)^2}\right)_{syst}+\left(\frac{Var(\Phi_n)}{(\Phi_n)^2}\right)_{syst} \quad (4)$$

The best observable to compare these data is the correlation (Corr) of two measurements defined as the covariance divided by the square root of the variances. Thus, this dimensionless quantity gives the degree of freedom of the data.

$$Corr(\langle\sigma_{(n,f)}\rangle_i;\langle\sigma_{(n,f)}\rangle_j)=\frac{Cov(\langle\sigma_{(n,f)}\rangle_i;\langle\sigma_{(n,f)}\rangle_j)}{\sqrt{Var(\langle\sigma_{(n,f)}\rangle_i).Var(\langle\sigma_{(n,f)}\rangle_j)}} \quad (5)$$

The main difficulties concern the assessment of solid angle covariances (eq.2 & 3) but these terms are bounded $Cov(\Omega_n;\Omega_l)=\lambda.\sqrt{Var(\Omega_n).Var(\Omega_l)}$ with $-1\le\lambda\le1$ in general case. This latter parameter represents the solid angle correlation. The geometry of the set-up leads to consider only positive correlation for λ. In the following, we use λ as a free parameter and we will discuss the weight of the solid angle correlation on the correlation of fission cross section measurements.

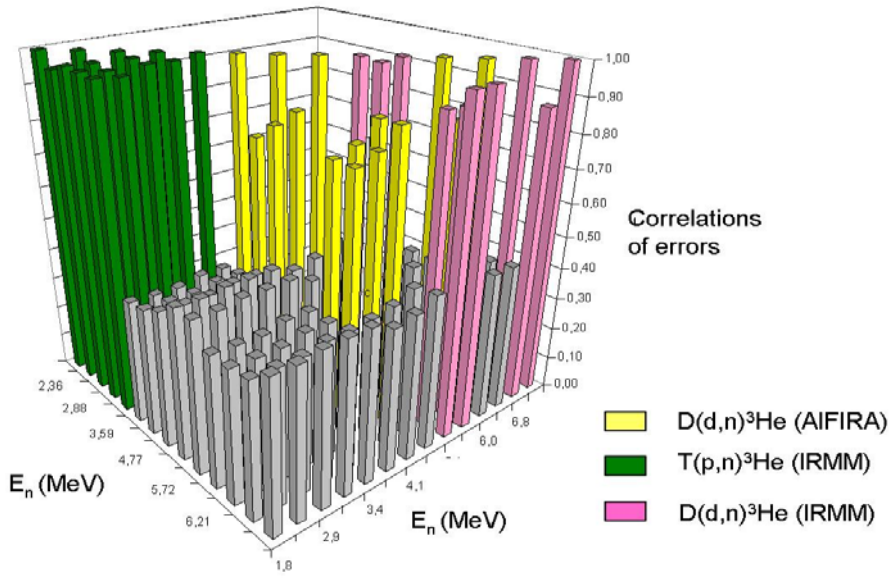

Figure 1. *Correlation matrix of fission cross section measurements in reference to the (n,p) elastic scattering cross section with null solid angle correlation (λ=0) as a function of neutron energy (E_n)). Correlations are maximal for a same* set *of measurements. The most important part of these correlations is due to the error on the position of the neutron source. Between two series, only systematic parameters of the method generate the correlations.*

In first step, we assume that all the parameters are independent ie $\lambda = 0$. The results are displayed in figure 1. For each series of measurements, we note a large correlation (>0.79) due to the error on solid angle and intrinsic systematic parameters of the method (quantities of matter, (n,p) elastic scattering cross section and efficiencies of detector). Between two series of measurements, only intrinsic systematic parameters of the method have been propagated and the correlations do not exceed 0.48 (Figure 1.). In a second step, a full correlation has been assumed. The limits of the fission cross section correlation matrix $(Corr(\langle\sigma_{(n,f)}\rangle_i;\langle\sigma_{(n,f)}\rangle_j) \leq 1)$ provide an upper limit on solid angle correlation: for one ^{243}Am target $\lambda_1 = 1$; for two ^{243}Am targets $\lambda_2 = 0.61$. The data provide by these two matrices have been compared using a singular value decomposition method [12]. Each singular value represents a quasi-independent state of the matrix. Singular values of the two limit matrices are displayed in figure 2. The results suggest that, in our case, variance-covariance matrix has provided the same information for all solid angle correlations $0 \leq \lambda_1 \leq 1$ and $0 \leq \lambda_2 \leq 0.61$. So, the standard deviations of fission cross section measurements are defined by two extreme values corresponding to the extreme correlation matrices (table 1.).

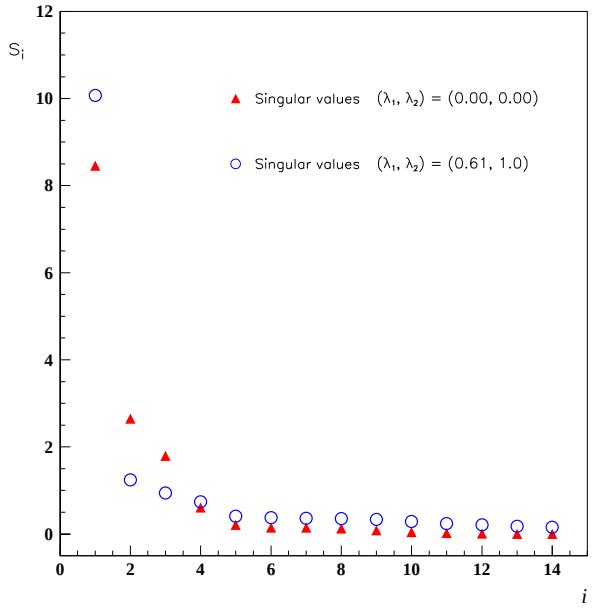

Figure 2. *Singular values of correlation matrices:* each value represents a quasi-independent state of the matrix. *We can conclude that data provided by the two limit matrices are similar.*

In conclusion, the limits on correlation matrix give the maximal solid angle correlations for the variances on systematic parameters used in this work. Thus, the limits on errors of measurements are content between 2.1 and 3.4% (IRMM data) or 3.2 à 4.6% (AIFIRA data) (table 1).

Neutron-induced fission cross section of ^{243}Am relative to ^{253,238}U

Cross-section measurements of ^{243}Am(n,f) relative to ^{235}U(n,f) were performed at the 4MV Van-de-Graaff facility of the CENBG at Bordeaux and that relative to the ^{238}U(n,f) one, have been realized at the new 4 MV facility (AIFIRA) at CENBG. The fast neutron flux over the neutron energy range 4 MeV to 6 MeV was produced using the D(d,n)^{3}He reaction. Back-to-back targets, consisting of one ^{243}Am one (550 µg/cm^2 thick) and one ^{238}U (462 µg/cm^2 thick), were placed at a distance of 40 mm from the neutron source and perpendicularly to the incident-neutron beam. Fission detectors were also composed of two sets of photovoltaic cells in a very compact geometry. The ensemble “Am target + fission fragment detector” were the same as the one used for the measurements relative to the (n,p) elastic scattering cross

section. The ensemble “U target + fission fragment detector” formed our neutron flux detector, then the results on the neutron flux are completely independent. The correlation within a same set of measurements varies between 0.53 and 0.87 range. While, the correlations between two measurements of two sets do not exceed 0.17 (from systematic errors on ^{243}Am fission rates).
Cross-section measurements of ^{243}Am(n,f) relative to ^{235}U(n,f) were performed with the same method. In this case, two other targets of ^{243}Am and ^{235}U were used: an ^{243}Am target of about 106 µg/cm^2 thick and an ^{235}U one of about 409 µg/cm^2. The correlations in a same set were found around 0.89. The correlations of these data with other series are definitely null as there were no common parameters between these data.

Table 1. *^{243}Am fission cross sections measurements relative to the (n,p) elastic scattering cross section. The standard deviation are presented (1) for a maximal correlation on ^{243}Am fission cross section (λ_1=1; λ_2=0.61), (2) without solid angle correlations (λ=0).*

E_n (MeV)	Standard deviation on E_n (MeV)	$\sigma_{(n,f)}$ (b)	Minimal standard deviation on $\sigma_{(n,f)}$ (%) (λ_1=1; λ_2=0.61)	Standard deviation on $\sigma_{(n,f)}$ (%) (λ=0)
Series n°1 Van de Graff IRMM – neutron source T(p,n)^{3}He				
1,841	0,100	1,506	2,21	3,35
2,361	0,090	1,583	2,25	3,37
2,876	0,085	1,602	2,14	3,30
2,876	0,085	1,617	2,15	3,31
3,387	0,076	1,551	2,16	3,32
Series n°2 Van de Graff IRMM – neutron source D(d,n)^{3}He				
5,122	0,074	1,498	2,12	2,89
5,721	0,059	1,554	2,12	2,89
6,824	0,045	2,192	2,96	3,74
7,350	0,042	2,289	2,16	2,92
Series n°3 AIFIRA CENBG – neutron source D(d,n)^{3}He				
3,592	0,198	1,585	3,74	4,58
4,070	0,117	1,600	3,58	4,45
4,768	0,074	1,537	3,25	4,19
5,997	0,050	1,636	3,47	4,36
6,213	0,042	1,823	3,46	4,36

Results and conclusion

Between 1 MeV and 8 MeV, 15 points of ^{243}Am fission cross section have been measured relative to the (n,p) cross section. Additional measurements have been done relative either to ^{238}U(n,f) (4 points) or to ^{235}U(n,f) (3 points). The overall precision of our data is better than 5% (the statistical uncertainty represents 1%). Figure 3 presents a comparison of our results with earlier measurements. On can see that our measurements contradict those of Behrens [5] and Laptev [7] which are about 15 % higher than the present data. Therefore our additional measurements (relative to ^{235}U and ^{238}U) are fully compatible with these findings. We are in close agreement with the data of Knitter [2] as well as the evaluated data files.
We have presented the first measurement of the fission cross section of ^{243}Am relative to the neutron-proton scattering cross section. Additional measurements have been performed relative to ^{238}U(n,f) and ^{235}U(n,f). The coherence between all these measurements validates the evaluated data files. In addition, we have used a statistical code developed at CENBG to for the modelling of the fission cross section below 10 MeV. Fundamental fission parameters such as fission barrier heights and curvatures have been determined. The model has been

used for the determination of other channel competing with fission that are much more difficult to measure such as capture, inelastic and (n,2n) cross sections [12].

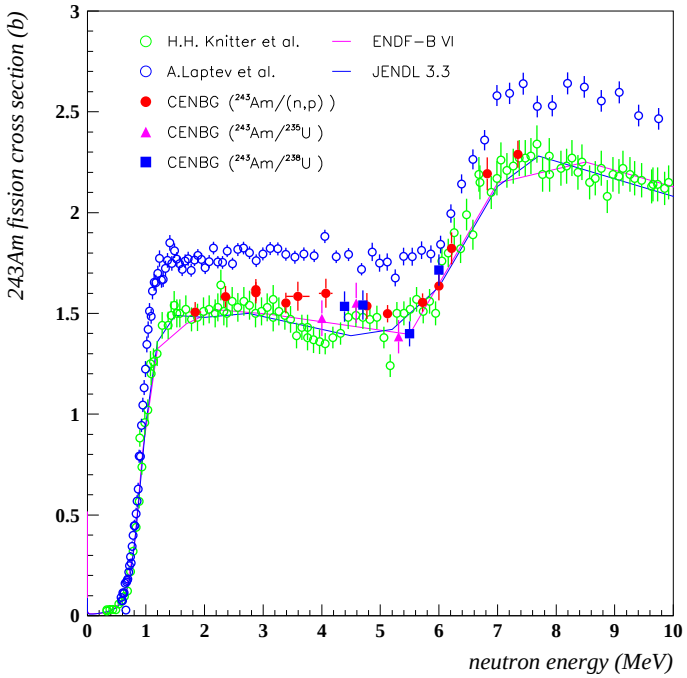

Figure 3. *Results for the ^{243}Am neutron-induced fission cross section of the present work are compared to* the evaluated data files *and experimental data from Knitter [2] and Laptev [7].*

Acknowledgments

This work has been supported by the CNRS programme PACE/GEDEPEON and the EURATOM Transnational Access Program NUDAME. We thank the Laboratory of Inorganic and, Nuclear Chemistry, NY 12201, to make available the ^{243}Am Target and the IPN Orsay for building the high-quality Si detector. The authors thank also the accelerator staff of the IRMM-Geel and CENBG for their great support during the experiments.

References

[1] M. Salvatores et al., Nuclear Science NEA/WPEC 26.
[2] H. H. Knitter et al., Nucl. Sci. Eng. 99 (1988) 1.
[3] B.I. Fursov et al., Atomnaya Energiya, Vol59, p339 (1985) Russia.
[4] P. A. Seeger et al., “Fission Cross Sections from Pommard,”LA-4220, 138, Los Alamos National Laboratory (1970).
[5] J. W. Behrens, J.C. Browne, NSE, 77, 444 (1981).
[6] A. A. Goverdovsky et al. Proc. Int. Conf. Nuclear Data for Basic and Applied Science, Santa Fe, New Mexico, May 13–17, 1985.
[7] A. B. Laptev et al., Nucl. Phys. A 734 (2004) E45.
[8] P. Talou, et al., Nucl. Sci. Eng. 155 (2007) 84.
[9] J. C. Hopkins and G. Breit, Nucl. Data Tables, A9 (1971) 137.
[10] D. Carlson, Private Communication.
[11] A. Aiche, G. Kessedjian et al., International Conference on Nuclear Data for Science and Technology 2007.
[12] G. Kessedjian, Ph.D thesis, Université de Bordeaux.

Development of a neutron counter for measuring prompt neutron multiplicity in (n,f) at the *LANSCE/WNR* facility

B. Laurent[1)], T. Granier[1)], G. Belier[1)], A. Chatillon[1)], J. Taieb[1)], A. Courtial[1)], R. C. Haight[2)], R. O. Nelson[2)], J. M. O'Donnell[2)], M. Devlin[2)]

1) CEA, DAM, DIF, F-91297 Arpajon, France
2) LANSCE-NS, Los Alamos National Laboratory
benoit.laurent@cea.fr

Abstract: A new high efficiency-neutron counter has been designed to perform experiments at the *WNR/LANSCE* facility. A first test experiment was performed last September and neutron multiplicity information could be extract from data analysis after background subtraction. Now, more complex experiments involving fragment kinetic energy measurement in coincidence with neutron detection are planned.

Introduction

The number of neutrons emitted in fission is a fundamental observable which governs primarily most of the applications of this phenomenon. From a basic point of view, this quantity is linearly related to the excitation energy of the primary fragments and is thus of high interest for inferring the scission configuration (deformation energy at scission point). The accurate knowledge of this observable and its variation as a function of incident neutron energy would give information about the complex mechanism of fission and help improve the theoretical models. In this purpose, experiments are planned at the *WNR* spallation neutron source of the Los Alamos Neutron Science Center. The goal is to study the variation with incident neutron energy En of the mean fission prompt neutron multiplicity $\bar{\nu}$ and the associated multiplicity distribution p(□). The coincident detection and identification of the fission fragments is also planned.
The mean neutron multiplicity in (n,f) for the major actinides has been subject to lots of experimental studies. Nevertheless only a few works concern the incident neutron energy domain above 6 MeV. Precision measurements were performed with detectors based on a tank containing Gd-doped liquid scintillator [1,2]. Although this type of detectors can have a high neutron efficiency, they are sensitive to □-rays. Moreover, the beam was stopped after each fission event, in order to reduce background noise during neutron counting.
Since it is not possible to stop the beam after each event at *WNR/LANSCE*, a new fission neutron counter based on ^{3}He tubes was developed at Bruyères-le-Châtel and tested at *WNR*.

Neutron counting setup

The neutron detection setup consists of ^{3}He neutron detectors arranged within a block of polyethylene. These proportional counters are essentially sensitive to thermal neutrons through the reaction ^{3}He(n,p). They are almost insensitive to gamma-rays. The role of the polyethylene block is to moderate the fission neutrons, making them detectable by the ^{3}He counters.
This neutron counter was tested first with a ^{252}Cf spontaneous fission source and later with the *WNR* "white" neutron beam using a ^{239}Pu fission chamber.
The neutron counting setup has been designed on the basis of calculations using the MCNP-4C3 computer code. These simulations have been validated by experimental tests with a prototype setup. The geometry of the setup has been chosen in order to optimize neutron detection efficiency as well as to comply with other experimental requirements. The selected design comprises twenty two 10 bar-^{3}He detectors disposed in two concentric rings along the beam direction (Fig. 1).

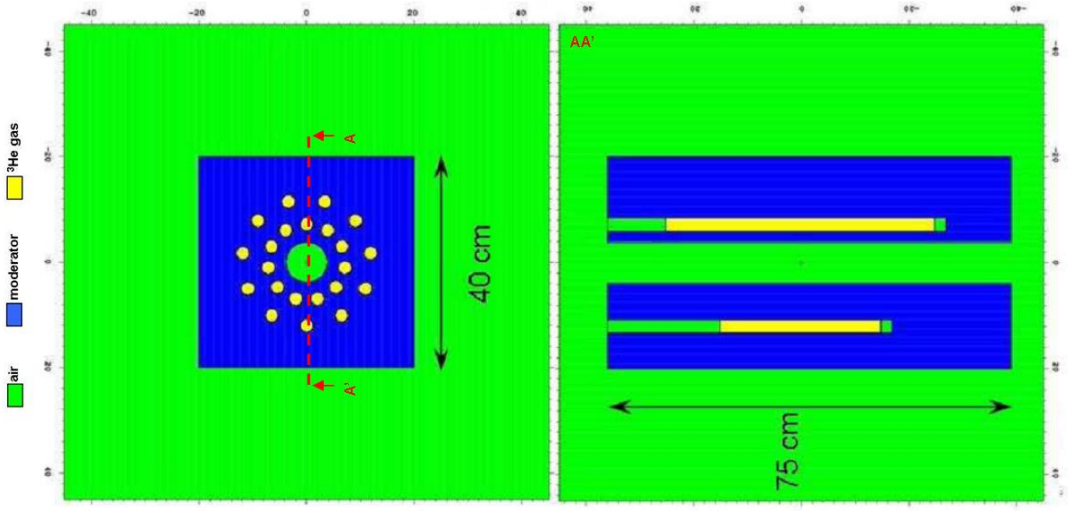

Figure 1. *MCNP simulation of the counter design.*

The detectors of the inner ring have a 50 cm sensitive length whereas that of the outer ring detectors is 30 cm. The sensitive diameter of the helium tubes is 25 mm.
Calculations show that the efficiency of such a setup to fission neutrons is about 50 %. The variation of efficiency with prompt neutron energy is given in Fig. 2.
The simulations have been validated by experimental tests with a prototype comprising eleven 30 cm ^{3}He tubes in the inner ring. A ^{252}Cf spontaneous fission neutron source was used for this purpose. With this prototype both calculations and measurements yield a 30% efficiency for fission neutrons.

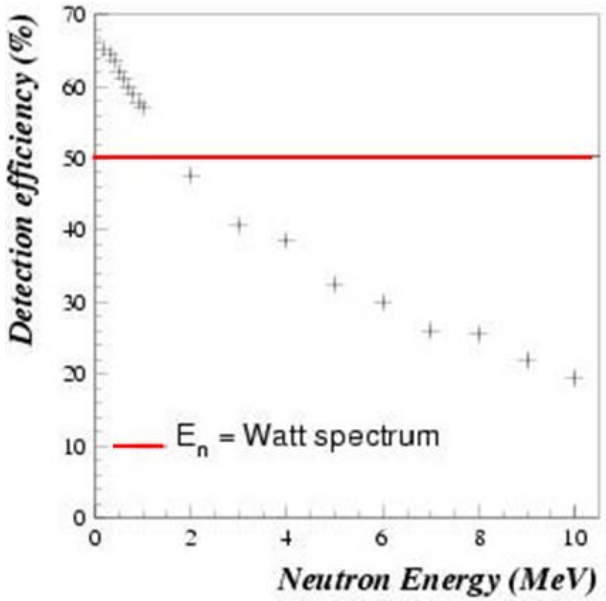

Figure 2. *Neutron detection efficiency as a function of neutron energy (calculations). The 50% value corresponds to the fission neutrons from ^{252}Cf.*

The propagation time before detection has also been investigated. The time distribution of the neutron detections obtained from the simulations is given in Fig. 3 and compared to the distribution obtained from ^{252}Cf tests of the prototype. It is found that 95% of the neutron detections occur within 200 μs after fission.

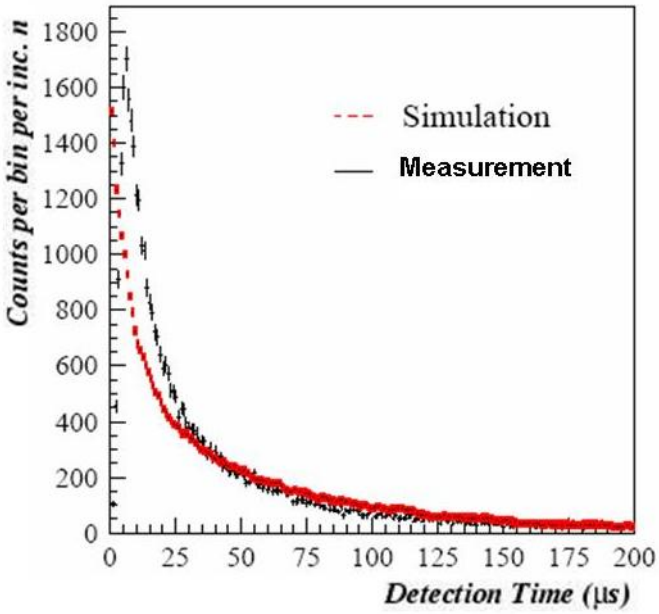

Figure 3. *Distribution of detection time for fission neutrons.*

The long moderation time inherent to polyethylene and the high efficiency of the setup yield a relatively high sensitivity to neutron ambiance. At *WNR*, scattered neutrons coming from the neighbouring beam lines are likely. Also, although the neutron line is well collimated, neutron halo is inevitable. These neutrons coming from the outside of the counter can be absorbed by adequate shielding. Calculations show that the use of a shielding composed of polyethylene on the outside to moderate the background neutrons and boron carbide to capture the moderated neutrons would reduce the instrument sensitivity to background neutrons entering the polyethylene from the outside by orders of magnitude. Particular attention was paid to design the shielding of the beam-facing side of the counter.

Experiment at *LANSCE*

At *WNR*, neutrons are produced by bombarding a tungsten target by the *LANSCE* 800 MeV proton beam. The ^{3}He counter was installed on the FIGARO neutron flight path (Fig. 5) at a distance of about 22 m from the spallation target. At this position, the neutron flux from 1 to 200 MeV is of about 10^{6} n/s/cm².

The experiment principle is outlined in Fig. 4. The target consists of a multi-plate fission chamber containing tens of milligrams of actinides. It is irradiated by a collimated neutron beam. The fission chamber delivers a signal every time a fission occurs. This signal is used to determine the incident neutron energy by measuring the time difference with respect to the beam RF signal (time-of-flight method). The fission signal is also used to trigger data acquisition from the neutron detectors.

For this experiment, a new acquisition system was developed, based on an universal logic module (FPGA-based memory) which during 200 μs after each trigger counts and time-stamps the neutron events. This is useful to reconstruct the time distribution of the neutron events.

The amount of structure material in this fission chamber is significant and neutron scattering constitutes thus an intense source of neutron background. Therefore, this source of noise was monitored online by implementing in the data acquisition trigger a uniform time sampling signal (electronic pulser). This signal is completely decorrelated from the fission events and allows us to measure online the contribution from scattered neutrons. This contribution can then be subtracted off-line in the data obtained with the fission trigger.

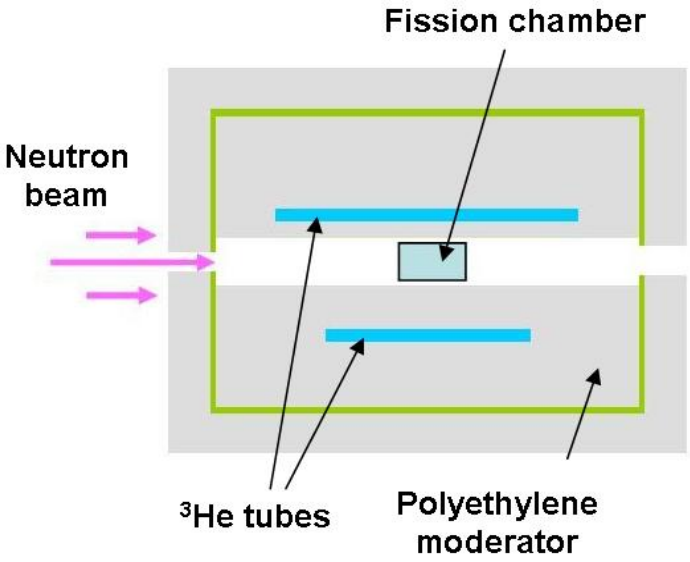

Figure 4. *Experimental principle.*

Figure 5. *Installation of the setup on the beam line. The left part shows the front side of the counter with the beam arriving from the left. The right part shows the rear side with the two concentric rings of tubes around the beam axis. The external shielding can be seen with the boron carbide (black plates) between the two blocks of polyethylene. The shielding of these front and rear faces was not yet installed on these pictures.*

Preliminary results

The time distributions of the neutron events after the fission chamber trigger (black) and the pulser trigger (red) are shown in Fig. 6. On the same figure, the time distribution obtained without beam with spontaneous fission from a ^{252}Cf fission chamber is also represented (blue). In this particular case, there is no contribution from neutron scattering and the distribution goes down to zero at longer times. With beam, the asymptote of the time distribution corresponds to neutron scattering induced by the quasi continuous neutron beam going through the chamber during the 200 μs-time window after the trigger.
This asymptote coincides with the measured contribution of neutron background obtained from the pulser trigger.

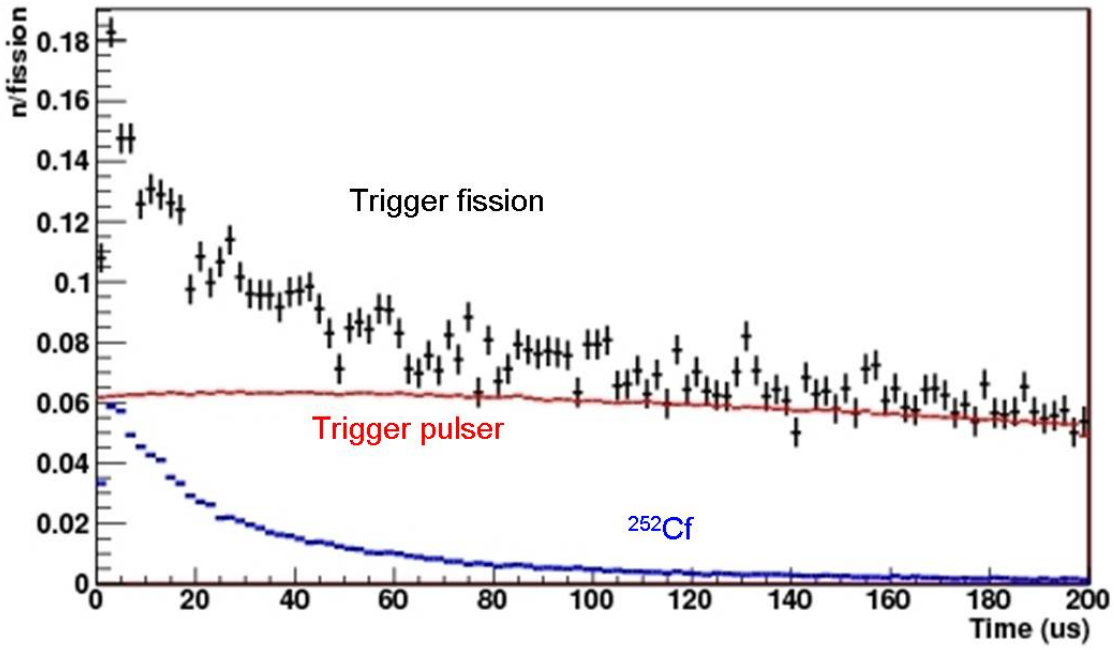

Figure 6. *Time distribution of the neutron events from different triggers for all incident neutron energies (normalized by the number of trigger events).*

The second step in the analysis consists in the measurement of the mean neutron multiplicity as a function of incident neutron energy E_n, obtained from the time-of-flight. The mean neutron multiplicity is obtained for bins of E_n after background subtraction and efficiency correction. The preliminary results from a data subsample are shown in Fig. 7. The mean neutron multiplicity is calculated as a function of E_n and the points of this work are compared to the earlier measurements performed by Frehaut with the ^{239}Pu(n,f) reaction. Even if these results are not comparable in terms of statistics, there is a good agreement.

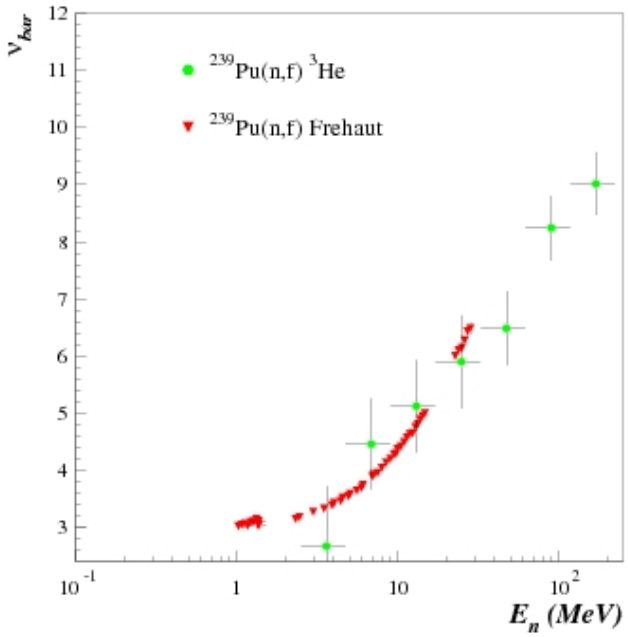

Figure 7. *Mean neutron multiplicity as a function of E_n for this work (green) and for earlier measurements performed by Frehaut and collaborators.*

Conclusion and outlook

A new high efficiency fission neutron counter insensitive to γ-rays has been developed and tested at *LANSCE/WNR* with a ^{239}Pu fission chamber. Although the principle has been validated, it was observed that the amount of structure material was a crucial parameter in order to obtain precise measurements. The use of special target with minimal structure material will be required in the future to study the evolution of the mean multiplicity of prompt fission neutron and the associated multiplicity distribution as a function of the incident neutron energy for major actinides. Also, in the framework of a collaboration with IRMM-Geel, it will used in coincidence with a double Frish-guided ion chamber to measure the mass and kinetic energy of the fission fragments.

References

[1] M. Soleilhac, J. Fréhaut, J. Gauriau, Journal of Nuclear Energy, 23 (1969) 257-282.
[2] J. Fréhaut, M. Soleilhac, G. Mosinski, National Soviet Conference on Neutron Physics, 1973.

Neutron production in neutron-induced reactions at 96 MeV on iron and lead

F.-R. Lecolley[1)], I.C. Sagrado García[1,2)],J.-F. Lecolley[1)], G. Ban[1)], J.-M. Fontbonne[1)], G. Iltis[1)], J.-L. Lecouey[1)], T. Lefort[1)], N. Marie[1)], J.-C. Steckmeyer[1)], Ch. Le Brun[3)], J. Blomgren[4)], C. Johansson[4)], J. Klug[4)], A. Orhn[4)], P. Mermod[4)], N. Olsson[4)], S. Pomp[4)], M. Osterlund[4)], U. Tippawan[4,5)], A.V. Prokofiev[6)], P. Nadel-Turonski[7)], M. Fallot[8)], Y. Foucher[8)], A. Guertin[8)], F. Haddad[8)], M. Vatre[8)]

1) LPC, ENSICAEN, UCBN and CNRS/IN2P3, Caen, France
2) DSM/DAPNIA, CEA-Saclay, France
3) LPSC, Grenoble, France
4) Department of Neutron Research, Uppsala University, Sweden
5) Fast Neutron Research Facility, Chiang Mai University, Thailand
6) The Svedberg Laboratory, Uppsala University, Sweden
7) George Washington University, Washington DC, USA
8) SUBATECH Nantes, France
fr.lecolley@lpccaen.in2p3.fr

Abstract: Double differential cross sections for neutron production were measured in 96 MeV neutron induced reactions at The Svedberg Laboratory (TSL) in Uppsala (Sweden). Measurements for iron and lead targets were performed using two independent set-ups: DECOI-DEMON, a time-of-flight telescope dedicated to the detection of emitted neutrons with energies between few MeV and 50 MeV, and CLODIA-SCANDAL, a device used to measure emitted neutrons with energies above 40 MeV. Double differential cross sections were measured for an angular range between 15 and 100 degrees and with low-energy threshold (1-2 MeV). Elastic cross sections, angular and energy distributions and total inelastic cross sections have been obtained from measured double differential cross sections. After a brief presentation of setups, data reduction and normalization procedure are discussed. The results are then compared with calculations performed with several models and transport codes (MCNPX, GEANT, TALYS and PHITS) and with other experimental data (EXFOR data base).

Introduction

Future Accelerator-Driven Systems (ADS) will coupe a high-energy intense proton beam (1 GeV & a few mA) with a spallation target and a sub-critical reactor core. Protons impinging on the ADS target will yield a large amount of spallation products, mainly neutrons, protons and light charged particles, with energies ranging in the MeV to the GeV region. Below 20 MeV the nuclear data libraries are nearly complete [1]. Above 200 MeV the cross section predictions by Intra Nuclear Cascade (INC) models are in good agreement with the experimental data [2,3,4]. For energies from 20 to 200 MeV there are few high-quality data, most of them for (n,Xlcp) and (p,Xn) obtained in the frame of the HINDAS collaboration [1]. Particularly for (n,Xn) inelastic measurements there is only one experimental measurement [5]. Within this context, the aim of this work included in the European collaboration EUROTRANS-NUDATRA [6] was to measure (n,Xn) double differential cross sections (DDCS). Measurements using lead and iron targets were carried out at The Svedberg Laboratory (TSL), Uppsala (Sweden), where a quasi-monoenergetic neutron beam at 96 MeV is available [7,8]. They were accomplished using two independent set-ups: DECOI-DEMON and CLODIA-SCANDAL which are briefly described in the following section. Then experimental results are presented and compared with several calculations using the main available transport codes. Finally we have used the few existing data to perform a qualitative study of the dependence of (n,Xn) cross sections on the target mass. The last section of this paper will summarize the mains results and conclusions obtained from this work.

Experimental setup

In order to obtain complete distributions, the measurements were carried out using two independent devices. Both devices as well as a detailed description of experimental techniques have been presented in reference [9, 10]
To measure the low-energy part of the neutron spectrum (1 – 50 MeV), a time-of-flight telescope labelled DECOI-DEMON was developed. DECOI is a neutron-to-proton converter made of a plastic scintillator. DEMON is a neutron detector made of a cylindrical scintillator. Incoming neutron, weakly deflected in DECOI, is detected and identified using a DEMON. The neutron energy is determined using the well-known time-of-flight technique.
To measure the high-energy part of the neutron spectrum (40 – 100 MeV) a new set-up labelled CLODIA-SCANDAL was developed. CLODIA consists of seven neutron-to-proton converters and eight multi drift chambers to measure the recoil proton trajectories and determine in which converter the neutron interaction took place. In addition, one SCANDAL arm was used to measure the energy of recoil proton. Neutron energy is deduced from the angle of the well-known backward elastic neutron-proton scattering and from the energy of the recoiling proton.

Experimental results

Figure 1 shows the complete double differential distributions for lead and iron targets for an angular range from 15 to 100 degrees and with an energy threshold of 1 – 2 MeV. Distributions below 50 MeV were obtained using the DECOI-DEMON data, above 40 MeV from measurements involving CLODIA-SCANDAL set-up. In the overlap region of the energy spectra, from 40 to 50 MeV, the two set of measurement are in agreement within 10%. This value corresponds to systematic errors (see [9,10] for details).

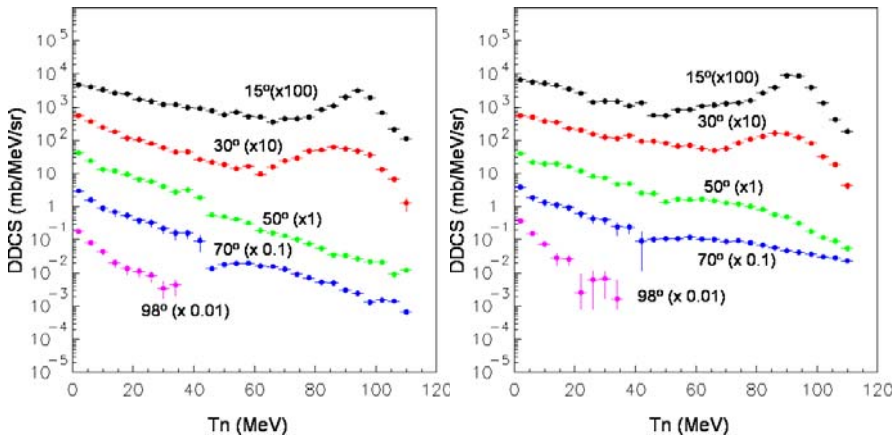

Figure 1. *(n,Xn) measured double differential cross section at 96 MeV for iron (left) and lead (right) in the angular range between 15 and 98 degrees.*

Double differential spectra are characterized by three components:
- a peak at the beam energy. This peak, only present in distributions measured at small angles, is characteristic to direct reactions between incident neutron and a neutron from the target. As expected, this elastic contribution decrease strongly with the emission angle, being more important at 15 degrees than at 30 degrees.
- a peak at low energy (1 – 15 MeV) characteristic for the evaporation process which is the dominant process at backward angles.
- in between these regions one can identify the pre-equilibrium which is a consequence of intra nuclear cascade process. This component also shows a strong dependence on the angle.

For small angles (below 30 degrees) elastic cross section can be calculated from double differential cross sections integrating over the elastic peak. On the other hand the DECOI-DEMON device allows the elastic cross section measurements at all angles [9,10]. The obtained results for lead and iron are compared with the existing experimental data [11,12,13] and with the theoretical calculations based on the optical model [14] (figure 2). Our results for both targets are in good agreement with previous experimental measurements as well as with

the optical model calculations. This allows the validation of the normalization procedure used to extract the double differential cross sections.

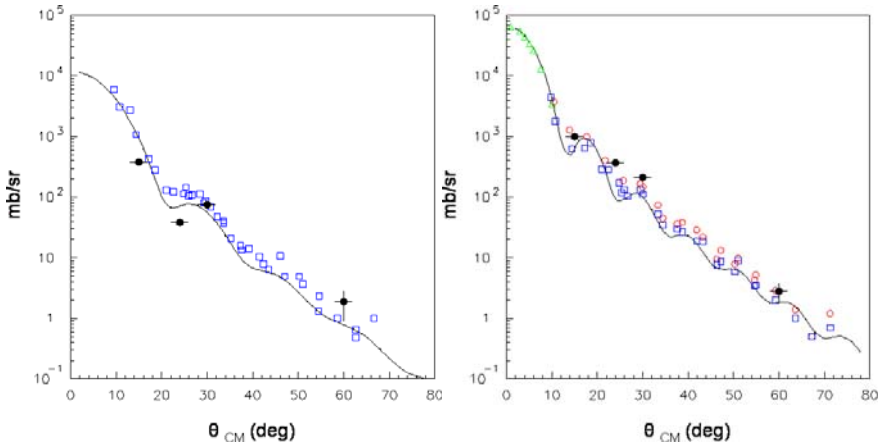

Figure 2. *Elastic cross section for iron (left) and lead (right) at 96 MeV. The experimental data are from this work (filled circles) and from previous measurements [11,12,13] (open symbols). The continuous line represents theoretical calculations based on the optical model [14].*

A detailed study shows that double differential cross section spectra at 98 degrees have all characteristics of the evaporation process in the frame of the Weisskofpt theory. The evaporation cross sections can be considered as isotropic. If we approximate elastic peak as a Gaussian function, then we can separate double differential distributions in components: evaporation, pre-equilibrium and elastic. This separation has been made for all double differential distributions presented in figure 1.

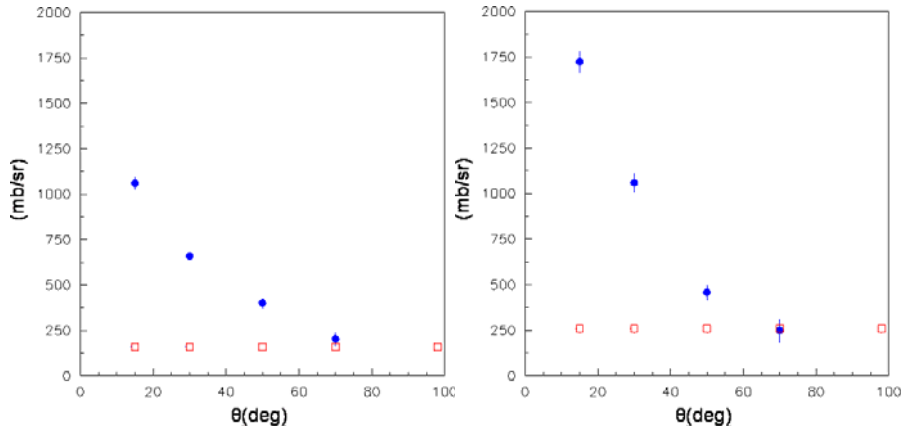

Figure 3. *Angular distributions for iron (left) and lead (right) at 96 MeV. Contribution from evaporation (open square) and pre-equilibrium (circles) process.*

Evaporation and pre-equilibrium angular distributions (figure 3) were then calculated by integration of double differential distributions. The resulting values of the pre-equilibrium emission decrease strongly with the angle preserving the same behaviour that the double differential distributions (figure 1). The data obtained for the evaporation emission are 159 ± 11 mb/sr for iron and 259 ± 23 mb/sr for lead. The relatively good agreement between these values and the values calculated using the Weisskofpt evaporation theory (respectively 148 and 306 mb/sr) suggests that double differential distributions measured at 98° are indeed the result of an evaporation process.

Energy distributions can be calculated from double differential cross sections using the Kalbach parameterization [15]. We have applied this parameterization using the complete double differential distribution (evaporation + pre-equilibrium). Results are shown in figure 4. Energy distributions have the same behaviour for iron and lead. We can observe an important

contribution at low energy due to evaporation process. This is a normal effect taking into account that neutrons are not affected by the coulomb barrier. As expected, energy cross sections for lead are higher than for iron and the difference is essentially constant over the entire energy range.

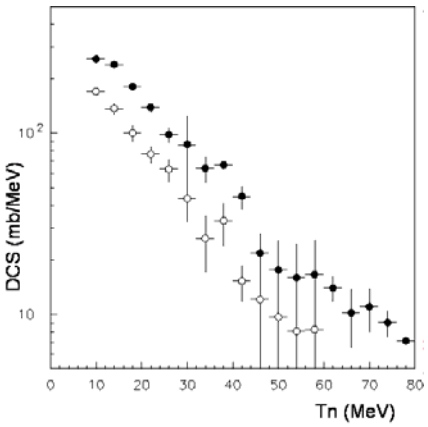

Figure 4. *Energy distributions for iron (open symbols) and lead (filled circles) derived from double differential distributions using the Kalbach parameterization [15].*

Theoretical calculations

Monte Carlo transport codes are usually employed for application, for the design and decommissioning of nuclear installations. Therefore performances of different codes and models are essential. In this section (n,Xn) energy differential distributions for lead and iron have been calculated using commonly used available transports codes and several physical models:

- MCNPX [16] with GNASH [17] and INCL4-ABLA[18,19],
- GEANT with GHEISA and FLUKA [20,21],
- TALYS [22],
- PHITS [23] with QMD [24] and SDM [25].

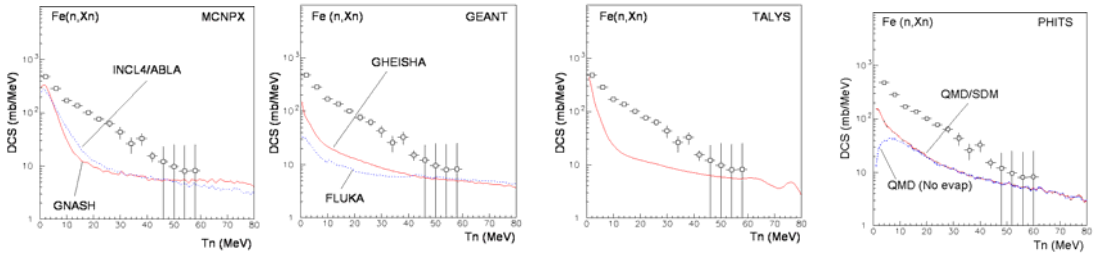

Figure 5. *Comparison between experimental data and calculated energy differential cross sections for Fe(n,Xn) reactions at 96 MeV using different available codes and models.*

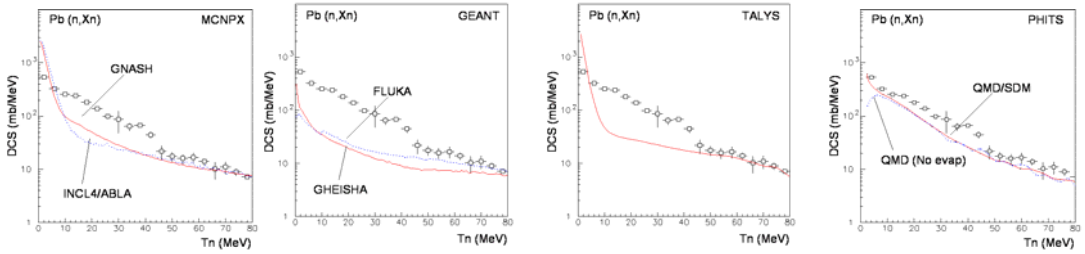

Figure 6. *Comparison between experimental data and calculated energy differential cross sections for Pb(n,Xn) reactions at 96 MeV using different available codes and models.*

Comparison between these calculations and the experimental data are shown in figures 5 and 6 for iron and lead respectively. In distribution obtained with TALYS and MCNPX we can identify two well defined contributions: an evaporative peak at low energy and a pre-equilibrium contribution at intermediate energies from 10 to 80 MeV. In distributions calculated with GEANT the effect is less visible but is also present. In these three calculated distributions, a sharp transition from pre-equilibrium to equilibrium is observed at energies around 10 MeV. Only calculations performed with QMS/SDM model using the PHITS transport show a different behaviour, allowing a better reproduction of the shape of the experimental distributions. PHITS calculation is the only one giving a reasonable agreement with measurements in all energy range in case of lead. All performed calculations give a systematic under-estimation in whole energy region in case of iron.

Cross section analysis

The EXFOR data base [26] contains few experimental data for (n,Xn) cross sections [5,27,28,29]. Available EXFOR data of double differential cross sections measured at 20° - 30° for several beam energies are presented in figure 7. One can see that the pre-equilibrium emission is not very sensitive to the incident neutron beam energy. The cross section values are comparable to the one obtains in this work.

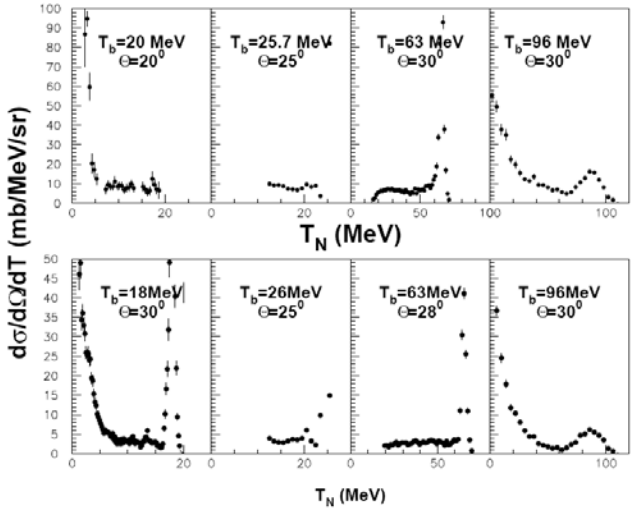

Figure 7. *Pb(n,Xn) (top) and Fe(n,Xn) (bottom) double differential cross sections at 20° - 30° for several beam energies Tb. Data are from this work and from references [5,27,28,29].*

To get a quantitative estimation of the pre-equilibrium contribution, a partial pre-equilibrium cross section σ has been derived from differential cross section by integration of the energy distribution with an energy threshold Tt. This energy threshold (Tt = 12 MeV) has been chosen to allow the use of all available data in the 18 – 100 MeV beam energy range. σ is presented as a function of the target mass (figure 8, left). Values from this work are larger than the others but we have to take into account that there is a difference of more than 70 MeV in the beam energy. To obtain a comparable quantity we have calculated the partial pre-equilibrium cross section per incident MeV. A good agreement between our data and the other experimental results is found (figure 8, right) giving confidence in data reduction and normalization procedures used in this work. Moreover a strong correlation is observed between the production ration per MeV and the size of the target.

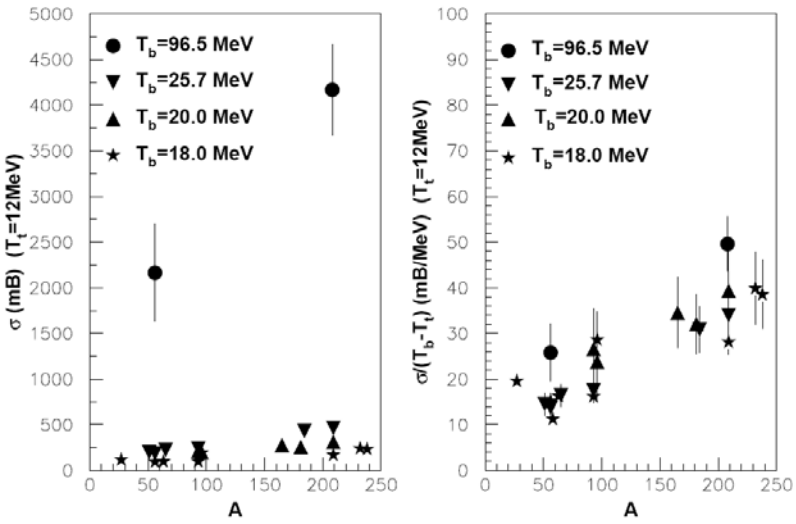

Figure 8. *Evaluated partial cross section σ with Tt = 12 MeV (left) and partial pre-equilibrium cross section per incident MeV σ / (Tb – Tt) (right) for several targets [27,28,29].*

Summary

Double differential cross sections for neutron production have been measured in 96 MeV neutrons induced reactions on iron and lead targets for an angular range between 15 and 98° and with an energy threshold of 1 – 2 MeV. Measured double differential cross section shows strong angle dependence. The elastic peak is only present at small angles (below 30°) disappearing for intermediate angles (50 – 70°) where only pre-equilibrium and evaporative contributions are present. At 98° there is only the contribution due to evaporation process.
Fe(n,n) and Pb(n,n) elastic cross sections have been extracted from double differential distributions and are in good agreement with existing experimental data and with optical model calculations. Angular distributions have been calculated for evaporative and pre-equilibrium processes. Energy distributions have been also obtained using the Kalbach systematic. Comparison between experimental data and calculations for lead show a reasonable agreement in the energy range between 40 and 80 MeV and an underestimation at low energy, except those performed with PHITS which gives a good agreement also at low energy. For iron, all calculations show a systematic underestimation in whole energy region. We have point out that only PHITS calculations are able to reproduce the shape of the measured distributions.
Comparison between the results obtained in this work and other experimental data shows that (n,Xn) double differential cross sections associated to the pre-equilibrium emission are not very sensitive to the neutron beam energy. Partial pre-equilibrium cross sections and partial pre-equilibrium cross sections per incident MeV have been calculated. Representing this as a function of target mass, a good agreement between our results and other experimental data is found.

References

[1] HINDAS. High and Intermediate energy Nuclear Data for Accelerator-Driven Systems, European Community, contract n° FI5W-CT-2000-0031.
[2] H.W. Bertini, Phys.Rev.188 (1969).
[3] A. Boudard, J. Cugnon, S. Leray and C. Volant, Phys. Rev. C66 (2002).
[4] H. Kumawat and V.S. Barashenkov, Eur. Phys. J. A26 (2005).
[5] E.L. Hjort et al, Phys. ReV. C53 (1996).
[6] EUROTRANS-NUDATRA, European Community, contract n° FI6W-CT-2004-516520.
[7] H. Condé et al, NIM A292 (1990).
[8] S. Pomp et al, ND2005, Santa Fe, AIP Conf. Proc. 769 (2005).
[9] G. Ban et al, NIM A, submitted.

[10] I.C. Sagrado Garcia et al, Proc. Intern. Workshop on Fast Neutrons Detectors and Applications, Cape Town, PoS (FNDA 2006).
[11] J. Klug et al, NIM A489 (2002).
[12] G.L. Salmon, Nucl. Phys. 21 (1960).
[13] A. Ohrn et al, to be published.
[14] A.J. Koning et J.P. Delaroche, Nucl. Phys. A713 (2003).
[15] C. Kalbach, Phys. Rev. C37 (1988).
[16] D.B. Pelowitz (Ed.), MCNPX user's Manual, LA-CP-05-0369, LANL (2005).
[17] M.B. Chadwick et al, LA-UR-98-1825, LANL (1998).
[18] A. Boudard et al, Phys. Rev. C66 (2002).
[19] A.R. Junghans et al, Nucl. Phys. A629 (1998).
[20] GEANT, CERN Program Library Long Write-up W5013.
[21] A. Fasso et al, Proc IV Int. Conf. On Calorimetry in High energy Physics, La Riodola, Italy (1993).
[22] A.J. Koning et al, NRG Report 21297/04.62741/P FAI/AK/AK (2004).
[23] H. Iwase et al, J. Nucl. Sci. Tech. 39 (2002).
[24] K. Niita et al, Phys. Rev. C52 (1995).
[25] O. Iwamoto et al, J. Nucl. Sci. Tech. 2 Suppl. (2002).
[26] EXFOR data base : http://www.nea.fr/html/dbsata/x4/.
[27] A. Marcinkowski et al, Nucl. Phys. A402 (1983) ; J. NSE 83 (1983).
[28] A. Marcinkowski et al, Nucl. Phys. A530 (1991) ; A561 (1993).
[29] S. Iijima et H. Yamakoshi, Proc. Int. Conf. Nuclear Data for Science and Technology, MITO (1988).

Characterization of neutron detectors for nuclear technology applications

T. Martínez[1)], J. Agramunt[2)], A. Algora[2)], A. Aprahamian[3)], D. Cano Ott[1)], L.M. Fraile[4)], A. Gottardo[5)], C. Guerrero[1)], M.D. Jordan[2)], H. Mach[3)], E. Mendoza[1)], M. Mosconi[6)], R. Nolte[6)], E. Reillo[1)], J.L. Tain[2)], J.J. Valiente[5)]

1) Centro de Investigaciones Energéticas, Medioambientales y Tecnológicas (CIEMAT) Avda. Complutense, 22, E-28040 Madrid, Spain
2) Instituto de Física Corpuscular (IFIC) Edificio de Institutos de Paterna, Apdo. Correos 22085, E-46071 Valencia, Spain
3) University of Notre-Dame, Notre Dame, IN-46556 Indiana, USA
4) Universidad Complutense de Madrid, Ciudad universitaria, E-28040, Madrid, Spain
5) Laboratori Nazionali di Legnaro (LNL-INFN) Viale dell'Universita', 2, I-35020 Legnaro, Italy
6) Physikalisch-Technische Bundesanstalt (PTB) Bundesallee, 100, D-38116 Braunschweig, Germany

trino.martinez@ciemat.es

Abstract: The development of neutron detector systems contributes greatly to improve nuclear data relevant to nuclear technologies for radioactive waste transmutation and management. Characterization of detectors at known irradiation fields and relevant energies is mandatory for a complete knowledge of the response function.

Introduction

Improvement on nuclear data has received a special attention in the last decades within the framework of "Technology Advances in Fast Reactors and Accelerator Driven Systems for Actinides and Long-Lived Fission Products Transmutation". Accurate nuclear data are essential for the detailed design, safety assessment and operation of these reactor systems [1,2]. Neutron cross-sections (capture, fission, inelastic) data for minor actinides (MA) are needed with improved accuracy. Decay heat data of MA-dominated fuels as well as delayed neutron data play also a crucial role within the uncertainty assessment. Additionally the need of improved decay heat data for conventional fuels has been stressed recently [3].

Uncertainty reduction in nuclear data involves the improvement of the measurement and detection techniques. Therefore, big efforts have been performed in order to develop facilities where to carry out the measurements and to design appropriate detection systems. An example is the n_TOF facility at CERN where several detection systems have shown their capabilities in measuring neutrons cross-section data [4].

Following the activities on development of detection techniques for nuclear data, our groups are involved in several detection system for the DESPEC experiment at the FAIR facility at GSI. Delayed neutron data from neutron rich isotopes will be obtained at DESPEC and will allow us to complete nuclear data libraries that would serve as input to more accurate delayed neutron summation calculation of interest in transmutation reactor systems, in particular delayed neutron of MA. Decay heat data will be obtained from the development of the DESPEC beta-decay total absorption gamma spectrometer. Decay properties (as the distribution of beta, gamma and neutrino energies) of exotic nuclei in particular neutron rich fission products could be studied with much greater accuracy.

Delayed neutrons are emitted by excited nuclei formed in beta decay of fission products, called neutron precursors. Absolute delayed neutron yield, the time dependence on the neutron activity and delayed neutron spectra have to be determined with high accuracy. A neutron spectrometer based on liquid organic scintillation cells has been proposed in order to extract information on neutron emission rate probabilities and neutron energy spectra by means of Time-of-Flight technique (TOF).

Delayed neutrons become a source of systematic uncertainty in the case of beta decay measurements with TAGS. The emitted neutron can be captured or inelastic scattered in the total absorption spectrometer and the subsequently emitted gamma-rays registered, which cannot be distinguished from the beta-delayed gamma-rays. Several scintillation materials have been considered for future spectrometers (NaI, CsI, BaF_2, $LaCl_3$:Ce) and detailed Monte Carlo simulations of this kind of background have been carried out showing the limitations of the present code models and data-bases, rendering necessary the experimental verification in order to minimize/correct for this component [5].
The characterization of detectors at known irradiation fields is mandatory for a acquiring a complete knowledge of the response function and for the improvement of their design. Features such as the light output functions for scattered proton and electrons, the neutron detection efficiency as well as the neutron sensitivity of different detector materials have been investigated at different neutron energies in the PIAF facility [6]. The status of the analysis and the preliminary results will be presented in this work.

Experimental set-up

In order to determine the response function of organic liquid scintillators and to measure the neutron sensitivity of inorganic crystal scintillators, two combined measurements have been performed with the two accelerators of the PIAF facility: the TCC CV-28 cyclotron and the 3.75MV Van de Graaff linear accelerator (VdG). The cyclotron has been used to produce mono-energetic neutron beams above 5MeV and the VdG for neutron beams below 5MeV.
Thus, two different type of experimental set-up have been arranged in order to irradiate the different detectors, which dimensions and details are reported in table 1. In the first case, liquid detectors as BC501A and BC537 (or C_6D_6) has been irradiated with neutron reference beams of 8, 10, 12 and 14 MeV at the cyclotron hall, produced through the D(d,n) reaction. The detectors were placed at a distance of 10.5 m from the target position. At the VdG hall the detectors were irradiated with neutron beams of 144, 250, 565, 1200 and 2500 keV produced through the Li(p,n) reaction. The detectors were placed at different distances, between 1 and 2.5 m depending on the intensity of the neutron fluence.
In the other hand, inorganic scintillators as NaI, CsI, BaF_2, $LaCl_3$ and $LaBr_3$ crystals were irradiated only at the VdG hall with neutron reference beams of 144, 250, 565, 1200 and 2500 keV. The detectors were placed at a distance of around 1m and at different angles, ±30 and ±61 degrees from the incident direction, being irradiated by neutrons with lower energies.

Table 1. *Design details of the different detectors used in the measurements.*

Detector	Diameter x Length (mm)	PMT	Light guide
BC501A	200 x 50	XP4512B	Y
BC537	101 x 76	XP4512B	N
NaI (Tl)	76 x 76	9265B03	N
CsI (Tl)	75 x 35	R-580	Y
BaF_2	50 x 50	E-9821QB	N
$LaCl_3$ (Ce)	76 x 76	XP5300B02	N
$LaBr_3$ (Ce)	38 x 38	XP20D0/B	N

The readout of the detector signals were carried out with two types of data acquisition system (DAQ): a digital system based on a flash-ADC board and, an analogue system based in CAMAC and VME standard electronics. The liquid detectors data were registered using both types of system in order to compare the performance of each system. The inorganic scintillators just used the CAMAC-based system. Specific software routines were developed to run both systems. The trigger of each system was build from the accelerator time signal and each detector signal. A 100 Hz clock signal was also included in the trigger system to evaluate the possible dead-time corrections. In the case of the digital system, a digital scaler based on a National Instruments board was used to account for the dead-time corrections.

Time of flight technique has been used to determine the deposited energy spectrum that corresponds to neutron energies as well as the gamma spectrum originated from the interaction of neutron with the detector material. The accelerators were run in pulsed mode to optimize the direct neutron events from scattered in surrounding materials and spurious background events. Energy calibration measurements were performed with a set of standard gamma calibration sources and an AmBe neutron source.

Data analysis

One of the objectives of the work is the determination of the light output function, $L_p(E)$, for protons in the energy range up to 20 MeVee with reference to photon calibration for liquid scintillation detectors. Thus, the analysis procedure will consist in an initial calibration of the electron light output function, $L_e(E)$, using a set of gamma calibration sources. The experimental response should be compared to a MC simulated response function, allowing us to determine the average calibration factor and the resolution function ($\Delta L/L$). Then, the neutron (or proton recoil) response spectrum should be obtained from the integration the pulses and by setting the appropriate time window cut on the time of flight spectrum and by applying a further cut on the delayed-to-total charge ratio. Such experimental spectrum should be corrected for the acquisition dead-time and normalized with the effective neutron fluence. Then the experimental proton recoil spectra will be compared with the MC simulated responses, convoluted with an appropriated resolution function in order to reproduce the upper part of the response functions. The results from these comparisons will allow to obtain the light output function, $L_p(E)$, for protons and the energy resolution as a function of the neutron energy beam.
A preliminary analysis has been performed for the irradiation beam energies produced with the cyclotron through the D(d,n) reaction. An example of time of flight spectrum recorded with the BC501A scintillator is plotted in figure 1 showing the gamma peak events at lower flight times (~35 ns) and the 14MeV neutrons peak at around 210 ns. The bump observed a larger flight times corresponds to break-up neutrons produced in the D-d reaction. A second tof spectrum is plotted to show the neutrons produced when the deuterium target gas has been removed from the target holder, the gas-out spectrum.

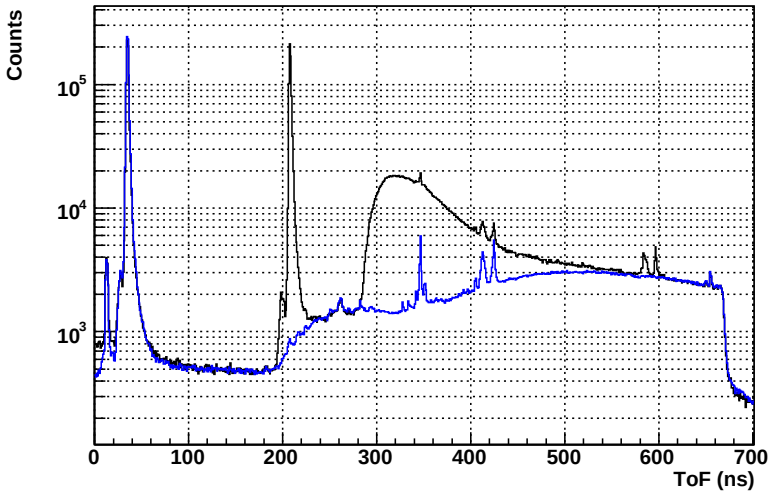

Figure 1. *Tof spectra for the D(d,n) reaction (black) and reaction of deuterium beam with holder without target (blue) measured with BC501A detector. The peak structure located at around 210 ns corresponds to neutron of 14MeV.*

After setting a cut in the time of flight window corresponding to 14MeV neutrons and by setting a bi-dimensional cut on the total versus delayed charge integration matrix that select the neutron events from gamma events, the corresponding total integration charge spectrum is plotted in figure 2. It shows the proton recoil response that should be compared to the Monte Carlo simulation response in order to determine the upper edge of the response function and obtain the value of the light output function for proton recoils originated from neutron energy of 14 MeV.

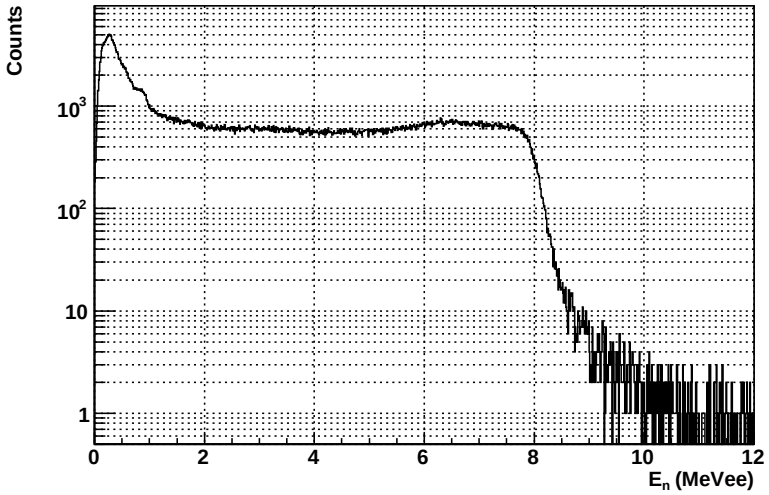

Figure 2. *Proton recoil response to mono-energetic neutron beam at 14MeV after cut in the tof spectrum an cut in the appropriate total-to-delayed charge ratio.*

Absolute neutron sensitivity and detection efficiency of detector cells at a given neutron energy can be deduced by integrating the corresponding response function normalized with the effective neutron fluence at each energy beam.
Another objective is the characterization of the neutron induced gamma-ray background through capture and inelastic scattering in the inorganic scintillators. Capture events are predominant at low neutron energies, while inelastic scattering dominates at higher energies. The intensity of gamma response due to neutron induced capture and inelastic events, should be determined after setting the corresponding cut on time-of-flight parameter for the neutron events. Energy calibration and dead time correction has to be applied to the experimental detector response as well as the normalization to the neutron fluence at each neutron energy. Experimental intensities will be compared with calculation obtained with neutron capture and inelastic cross section data available from the ENDF/B database for the different scintillation materials.
At present, the data analysis is ongoing and results will be available soon.

Conclusions

Several detectors, organic liquid and inorganic scintillators, considered as a prototypes of the final detection systems for the DESPEC experiment have been characterized with monochromatic neutrons beams and gamma sources at the PTB Accelerator Facility.
The performance of liquid organic scintillators have been tested in terms of light output functions for electrons and protons and energy resolution. The response function of inorganic scintillators has been studied in terms of gamma background originated from neutron interaction through capture and inelastic scattering.
Time of flight technique has been used to determine the deposited energy spectrum with a reduction of the unwanted events produced from scattered neutrons and background. The performance of different kind of data acquisition systems have also been tested during the PTB run. The analysis of the data is ongoing.

Acknowledgements
Special thanks go to EFNUDAT program for funding support. We would like to thank R. Nolte and collaborators of the Neutron Dosimetry Group for their help during the run and the accelerator staff of PTB. The technical support of Ciemat staff is also acknowledged.

References

[1] M. Salvatores. “Future nuclear power systems and nuclear data needs”. J. Nucl. Sci. and Tech. Supplement 2, 4-12 (2002).
[2] Y. Ikeda. “Nuclear data relevant to accelerator driven systems”. J. Nucl. Sci. and Tech. Supplement 2, 13-18 (2002).
[3] T. Yoshida, A.L. Nichols, “Assessment of fission product decay data for decay heat calculations”, WPEC-25/NEA-OECD, http://www.nea.fr/html/science/wpec/.
[4] n_TOF Collaboration. http://pceet075.cern.ch.
[5] J.L. Tain, “Beta decay total absorption measurements for nuclear technology and astrophysics”, Proceed. Int. Conf. ND2007, Nice, April 22-27, 200.
[6] Physikalisch-Technische Bundesanstalt (PTB). http://www.ptb.de.

Protactinium neutron-induced fission up to 20 MeV

V. M. Maslov

Joint Institute for Nuclear & Energy Research, 220109, Minsk-Sosny, Belarus
maslov@bas-net.by

Abstract: The robust evaluation of ^{230,231,232,233}Pa(n, F) is supplemented by consistent description of fission probability data, coming from transfer reactions. ^{230,231,232,233,234}Pa and ^{231}Th fission probability and ratios of fission probabilities, surrogate for neutron-induced fission of respective target nuclides, of various excitation energy ranges, including emissive fission domain, are critically analyzed. First chance fission cross sections trends are based on consistent description of ^{232}Th(n, F), ^{232}Th(n,2n) and ^{238}U(n, F), ^{238}U(n,xn) data. The theoretical approach employed is supported by the ratio surrogate data for the ^{237}U(n, F) reaction. Recent ratio surrogate data on the fission probabilities of ^{232}Th(^{6}Li,^{4}He)^{234}Pa and ^{232}Th(^{6}Li,d)^{236}U by Nayak et al. (2008), relevant for the E_n=11.5-16.5 MeV, support the predicted ^{233}Pa(n, F) cross section. The predicted trend of ^{231}Pa(n, F) cross section up to E_n=20 MeV, which is similar to that of ^{233}Pa(n, F), is consistent with fissilities of Pa nuclides, stemming from ^{232}Th(p, F) data analysis.

Introduction

Protactinium-231 can initiate ^{232}U production in uranium- and thorium-uranium-fueled nuclear reactors by capture of neutrons and subsequent β-decay. This chain also could be initiated after capture and (n, 2n) reactions on ^{230}Th (^{230}Th(n, γ)^{231}Th(β$^-$)^{231}Pa(n, γ)^{232}Pa(β$^-$)^{232}U) or ^{232}Th (^{232}Th(n,2n)^{231}Th(β$^-$)^{231}Pa(n, γ)^{232}Pa(β$^-$)^{232}U) nuclides, respectively. Protactinium-233 is a precursor of the ^{233}U, which is formed after capture of neutrons by ^{232}Th and two subsequent β$^-$-decays, i.e., ^{232}Th(n, γ)^{233}Th(β$^-$)^{233}Pa(β$^-$)^{233}U. Because of rather long β$^-$-decay half-life of 27 days, ^{233}Pa inventory is very important for the nuclear reactor reactivity control. However, ^{233}Pa half-life is still short, which prohibited extensive neutron cross section measurements until recently. Neutron-induced fission measured database for ^{231}Pa(n, F) and ^{233}Pa(n, F) was enriched by a few data sets [1,2,3], however they still do not cover the energy range of 0.001-20 MeV. The direct fission (neutron-induced cross sections of ^{231}Pa(n, F) and ^{233}Pa(n, F)) data might be complemented with a surrogate fission data. Namely, fission probabilities of ^{230,231,232,233,234}Pa nuclides, measured in ^{232}Th(^{3}He,d)^{233}Pa, ^{231}Pa(d,p)^{232}Pa, ^{230}Th(^{3}He,d)^{231}Pa and ^{230}Th(^{3}He,t)^{230}Pa at excitation energies 6~11.5 MeV [4] and fission probabilities of ^{232}Th(^{3}He,p)^{234}Pa, ^{232}Th(^{3}He,d)^{233}Pa, ^{232}Th(^{3}He,t)^{232}Pa at excitation energies 6~15 MeV [5]. However, in an emissive fission domain data by Petit et al. [5], as well as older indirect data by Birgul et al. [6] may provoke rather exotic assumptions about the fission chances contributions to the observed ^{233}Pa(n, F) and ^{231}Pa(n, F) fission cross sections. Description of these data needs steep decrease of the first-chance fission cross sections and systematically lowered fission probabilities of relevant Pa nuclides [7]. At excitations near fission threshold surrogate data [4,5] are model-dependent via assumed neutron-absorption cross section and different angular momentum spectra of excited and fissioning states in neutron-induced and transfer fission reactions [8, 9]. At excitations higher than emissive fission threshold the sensitivity of the surrogate data to the angular momentum spectra of the nuclide fissioning in (n, nf) reaction may again increase. Another source of possible discrepancies might be pre-equilibrium effects, which are pronounced in (n, F) reactions. Recently developed surrogate ratio method [10,11,12] largely removes the uncertainty, imposed by pre-equilibrium effects and different angular momentum spectra of excited and fissioning states in neutron-induced and transfer reactions. The theoretical approach, which would be employed for the $^{229\text{-}233}$Pa(n, F) cross section predictions, was independently supported by the ratio surrogate fissility data [10,11,12] for the ^{237}U(n, F) reaction [13,14]. In [10,11] the ratio of fission probabilities of ^{238}U and ^{236}U, excited in (d,d') reactions was measured with the strong "background" of ^{238}U(d, F) and ^{236}U(d, F) fission reactions. In [12] the ratio of fission probabilities of ^{238}U and ^{236}U, excited in (α, α') reaction, was measured. Recent ratio surrogate data on fission probability of ^{232}Th(^{6}Li, ^{4}He)^{234}Pa and ^{232}Th(^{6}Li, d)^{236}U

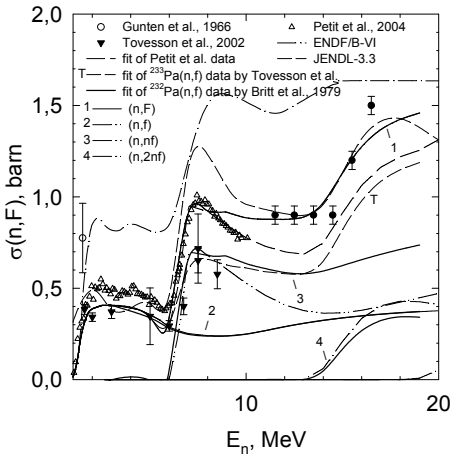

Figure 1. *Cross section of ^{231}Pa(n, F).*

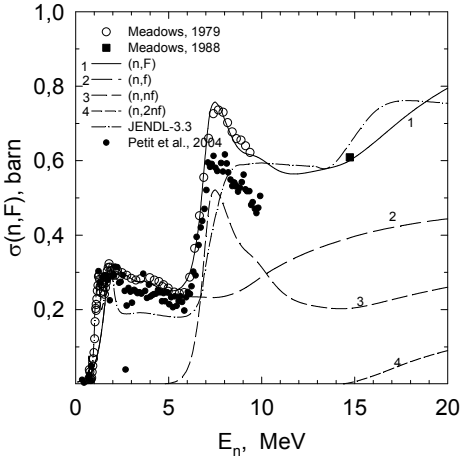

Figure 2. *Cross section of ^{230}Th(n, F).*

by Nayak et al. [15], relevant for the E_n = 11.5-16.5 MeV, nicely support the described approach, first presented at ND2004 Conference [16].
The major justification for the robust improvement of ^{229,230,31,232,233}Pa evaluated data comes from a consistent description within Hauser-Feshbach statistical model of direct neutron-induced and surrogate fission data for the mass chain A=229-234.

^{233}Pa(n, F), ^{232}Pa(n, F)

Fission cross section of ^{233}Pa(n, F) measured in [2, 3] between ~1 and ~3 MeV and ~5 and ~8.5 MeV, are rather discrepant with fission data [5], surrogate for ^{233}Pa(n, F) reaction. Fission probability $P_F^{\exp}$ was extracted in [5] from the transfer reaction ^{232}Th(^{3}He,p)^{234}Pa for E_n =0.5 ~ 10 MeV. The cross section obtained as $\sigma_{nf} = \sigma_{CN} P_f^{\exp}$ is used as a surrogate for the neutron-induced fission of ^{233}Pa, neutron absorption cross section was calculated with deformed optical potential [16, 17]. The surrogate data [5] are appreciably higher than direct ^{233}Pa(n, F) data [2, 3] both around (n, f) and second-chance (n, nf) fission thresholds (see Fig. 1). Similar discrepancies of direct and surrogate neutron-induced fission data were addressed by Arthur [18] in a combined analysis of the ^{235}U(n, f) data and ^{234}U(^{3}He,p)^{236}U reaction at E_n<3 MeV. It was observed [18] that when surrogate neutron-induced fission cross section is defined either as $\sigma_{nf} = 3.1 P_{nF}^{\exp}$, $\sigma_{CN} = 3.1$ barn being the estimate of the neutron compound reaction cross section, or using optical model neutron absorption cross section as

$$\sigma_{\mathrm{nf}}(\mathrm{E_n}) = \frac{\pi\lambda^2}{2(2I+1)} \sum_{\mathrm{lJ}\pi} (2\mathrm{J}+1)\mathrm{T_{lj}}(\mathrm{E_n})\mathrm{P_f^{exp}}(\mathrm{E_n}), \qquad (1)$$

the surrogate fission cross section overestimates σ_{nf} for E_n ≤2 MeV by 10~20 %. That is the consequence of the of the spin population differences in transfer and (n, f) reactions [18, 19]. In case when the observed fission probability data of transfer reactions $P_f^{\exp}(\mathrm{E_n}) = \sum_{\mathrm{lJ}\pi} \mathrm{P_f^{J\pi}}(\mathrm{U})\alpha^{J\pi}(\mathrm{U})$, where $\alpha^{J\pi}(\mathrm{U})$ defines the spin populations, are fitted and $P_f^{J\pi}$ are used in Eq. (1), the discrepancy of the direct and surrogate data diminishes [18,19].

Much larger discrepancy is observed at the onset of the second chance fission ^{233}Pa(n, nf), the direct fission data being much lower (see Fig.1). In principle it could be traced to oversimplified procedure of obtaining surrogate data as $\sigma_{nF} = \sigma_{CN} P_F^{\exp}$ in the emissive fission domain, pre-equilibrium emission sensitivity and influence of spectroscopic properties of transition states of ^{233}Pa, fissioning in ^{233}Pa(n, nf) reaction. The latter effect for odd-even nuclide ^{233}Pa should be excluded, unlike the observed discrepancy of direct and surrogate ^{230}Th(^{4}He,^{3}He)^{231}Th data for ^{230}Th(n, F), which might be traced back to properties of e-e nuclide ^{230}Th, fissioning in ^{230}Th(n, nf) reaction. Note that the discrepancy is of different “sign”, than shown on Fig. 1 for ^{233}Pa(n, F) reaction. However, its origin would be of much interest for

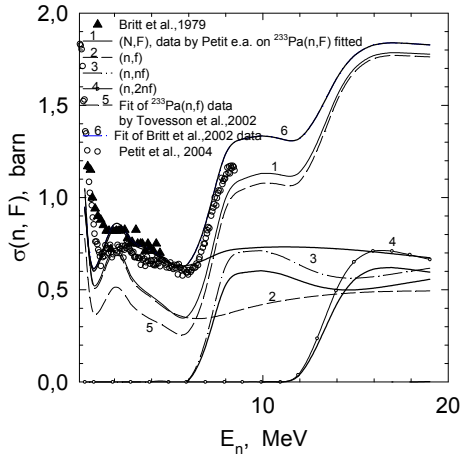

Figure 3. *Cross section of ^{232}Pa(n, F).*

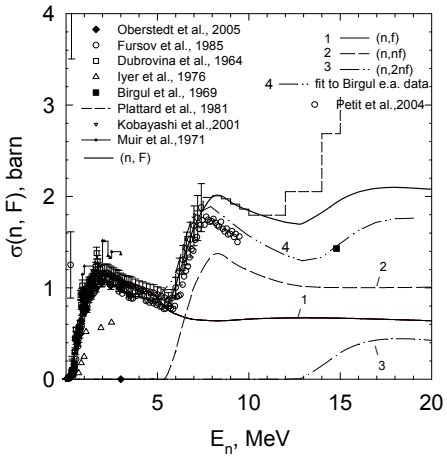

Figure 4. *Cross section of ^{231}Pa(n, F).*

^{231,232}Pa target nuclides. The shape of the ^{230}Th(n, F) cross section at E_n~6-9 MeV is controlled by the spectroscopic properties of the transition states of e-e ^{230}Th, fissioning in ^{230}Th(n, nf) reaction. Wide peak around E_n~8 MeV, observed in [20] is described by lowering the negative parity octupole band of ^{230}Th due to mass-asymmetry of outer saddle deformations. The step-like irregularity at E_n~9 MeV was interpreted as being due to the excitation of two-quasi-particle states in the ^{230}Th at outer saddle deformations [21, 22]. The estimated fission probability of ^{232}Th is compatible with data [8, 9], surrogate for the ^{231}Th(n, f) reaction. Similar cross section shape was observed [23] and predicted [22] for ^{229}Th(n, f) reaction. The increasing trend of the first-chance fission cross section ^{230}Th(n,f) is supported by data [24] at 14 MeV. Similar peculiarities are observed in ^{232}Th(n, F) and interpreted in [21, 22]. It might be concluded that the discrepancy of surrogate and direct fission data for ^{230}Th target nuclide above (n, nf) fission threshold is of systematic character, possibly due to factorization of the fission probability and neutron absorption cross section to get surrogate fission cross section.
For incident neutron energies up to E_n~2.5 MeV the threshold shape of ^{233}Pa(n, f) cross section is roughly reproduced with adopted level density description by varying the density of one-quasiparticle states of residual nuclide ^{233}Pa , as described in [16,17] (see Fig.1). The decreasing trend of the data above E_n~3 MeV is fitted with the correlation function value Δ_f at the outer fission barrier saddle of ^{234}Pa, which controls the cross section slope.
Above emissive fission threshold contributions to the observed fission cross section coming from (n,xnf), x= 1, 2, 3...X, fission of relevant equilibrated uranium nuclei, is calculated as

$$\sigma_{\mathrm{nF}}(E_n) = \sigma_{\mathrm{nf}}(E_n) + \sum_{x=1}^{X} \sigma_{\mathrm{n,xnf}}(E_n), \qquad (2)$$

emissive fission contributions are calculated using $P_{fx}^{J\pi}$ fission probability estimates

$$\sigma_{\mathrm{n,xnf}}(E_n) = \sum_{J\pi}^{J} \int_0^{U_{\max}} W_{x+1}^{J\pi}(U) P_{f(x+1)}^{J\pi}(U) dU, \qquad (3)$$

where $W_x^{J\pi}$ is the population of (x+1)-th nucleus at excitation energy *U* after emission of x neutrons, excitation energy U_{max} is defined by the incident neutron energy E_n and energy, removed from the composite system by ^{233}Pa(n,xnf) reaction neutrons. Fission threshold fission probabilities $P_{fx}^{J\pi}$ of ^{233}Pa and ^{232}Pa nuclides, fissioning in ^{233}Pa(n, nf) and ^{233}Pa(n, 2nf) reactions, are estimated using data of ^{232}Th(^{3}He,d)^{233}Pa [4, 5] and ^{231}Pa(d,p)^{232}Pa [5].
Overall consistency of ^{232}Th(^{3}He,d)^{233}Pa fissility data measured in [4] and [5] is demonstrated on Fig. 3 showing neutron-induced fission cross section of ^{232}Pa(n, F). Contribution of the first-chance fission to the observed fission cross section is defined by preequilibrium emission

of first neutron and level densities of fissioning and residual Pa nuclides. The behavior of the first-chance fission cross section σ_{nf} is defined via P_{f1}:

$$\sigma_{nf} = \sigma_c(1 - q(E_n))P_{f1} \,. \qquad (4)$$

The first neutron pre-equilibrium emission rate $q(E_n)$ is fixed by the consistent description of ^{238}U(n,f), ^{238}U(n,xn) and ^{232}Th(n,f), ^{232}Th(n,2n) data [25]. Fission barriers of Pa nuclei are believed to be three-humped, that is, the outer barrier has one more shallow well. However, the inner barrier height is rather low as compared with the outer splitted one. So, in the first "plateau" region and at higher energies we can safely use double-humped barrier model and relevant barrier parameters. The first-chance fission probability P_{fx} of the $^{233.233,234}$Pa nuclides depends only on the level density of fissioning and residual nuclei. We consider the adopted $\delta W_{fA(B)}$ [26,27] to be effective, provided that δW_n are obtained with the liquid drop model.

Neutron-induced fission cross section ^{233}Pa(n, F) should demonstrate strong step-like structures, relevant to the contributions of (n,xnf) reactions, since fission probability of ^{234}Pa nuclide is rather low. The ^{233}Pa(n,f) fission cross section shape predicted by the measured data [2,3], could be fitted, but for that the contribution of the second chance fission reaction ^{233}Pa(n, nf) to the ^{233}Pa(n, F) would be extremely low. Consequently, calculated ^{232}Pa(n,f) cross section would be drastically discrepant with the indirect data [4] on ^{232}Pa(n,f) at E_n~0.5 –5 MeV (see Fig. 3). Above (n,nf) reaction threshold the indirect data by Petit et al. [5] could be fitted up to E_n~10 MeV. Steep lowering of ^{233}Pa(n,f) cross section above E_n~7 MeV is obtained by increasing the parameter value $\delta_f = \Delta_f - \Delta_o$, for ^{233}Pa from δ_f =0.075 MeV to δ_f =0.165 MeV. The former value of δ_f =0.07 MeV corresponds to the δ_f value for the ^{231}Pa fissioning nuclide (^{231}Pa(n,nf) fission reaction), which produces similar description of the ^{230}Pa(n,f) data by Britt and Wilhelmy [4] in E_n~2-5 MeV incident neutron energy range.

When fission probability of the ^{233}Pa is tuned to fit the decreasing trend of the surrogate data by Petit et al. [9] above (n,nf) fission threshold, ^{232}Pa(n, f) cross section remains systematically lower than surrogate data [4] at E_n~0.5 –5 MeV (see Fig. 3). In case of fitting surrogate data [4] on ^{232}Pa(n,f) at E_n~2-5 MeV the calculated ^{233}Pa(n, f) cross section remains rather flat in the second plateau region [16,17] (see Fig. 1). Fig. 3 compares calculated fission cross sections of ^{232}Pa(n,f) with surrogate data [4, 5]. The latter data are obtained as factorization of the measured fission probability and neutron absorption cross section of [17]. The discrepancies of the calculated curve and simulated data below E_n~2 MeV are explained by the entrance channel influence in transfer reactions and neutron-induced fission reaction. Shape of the ^{233}Pa(n, F) calculated cross section, obtained by fitting ^{232}Pa(n,f) data by Britt and Wilhelmy [4] in E_n~2-5 MeV energy range in [16,17] is nicely supported by recent ratio surrogate data on the fission probabilities of ^{232}Th(^{6}Li,^{4}He)^{234}Pa and ^{232}Th(^{6}Li,d)^{236}U by Nayak et al. [15], relevant for the E_n = 11.5-16.5 MeV. These data as well as ratio data [10,11,12] are free of most strong systematic uncertainties of surrogate data, since only coincidences of fission and correlated particle are measured.

^{231}Pa(n, F), ^{230}Pa(n, F)

Observed neutron-induced fission cross section of ^{231}Pa(n,f) reaction (see Fig. 4) demonstrates strong step-like structures, relevant to the contributions of (n,xnf) reactions. Above (n,nf) reaction threshold calculated curve is compatible with measured data by Fursov et al. [28] - up to E_n~7 MeV, and up to E_n~10 MeV with data by Plattard et al. [29] . Data point by Birgul et al. [6] at E_n~14 MeV is incompatible with the direct data trend. The Petit et al. [5] data are obtained as factorization of the fission probability and neutron absorption cross section of [16,30]. The situation here is quite similar to that encountered in case of calculated and surrogate ^{233}Pa(n, F) cross section. The data, surrogate for ^{231}Pa(n, F) reaction are systematically lower, than direct (n, F) data above E_n~7 MeV. Actually, this trend and data by Birgul et al. [6] at E_n~14 MeV could be reproduced. For that the contribution of the ^{231}Pa(n,nf) should be much lower, than predicts fission probability for the fissioning nuclide ^{231}Pa, estimated using fission probability data of ^{230}Th(^{3}He,d)^{231}Pa reaction [4]. Then observed ^{231}Pa(n, F) cross section would be discrepant with data by Plattard et al. [29] at $E_n \geq 7$ MeV. Fig. 7 compares calculated cross sections of ^{230}Pa(n, F) with surrogate data [4]. Discrepancy

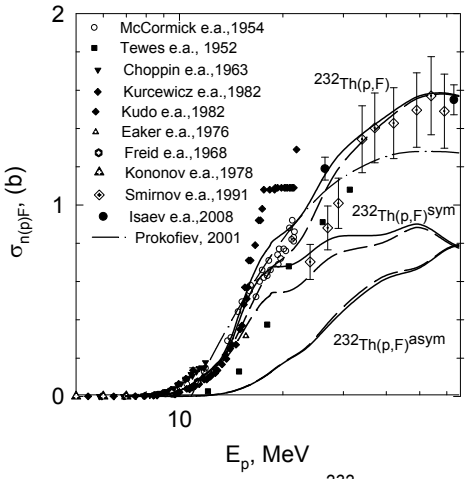

Figure 5. *Cross section of ^{232}Th(p, F).*

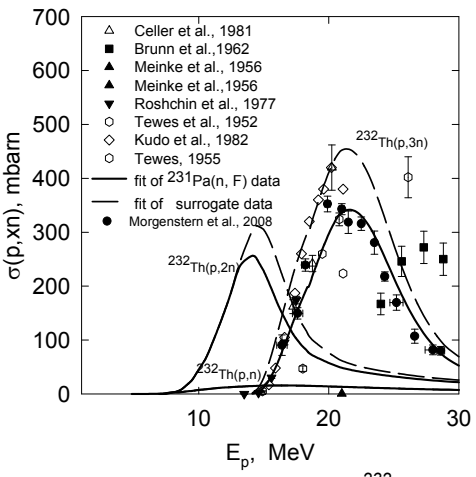

Figure 6. *Cross section of ^{232}Th(p, 3n).*

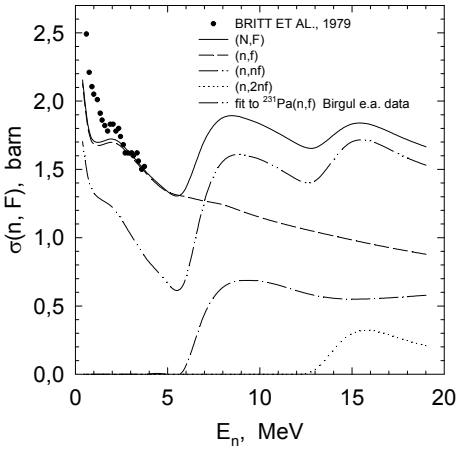

Figure 7. *Cross section of ^{230}Pa(n, F).*

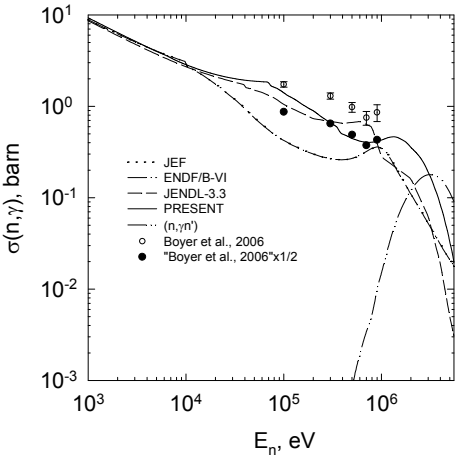

Figure 8. *Cross section of ^{233}Pa(n, γ).*

of the calculated curves and surrogate data for E_n~2 MeV is explained by the entrance channel influence for transfer reactions and neutron-induced fission reaction. Double-dot dashed curve shows the ^{230}Pa(n,f) fission cross section, decreased to fit the data point by Birgul et al. [6]. Fission probability for the nuclide ^{230}Pa, fissioning in ^{231}Pa(n, nf) reaction, was estimated using fission probability data from the transfer reaction ^{230}Th(^{3}He,t)^{230}Pa [4]. For ^{231}Pa(n,f) reaction we could describe the general shape of the fission cross section data by Kobayashi et al. [31] starting from ~0.01 keV [30]. The predicted trend of ^{231}Pa(n, F) cross section up to E_n=20 MeV, which is similar to that of ^{233}Pa(n, F), is consistent with fissilities of Pa nuclides, stemming from consistent analysis of ^{232}Th(p, F) and ^{232}Th(p,3n) data analysis. The data base for p+^{232}Th interaction was enlarged by new data on ^{232}Th(p, F) [32] and ^{232}Th(p,3n) [33] for the excitation energy range , corresponding to E_p=15~30 MeV, where the fission probabilities of ^{231}Pa and ^{230}Pa are of major importance (see Figs. 5,6, and [34]). Higher for ^{232}Th(p, F) and lower curves for ^{232}Th(p,3n) cross sections correspond to present description of ^{231}Pa(n, F), while lower and higher, respectively, to the fit of indirect data. Strong discrepancies with phenomenological estimates of [35] are demonstrated.

For incident neutron energies up to ~2.5 MeV the threshold shape of ^{231}Pa(n,f) cross section is roughly reproduced with adopted level density description by varying the density of one-quasiparticle states of residual nuclide ^{231}Pa, as described in [36]. In the same manner was calculated the sub-threshold behavior of ^{233}Pa(n,f) cross section. The capture cross section ^{233}Pa(n,γ) was estimated with transfer reaction ^{232}Th(^{3}He,p)^{234}Pa in [37] up to E_n~1 MeV. Fig. 8 compares surrogate data, measured in 2006, with calculated ^{233}Pa(n,γ) capture cross section [16,17] and previous evaluated data. The measured data are much higher, except E_n~0.1 MeV, though the energy variation of the data in keV-energy range is roughly reproduced with our previous evaluation, for that the data [37] are shown multiplied by 1/2.

Conclusion

The improved evaluation of ^{230,231,232,233}Pa(n, F) evaluated data is shown to be possible based on consistent description of fission probability data, coming from transfer reactions. Discrepancy of surrogate and direct fission data for ^{230}Th target nuclide at excitations higher than (n, nf) emissive fission threshold is of systematic character, applicable for ^{231,233}Pa targets as well, possibly due to factorization of the fission probability and neutron absorption cross section to get fission cross section. The theoretical approach employed is supported by the ratio surrogate data for the ^{237}U(n, F) reaction. Recent ratio surrogate data on the fission probabilities of ^{232}Th(^{6}Li,^{4}He)^{234}Pa and ^{232}Th(^{6}Li,d)^{236}U by Nayak et al. [15], relevant for the emissive fission domain, support the theoretical approach in case of ^{233}Pa(n, F) reaction. The predicted trend of ^{231}Pa(n, F) cross section up to E_n=20 MeV, which is similar to that of ^{233}Pa(n, F), is consistent with fissilities of Pa nuclides, stemming from consistent analysis of ^{232}Th(p, F) and ^{232}Th(p,3n) data analysis.

Acknowledgements
This work supported within Project B-1604 of International Science and Technology Center.

References

[1] S. Oberstedt, S. Oberstedt, F-J. Hambsch et al., Ann. Nucl. Energy 32 (2005) 1867.
[2] F. Tovesson, A. Oberstedt, F-J. Hambsch et al., Phys. Rev. Lett. 88 (6), 062502-1(2002).
[3] F. Tovesson, F-J. Hambsch, A. Oberstedt et al., Nucl. Phys. A, 733, 3 (2004).
[4] H.C. Britt, J.B. Wilhelmy, Nucl. Sci. Eng., 72, 222 (1979).
[5] M. Petit, M. Aiche, G. Barreau et al., Nucl. Phys. A, 735, 3 (2004).
[6] O. Birgul, S.J.J. Lyle, Radiochimica Acta, 11, 108 (1969).
[7] G. Vladuca, F.-H. Hambsch, A. Tudora et al., Nucl. Phys. A 740 (2004)3.
[8] W. Younes and H.C. Britt, Phys. Rev. C 68, 034610 (2003).
[9] W. Younes and H.C. Britt, Phys. Rev. C 67, 024610 (2003).
[10] C. Plettner, H. Ai, C.W. Beausange et al., Phys. Rev. C 71 (2005) 051602(R).
[11] C. Plettner, H. Ai, C.W. Beausange et al., J. Phys. G: Nucl. Phys. 31 (2005) S1573.
[12] J.T. Burke, L.A. Bernstein, J. Escher et al., Phys. Rev. C 73 (2006) 054604.
[13] V.M. Maslov, Phys. Rev. C 72 (2005) 044607.
[14] V.M. Maslov Phys. Atom. Nucl., 71 (2008) 9.
[15] B.K. Nayak, A. Saxena, D.C. Biswas et al., Phys. Rev. C 78, 061602(R) (2008).
[16] V.M. Maslov et al., Proc. of the International Conference on Nuclear Data for Science and Technology, September 26 - October 1, 2004, Santa Fe, USA, p. 354.
[17] V.M. Maslov et al., INDC(BLR)-020, Vienna, 2004.
[18] E.D. Arthur, Trans. Amer. Nucl. Soc. 1984 Annual Meeting, New Orleans, June 3-7, 1984, vol. 46, TNSAO 46, p. 759.
[19] J. Escher and F.S. Dietrich, Phys. Rev. C 74 (2006) 054601.
[20] J.W. Meadows, in Proc. Int. Conf. on Nuclear Cross Sections for Technology, Knoxville, Tennessee, 22-26 Oct 1979, p. 479 (1979).
[21] V.M. Maslov, Nucl. Phys. A 743 (2004) 236.
[22] V.M. Maslov, Phys. Lett. B649 (2007) 376.
[23] B.M. Gohberg, G.A. Otroshchenko, V.A. Shigin, Dok. Akad. Nauk USSR, 128 (1959) 911.
[24] J.W. Meadows, Journ. Ann. Nucl. Energy 15 (1988) 421.
[25] V.M. Maslov et al., Phys. Rev. C 68, 034607 (2004).
[26] W.M. Howard and P. Moller, Atomic Data and Nuclear Data Tables, 25, 219 (1980).
[27] S. Bjornholm and J.E. Lynn, Rev. Mod. Phys. 52, 725 (1980).
[28] B.I. Fursov et al., Atomnaya Energiya, 59 (4), 339 (1985).
[29] S. Plattard, G.F. Auchampaugh, H.W. Hill et al. Phys. Rev. Lett., 46, 633 (1981).
[30] V.M. Maslov et al., INDC(BLR)-019, Vienna, 2004.
[31] K. Kobayashi, S. Yamamoto, S. Lee et al, Nucl. Sci.Eng., 139, 273 (2001).
[32] S. Isaev, R. Prieels,Th. Keutgen et al., Nucl. Phys. A809 (2008) 1.
[33] A. Morgenstern et al., Appl. Rad. and Isot., 66 (2008) 1275.
[34] V.M. Maslov, NEMEA-4 Neutron Measurements, Evaluations and Applications. JRC Scientific and Technical Reports, p. 171 (EUR 23235 EN-2008), 2008.
[35] A.V. Prokofiev, Nucl. Instr. Meth. In Phys. Res., A463 (2001) 557.
[36] V.M. Maslov, Physics of Atomic Nuclei, 63, 161 (2000).
[37] S. Boyer, D. Dassie, J.N. Wilson et al., Nucl. Phys. A, 775 (2006) 173.

Testing fast digitizing data acquisition system (FDDAS) at FZD

A. Matić[1)] R. Hannaske[1,2)], R. Beyer[1)], A. Dammrau[1)], E. Birgersson[1)], T. Kögler[2)], E. Grosse[1,2)], A. Junghans[1)], A. Wagner[1)]

1) Institut für Strahlenphysik, Forschungszentrum Dresden-Rossendorf, 01314 Dresden, Germany
2) Technische Universität Dresden, 01062 Dresden, Germany
a.matic@fzd.de

Abstract: *S*tate-of-the-art fast digitizer cards Acqiris DC282 were acquired as part of EFNUDAT project at FZD. HPGe preamplifier signals and photo multipliers signals from BaF_2 and plastic detectors are digitised and stored. A ROOT based data analysis software is being developed and algorithms for pulse height and precise timing determination were used for HPGe γ-energy resolution and timing determination for scintillation detectors, respectively. Data analysis of HPGe energy resolution shows that energy resolution achieved by a 14-bit peak sensing ADC is better than energy resolution obtained with 10-bit digitizers. However, digital methods give better time resolution for scintillation detectors in sub-ns timing than analogue signal processing.

Introduction

The necessity for higher quality experimental data for waste transmutation is highlighted in Ref. [1]. Better quality of measurements can systematically be improved by increasing the data acquisition speed in order to collect data of higher statistical significance in a given time and by improving existing pulse processing. These objectives can be achieved by the use of fast digitizers in measurements. Development of Fast Digitizing Data Acquisition System (FDDAS) system is part of Joint Research Activities (JRA) 1 within EFNUDAT project. This system should be modular, flexible and easy to implement within partner laboratories and to accommodate for a wide spectrum of experiments.

FDDAS at FZD

FDDAS at FZD is based on Acqiris (Agilent) DC282 digitizing cards [2]. DC282 cards have four sampling channels, each with a sampling rate up to 2 Gs/s and resolution of 10 bit. The card allows an increase of the sampling rate on 4 Gs/s or 8 Gs/s by combining 2 or 4 channels, respectively, to digitize one signal. The acquisition memory is 256000 points per channel and can be segmented in order to use Simultaneous Multi-buffer data Acquisition and Readout mode (SMAR). This feature theoretically gives an opportunity for zero dead time. Any channel in the card can be used as internal trigger, also an external trigger can be used. Furthermore, several cards can be synchronized and triggered via ASBus[2] connectors. FZD has 8 DC282 cards with 2 CC105 crates [3]. The crate enables data transport from the digitizing cards to a single board computer via 64-bit 66 MHz compactPCI (*cPCI*) backplane.
Two separate controlling and storage systems exist in the lab. The “small” solution is a 1.6 GHz Pentium single board computer [4] with Suse Linux operating system installed with Acqiris drivers and acquisition software. This system satisfy requirements for an open source system and is adaptable for different set ups. Storage of data is done via a SCSI card to an external HD with a theoretical maximal transfer speed of 300 MB/s.
The “large” system has a single board computer, PowerMidas C500 (IBM 440GX PowerPC with VxWorks operating system) [5], connected with VS-FC41F Storage device (JBOD, 12 disks with 300 GB each) [6] and a SAN Access Kit (2 Gb/s fibre channel host bus adapter for analysis server + software) [7]. The maximal transfer rate of this system is 450 GB/s.

Pulse height analysis of HPGe preamplifier signals

Measurements with an HPGe detector and ^{22}Na source

Coaxial n-type HPGe ORTEC GMX-100 [8] coupled with the digitizing card was used to determine an energy resolution of the FDDAS system. Spectra of an encapsulated ^{22}Na source were collected. The half-life of ^{22}Na is 2.6 years. It decays by electron capture (9.5 %) and β^+ decay (90.5 %). with to 1275.53 keV 2^+ state of ^{22}Ne. Therefore, both annihilation 511 keV line and 1275.53 keV line can be observed in the spectra and used for a channel to energy calibration.

For FDDAS trigger we used a logical signal (TTL standard), which was generated by analogue constant-fraction discriminator from a HPGe preamplifier signal. Trigger thresholds for negative HPGe and BaF_2 signals were set to a positive value to prevent triggering. Signals were sampled with 2 Gs/s rate and with 10 bits resolution. The pre-trigger-delay (number of points saved before trigger) was set to 3200 points and in total 10000 points per event were recorded.

For comparison between analogue and FDDAS systems, ^{22}Na spectra were also collected with state-of-the-art signal-processing and data acquisition system of the photon-scattering facility at ELBE [9]. The Preamplifier signal was shaped by *ORTEC 671* spectroscopy amplifier [10] and the pulse height was determined by the 14-bit peak-sensing ADC *SILENA 7423* [11].

Digitally processed data

A ROOT based software for FDDAS data analysis has developed in house as part of R. Hannaske's diploma thesis [12]. In Its library consists of: auxiliary functions, filters, shaper, timing and finite-decay time correction algorithms.

The baseline offset between -6.8 mV and -7.8 mV were determined, in the pre trigger part of the spectra, by averaging the baseline. This offset is then subtracted from the original signal in order to suppress response of applied algorithms to step at $t = 0$. In order to compensate for ballistic deficit a Moving Window Deconvolution (MWD) algorithm [13] was used. A MWD algorithm restores original charge information and shapes of the preamplifier signal. A few different shaping algorithms (CR-(RC)^n filter, Triangular and Trapezoidal shaper and Truncated Cups-like shaper) [12] were tested. The height of shaped signals are determined and filled in histograms and intensive γ peaks are fitted by an asymmetric Gaussian function [12] see Fig 2. The best energy resolution and stability over wide range of slope length parameter parameter *k* is obtained with truncated cups-like shaper Fig 1.

The energy resolution for analogue collected data are 3.46 keV and 2.88 for 511 keV and 1275.53 keV peaks, respectively. And for the data collected with FDDAS energy resolution are 4.75 keV at 511 keV and 5.37 keV for plateau length m = 1500 and slope length k = 3000. The impact of the MWD algorithm on energy resolution can be seen on Fig 1.

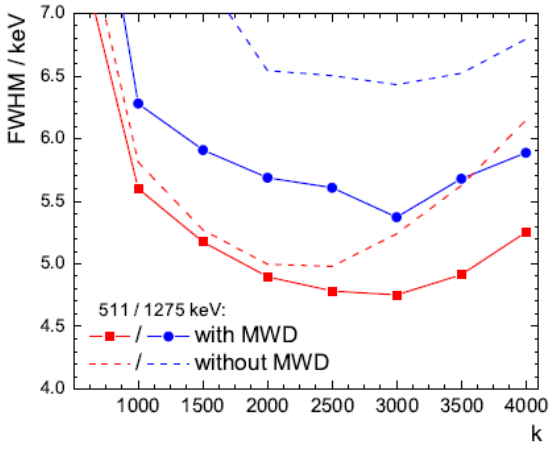

Figure 1. *Energy resolution (FWHM) achieved with truncated cups-like shaper with the plateau length m = 1500 as function of slope length k,with and without MWD.*

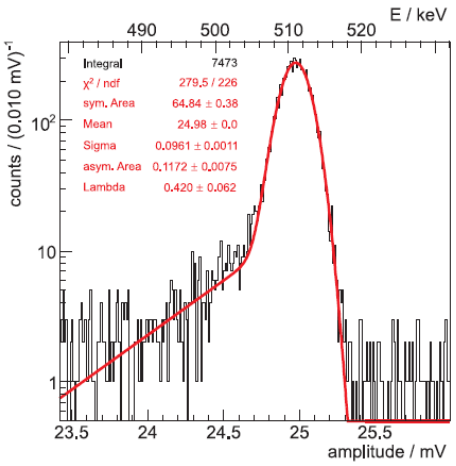

Figure 2. *Peak in DSP pulse height spectrum at 511 keV is fitted with an asymmetric gaussian function. Its energy resolution is 4.75 keV.*

Time resolution of scintillation detectors

Scintillation detectors and measurements

Scintillation detectors used at nELBE facility are plastic scintillation detector made from EJ-200 material for neutron detection and BaF_2 detectors for gamma detection REF[BAYER]. Plastic detectors are strips with a size 1000 mm x 42 mm x 11 mm with Hamamatsu R2059-01 photomultiplier tubes on each end. BaF_2 detectors are 19 cm long with a hexagonal cross section and inner diameter of 53 mm, also readout with R2059-01 photomultiplier tubes. The time information is measured by a multi event TDC CAEN V1190A, the complete information of nELBE DAQ can be found in Ref. [14].

Experimental data taken with FDDAS system were collected during the 56Fe(n,n'γ)56Fe experiment at nELBE facility in August 2008. The neutron beam was impinged on a 40 g iron target, consisting of 91.754 % of ^{56}Fe. The Neutron beam is produced by the 32 MeV pulsed (101 kHz repetition rate) electron beam from the super conductive accelerator ELBE. The electron beam impinges on a liquid-lead target [15] and neutrons are produced via (γ,n) reaction initialized by Bremsstrahlung produced by the electrons in liquid-lead target.

A typical time of flight spectrum from a plastic detector is shown in Fig. 3. The 1st peak originates from background through a door, 2nd peak originates from γ-flash at liquid lead target, and events after 300 ns are detected neutrons. Time of flight measurements for both type of scintillation detectors is measured relative to RF signal from ELBE-accelerator.

FDDAS data are taken with one DC282 2GS/ s card and with a VMETRO recording card. In the 1st measurement signals for #1, #5, #9 BaF_2 crystals are collected together with RF accelerator signal. The signals were collected in a range of -1900 mV to 100 mV, where internal trigger for BaF2 signals was -300 mV from a leading edge and a negative slope. In the 2nd measurement signals from photomultiplier tubes were collected together with RF signal in a range from -4900 mV to 100 mV. A threshold for leading edge of negative slope signal for plastic detector signal was setted at -900 mV. 5000 points were recorded per channel with before trigger delay of 512 and 2048 points for the 1st and 2nd measurements, respectively. In total 60 GiB data were collected.

Digitally processed data

Since electron bunches are very short (order of few ps) and small dimensions of liquid-lead radiator (approximately 1 cm) uncertainties of the γ-generation time can be neglected. The time resolution of the scintillation detectors was determined by fitting the 2nd peak (Fig. 3) with a gaussian function. Achieved resolution for analogue collected data was 1.08 ns, 0.82 ns, 0.79 ns and 0.98 ns for BaF_2 #1, #5, #9 and plastic detector respectively. These resolutions are marked with horizontal dashed lines in Figs. 4. and 5.

Several different timing algorithms were tested in FDDAS data analysis: Leading Edge Timing (LET), Extrapolated Leading Edge Timing (ELET), Zero-Crossing Shaper Timing (ZCT), Zero Crossing Constant Fraction Timing (ZCCFT), Constant Fraction Timing (CFT) and Fitting Constant Fraction Timing (FCFT) [12]. The best results from all these algorithms were compared with analogue processed data.

The LET and ELET algorithms gave worse resolution than analogue data for every threshold value. The ZCT method for BaF_2 detectors gave better results for a time constant τ between 0.1 ns to 1 ns, but time resolution of the plastic detector was all time worse than analogue ones, see Fig. 4.

The ZCCFT method we varied delay parameter *m* to be 3, 5 and 10 points. The attenuation factor a_{cf} was varied between 0.05 and 0.60. From Fig 5 it can be seen that every function has a minimum. Furthermore, for all BaF_2 detectors time resolution was much better than analogue ones. For the plastic detector better resolution was achieved only for delay time of 10 points (5 ns).

For CFT and FCFT methods, fraction parameter c_{cf} was varied between 0.025 and 0.80. In Fig 6. it can be seen that the resolution for digitally recorded data is better than for analogue. The difference between CFT and FCFT methods was small, which suggests that linear interpolation in CFT method is competitive with the fit used in FCFT [16]. More detailed description can be found in Ref. [12].

Conclusion and outlook

FDDAS system was tested under real experimental conditions with one recording card and 2GS/s sampling rate. We showed that 10-bit digitizers with 2 GS/s sampling rate is not competitive to state of the art analogue -signal processing system with 14-bit ADC. At same time we proved that better timing resolution can be achieved with FDDAS compared to analogue system, by using ZCCFT and CFT algorithms.
Further testing with “small” and “large” recording systems are ongoing. It has been shown that the system can work with 4 GS/s and 8 GS/s sampling rate for maximum 8 and 4 detectors, respectively.
A filter function for data reduction is implemented in data acquisition software. Furthermore, code for decoding of VMETRO and Acqiris ASCII formats has been developed and included in ROOT based data analysis software. Library of procedures for data handling, peak height reconstruction for HPGe detector and timing information for scintillation detectors are included. Routines for pulse-shape analysis are under development.

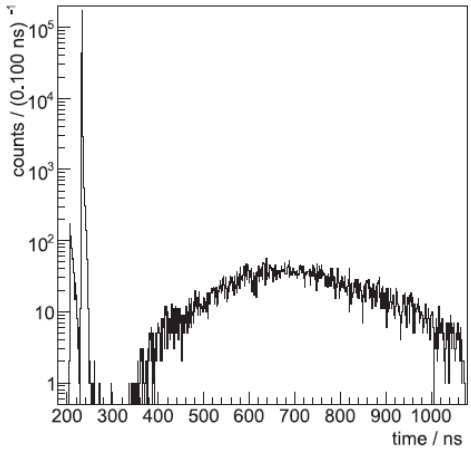

Figure 3. *Full TOF spectrum for plastic detector from digitally processed signals.*

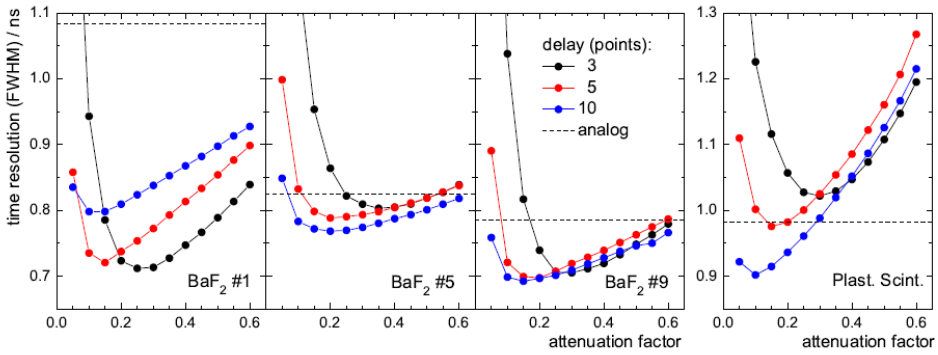

Figure 4. *Time resolution achieved with ZCCFT.*

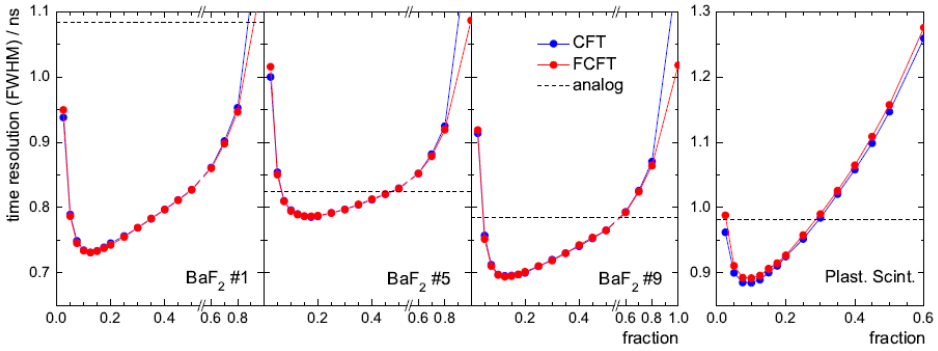

Figure 5. *Time resolution achieved with CFT and FCFT methods.*

References

[1] Nuclear Science NEA/WPEC-26 ISBN 978-92-64-99053-1.
[2] http://cp.literature.agilent.com/litweb/pdf/U1092-90004.pdf.
[3] http://cp.literature.agilent.com/litweb/pdf/U1092-90018.pdf.
[4] http://cp.literature.agilent.com/litweb/pdf/5989-7112EN.pdf.
[5] http://www.cwcembedded.com/products/0/3/562.html.
[6] http://www.vsystems.it/category3836.html.
[7] http://www.vsystems.it/category3859.html.
[8] http://www.ortec-online.com/detectors/photon/b2_2.htm.
[9] R. Schwengner et al., Nucl. Instr. Meth. Phys. Res. A 555 (2005) 211.
[10] http://www.ortec-online.com/electronics/amp/671.htm.
[11] http://www.geocities.com/silena_spa/7423uhss.htm.
[12] R. Hannaske, Wissenshaftlich-Technische Berichte, FZD – 510 2009, ISSN 1437-322X.
[13] A. Georgiev et al., IEEE Trans. Nucl. Sci. 40, 4 (1993) 770–779.
[14] R. Beyer et al., Nucl. Instr. Meth. Phys. Res. A 575 (2007) 449.
[15] E. Altstadt et al., Ann. Nucl. Energy 34 (2007) 36–50.
[16] F. Bečvář et al., Nucl. Inst.r Meth. Phys. Res. A 539 (2005) 372.

Characterization of the ANITA white neutron beam

R. Nolte[1)], S. Röttger[1)], A. Prokofiev[2)]

1) Physikalisch-Technische Bundesanstalt, PO Box 3345, D-38023 Braunschweig, Germany
2) The Svedberg Laboratory, Uppsala University, Box 533, SE-75121 Uppsala, Sweden

ralf.nolte@ptb.de

Abstract: The high-intensity neutron beam facility ANITA was installed recently at the Gustav-Werner cyclotron of the The Svedberg Laboratory in Uppsala/Sweden. A neutron beam with continuous energy distribution is produced by a 177 MeV proton beam impinging on a stopping-length tungsten target. The neutron emission in the forward direction is collimated using a set of steel collimators of variable size. The spectral distribution of the neutron beam extends from the keV region to about the energy of the proton beam and exhibits a low-energy component resulting from neutron evaporation and a high-energy component from (p,xn) reactions. The ANITA neutron spectrum was characterised using a ^{238}U fission ionization chamber and the time-of-flight method. Due to the limited time resolution and fixed repetition frequency of the accelerator, several measurements at different distances had to be combined to derive the spectral fluence above the cut-off energy of about 10 MeV. This was accomplished by using a parameterized model of the neutron spectrum. The most probable value of the parameters was determined by analysing all available measurements simultaneously using the WinBUGS software. The results of this analysis are compared with MCNPX simulations using the recently released TENDL library.

Introduction

The increase of the integration density in modern semiconductor devices makes them also more sensitive to effects induced by ionizing radiation of high linear energy transfer (LET). Therefore, devices intended for use in critical positions of the IT infrastructure, such as server computers, or in locations with increased radiation levels, require intensive testing of the failure rates induced by radiation. Such environments are found, for example, in nuclear power plants, around high-energy accelerators, at flight altitudes or in earth orbits. Usually accelerated tests are carried out by irradiating the devices at higher dose rates in radiation fields representative for the conditions encountered during the actual use of the device.
At ground level and at flight altitudes, a significant contribution of the high-LET component of the radiation field results from secondary charged particles produced by interactions of high-energy neutrons with air or with the device materials. Hence, a testing facility should provide a broad ('white') neutron spectrum with a spectral shape similar to that of the ambient neutron spectrum, i.e. it should exhibit a high-energy spallation contribution and a low-energy evaporation part. To achieve consistent results from different testing facilities a proper characterization of the spectral distribution of each facility is crucial.
The present work describes the characterization of the novel device testing facility ANITA (**a**tmospheric-like **n**eutrons from th**i**ck **ta**rget) which was recently set up at the The Svedberg Laboratory (TSL) in Uppsala /Sweden.

The ANITA facility

The ANITA facility is part of the TSL neutron beam facility installed at the Gustav-Werner cyclotron which includes also a quasi-monoenergetic neutron beam. An overview of the facility is shown in Figure 1. A 176.6 MeV proton beam is directed at a 24 mm thick cylindrical water-cooled tungsten target at an incidence angle of about 3°. The thickness of the tungsten disc is sufficient to stop the proton beam inside the target. The target is surrounded by a cylindrical lead shield to absorb γ-rays. The neutrons emitted in the forward direction are collimated using a lead pre-collimator and a steel collimator 100 cm in length. The collimator has various exchangeable inserts with different diameters and shapes. For the present measurements, a cylindrical insert with a diameter of 102 mm was used. The whole facility is surrounded by a massive concrete shield which separates the neutron production cave from

the irradiation (user) area. In the irradiation area, the collimated neutron beam propagates over more than 15 m of air before it is stopped in a beam dump located inside a tunnel.

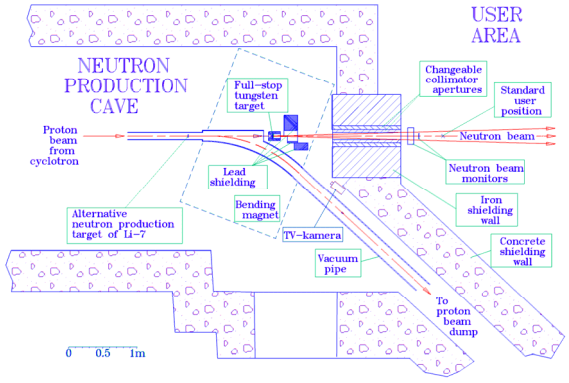

Figure 1. *Overview of the ANITA 'white' neutron beam facility at the Gustav-Werner cyclotron of the The Svedberg Laboratory in Uppsala/Sweden. The energy of the proton beam incident on a stopping-length tungsten target is about 177 MeV.*

At energies above 100 MeV, the Gustav-Werner cyclotron is operated in the synchrocyclotron mode. Hence, the 176.6 MeV proton beam has a micropulse/macropulse time structure. The time separation of the micropulses is about 45.2 ns. The duration of the micropulses is estimated to be about 5 ns and the duration of the macropulses is about 0.82 ms. The repetition frequency of the macropulses is 160 Hz, resulting in an overall macropulse duty cycle of 13 %. The neutron emission is monitored by a ^{238}U fission ionization chamber (IC) and by thin-film breakdown counters (TFBC) located behind the collimator exit. In addition, the integrated target current (Q) can be used as a monitor. More details of the ANITA facility are described elsewhere [1,2].

Characterization of the ANITA neutron spectrum

TOF measurements

Time-of-flight (TOF) measurements were carried out using the ^{238}U fission ionization chamber H21 of PTB [3]. This instrument has ten fissile deposits with masses per area of about 400 µg/cm² and active diameters of 78 mm. The total ^{238}U mass is (197.8±0.5) mg. The enrichment of ^{238}U is larger than 99.9% which makes the instrument virtually insensitive to thermal neutrons. The time resolution of the instrument is about 3 ns to 4 ns. The efficiency for the detection of fission fragments is about 0.95 with a small energy dependence due to the transfer of linear momentum to the fission fragments. The efficiency was calculated using Carlson's analytical approach [4]. The TOF measurements were carried out using the usual 'inverted' method, i.e. the measurement was started by the fission chamber and stopped by a signal derived from the accelerator RF.

With the given time structure of the proton beam, it was impossible to characterize the ANITA spectrum with a single TOF measurement, because good energy resolution and low frame-overlap threshold require long and short flight distances, respectively. This is demonstrated in table 1 which lists the variation $(\mathrm{d}E_\mathrm{n}/\mathrm{d}t_\mathrm{n})(E_{\mathrm{n},0})$ of the neutron energy E_n with flight time t_n for neutrons with an energy $E_{\mathrm{n},0}$ = 180 MeV and the frame-overlap threshold energy $E_{\mathrm{n,ov}}$ for several flight distances d. Hence, several measurements at different distances had to be combined to arrive at a characterization of the neutron spectrum above 10 MeV with sufficient energy resolution at the high-energy edge around 170 MeV. This procedure requires, however, that the neutron spectra measured at different distances d follow a $1/d^2$-dependence so that they can be combined without problems.

The prompt photon emission at ANITA is insufficient to produce a photofission peak in the TOF spectra which could be used to determine the position of the origin t_0 of the TOF scale. Hence, additional measurements using a 23.5 mm thick ^{7}Li target located 124 cm closer to the cyclotron were carried out in parallel to the measurements with the ANITA target. The mean energy of the neutrons resulting from the transition to the ground state and the first excited state of ^{7}Be was calculated from the proton beam energy and the position of the corresponding TOF peak was used as a reference.

Table 1. *Variation (dE_n/dt_n) of the neutron energy E_n with flight time t_n for neutrons with an energy of 180 MeV and frame-overlap threshold energy $E_{n,ov}$ for several flight distances d.*

d / m	(dE_n/dt_n) / (MeV/ns)	$E_{n,ov}$ / MeV
2.5	26.9	9.1
5	14.7	23.7
10	7.4	49.9

Analysis using the WinBUGS software

Since the ANITA thick-target neutron spectrum extends to the keV energy region, a frame-overlap correction was necessary even for the smallest flight distances possible in the present experiment. This correction was carried out by fitting a parameterized analytical model of the spectral fluence per beam charge (Φ_E/Q) to the TOF spectra. This model comprises separate descriptions of the evaporation and the 'spallation' part of the neutron spectrum by generalized Maxwellian Y_1 and a modified Fermi distribution density Y_2, respectively.

$$(\Phi_E/Q) = \frac{f}{d^2}\sum_{i=1}^{2} Y_i(E) \text{ with}$$
$$Y_1 = \frac{r}{E_{0,1}}\left(\frac{E}{E_{0,1}}\right)^x \exp\left(-\frac{E}{E_{0,1}}\right),\ Y_2 = \frac{\lambda_2(1-\exp(\lambda_2))}{E_{0,2}}\frac{\exp\left(\lambda_2\left(E/E_{0,2}-1\right)\right)}{1+\exp\left(\delta^{-1}\left(E/E_{0,2}-1\right)\right)} \quad . \tag{1}$$

For the spallation component, the parameters $E_{0,2}$ and δ_2 represent the energy and the width of the high-energy edge of the neutron spectrum while λ_2 models the slope in the energy region well above $E_{0,1}$. The parameterization is transformed to the 'inverted' TOF scale with its origin at t_0 according to

$$(\Phi_t(t)/Q) = (\Phi_E/Q)\frac{dE}{dt} = (\Phi_E/Q)\frac{\beta^2}{\sqrt{(1-\beta^2)^3}}\frac{mc^2}{t-t_0} \quad \text{with } \beta = \frac{v}{c}. \tag{2}$$

The number of fission events per TOF interval and per beam charge ($N_{f,t}/Q$) is then given by

$$(N_{f,t}(t)/Q) = kN_U \int R(t,t')\cdot(\Phi_t(t')/Q)\,dt' \tag{3}$$

where N_U and k denote the number of ^{238}U nuclei in the fission chamber and the product of correction factors for dead time losses, detection efficiency for fission fragments etc., respectively. The time response function $R(t, t')$ of the fission chamber is modelled by a Gaussian with an FWHM of 4.0 ns, as determined from the measurements with the Li target.

The energy region below 10 MeV is not accessible for TOF measurements at ANITA, because the smallest possible flight path is about 2.4 m. Therefore, the parameters x and $E_{0,1}$ of the evaporation component Y_1 were fitted to the neutron emission spectrum calculated for a 180 MeV proton beam incident on a stopping-length tungsten target using MCNPX [5] with the TENDL library [6] (see below). The fit was restricted to the energy range from 1 MeV to 10 MeV and resulted in x = -1.27 and $E_{0,1}$ = 5.4 MeV.

The WinBUGS software [7] was used to estimate the remaining parameters f_i *(i = 1-3)*, r, δ_2, $E_{0,2}$ and λ_2 from three TOF measurements carried out at distances d of 2.579 m, 4.429 m and 8.858 m. WinBUGS uses the Markov chain Monte Carlo method to perform Bayesian parameter estimations. Using these techniques, the available pre-information can be specified by distribution densities for all parameters of the model. In the present case the pre-information was generated from the results of MCNPX simulations (see below).

The mean values of the parameters, their variances and distribution densities as well as their covariances are updated using the additional information from the experiment under analysis. To limit the computation time to acceptable values, the experimental TOF spectra were compressed by grouping 8 bin of the experimental spectra together which increased the bin size from 52 ps per bin to 417 ps per bin.

The result of the parameter estimation procedure is shown in Figure 2. The experimental TOF spectra are indicated by the black histograms. The solid red lines are the TOF spectra calculated using the mean values of the estimated parameters while the blue lines show the frame-overlap continuum underlying the TOF spectra. These frame-overlap continua have to be subtracted from the experimental TOF spectra before they can be transformed to the

energy scale to yield the spectral fluence Φ_E. The number of frame overlaps to be subtracted varies from 2 at 2.579 m to 12 at 8.858 m. It should be noted that the measurement at 3.376 m was not included in the parameter estimation procedure.

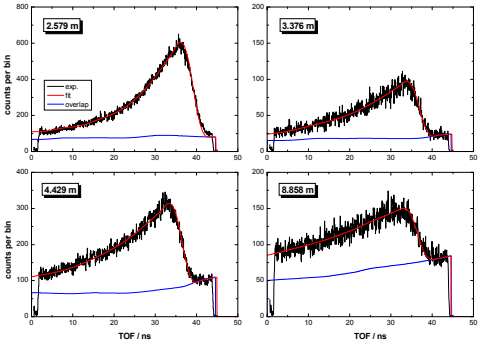

Figure 2. *Experimental TOF spectra (black histograms) measured using the ^{238}U fission ionization chamber at different distances. The solid red lines show the TOF spectra calculated using the analytical model given by eq.s (1-3). The solid blue lines indicate the frame-overlap component which varies from 2 frame overlaps at 2.579 m to 12 frame overlaps at 8.58 m.*

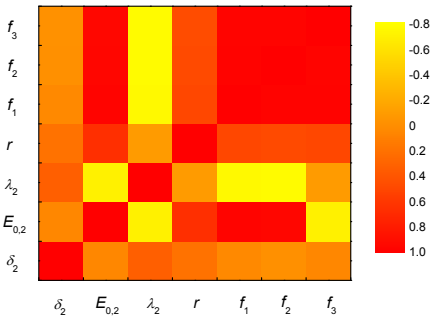

Figure 3. *Correlation matrix for the parameters of the analytical model. The parameters f_i (i = 1-3) denote the normalization parameters for the three measurements at distances of 2.579 m, 4.429 m and 8.858 m.*

Figure 3 shows the colour-coded correlation matrix for the parameters with negative and positive correlation indicated in yellow and red, respectively. Obviously, there are still strong correlations among the parameters although it was attempted to formulate the model so that the parameters become as independent as possible. It should be noted that the strong correlation of the parameters f_i (i = 1-3) is not surprising since the dependence of the number of events in the measured TOF spectra on distance d_i and beam charge Q_i is already reflected in the model (cf. eq. (1) and (2)).

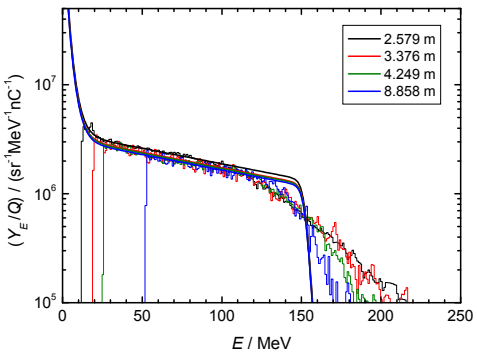

Figure 4*. Spectral yields Y_E obtained from the experimental TOF spectra after correction for frame overlap (histograms) and calculated from the analytical model (solid lines) for different flight distances.*

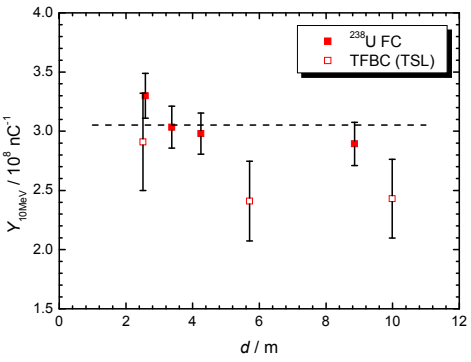

Figure 5*. Yield above 10 MeV Y_{10MeV} measured for the ^{nat}W ANITA target using the ^{238}U fission ionization chamber (closed symbols) and TFBCs (open symbols) [1]. The dashed line shows the mean of the FC data.*

After the subtraction of the frame-overlap continua determined from the experimental TOF spectra using WinBUGS, the net spectra were transformed to the energy scale, divided by the ^{238}U(n,f) cross section from the INDC evaluation [8] and converted to spectral yields per beam charge Y_E. Figure 4 shows the data obtained for the different flight distances d together with

the spectral yields calculated directly from the analytical model for d = 4.429 m (i = 2). The effect of the flight distance on the energy resolution of the TOF measurements is obvious. Thus, the measurements at different distances have to be combined to cover the full energy range above 13.5 MeV. This combined spectrum is depicted by the histogram in Figure 6. The parameter δ_2 = (12±4) keV describing the width of the high-energy edge at $E_{0,2}$ = (152.4±0.3) MeV is very small, most likely, because the increased bin size used for the WinBUGS analysis made the algorithm insensitive to the small contribution from the 'physical' width of the edge compared with the larger width resulting from the TOF resolution.
Figure 5 shows the yields Y_{10MeV} for a low-energy cut-off at 10 MeV. The uncertainties of the yields measured using the ^{238}U fission chamber have a 5% contribution from the uncertainty of the ^{238}U(n,f) cross section. There is a slight deviation from the $1/d^2$ dependence for the smallest distance to the tungsten target which is also visible in Figure 4. The data measured earlier by Prokofiev et al. [1] using TFBCs show the same trend but are systematically lower by about 15 %.

MCNPX simulations

A detailed simulation of the ANITA facility was carried out using the MCNPX Monte Carlo code [5]. The main focus of this work was to investigate the effect of neutron interactions with the target setup and the collimators on the neutron spectrum and to calculate the neutron background in the experimental area. Most of the cross section data were taken from the recently released TENDL libraries [6] for incident neutrons and protons which are based on the TALYS code [9]. In particular, TENDL emission cross sections were used for the source term, i.e. ^{182,183,184,186}W(p,xn). The maximum energy of the TENDL library is 200 MeV. Therefore, the use of nuclear models for high-energy neutrons and protons could be avoided to a large extent. The only exceptions were ^{1}H, ^{14}N and ^{16}O for which data from the LA150 libraries [10] were used up to 150 MeV, and the Bertini intranuclear cascade model plus the Dresner evaporation model above 150 MeV. Thermal scattering data for water at 300 K were taken from the ENDF/B-VI library. Disc-like track-length estimators with the same diameter as that of the fission chamber (78 mm) and larger spherical track-length estimators for the background outside the beam area were used throughout the problem since the use of nuclear models prevented the application of point detectors. The mass fractions used for the concrete shield were 0.3% H, 45.3% O, 32.3% Si, 14.1% Ca and 8.0% Fe (density ρ = 2.3 g/cm^3). The mass fractions for the stainless steel used for the collimator inserts were 19.5% Cr, 70.5% Fe and 10% Ni (ρ = 7.84 g/cm^3) . The composition used for the air was 76.5% N and 23.5% O (ρ = 1.22 mg/cm^3). Reference data for densities and isotopic composition were employed for the other materials.

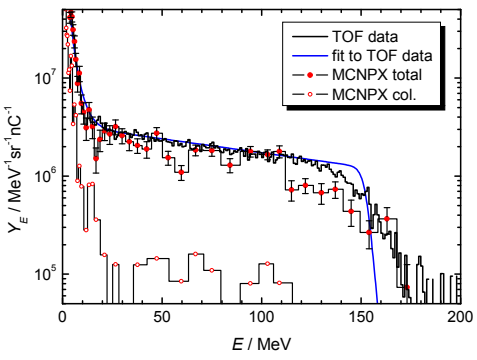

***Figure 6**. Spectral yield Y_E calculated with MCNPX at the SUP. The red circles show the total tally contribution while the open circles indicate the contribution from neutrons which had at least one interaction with the material surrounding the target. The histogram and the solid lines indicate the experimental results.*

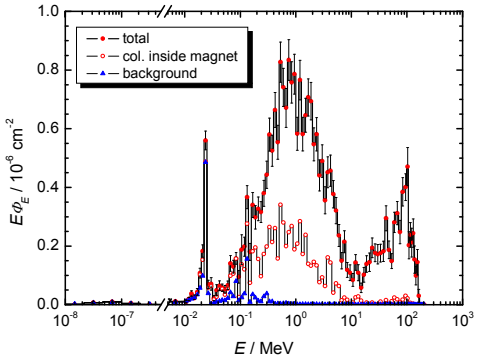

***Figure 7**. Energy-weighted spectral fluence $E\Phi_E$ per source proton at the SUP. The total contribution and the contribution with collisions inside the magnet gap are shown by the closed and open red circles. The background below the beam is shown by the blue triangles.*

The fluence in the neutron beam was tallied at the actual positions of the ^{238}U fission chamber and at the standard user position (SUP) at a distance of 250 cm from the tungsten target. Figure 6 shows the calculated and measured spectral yield Y_E at the SUP. A total number of $1.25 \cdot 10^8$ protons was used for the calculations corresponding to a computation time of about 400 h on a standard PC. The simulated spectral yield is only slightly below the experimental one in the energy region below 100 MeV but discrepancies are visible above 100 MeV, where the simulated spectral yield is about a factor of 2 less than the measured one. In the energy region above 20 MeV, the relative contribution of neutrons undergoing an additional collision with the material in the magnet gap outside the tungsten disc is only about 5%.
Figure 7 shows the energy-weighted fluence $E\Phi_E$ over the full energy range from thermal to 180 MeV. About 80% of the total ANITA fluence is located in the energy region below 10 MeV which could not be investigated by TOF measurements in the present work. In the energy region between 10 keV and 10 MeV the fraction of neutrons with additional collisions outside the target rises to about 30%. The background outside the beam is rather small with a prominent contribution from transmission through the iron shield in the energy region around the ^{56}Fe resonance at about 24 keV. The thermal fluence below the Cd threshold at 0.68 eV is only about 2.8% of the fluence above 10 MeV.

Conclusions

It could be demonstrated that TOF measurements can be used to measure the spectral neutron distributions of 'white' neutron sources even if the time structure of the beam is not optimized for this method by the use of a beam pulse selector device. The necessary frame-overlap correction can be carried out if additional pre-information on the low-energy part of the spectrum is available from Monte Carlo simulations or other experimental methods. A flexible analytical description of the spectral shape and the use of the WinBUGS software was instrumental in carrying out the corrections, including the determination of the contribution to the measurement uncertainty. Using these methods, the ANITA white neutron beam could be characterized in the energy region above 10 MeV, which is most important for the use of the ANITA facility for radiation damage studies.

Acknowledgements
The authors would like to thank the TSL staff for providing the beams and for their excellent support during the measurements. R. Nolte is indebted to M. Reginatto for introducing him to the use of the WinBUGS software and for numerous discussions on the subject. The present work was partly funded by the European Commission under the Integrated Infrastructure Initiative EFNUDAT.

References

[1] A.V. Prokofiev, J. Blomgren, R. Nolte, S.P. Platt, S. Röttger and A.N. Smirnov, Proceedings from the 8th European Workshop on Radiation Effects on Components and Systems (RADECS), September 10 - 12, 2008, Jyväskylä, Finland, 260 – 267.
[2] A.V. Prokofiev, J. Blomgren, O. Byström, C. Ekström, S. Pomp, U. Tippawan, V. Zieman and M. Österlund, Radiat. Prot. Dosimetry 126 (2007), 18-22.
[3] D.B. Gayther, Metrologia 27, 211 (1990).
[4] G.W. Carlson, Nucl. Instrum. Meth. 119, 97 (1974).
[5] D.B. Pelowitz, Laboratory Report LA-CP-050369, Los Alamos National Laboratory (2005).
[6] A.J. Koning and D. Rochman, Report JEFF-DOC 1262, November 17, 2008.
[7] D.J. Spiegelhalter, A. Thomas and N.G. Best, WinBUGS Version 1.4, MRC Biostatistics Unit (2003), the WinBUGS software is available from http://www.mrc-bsu.cam.uk/bugs.
[8] A. D. Carlson, S. Chiba, F.-J. Hambsch, N. Olsson, A. N. Smirnov, Proc. Int. Conf. Nuclear Data for Science and Technology, Trieste, May 19-24, 1997 p. 1223 and summary report on a consultants meeting at the IAEA headquarters in Vienna, December 2-6, 1996, H. Wienke, Ed., International Atomic Energy Agency, report INDC(NDS)-368 (April 1997).
[9] A. Koning, S. Hilaire, M.C. Duijvestijn, Proceedings of the International Conference on Nuclear Data for Science and Technology - ND2004, Sep. 26 – Oct. 1, 2004, Santa Fe.
[10] M.B. Chadwick, P.G. Young, S. Chiba, S.C. Frankle, G.M. Hale, H.G. Hughes, A.J. Koning, R.C. Little, R.E. McFarlane, R.E. Prael, L.S. Waters, Nucl. Sci. Eng. 131 (1999), 293-328.

Information on the super-deformed ground state in ^{235}U*

A. Oberstedt[1)], S. Oberstedt[2)], M. Gawrys[3)], F.-J. Hambsch[2)], N. Kornilov[2)], M. Vidali[2)]

1) School of Science and Technology, Örebro University, Fakultetsgatan 1, 70182 Örebro, Sweden
2) European Commission, Joint Research Centre, Institute for Reference Materials and Measurements, Retieseweg 111, 2440 Geel, Belgium
3) Department of Fundamental Physics, Chalmers University of Technology, 41296 Göteborg, Sweden

andreas.oberstedt@nat.oru.se

Abstract: Two neutron-induced experiments on ^{234}U were performed at EC-JRC IRMM in order to obtain information on the super-deformed (SD) ground state in ^{235}U*. The first one was carried out with the isomer spectrometer NEPTUNE and from delayed fission events the isomeric fission half-life and the corresponding cross-section could be determined to $T_{1/2}$ = (3.6 ± 1.8) ms and σ_{if} = (10 ± 8) μb, respectively. With the experimental confirmation of the existence of a (SD) shape isomer one has come one step closer to the precise knowledge of the distinct structure of the fission barrier in an odd-uranium isotope for the first time. However, for the determination of the outer fission barrier height E_B and the penetrability $\hbar\omega_B$, also the SD ground state energy E_{II} needs to be known. For this purpose another experiment was conducted, this time at the Geel linear accelerator facility (GELINA). It represented a feasibility study for the search of γ-rays populating the shape-isomeric ground state in ^{235}U* via neutron-capture in ^{234}U, from which E_{II} may be determined directly by measuring γ-rays following neutron capture in the energy region of the intermediate structure (IS) in the sub-threshold region of the fission cross-section.

Introduction

The appearance of a second minimum in the nuclear potential energy surface of actinide nuclei is explained by the superposition of microscopic shell corrections to the nuclear binding energy, varying periodically with deformation, and the unstructured macroscopic part of the deformation energy, usually described by the liquid-drop model [1]. As a consequence, fission isomers exist as discovered in a variety of nuclei ranging from ^{234}U to ^{245}Bk since the early 1960s [2,3]. However, one of the still persisting problems today is the lack of shape-isomer half-life data for odd-N uranium and neptunium isotopes. Only for ^{239}U the population of the super-deformed ground state in a neutron-induced capture experiment was observed [4,5]. Since for these isotopes fission half-lives are expected to be in the order of several hundreds of μs or even longer, the detection with commonly used pulsed particle beams is very difficult. It is even more difficult in neutron-induced reactions, where the environmental background, as created from sub-sequent pulses, is extremely disadvantageous. Together with the extremely low production cross-section for shape isomers, typically of the order of a few μb [6,7], as well as half-life predictions ranging in some cases over five orders of magnitude [8-10], the measurement of shape-isomer decay data implies a huge challenge for the experimentalist. However, a recent theoretical work [10], giving reliable predictions for half-lives for isomeric fission in the reaction ^{234}U + n, motivated an experiment, which was performed with the isomer spectrometer NEPTUNE of the EC-JRC IRMM [11].

Still, the exact determination of the potential energy landscape around the double-humped fission barrier, the fission barrier heights E_A and E_B for the inner and outer barrier, respectively, and the corresponding penetrabilities through both barriers, $\hbar\omega_A$ and $\hbar\omega_B$, as well as the ground state energy E_{II} of the super-deformed ground state, where the axis ratio of the nuclear shape is around 2:1, remains a challenge, in particular in odd-A uranium isotopes. In the past the investigation of the intermediate structure (IS) in the sub-threshold fission cross-section of non-fissile isotopes has been the tool to obtain information on the nuclear energy landscape around the fission barrier [6,12-14]. The resonances belonging to an IS are supposed to be linked to so-called class-II compound nuclear states located within the second minimum of the energy landscape above the shape isomer. From the class-II resonance

spacing relative to the one of normal class-I states, deduced from neutron transmission or capture cross-section data, the required information may be obtained. However, the data for uranium and neptunium isotopes are in discrepancy with corresponding data obtained from analyzing the fission cross-section around fission threshold. Apart from studying the intermediate structure in sub-threshold fission cross-sections, the direct measurement of shape-isomeric decay properties, like the half-life, the particular decay mode and the excitation function, provides information about the double-humped fission barrier. After a successful half-life determination of the SD ground state of ^{235}U, the next step would be to determine the ground state energy of the SD isomer, E_{II}. Together with $T_{1/2}$ the outer fission barrier height E_B, and penetrability $\hbar\omega_B$, are then well defined.

The NEPTUNE experiment

In this experiment a quasi mono-energetic neutron source was used with a tuneable pulse frequency in the Hz- to kHz-range and an individually adjustable neutron pulse width in connection with an appropriate detector system [11]. The fission fragments were detected with a twin Frisch-grid ionization chamber (IC) with common anode. A 1.364 mg sample of ^{234}U was placed in the center of the cathode closest to the neutron source. The contamination from ^{235}U was smaller than 9×10^{-4}. A sample with 2.38 mg of ^{235}U served as monitor for scattered and thermalized neutrons and was mounted on the second cathode of the IC. Both samples had a circular shape with a radius of 2.8 cm. Fast neutrons were monitored with a NE213-equivalent scintillation detector (4 inches in diameter $\times$ 1 inch thickness), employing the pulse-shape technique for n/γ separation. Measurements were performed at E_n = 0.95 and 1.27 MeV at pulse frequencies ν = 100 Hz and 50, 100 and 150 Hz, respectively. In all settings a duty cycle of 30% was chosen. The neutron beam was produced by employing the T(p,n) reaction. With an average beam current of 10 μA on a Ti:T target of initially 2 mg cm^{-2} thickness, a neutron flux of about 2.0×10^6 cm^{-2} s^{-1} was obtained at ^{234}U target position. Both incident neutron energies were chosen, since they correspond to the position of vibrational resonances in the neutron-induced fission cross-section [4], and one could hope that the population of the shape isomer was enhanced due to coupling to excited states above the second minimum. This was observed in the reaction ^{238}U(n,f) around 720 eV [5,6]. The energy resolution was 300 keV (FWHM), mainly determined by the thickness of the production target and the solid angle. The frequencies were varied as mentioned above in order to optimize the half-life measurement. However, during the experiment it became soon obvious that the time period corresponding to 150 Hz was too small. Hence, only few events were measured with this setting and further analysis of them was not possible.

The GELINA experiment

Following the experimental approach in Refs. [15,16], the determination of E_{II} is possible by measuring γ-rays following neutron capture in the energy region of the IS in the sub-threshold region of the fission cross-section. The population of the SD ground state in slow neutron-capture reactions proceeds through γ-decay of an excited quasi class-II state, which is mainly located above the SD minimum. As a consequence additional γ-rays, which appear exclusively in resonances belonging to an IS, are candidates for a possible decay towards the SD ground state. Best-suited candidates are neutron resonances with a low neutron width Γ_n, and a large fission width Γ_f, indicating a high fraction of a class-II state. In the case of the target nucleus ^{234}U, two resonances exhibit a ratio $\Gamma_f/\Gamma_n > 2$, at E_n = 387,6 and 1092,5 eV. The experiment was performed at GELINA of EC-JRC IRMM. The population of the SD ground state was achieved by irradiating a thick ^{234}U sample (2.12 g with about 3 cm in diameter) with a pulsed white neutron spectrum, whose neutron pulse width and repetition frequency was 1 ns and 800 Hz, respectively. The neutron energy of interest was between 5 and 1500 eV and coincides with the region of IS in the neutron-induced fission cross-section of ^{234}U.

The experiment was set up at flight path FP5 with a distance from the neutron source of about 10 m. With the available sample the expected number of measured γ-rays, populating the shape isomer, was relatively low within the scheduled beam time of two weeks. Hence, the detection had to depend strongly on the general experimental conditions, e.g. environmental background radiation and detector resolution. Therefore, this experiment was considered as a feasibility study to establish precise γ-ray spectra for clearly identifying decay from excited ^{235}U as well as from the radioactive decay of the target material, and to estimate the amount

of sample material and/or total beam time needed to identify γ-decay towards the SD shape-isomeric ground state. The γ-rays were detected with two high-purity Germanium detectors (ORTEC HPGE with X-coolers, n-type) and two planar Germanium detectors (Canberra LEGe, n-type), whose relative efficiency was 45 % and 7 %, respectively. The detectors were placed at a distance of 23 cm (one at 17 cm) from the target, at angles of 110° and 150°, which in principle allows for the determination of the multi-pole order of the γ-radiation.

Results and discussion

During two weeks of beam time with NEPTUNE, corresponding to 11.7 days of actual run time, 55 delayed fission events from the ^{234}U target were identified in total. Fission fragment pulse heights were corrected for angular-dependent energy loss based on the analysis of the pulse height of the prompt fission events as a function of the cathode signal, which is proportional to the fragments' range times the cosine of the emission angle θ [17]. Taking into account only events with $\cos\theta > 0.45$ allowed an efficient suppression of the α-particle background from the natural decay of ^{234}U. The resulting distribution of delayed fission events from ^{235}U* is shown in Fig. 1. In the upper left part the decay time, taken relative to the end of the neutron pulse, versus the fragment pulse height is depicted. Also shown are the projections on the time axis (upper right part) as well as on the pulse-height axis (lower left part). Since all recorded events fulfilling the conditions above are shown, corrections for either ^{235}U contaminants or scattered neutrons were not applied to the data displayed in both plots. The typical double-humped pulse-height distribution measured in the "beam off" time interval allows us to conclude that delayed fission events were detected. In the lower right part of Fig. 1 the pulse height spectrum of fragments from prompt fission of ^{235}U* is shown for comparison. Here contributions due to the ^{235}U admixture are negligible. The delayed fission events were then corrected for possible fission induced by residual background neutrons between the neutron pulses, which may origin from three processes: firstly, thermalized neutrons, which have a lifetime comparable with the investigated time interval, might have induced fission in the ^{235}U admixture in the ^{234}U target; secondly, a time-independent background and, finally, a time-dependent background due to fast-neutron induced fission, if the proton beam was not perfectly deflected. The first component was monitored with the ^{235}U monitor sample. For each setting, the number of "late" fission events, i.e. beam off-target, induced in the ^{235}U sample was determined. In total, their number was 8789, which corresponds to a contribution of 4.2 (out of 55) in the ^{234}U sample. The time dependence was described by the sum of two Exponentials, scaled to the ^{235}U content in the ^{234}U sample and corrected for each individual time bin. The last two components were monitored with the liquid scintillation detector. The analysis of the data for all measurements did not show any time-dependent background, and the time-independent background agrees reasonably well with the "accelerator off" condition. It was detected as proton recoil with energies larger than 3 MeV and may be attributed to cosmic rays. Assuming these particles being neutrons with energies around 6 MeV results in at most one possible fission induced in the ^{234}U sample during one week of measurement. This, again, agrees with the fission rate obtained during an "accelerator off" run. The final decay curves are obtained in the following way: the observed delayed fission events are collected in time bins of 3 ms width, normalized with the time of measurement and background corrected as described above. Due to the statistical nature of decay, the detected events are not homogenously spread over a time bin. Hence, the position is usually not the middle of the bin, instead the average time of all events in the bin was chosen to represent the locations of the corresponding bins. Consequently, the error bars for the time positions are determined by the standard deviations of the time values of the events in each bin. The result is shown in Fig. 2 separately for both incident neutron energies and fitted to Exponentials. The given error bars include statistical errors as well as systematical errors with respect to the background. From both fits one obtains a weighted average half-life $T_{1/2}$ = (3.6 $\pm$ 1.8) ms. A shape isomer population probability was determined by dividing the integrals of the fitted Exponentials with the measured prompt fission yields from ^{234}U + n. The mean value is P_{iso} = (7.5 $\pm$ 6.0) $\times$ 10^{-6}. With the known prompt neutron-induced fission cross-section of ^{234}U, this corresponds to a production cross-section of the shape isomer of (10 $\pm$ 8) μb. No statistically significant enhancement of the production cross-section in the vibrational resonance at E_n = 1.27 MeV was observed.

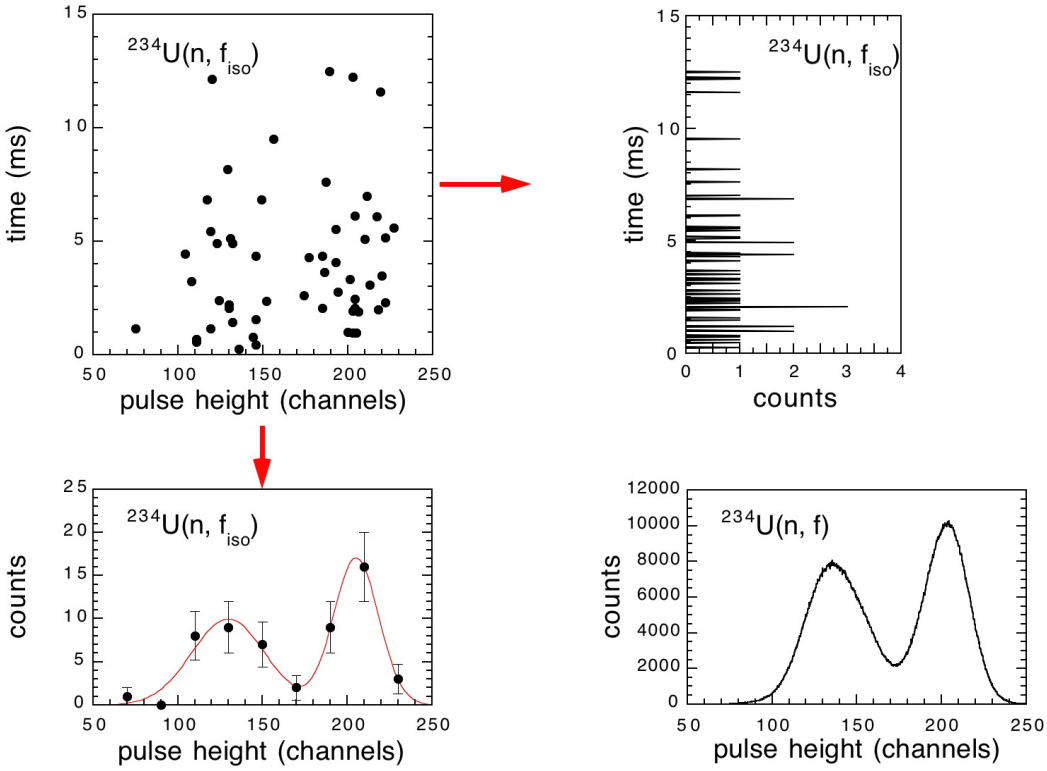

Figure 1. *Fission fragments from the decay of the shape isomer in $^{235}U^*$: Decay time relative to the end of the neutron pulse vs. angular-dependent energy-loss corrected fission fragment pulse height (upper left part), time distribution of shape isomeric fission events from $^{235}U^*$ prior to any background subtraction (upper right part), and shape isomeric (delayed) fission-fragment pulse height distribution corrected for angular-dependent energy loss prior to any background subtraction (lower left part). For comparison the corresponding pulse height distribution from prompt fission of $^{235}U^*$ is shown, too (lower right part).*

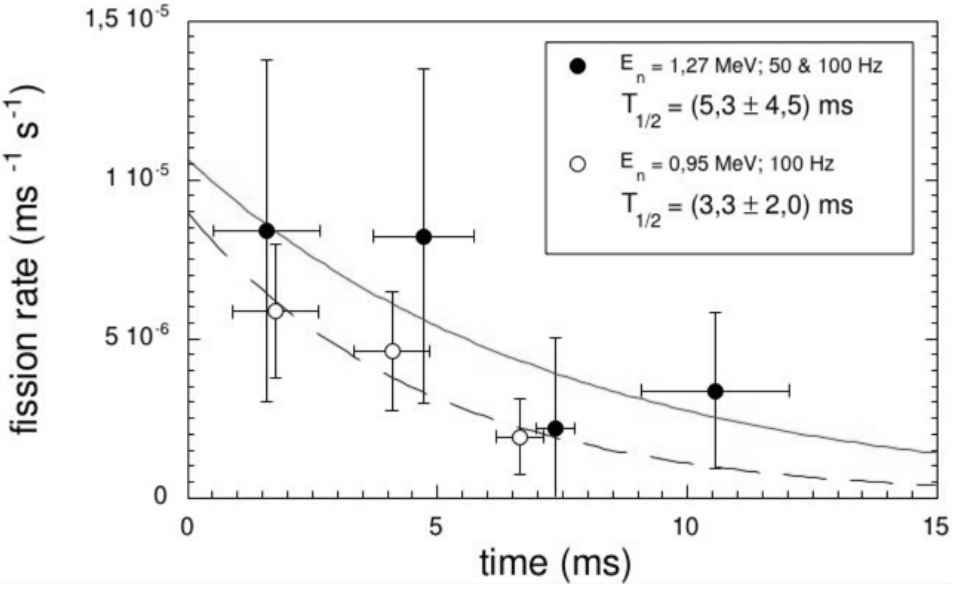

Figure 2. *Fission decay curve of the shape isomer in $^{235}U^*$: events are summed in time bins of 3 ms and background corrected as outlined in the text.*

As shown in Ref. [18], the measured half-life together with values for the relative outer fission barrier height and the shape isomeric ground state energy from Ref. [6] can be used to calculate a barrier penetrability $\hbar\omega_B$ = (0.47 ± 0.06) MeV. This is lower than the recommended value of $\hbar\omega_B$ = 0.52 MeV [6], but still compatible within the error bars. This result points towards the existence of a double-humped outer barrier in ^{235}U, well in agreement with results for ^{234}U and ^{236}U reported e.g. in Refs. [19,20].
Although two weeks of beam time were granted for the GELINA experiment, only a couple of days had effectively become available. Naturally, problems occurred basically due to the high γ-count rates, caused by the highly radioactive ^{234}U sample ($A_\alpha \approx 4{,}9 \times 10^8$ Bq) and the short distance between the source and the detectors. Since these distances could not be increased at the experimental setup that was available due to a lead wall at FP5, we had to switch off the closest of the four detectors and to cover the entrance windows of the others with a 5 mm thick lead shielding. An additional coincidence condition between a γ-ray and the pulsed neutron beam was imposed, which on one hand reduced the count rate also for events of our interest, but on the other hand increased the signal-to-background ratio due to the higher neutron capture γ-ray multiplicity (n-capture is followed by the emission of about 5 γ-rays, compared to about 1 γ-ray in α-decay). Nevertheless, the Germanium detectors were calibrated with known ^{60}Co and ^{22}Na sources as well as with the 511 keV annihilation radiation, and considering the extremely high activity of the ^{234}U sample, an energy resolution of about 0.5% at E_γ = 1.33 MeV for the Ge-detectors was achieved. Despite the little time that was available for actual data taking, neutron time-of-flight spectra were eventually recorded. Fig. 3 shows such a neutron spectrum, however converted to neutron energy. The grey-shaded areas indicate the regions for resonances with largest capture width Γ_n [21] and, actually, the position of the resonances may be anticipated.

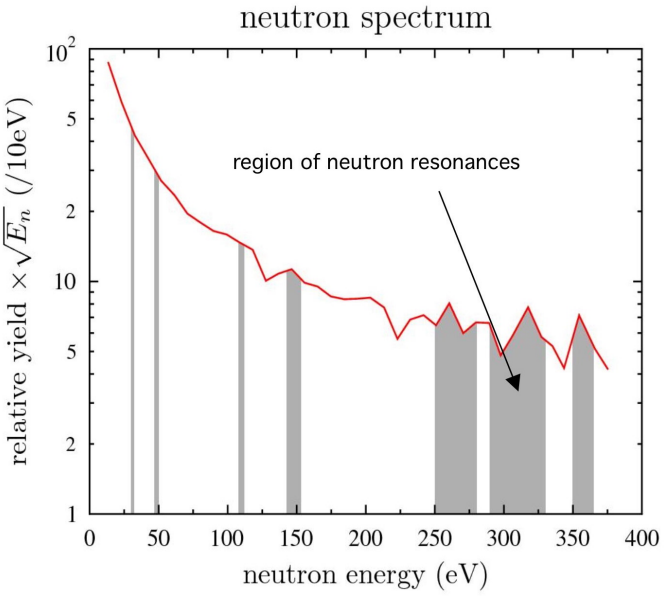

Figure 3. *Neutron energy spectrum indicating resonances (see text for details).*

Conclusions

In conclusion, we have reported on the first identification of a super-deformed isomer in odd-uranium isotopes in the case of ^{235}U*. From the measurement of neutron-induced delayed fission events, the fission half-life for the shape isomeric ground state and its population probability were determined for the first time [18]. In this experiment the isomer spectrometer NEPTUNE has proven how valuable it is for this kind of investigations. The feasibility of a direct measurement of E_{II} was studied as well by populating the shape-isomeric ground state in ^{235}U* by neutron-capture in ^{234}U, and measuring decay γ-rays from the excited states above the shape isomer. As expected, several problems were encountered. However, they were also identified and partially resolved already. We reckon that repeating the GELINA experiment should be successful under certain circumstances. Necessary improvements

concern basically an increased distance between the sample and the detectors as well as more beam time. With these conclusions in mind we consider that the aim of this second study was fulfilled. We believe that the results obtained in this work imply necessary and important information for the understanding of the multi-humped potential energy landscape in heavy nuclei. Actually, it is believed that the U and Np isotopes might represent a region of transition nuclides with respect to the depth of the third minimum, and amongst these ^{235}U is now the only odd-N nuclide, for which a shape isomer was identified. For these nuclides, the depth of the third minimum seems to increase compared to Th and Pa isotopes, until the third barrier drops off, starting with plutonium isotopes.

Acknowledgements
We are indebted to the operating teams of the 7 MV Van-de-Graaff accelerator and GELINA as well as the Radiation Protection Unit for their support during the measurements. In particular, J.-C. Drohé and R. Wynants have to be mentioned. We are also grateful to P. Schillebeeckx for providing the space at FP5. This work was supported by the European Commission within the Sixth Framework Programme through NUDAME (EURATOM contract no. FP6-516487).

References

[1] V. M. Strutinsky, Nucl. Phys. A95, 420 (1967).
[2] R. Vandenbosch, Annu. Rev. Nucl. Sc. 27, 1 (1977).
[3] B. Singh, R. Zywina and R. B. Firestone, Nuclear Data Sheets 97, 241 (2002).
[4] S. Oberstedt and F. Gunsing, Nucl. Phys. A589, 435 (1995).
[5] S. Oberstedt and F. Gunsing, Nucl. Phys. A636, 129 (1998).
[6] S. Björnholm and J. E. Lynn, Rev. Mod. Physics, Vol. 52(4), 725 (1980).
[7] JANIS 2.1, released July 2004, www.nea.fr/janis/welcome.html.
[8] H. Weigmann and J. P. Theobald, Nucl. Phys. A187, 305 (1971).
[9] V. Metag, in Ref. [6], p. 784ff.
[10] R. Zhongzhou and Xu Chang, Nucl. Phys. A759, 64 (2005).
[11] S. Oberstedt *et al*., Exploratory Research at IRMM 2004, Final Report, GE/SCIRMM/ER/2005 (2005) D1, to be published.
[12] S. F. Mughabghab, Neutron Cross Sections, Vol 1, part B, Academic Press, New York (1984).
[13] F. C. Difilippo et al., Phys. Rev. C21, 1400 (1980).
[14] G. F. Auchampaugh et al., Phys. Rev. C33, 125 (1986).
[15] S. Oberstedt and F. Gunsing, Nucl. Phys. A589, 435 (1995).
[16] S. Oberstedt and F. Gunsing, Nucl. Phys. A636, 129 (1998).
[17] C. Budtz-Jørgensen, H.-H. Knitter, Ch. Straede, F.-J. Hambsch, and R. Vogt, Nucl. Instr. Meth. A258, 209 (1987).
[18] A. Oberstedt, S. Oberstedt, M. Gawrys, and N. Kornilov, Phys. Rev. Lett. 99, 042502 (2007).
[19] M. Csatlos et al., Phys. Lett. B 615, 175 (2005).
[20] A. Krasnahorkay et al., Phys. Lett. B 461, 15 (1999).
[21] S. F. Mughabghab, Atlas of Neutron Resonances: Thermal Cross Sections and Resonance Parameters. Amsterdam: Elsevier (2006).

The target laboratory at IPN, Orsay

*V. Petitbon-Thévenet, J. Mottier**

Institut de Physique Nucléaire d'Orsay (IPNO) CNRS : UMR8608 – IN2P3
Université Paris Sud - Paris XI
petitbon@ipno.in2p3.fr, mottier@ipno.in2p3.fr

* EFNUDAT fixed term contract

Abstract: The target laboratory at IPNO (Orsay Nuclear Physics Institute) has a long history of production of stable thin layers. Various types of target can be produced: self-supported or deposited on a backing, possibility of multilayers, large surfaces … The techniques mainly used are Joule effect, electron gun, electronic bombardment, chemical techniques, and electrodeposition. Lamination and centrifugation are also foreseen. The laboratory is also involved in the CACAO project which aims to produce radioactive layers by electrodeposition. All these techniques will be presented and compared, in terms of performances with respect of target characteristics

Introduction

The Target laboratory at IPNO has been in operation since 1963 first for local accelerators then for the national and international community as much as for accelerators and lasers. This laboratory can deposit various types of layers:

- Thin layers on a backing (25% of the production
- Thin self supporting layers (60% of the production)
- "Exotic" layers like thermocouples…

In the target laboratory, different techniques are used to make these layers

- Physical Vapor Deposition (PVD)
- Chemical techniques
- Electrodeposition

The choice of the method depends on different parameters:

- The toxicity of the material
- The availability of the material
- How easily the material oxidizes in air
- How the material degasses, decomposes or micro-explodes
- The risk of reactions with the evaporation sources
- The tendency to manufacture an alloy
- Whether the deposit is on a backing or is self supported

The technique of PVD

The PVD technique consists in vaporizing a material in vacuum to deposit it on a surface. Different techniques can be used to heat the sample. Different atmospheres can be used (with or without a gas, inert or reactive gas). An electric field can be used to create a plasma.

The electron gun

We have 3 electron guns: 2 are equipped with diffusion pumps which allow for one experiment a day, 1 is equipped with a cryogenic pump which allows 2 or 3 experiments a day because the speed of pumping is faster.
Figure 1 shows the functional diagram of an electron gun.

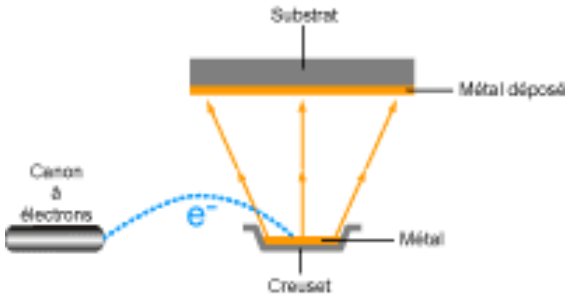

Figure 1. *Functional diagram of an electron gun.*

The crucible is divided into 4 sites and is in copper. This allows us to make multilayers without breaking the vacuum. Some precautions must be taken in certain cases:

- if the material has a higher melting point than copper, an intermediate liner must be used like boron nitride
- if the material is a good heating conductor, thermal losses will occur in the copper so that the evaporation speed will not be sufficient. In this case, a carbon liner can be used.

The crucible is cooled with water and bombarded by an electron beam with an energy from 1 to 10 KeV emitted by a tungsten filament heated at high temperature (2500/2800°C). The deposit is made in vacuum (10-6/10-7 mbar) to protect the filament and to avoid the dispersion of the beam due to collisions with atoms or molecules. The filament is not facing the crucible so that the evaporation material does not pollute it. The electrons are scanned in the X and Y planes to homogenize the surface of evaporation. The electrons are accelerated by an electric field. All of this is placed in a magnetic field to focalize the electrons on the crucible.
With this method, no alloys can be created with the crucible because it is cooled and an liner is used.
The main advantages of this technique are the following:

- Materials with a high melting point can be deposit
- Large surfaces with a good homogeneity (900 cm2) can be obtained.
- A material is deposited on a backing with a better adherence than with the other techniques developed in the laboratory
- The evaporation speed is well controlled through a good control of the power supplies
- Multilayers can be made
- Thick layers can be deposited (several µm) because the liner has an important volume. Self supporting layers can be made because a release agent can be deposit by Joule effect in an electron gun.

In order to make a self supporting layer, a very clean piece of glass is used. A release agent is deposited followed by the material. The system is slowly immersed in water to dissolve the release agent and the material ends up by floating on the surface. The material can then be put on the frame. In the case of oxidising materials, the process takes place in a glove box under controlled atmosphere and the release agent is a polymer.

Evaporation using the Joule effect
We have 2 evaporators using the Joule effect. We can put 2 crucibles, one for the material and one for the release agent.
Figure 2 shows the functional diagram of an evaporation using the Joule effect.

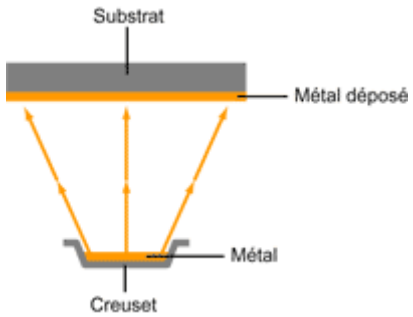

Figure 2. *Functional diagram of an evaporation using the Joule effect.*

The method is well suited for materials with a low melting point
The crucible is heated in vacuum under 10V/600A.
The atoms of the material are at low energy thus the layers are less adherent than with an electron gun. In our case, it does not matter because the Joule effect is used particularly for self supporting layer with the release agent between the material and the substrate.
When a physicist needs a very pure material on a backing, it is easier to clean a Joule effect apparatus than a electron gun (smaller volume, less pieces to clean…) but some materials need an undercoat to adhere. For example, gold does not adhere on a glass substrate, the undercoat is titanium or chromium.
To evaporate using the Joule effect, the choice of the vacuum evaporation source is fundamental.
The size of the evaporation source is limited. It is difficult to make thick layers. Lists exits which give recommended source for a given material. It is the result of experiments. Sometimes, 2 lists do not give the same information for the same material.
For some particular cases, the evaporation source is made in our machine shop. For example, to evaporate ^{70}Zn, an evaporation source was designed in tantalum with a system to avoid projections and obtain the right thickness. The best results were obtained with the least possible material.
Some examples are described below. [1]
Figure 3 shows a boat source in tantalum, tungsten or molybdenum. A refractory material (alumina) can be deposited on the surface. A lot of materials can be evaporated in these boats.

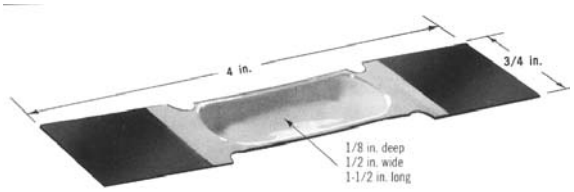

Figure 3. *Boat source in tantalum, tungsten or molybdenum.*

Figure 4 shows a crucible made in a refractory material (boron nitride) heated by a tungsten filament. This crucible is used for aluminium. In a regular boat, aluminium overflows inducing a short circuit. 2 or 3 tungsten wires are inserted in the crucible with the aluminium. When the aluminium boils, it wets the tungsten wires and 95% of aluminium stays in the crucible.

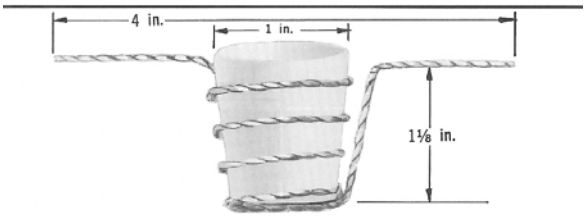

Figure 4. *Crucible made in a refractory material (boron nitride) heated by a tungsten filament.*

Figure 5 shows a sublimation source. Figure 6 shows the interior of this evaporation source. This source is well suited for materials that degas like silicon monoxide, it degases causing

ejection of material. Holes appear in the layer. The gas stays in the buffer volume. The material is evaporated through the other chimney.

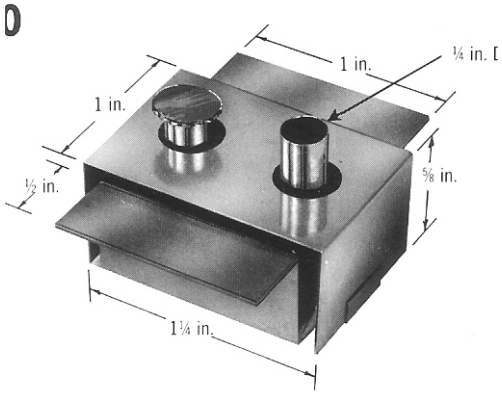

Figure 5. *Sublimation source.*

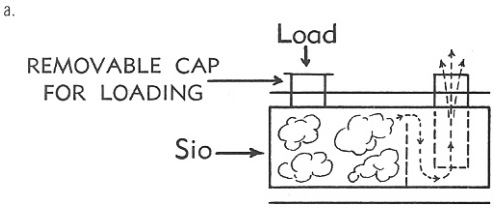

Figure 6. *Interior of an evaporation source.*

Electronic bombardment

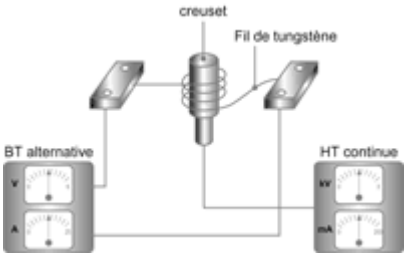

Figure 7. *Functional diagram of electronic bombardment.*

Figure 7 shows the functional diagram of electronic bombardment. A tungsten filament is wounded around a crucible without touching it. The filament is heated at low voltage. The crucible is connected to high voltage. The strongly positive potential attracts the electrons. The impact of the electrons induces an overheating of the crucible. This is indirect evaporation. This method is well suited to evaporate small samples. It is used for isotopic materials which are expensive. The crucible is a small vertical cylinder and the deposit is very directive but the thickness is limited by the quantity of material available in the tube. The target diameters are less than 15 mm.

Electrical arc for carbon deposit

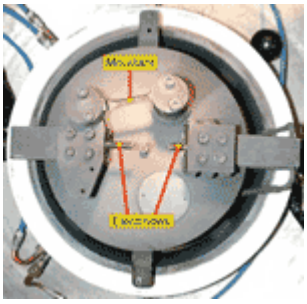

Figure 8. *Interior of the carbon deposit apparatus with 2 graphite rods.*

Figure 8 shows the interior of the apparatus for carbon deposit with 2 graphite rods. The electric arc low voltage (24V) and high current (up to 300A) in vacuum vaporises the material off the graphite electrodes. The 2 rods are brought close to each other to induce an arc discharge which in turn causes the carbon to sublimate. The support and the connections are water cooled. It is not possible to evaporate a lot of carbon at one time because of the powerful heating. The procedure is repeated until the right thickness is reached.

Chemical techniques

The laboratory uses three chemical techniques to make polymer layers.
At first, the polymer powder is dissolved in the appropriate solvent.

- The first technique consists in soaking a piece of glass in the solution with an automatic system which plunges the piece of glass and brings it back up.
- The second method consists in dissolving the powder in a hot solvent and deposing quickly the solution on a horizontal piece of glass.
- The third technique consists in using a spin coater (0-6000rpm). This method gives a better homogeneity than the others.
- These techniques work well with polystyrene, polyethylene, polyethylene D2, collodion…but others can be studied.

Other methods which are not used in the laboratory.

Other techniques exist but they are not used in the laboratory:
- Ion Beam Assisted Deposition: IBAD
- Molecular Beam Epitaxy (MBE)
- Sputtering
- Laser ablation
- Chemical vapour deposition (CVD)
- Mass separator

It seems interesting to study the IBAD method. It is possible to adapt this kind of system in an evaporator. The layers have a better adherence, a longer lifetime, a better chemical composition …

Other methods which will be developed in the target laboratory

- Centrifugation [2]

This is an interesting method to make isotopic layers with a backing. It consists in depositing the isotopic material on a foil as a powder.
The powder is wetted with ethyl acetate and then put in suspension in a mixture of chloroform and polystyrene the viscosity of which depends on the density of the powder and the desired thickness of the layer. The deposit is made by centrifugation.
The equipment exists in the laboratory and the technique will be developed.

- Lamination

It is a method to make thick layer with bulk material (no powder). By the end of 2009, the target laboratory will be equipped with a rolling press.

Electrodeposition (project CACAO) [3]

There are, in fact, many techniques to make radioactive targets. The two most commonly used are the electrodeposition technique and the evaporation using the Joule effect. The equipment using the Joule effect does not exist in the laboratory for radioactive evaporation because it is necessary to have a dedicated equipment (1 equipment = 1 radioactive element). To begin with the electrodeposition technique is easier. The first tests are planned with stable material: lanthanum, thallium and lead deposits on a 6 µm aluminum foil. The first tests with radioactive layers will be the manufacture of a uranium target on polyimide with a 30 nm thick carbon layer for CEA. These first tests are planned to begin in May 2009.
The technique consists in dissolving a compound of the radioactive material and to deposit it on the backing by electrodeposition.

Conclusion

The following table shows a non exhaustive list of the different samples that we have made.

Name	Self supporting	On a support
Silver	Yes	Yes
Aluminium	Yes	Yes
Antimony	Yes	Yes
Bismuth	Yes	
Boron 11		Yes
Calcium 40/48	Yes	Yes
Carbon natural /12/13	Yes	Yes
Caesium iodide		Yes
Chromium	Yes	Yes
Cobalt	Yes	Yes
Collodion	Yes	
Copper	Yes	Yes
Deuterium	Yes	
Tin	Yes	
Iron		Yes
Indium	Yes	
Indium oxide doped with tin		Yes
Lithium6/7	Yes	
Lithium fluoride	Yes	
Glycine		
Guanine		
Mg nat./26/28/30	Yes	Yes
Magnesium oxide nat./24	Yes	
Nickel	Yes	
Gold	Yes	Yes
Phenylalanine		Yes
Platinum	Yes	Yes
Nat.lead/208	Yes	Yes
Polystyrene	Yes	
Polyethylene	Yes	
Polyethylene d4	Yes	
Samarium	Yes	Yes
Silicon	Yes	Yes
Silicon dioxide		Yes
Silicon monoxide		Yes
Strontium	Yes	
Tantalum	Yes	Yes
Tantalum oxide	Yes	
Titanium	Yes	Yes
Titanium nitride		Yes
Nat. tungsten/182/186	Yes	Yes
Tungsten oxide	Yes	Yes
Vanadium		Yes
Ytterbium	Yes	
Yttrium		Yes
Zinc nat/70		Yes
Zirconium	Yes	Yes

References:

[1] Vacuum evaporation sources catalogue – R.D. Mathis Company D.C.
[2] Préparation de cibles par centrifugation de poudre métallique – M. Bouriant, A. Gallois, A. Pelissier, J .P. Richaud – ISN 76,37 Rapport interne juin 1976.
[3] Ch.O. Bacri, paper on CACAO project, contribution to this conference.

Measurements of Scattering Cross Sections of ^{nat}Pb and ^{209}Bi in the Energy Range from 2 MeV to 4 MeV

E. Poenitz[1,], R. Nolte[1], D. Schmidt[1]*

1) Physikalisch-Technische Bundesanstalt (PTB), Bundesallee 100, 38116 Braunschweig, Germany
*) Present address: University of Technology Dresden, Institute of Nuclear and Particle Physics, 01062 Dresden, Germany
poenitz@asp.tu-dresden.de

Abstract: At the PTB TOF spectrometer, cross sections were measured for the elastic and inelastic scattering of neutrons on ^{nat}Pb and ^{209}Bi in the energy range from 2 MeV to 4 MeV using the (n,n') method. The ^{15}N(p,n)^{15}O reaction was used for the production of mono-energetic neutrons. Angle-integrated cross sections were obtained by fitting a Legendre polynomial expansion to the experimental data. The cross sections were normalized to the ENDF/B-V hydrogen scattering cross section. The results are compared with existing experimental and evaluated data. Additional measurements for the monoisotopic ^{209}Bi sample in the same energy range are in progress.

Introduction

Reliable cross section data are required for lithium-lead tritium-breeding blankets for fusion reactors and for the design of Accelerator-Driven Systems (ADS). In particular the neutron transport in a lead spallation target is strongly dependent on the inelastic neutron scattering cross sections between 1 MeV and 4 MeV [1,2].
So far, the PTB time-of-flight (TOF) spectrometer has already been used to measure differential and double-differential cross sections for lead in the energy range from 8 MeV to 14 MeV [3]. For these measurements, a D_2 gas target was used for the production of neutrons by the D(d,n) reaction. Recently, the energy range was extended to lower energies by using the ^{15}N(p,n)^{15}O reaction. With this reaction, monoenergetic neutrons with energies up to 5.7 MeV can be produced. NE213 liquid scintillation detectors were used for neutron detection. The data analysis is based on a realistic simulation of the measured TOF spectra. This procedure, as well as the detailed description of the detector properties (time response, detection efficiencies), allow a very reliable determination of the cross sections.
Differential cross sections were measured at 4 energies for the elastic scattering on ^{nat}Pb as well as for the inelastic scattering with excitation of the first isolated levels of ^{206}Pb and ^{207}Pb. Angle-integrated cross sections were obtained by fitting a Legendre polynomial expansion to the experimental data points. The experimental data were normalized to the ENDF/B-V hydrogen scattering cross section using a polyethylene sample with a well-known hydrogen content.
Measurements were also carried out for the monoisotopic element ^{209}Bi at three energies. The data analysis for ^{209}Bi is not yet completed for all energies. Additional measurements in the energy range from 2 MeV to 4 MeV are in progress.

The PTB TOF Spectrometer

An overview of the PTB TOF spectrometer is shown in fig. 1. The cyclotron (denoted by CY) can be rotated from -20° to +110° with respect to detector D1, resulting in scattering angles between 0° and 160°. Pulsed beams with a time width of 0.8 ns to 2.0 ns can be produced. The gas target T has a length of 3 cm. Its entrance window consists of a 5 µm Mo-foil. The scattering sample S is located at the pivot point. The flight path of the scattered neutrons is 12 m. The distance between the centre of the gas target and the pivot point is 17.5 cm. The detectors D1 (Ø 4" × 1"), D2 – D5 (Ø 10" × 2") and the neutron fluence monitor detector M are NE213 liquid scintillation detectors which are sensitive to γ-rays and fast neutrons. A detailed description of the PTB TOF spectrometer can be found in ref. [4].

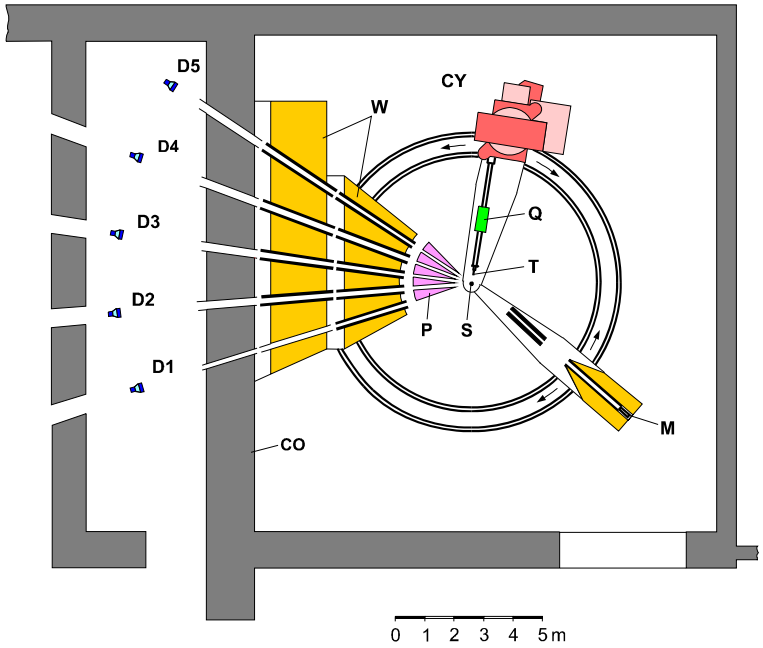

Figure 1. *Schematic view of the PTB TOF spectrometer (see also text).*

The ^{15}N(p,n)^{15}O Reaction as a Source for Monoenergetic Neutrons

Neutron scattering cross sections have been determined with high precision at PTB for more than twenty years. So far, primarily the D(d,n) reaction has been used for the production of neutrons. Due to the Q value of +3.27 MeV and the deuteron energies available at the cyclotron, neutrons in the energy range from 6 MeV to 16 MeV can be produced. For the measurement of neutron scattering cross sections below 6 MeV, however, the implementation of a new neutron source was necessary.

With the ^{15}N(p,n) reaction, monoenergetic neutrons with energies up to 5.7 MeV can be produced. At higher energies there is an additional neutron production via excited states of ^{15}O. A gas target allows background subtraction by gas-in/gas-out difference measurements as well as the easy variation of the target thickness by changing the gas pressure. ^{15}N is a stable isotope and the produced ^{15}O activity does not pose a radiological problem due to its short half life $T_{1/2}$ = 122 s. In contrast to this, the use of the T(p,n) reaction which is commonly used for the production of neutrons in the few MeV region is not possible at the PTB TOF spectrometer because of the radioactive hazard.

A disadvantage of this reaction is the large energy loss of protons in $^{15}N_2$ gas compared to that of deuterons in D_2 gas. The ^{15}N(p,n) cross section shows a strong resonance structure. In contrast to the D(d,n) reaction, angular distributions are not always forward-peaked. In addition, only limited experimental cross section data exist. There are also many discrepancies in the existing data. The PTB TOF spectrometer was also used for the measurement of differential cross sections for the ^{15}N(p,n) reaction at selected energies. Differential ^{15}N(p,n) cross sections for 0° are shown in fig. 2.

Due to the strong resonance structure of the reaction cross section, the measurement of inelastic scattering cross sections is only meaningful at selected energies, i.e. $E_n(0°)$ = 2.24 MeV, 2.71 MeV, 4 MeV, 5.3 MeV. However, differential cross sections for 0° of the ^{15}N(p,n) reaction are, even in the resonances, a factor of 2 – 3 smaller than those of the D(d,n) reaction for the same projectile energy range. The lower differential cross sections and the larger energy loss lead to a neutron yield that is a magnitude lower than in scattering experiments using the D(d,n) reaction.

For a ^{nat}Pb sample, cross section measurements are limited to an incident neutron energy range of 2 MeV to 4 MeV. The lower limit is given by the decrease of the detection efficiency around 1.5 MeV for a detection threshold of about 0.9 MeV which is caused by the properties of the large scintillation detectors. The upper limit is given by the inelastic cross sections which decrease with increasing neutron energy. Because of the lowered neutron yield,

reliable neutron cross section measurements using the ^{15}N(p,n) reaction are limited to the differential cross sections $d\sigma/d\Omega$ greater than 10 mb/sr.

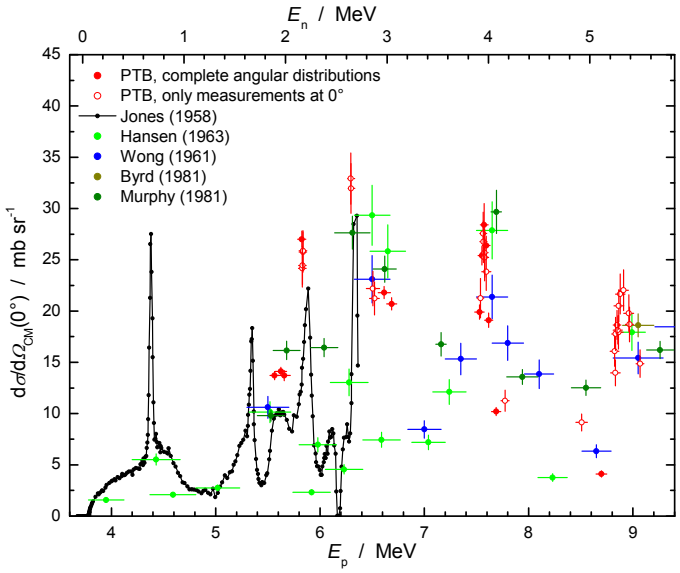

Figure 2. *Differential cross sections for 0° of the ^{15}N(p,n) reaction. The red dots are measurements of complete angular distributions. The red circles are measurements at 0° only. Other data are taken from references [5 – 9].*

Neutron Scattering Cross Sections: Measurements and Data Analysis

Measurements for the ^{nat}Pb sample were carried out at E_n = 2.24 MeV, 2.71 MeV, 2.94 MeV and 4.02 MeV. The pressure of the $^{15}N_2$ gas was chosen to be between 0.4 hPa and 0.5 hPa. This leads to an energy resolution of 90 – 100 keV. Thus, the time-of-flight peaks of the 1st level of ^{206}Pb (E_x = 803 keV) and the 2nd level of ^{207}Pb (E_x = 898 keV) can be separated. For ^{209}Bi, the incident neutron energies were E_n = 2.24 MeV, 2.71 MeV and 3.99 MeV.
The lead and bismuth cross sections were normalized to the ENDF/B-V hydrogen scattering cross section. For this measurement, a polyethylene sample with a well-known hydrogen mass content was used. The scattering samples used in the experiments are full cylinders with nearly identical diameters and heights. The data of all samples are given in table 1.

Table 1. *The data of the scattering samples.*

Sample	Mass m / g	Diameter / mm × Height / mm	Atom density n / 10^{22} cm^{-3}	Remarks
PE	22.455	24.56 × 49.74	8.1416 (H) 4.0946 (C)	hydrogen mass content: (14.30 ± 0.07) %
^{nat}Pb	278.26	25.02 × 50.02	0.04353 (^{204}Pb) 0.86170 (^{206}Pb) 0.68524 (^{207}Pb) 1.69822 (^{208}Pb)	chem. purity: 99.9% isotopic abundance de-termined at PTB group “Inorganic Analysis”
^{209}Bi	240.16	25.00 × 50.00	2.82016	chem. purity: 99.9 %

The data analysis is carried out by iteratively fitting a realistic Monte Carlo simulation of the neutron production, scattering and detection process to the measured time-of-flight spectra. The Monte Carlo code STREUER [10] was used for this simulation. With the simulation, data are corrected for finite geometry, multiple scattering and flux attenuation in the sample and the surrounding air. Fig. 3 shows a simulated and a measured TOF spectrum as an example. The measured spectrum is corrected for the empty-target background and scattering from the air and the sample holder.

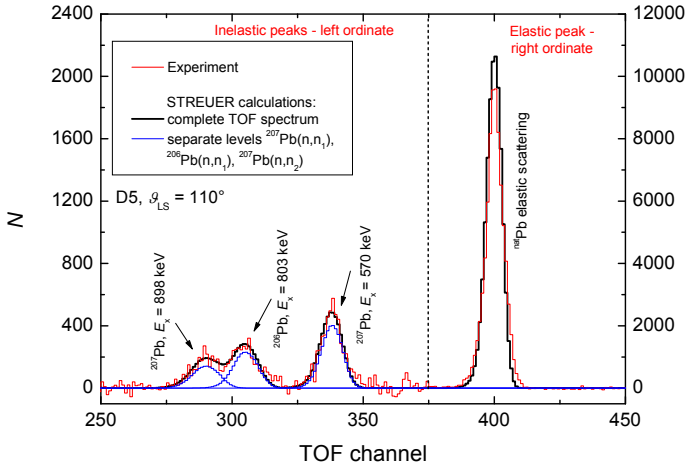

Figure 3. *Simulated and measured TOF spectra of neutrons scattered from a ^{nat}Pb sample for a scattering angle ϑ_{LS} = 110°. Note the different ordinates for the left peak (right axis) and the inelastic peaks (left axis). One TOF bin corresponds to 1.08 ns.*

Results for Pb

In fig. 4, angular distributions of the elastic scattering on ^{nat}Pb at E_n = 2.71 MeV (left) and 4.02 MeV (right) are shown. Compared with the ENDF/B-VI.8 [11] evaluation, the measured angular distribution is more forward-peaked. The JENDL 3.3, BROND 2.2 and JEFF 3.1 [11] evaluations show better agreement. Wick's limit is a lower limit for the differential elastic scattering cross sections for 0°. In the figures, the value of Wick's limit is marked on the left axis. The measured angular distributions, JENDL, BROND and JEFF fulfill Wick's limit. Surprisingly, it is not fulfilled by ENDF/B-VI.8. However, the angle-integrated elastic scattering cross sections are in very good agreement with all evaluations.

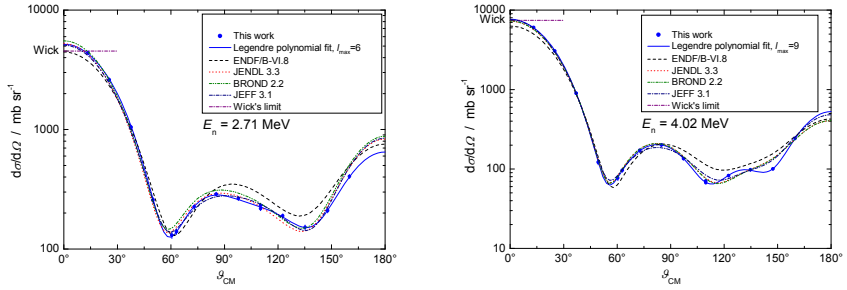

Figure 4. *Angular distributions of the elastic scattering on ^{nat}Pb at E_n = 2.71 MeV (left) and 4.02 MeV (right). Angular distributions from the ENDF/B-VI.8, JENDL 3.3, BROND 2.2 and JEFF 3.1 evaluations [11] are included for comparison. Wick's limit is a lower limit for the differential 0° cross section.*

In fig. 5, angular distributions for the inelastic scattering with excitation of the 1st level of ^{207}Pb for E_n = 2.71 MeV (left) and the 1st level of ^{206}Pb for E_n = 4.02 MeV (right) are depicted. The data points have larger uncertainties because only one isotope contributes and the cross sections for the inelastic scattering are smaller than those for the elastic scattering. In general, there is better agreement with ENDF. JENDL is often discrepant, especially at higher energies.

Angle-integrated cross sections were obtained by fitting a Legendre polynomial expansion to the experimental data using least-squares methods. In fig. 6, angle-integrated cross sections for the inelastic scattering with excitation of the 1st level of ^{207}Pb and the 1st one of ^{206}Pb are shown. Generally, there is good agreement with the cross sections of the evaluations

ENDF/B-VI.8, BROND 2.2 and JEFF 3.1 as well as with measurements by Ramström [12] and Cranberg [13]. For the 1st level of ^{206}Pb, the cross sections by Hicks [14] and Landon [15] are slightly larger than those of this work. The measurement by Abdel-Harith [16] is in good agreement for the 1st level of ^{207}Pb, but larger for the other levels. The deviation increases with rising excitation energy.

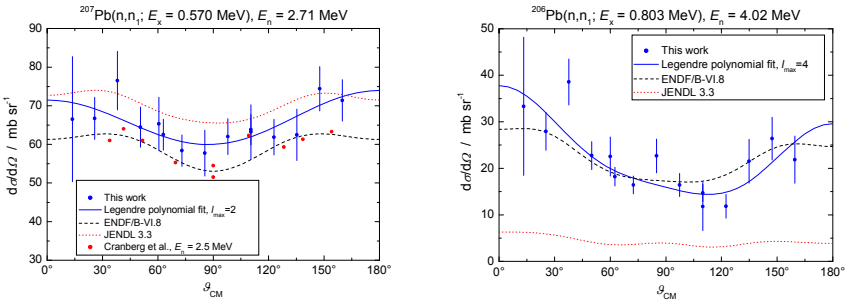

Figure 5. *Angular distributions of the inelastic scattering with excitation of the 1st level of ^{207}Pb at E_n = 2.71 MeV (left) and the 1st level of ^{206}Pb at 4.02 MeV (right).*

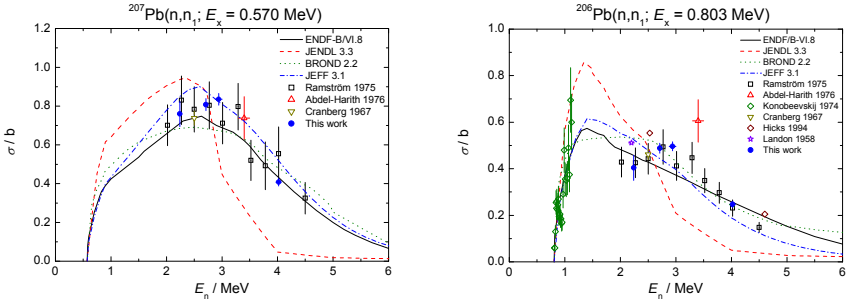

Figure 6. *Angle-integrated cross section for the inelastic scattering with excitation of the 1st level of ^{207}Pb and the 1st level of ^{206}Pb.*

Results for ^{209}Bi

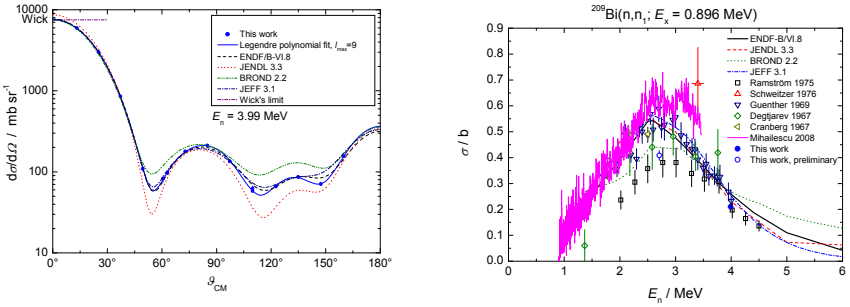

Figure 7. *Angular distribution for the elastic scattering on ^{209}Bi at E_n = 3.99 MeV (left) and angle-integrated cross section for the inelastic scattering with excitation of the 1st level of ^{209}Bi (right).*

In fig. 7, the angular distribution of the elastic scattering on ^{209}Bi at E_n = 3.99 MeV (left) and angle-integrated cross sections for the inelastic scattering with excitation of the 1st level of ^{209}Bi (right) are depicted. The angular distribution of the elastic scattering shows good agreement with those of ENDF and JEFF. For the inelastic scattering, however, the existing evaluated and experimental cross sections scatter strongly. At E_n = 3.99 MeV, the results of

this work are in rather good agreement with all evaluations and the experimental data by Ramström [12] and Guenther [17]. At E_n = 2.71 MeV, there is good agreement with the BROND evaluation and experimental data by Ramström. All other data, including the precision measurement by Mihailescu [18], are significantly larger. Unfortunately, an energy instability of the ion accelerator occurred during this experiment. Although the true value of the cross section may be up to 10 % larger than the value shown in the figure, the energy instability is not sufficient to explain the deviation between the results of Ramström and the present work on the one hand and those of Mihailescu on the other hand.
An additional measurement for ^{209}Bi for E_n = 2.24 MeV was carried out, but the data analysis is not yet completed. At this energy, the decay scheme of ^{209}Bi is quite simple as only 2 levels can be excited. This measurement may be helpful to solve discrepancies between the existing experimental data.

Summary

Scattering cross sections were measured for a ^{nat}Pb sample in the incident neutron energy range from 2 MeV to 4 MeV. Additionally, measurements were carried out for the monoisotopic element bismuth. The ^{15}N(p,n)^{15}O reaction was used for the production of monoenergetic neutrons.
Angular differential and integrated cross sections were determined for elastic scattering as well as for inelastic scattering at the first levels of ^{206,207}Pb and ^{209}Bi. Because of the low neutron yield of this reaction compared with the D(d,n)^{3}He reaction, longer measurement times are required than in earlier experiments at the PTB TOF spectrometer using the D(d,n) neutron source.
For Pb, the angular distributions of the elastic scattering are in good agreement with those of the JENDL, JEFF and BROND evaluations. Inelastic cross sections of lead and all data for bismuth are in better agreement with the ENDF and JEFF evaluations. The measurements confirm the measurements of inelastic scattering cross sections by Ramström, but have smaller uncertainties in the most cases.
Additional measurements for ^{209}Bi in the energy range from 2 MeV to 4 MeV are in progress.

References

[1] M. Embid et al., Systematic Uncertainties on Monto Carlo Simulation of Lead Based ADS, Actinide and Fission Product Partitioning and Transmutation, Proceedings of the Fifth International Information Exchange Meeting, Mol, Belgium, 25-27 Nov 1998.
[2] G. Aliberti et al., Nucl. Sci. Eng. 146 (13 – 50) 2004.
[3] D. Schmidt et al., Differential Cross Sections of Neutron Scattering on Elemental Lead at Energies between 8 MeV and 14 MeV, report PTB-N-27, Braunschweig 1996, ISBN 3-89429-802-2.
[4] D. Schmidt et al., Precise Time-of-Flight Spectrometry of Fast Neutrons - Principles, Methods and Results, report PTB-N-35, Braunschweig 1998, ISBN 3-89701-237-5.
[5] K.W. Jones et al., Phys. Rev. 112 No.4 (1252 – 1256) 1958.
[6] L.F. Hansen et al., Phys. Rev., 132 No. 3 (1123 – 1130) 1963.
[7] C. Wong et al., Phys. Rev.123, No. 2 (598 – 605) 1961.
[8] R.C. Byrd et al., Nucl. Phys. A351 (189 - 218) 1981.
[9] K. Murphy et al., Nucl. Phys. A355 (1 – 12) 1981.
[10] D. Schmidt et al., Fast Neutron Spectrometry and Monte Carlo Simulation - the Codes SINENA and STREUER, report PTB-N-40, Braunschweig 2000, ISBN 3-89701-531-5.
[11] ENDF/B-VI.8, JENDL 3.3, BROND 2.2 and JEFF 3.1 data taken from the NEA database, www.nea.fr.
[12] E. Ramström, EXFOR 20788, www.nea.fr/exfor.
[13] L. Cranberg et al., Phys. Rev. 159 (969 – 979) 1967.
[14] S.F. Hicks et al., Phys. Rev. C 49 No. 1 (103 – 115) 1994.
[15] H.H. Landon et al., Phys. Rev. 112 No. 4 (1192 – 1200) 1958.
[16] M. Abdel-Harith et al., EXFOR 30464, www.nea.fr/exfor.
[17] P.T. Guenther et al., Nucl. Sci. Eng. 75, 69, 1980, EXFOR 10846, www.nea.fr/exfor.
[18] L.C. Mihailescu et al., EXFOR 22741, www.nea.fr/exfor.

Fragment mass yields in neutron-induced fission of ^{232}Th and ^{238}U at 32, 45 and 60 MeV

I.V. Ryzhov[1)], G.A. Tutin[1)], M.S. Onegin[2)], L.A. Vaishnene[2)]
V.D. Simutkin[3)], J. Blomgren[3)], S. Pomp[3)], M. Österlund[3)], P. Andersson[3)]
R. Bevilacqua[3)], J.P. Meulders[4)], R. Prieels[4)]

1) Khlopin Radium Institute, 2nd Murinski pr. 28, 194021, St. Petersburg, Russia
2) Petersburg Nuclear Physics Institute of Russian Academy of Science, 188350, Gatchina, Leningrad district, Russia
3) Division of Applied Nuclear Physics, Department of Physics and Astronomy, Uppsala University, Box 525 S-751 20, Uppsala, Sweden
4) FNRS and Institute of Nuclear Physics, Université catholique de Louvain, B-1348 Louvain-la-Neuve, Belgium

ryzhov@khlopin.ru

Abstract: Preliminary data on fission fragment mass yields measured for the ^{232}Th(n,f) and ^{238}U(n,f) reactions at 32.8, 45.3 and 59.9 MeV are presented. The measurements have been carried out at the neutron beam of the Louvain-la-Neuve cyclotron facility CYCLONE. A multi-section Frisch-gridded ionization chamber has been used as a fission fragment detector. The measured data are compared with the ones obtained for the proton-induced fission of ^{232}Th and ^{238}U in the energy range 30-60 MeV. A comparison of the experimental data with the TALYS calculations is also presented.

Introduction

An experimental campaign aimed at measuring fission data at intermediate neutron energies has been organized by Khlopin Radium Institute and Petersburg Nuclear Physics Institute in collaboration with Uppsala University and Université catholique de Louvain. This activity was motivated by nuclear data needs for Accelerator Driven Systems (ADS). At the fist stage, neutron-induced fission cross sections of 21 nuclides (ranging from tantalum to heavy actinides) have been measured in the energy range from 1 to 200 MeV (see, e.g., [1] and references therein). The next step is a measurement of fission yields in intermediate energy neutron-induced fission of actinides.

Recently, energy dependent fission product yields for actinide fission induced by neutrons and charged particles with energies up to 150 MeV have been requested by the JEFF project. In response to the request, the UKFY4.1 library has been produced [2] making use of the CYPF [3]. It should be noted that the CYPF code is based on an empirical fit to low energy data. Therefore, the predictive power at energies above 20 MeV is expected to be limited. To improve the situation, concerted experimental and theoretical efforts are necessary.

Here we present our results of fission yields measurement from neutron-induced fission of ^{232}Th and ^{238}U. These fertile nuclei play an important role in the ADS performance regardless of fuel mixtures and burn-up schemes. In addition, fast neutron induced fission of ^{232}Th and ^{238}U is a way to produce intense beams of neutron-rich nuclei in Radioactive Nuclear Beam facilities (EURISOL, SPIRAL-2).

The experimental part of the present work will be described in detail elsewhere [4], so only a brief description of the measurement procedure and the data analysis is given here. The measurement results must be considered as preliminary.

Experimental arrangement

Neutron beam facility and detector setup

The measurements have been carried out at the neutron beam of the Louvain-la-Neuve cyclotron facility CYCLONE [5]. Quasi-monoenergetic neutrons were produced by protons impinging on a 5 mm thick lithium target. A multi-section Frisch-gridded ionization chamber (MFGIC) similar to that described in [6] was used as a fission fragment detector. The fissile targets were prepared by vacuum evaporation of $^{nat}UF_4$ and $^{232}ThF_4$ onto 30 μg/cm^2 thick formvar backings. The backings were covered by 10-15 μg/cm^2 Au to make them electrically

conducting. The average thickness of the fissile targets was 130 and 70 μg/cm^2, respectively, for the thorium and uranium deposits. The MFGIC sections 1-3 (in order of increasing distance from the Li target) were loaded with the thorium targets, while the uranium ones were placed into the sections 5-7. In the central (the fourth) section, a calibration ^{252}Cf source was mounted. It was prepared by self-sputtering onto a 50 μg/cm^2 thick Al_2O_3 backing covered by an Au layer with a thickness of about 15 μg/cm^2. The first fissile target was located at a distance of 375 cm from the Li target. The target spacing was 6.4 cm. At the target positions, the fluence rate of peak neutrons was about 10^5 cm^{-2}s^{-1}.

Treatment of the detector signals

Fig. 1 shows a block diagram of the electronics used to process the signals from the MFGIC. Each of the seven sections operates as a twin Frisch-gridded ionization chamber delivering two anode signals and a cathode signal to charge-sensitive preamplifiers (PA). To simplify the data acquisition system, the alternate anodes were connected together, so only two spectroscopy channels (instead of 14) were used to treat the anode signals from all sections. Each anode PA was placed in a common housing with a spectroscopy amplifier. The amplified and shaped anode signals were fed to peak sensing analog-to-digital converters (ADC) to measure the fragment energies. The timing outputs of the anode PAs were fed to timing filter amplifiers (TFA) with the shaping time constants τ_{int} = 20 ns, τ_{dif} = 200 ns and then to leading edge discriminators (LED). The logic signals from LEDs were used as stop signals in time-to-digital converters (TDC) to determine fragment emission angle by measuring time delay between the cathode and anode signals.

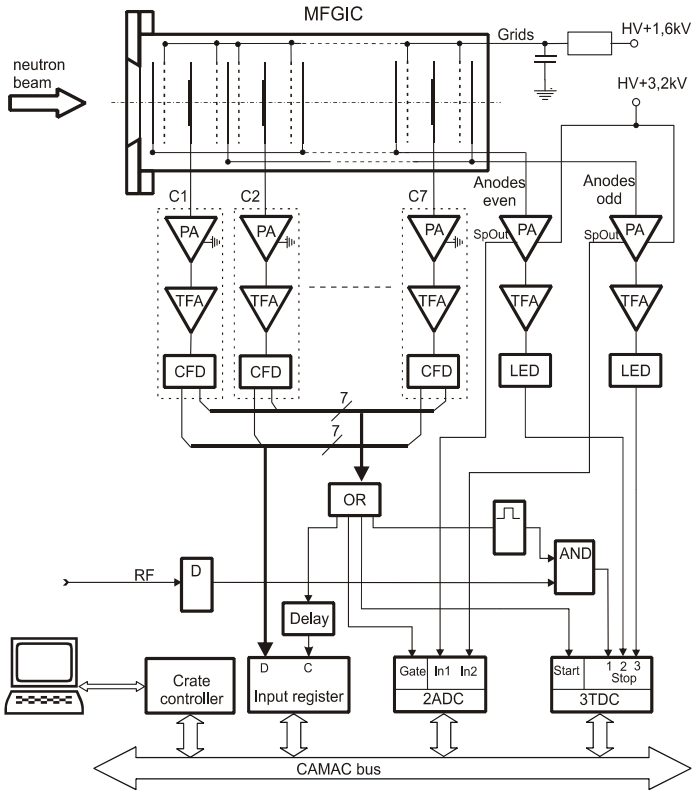

Figure 1. *Electronic block-diagram.*

The cathode signals were used to deliver the start for the neutron energy measurement by the time-of-flight method as well as to identify the chamber fired. The timing output of the cathode PA was fed to TFA with the shaping time constants τ_{int} = τ_{dif} = 20 ns. The output signal of TFA was input to constant fraction discriminator (CFD). Each of seven CFD delivers two output signals. One logic signal from CFD entered input register to identify the number of the chamber fired. The other signal was split into four branches to strobe ADC and input register, to form the start and stop signals linked to fission fragment and the cyclotron RF, respectively.

Data analysis

Having the energies of the complementary fragments in the c.m. system one can determine the fragment masses using the double kinetic energy method based on the conservation laws of mass and linear momentum. The corresponding iteration procedure will be described in [4]. A short micropulse spacing (55-72 ns) at the LLN facility results in a so-called wraparound background caused by slow neutrons arriving at the detector simultaneously with fast neutrons from the next micropulses. A proper subtraction of the wrap-around background can be done provided that we know how many neutrons of given energy are under the high-energy peak. For this purpose, the time distributions were simulated by a Monte-Carlo folding of the neutron-induced fission cross sections of ^{232}Th and ^{238}U [7] with the neutron spectra [5]. The cyclotron RF period, the detector time resolution, and the neutron flight path were taken into account to fit the experimental conditions. An example of measured and simulated time distributions in case of uranium fission is given in the left part of Fig. 2. With the knowledge of the frame-overlap structure of the time distributions, the background mass distributions were obtained using, as a first approximation, the Wahl's evaluation [3] (see the right part of Fig. 2).

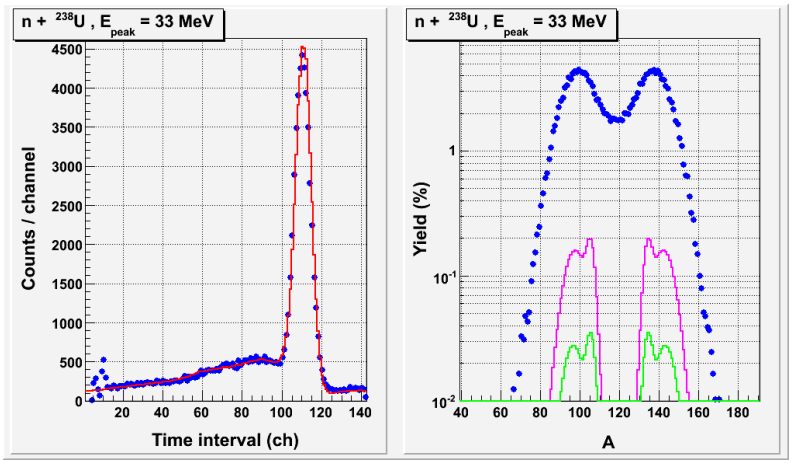

Figure 2. *Left: measured (symbols) and simulated (line) distributions of time intervals between the fission events and the RF signals (the channel width is 0.5 ns). Right: fragment mass distribution for the reactions induced by neutrons under the high-energy peak (symbols) and the simulated background distributions (lines) due to wrap-around neutrons.*

The pre-neutron emission fragment mass distributions obtained as described above were then corrected for the mass resolution. The mass resolution function was calculated taking into account the "inherent" broadening due to prompt neutron emission as well as the instrumental broadening caused by the measurement technique. An example of the unfolding results is given in Fig. 3 [4].

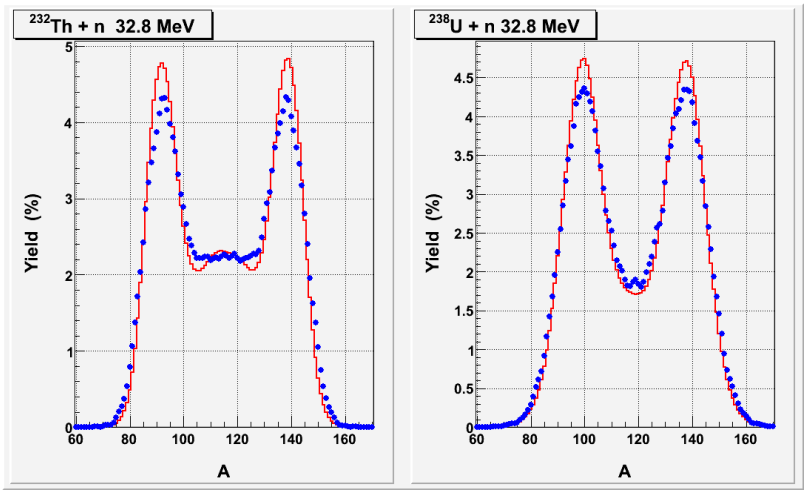

Figure 3. *Pre-neutron emission fragment mass distributions uncorrected (symbols) and corrected (lines) for the mass resolution.*

Measurement and calculation results

Pre-neutron emission fragment mass yields measured for the ^{232}Th(n,f) and ^{238}U(n,f) reactions at 32.8, 45.3 and 59.9 MeV are presented in Fig. 4. Our data obtained for ^{238}U are compared with other data measured in neutron [8] and proton [9] induced fission in Fig. 5. Note that although only data sets compiled in EXFOR have been taken for the comparison, the other data have recently been measured in proton-induced fission of actinides [10]. One can see that our results at 32.8 and 45.3 MeV agree well with the Zoller data [8] while it is worse at 59.9 MeV. The proton data [9] reveal a substantially increased symmetric to asymmetric fission ratio as compared to the neutron data. For a proper comparison, it should be realized that we detected fragments within a cone around the neutron beam axis, while the other measurements were done at fragment emission angles close to 90 degrees.

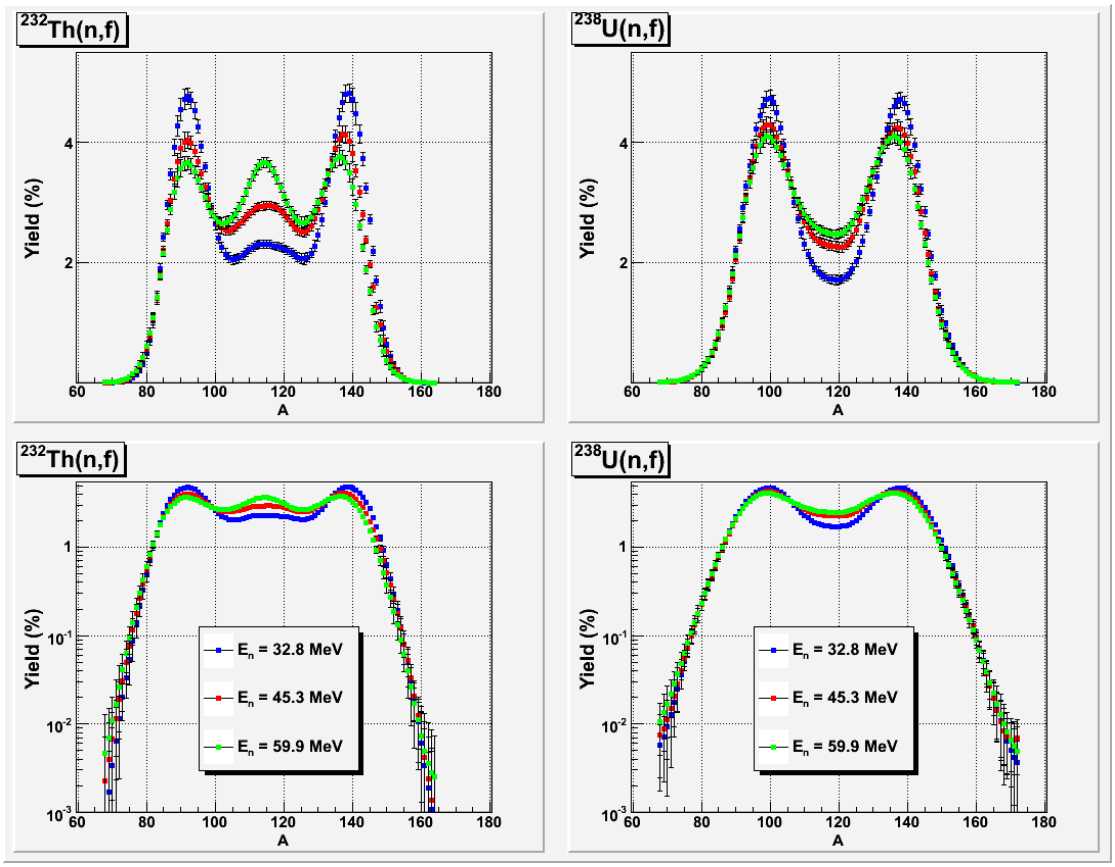

Figure 4. *Pre-neutron emission fragment mass distributions measured for neutron-induced fission of ^{232}Th (left) and ^{238}U (right) at 32.8, 43.5 and 59.9 MeV.*

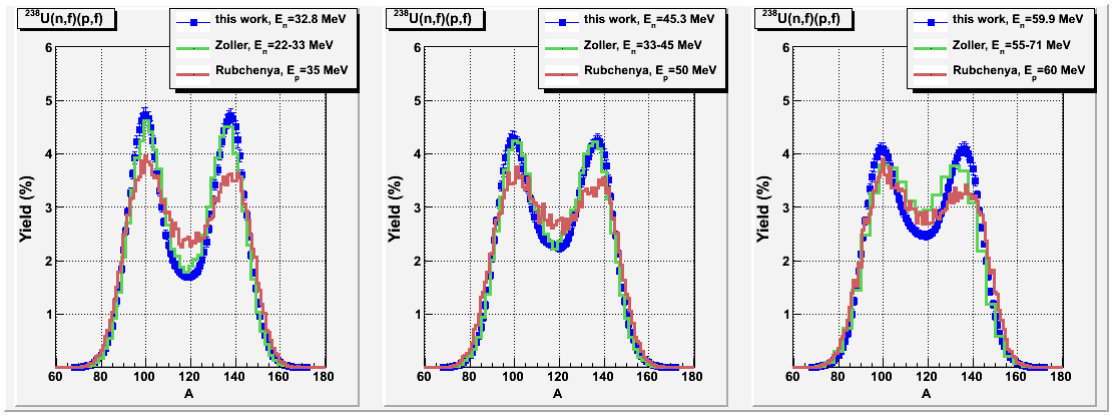

Figure 5. *The present data for ^{238}U in comparison with other data on fragment mass yields in neutron- and proton-induced fission of ^{238}U* [8, 9].

Fig. 6 shows a comparison of the uranium data with model calculations carried out using the TALYS code [11] with the default inputs.

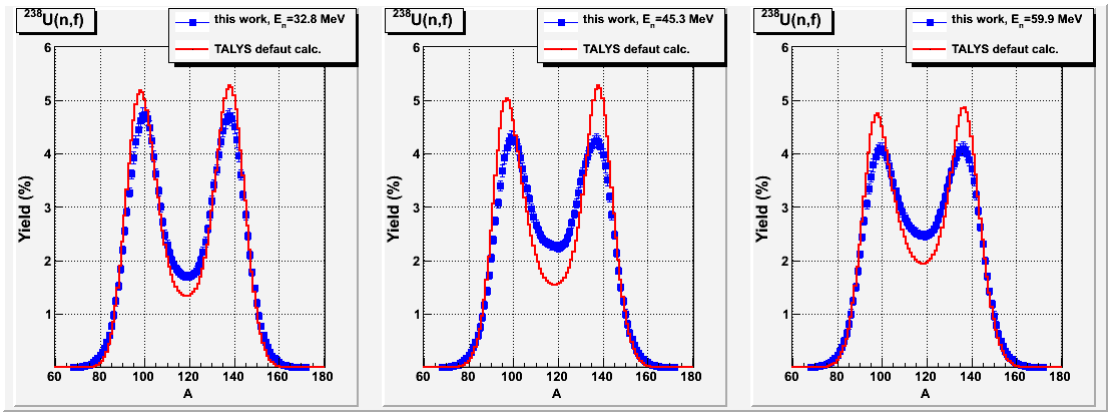

Figure 6. *The present data for ^{238}U in comparison to the model calculations with default inputs.*

The fission yields calculation is based on the Brosa model [12] which can predict the channel mass yields, but not the channel probabilities. We undertook an attempt to deduce the channel probabilities from the experimental data obtained. For this purpose, the measured bidimensional distributions Y(A,TKE) were fitted with a function

$$Y(A,TKE) = \sum_{c} y_c(A)\; y_c(TKE)\,, \qquad (1)$$

where the channel mass yields $y_c(A)$ and the TKE distributions $y_c(TKE)$ were defined as in Ref. [13]. From the 2D fits the channel probabilities averaged over excitation energy of fissioning nuclei were obtained. A comparison of the re-calculated fragment mass yields with the experimental data is given in Fig. 7. Note that in spite of a good agreement between the data and the model calculations a problem of variation of the channel probabilities with excitation energy remains unresolved for the multi-chance fission. Further theoretical work is under way.

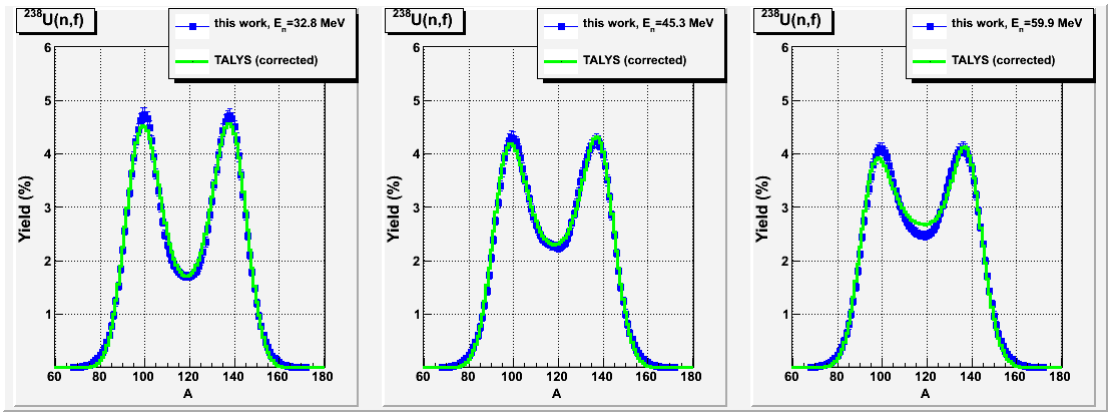

Figure 7. *The present data for ^{238}U in comparison to the model calculations with the corrected channel probabilities.*

Acknowledgements
The authors wish to thank the operating crew of the Louvain-la-Neuve cyclotron facility for the excellent neutron beams they provided for these experiments. This work was supported in part by the International Science and Technology Center (project #3192) and the European Commission within the Sixth Framework Programme through I3-EURONS (contract no. RII3-CT-2004-506065).

References

[1] I.V. Ryzhov, “Fission reaction data at intermediate energies: measurement techniques”, 5th Workshop on neutron measurements, evaluations and applications, October 27-29, 2008, Ljubljana, Slovenia.

[2] R.W. Mills, “UKFY4.1: A set of prototype fission product yield library for neutron, proton, deuteron, alpha particle, photon and spontaneous fission, developed from UKFY4.0.”, JEF/DOC-1232, http://www.nea.fr/html/dbdata/projects/jeffdoc.html.

[3] A.C. Wahl, “Systematics of Fission-Product Yields”, Los Alamos National Laboratory report LA-13928 (2002).

[4] I.V. Ryzhov, G.A. Tutin, J.P. Meulders, R. Prieels, V.D. Simutkin, J. Blomgren, S. Pomp, “Measurement of fragment mass distributions in neutron-induced fission reactions at intermediate energies”, 4th International workshop on nuclear fission and fission product spectroscopy, May 13-16, 2009, CEA, Cadarache, France.

[5] H. Schuhmacher, H.J. Brede, V. Dangendorf, M. Kuhfuss, J.P. Meulders, W.D. Newhauser, R. Nolte, “Quasi-monoenergetic neutron beams with energies from 25 to 75 MeV”, Nucl. Instrum. and Meth. A 421, 284 (1999).

[6] I.V. Ryzhov, G.A. Tutin, A.G. Mitryukhin, V.S. Oplavin, S.M. Soloviev, J. Blomgren, P. U. Renberg, J.P. Meulders, Y.El Masri, Th. Keutgen, R. Prieels and R. Nolte, “Measurements of neutron-induced fission cross sections of ^{205}Tl, $^{204, 206, 207, 208}$Pb and ^{209}Bi with a multi-section Frisch-gridded ionization chamber”, Nucl. Instrum. and Meth. A 562, 439 (2006).

[7] Evaluated Nuclear Data File, http://www-nds.iaea.org/exfor/endf.htm.

[8] C.V. Zöller, “Untersuchung der neutrnoneninduzierten Spaltung von ^{238}U im Energiebereich von 1 MeV bis 500 MeV”, PhD thesis, TH Darmstadt, 1995.

[9] V.A. Rubchenya, W.H. Trzaska, D.N. Vakhtin, J. Äystö, P. Dendooven, S. Hankonen, A. Jokinen, Z. Radivojevich, J.C. Wang, I.D. Alkhazov, A.V. Evsenin, S.V. Khlebnikov, A.V. Kuznetsov, V.G. Lyapin, O.I. Osetrov, G.P. Tiourin, A.A. Alexandrov, Yu. E. Penionzhkevich,”Neutron and fragment yields in proton-induced fission of ^{238}U at intermediate energies”, Nucl. Instr. and Meth. A 463, 653 (2001).

[10] S. Isaev, R. Prieels, Th. Keutgen, J. VanMol, Y. El Masri, P. Demetriou, “Proton-induced fission on actinide nuclei at energies 27 and 63 MeV”, Nucl. Phys. A 809, 1 (2008).

[11] A.J. Koning, S. Hilaire, M.C. Duijvestijn, “TALYS: Comprehensive Nuclear Reaction Modeling”, Proc. Int. Conf. on Nuclear Data for Science and Technology, Santa Fe, USA, 2004, vol. 769, p. 1154.

[12] U. Brosa, S. Grossmann, A. Müller, “Nuclear scission”, Phys. Rep. 197, p.167 (1990).

[13] S. Oberstedt, F.-J. Hambsch, F. Vives, “Fission-mode calculations for ^{238}U, a revision of the multi-modal random neck-rupture model”, Nucl. Phys. A 644, 289 (1998).

Neutron-induced activation cross sections on hafnium isotopes from the threshold to 20 MeV

V. Semkova[1)], R. Jaime Tornin[2)], N. Janeva[1)], N. Koyumdjieva[1)], A. Moens[2)], A. J. M. Plompen[2)], K. Volev[1)]

1) Institute for Nuclear Research and Nuclear Energy, Bulgarian Academy of Science, 72 Blvd. Tzarigradsko chaussee, 1784 Sofia, Bulgaria
2) European Commission, Joint Research Centre, Institute for Reference Materials and Measurements, Retieseweg 111, 2440 Geel, Belgium

arjan.plompen@ec.europa.eu

Abstract: Herein we report on ^{174}Hf(n,2n)^{173}Hf, ^{176}Hf(n,2n)^{175}Hf, ^{177}Hf(n,3n)^{175}Hf, ^{177}Hf(n,p)^{177g}Lu, ^{178}Hf(n,x)^{177g}Lu reaction cross section measurements using the activation technique. The irradiations were carried out at the 7-MV Van de Graaff accelerator at IRMM, Geel. Quasi-monoenergetic neutrons with energies between 14.8 and 20.5 MeV were produced via the ^{3}H(d,n)^{4}He reaction at E_d = 1, 1.4, 2, 3, and 4 MeV. Both natural and samples enriched in ^{177}Hf and ^{17}8Hf were used to account for the interference between reactions leading to the same product. The radioactivity of the samples was determined by γ-ray spectrometry using a HPGe detector. The current measurements are compared with the data from other authors and evaluated nuclear data files. Cross sections for three of the studied reactions are reported for the first time.

Introduction

Neutron-induced reaction cross sections for hafnium isotopes are of importance for nuclear technologies research and development [2]. Activation and transmutation analyses for the high intensity neutron sources require a full set of cross section data comprising all target nuclides that may be present in the materials to be irradiated. Accurate knowledge on neutron-induced activation cross sections is of interest for testing nuclear models as well [1]. A large number of the neutron-induced reactions on Hf isotopes involve population of an isomeric level in the reaction products, thus providing data sensitive to the structure and nuclear properties of the particular nucleus. The experimental database available in EXFOR is very scanty and covers mainly the energy range around 14 MeV.

Experimental procedure

The present cross section data were determined by the activation. The measurement procedure and data analyses that were applied have been detailed in Refs. [4,5]

Samples and irradiation procedure

Natural and enriched materials were employed in the present measurements to account for the interferences between reactions on different isotopes leading to the same nuclide. Natural samples were prepared by punching disks of 10 mm diameter and 0.2 mm thickness from metallic foils of 97% hafnium and 3% zirconium composition, supplied by Goodfellow Metals, Cambridge, UK. The enriched samples were prepared by canning about 125 mg of enriched HfO_2 powder in plexiglass containers. The isotopic composition of the natural and enriched sample materials is given in Table 1. High purity metallic aluminum, niobium, iron, indium and nickel foils of 10 mm diameter were attached to the hafnium samples in order to determine neutron flux density distribution.

The irradiations were carried out at the 7 MV Van de Graaff accelerator at IRMM, Geel. Quasi mono-energetic neutrons with energies between 14.8 and 20.5 MeV were produced via the ^{3}H(d,n)^{4}He reaction (Q = 17.59 MeV) at incident deuteron energies of 1,1.4, 2, 3 and 4 MeV. The samples, each sandwiched between monitor foils, were placed at angles between 0° and 75° relative to the incident deuteron beam and at a distance between 2 and 4 cm from the centre of the target.

Table 1. *Isotopic composition of the natural and enriched samples*.

Sample	Abundance (%)					
	^{174}Hf	^{176}Hf	^{177}Hf	^{178}Hf	^{179}Hf	^{180}Hf
Natural	0.16	5.26	18.6	27.3	13.6	35.1
^{177}Hf	<0.05	1.0	85.4	11.3	0.9	1.4
^{178}Hf	<0.05	0.8	1.9	92.4	3.3	1.6

The time profile of the neutron flux during the irradiations was recorded by a long-counter operated in multichannel-scaling acquisition mode.
The energy and yield distributions of the primary neutrons as a function of deuteron energy and emission angle were determined by the program code EnergySet that uses the ^{3}H(d,n)^{4}He reaction cross section of DROSG-2000 of IAEA, version 2.1 and the stopping powers of Ziegler and by the Monte Carlo code TARGET [5].
All studied reaction cross sections were measured relative to the ^{27}Al(n,α)^{24}Na ENDF/B-VII standard cross section.
The neutron flux density distributions were determined by an unfolding procedure that combines the time-of-flight spectrum measurements and the spectral index method that involves dosimetry reactions with distinct energy thresholds namely, ^{115}In(n,n´)^{115m}In, ^{58}Ni(n,p)^{58}Co, ^{27}Al(n,p)^{27}Mg, ^{27}Al(n,α)^{24}Na, ^{56}Fe(n,p)^{56}Mn, and ^{93}Nb(n,2n)^{92m}Nb.
The radioactivity induced in the samples during irradiation was measured by γ-ray spectrometry using HPGe detector with 100 % relative efficiency. Calibrated standard gamma sources supplied by PTB, Braunschweig, Germany and by DARMI, Gif-sur-Yvette, France were employed for the total and photo-peak efficiency calibration. The measured calibration points were fitted with an analytical function as described in Ref. [3]. The samples were placed directly on the detector cap in order to enhance the counting statistics. Due to the close measurement geometry a correction for the coincidence summing effects was applied in the case of ^{173}Hf and ^{177g}Lu activity measurements. The calculated values were verified by control measurement at 8 cm distance from the detector.

Table 2. *Decay data of measured reaction products ref. [6].*

Reaction	$T_{1/2}$	E_γ (keV)	I_γ (%)
^{174}Hf(n,2n)^{173}Hf	23.6(2) h	123.675(15)	83(3)
		296.974(16)	33.9(14)
^{176}Hf(n,2n)^{175}Hf	70(2) d	343.4	84(3)
^{177}Hf(n,3n)^{175}Hf			
^{177}Hf(n,p)^{177g}Lu	6.647(4) d	208.3662(4)	10.36(4)
^{178}Hf(n,x)^{177g}Lu		112.9498(4)	6.17(7)

The cross sections were determined by the well-known activation formula. The values for the decay constants and for the γ-ray emission probabilities, given in Table 2, were taken from the Evaluated Nuclear Structure Data File (ENSDF) [6]. The count rates were corrected for γ-ray self-absorption, coincidence effects, detector efficiency, neutron flux fluctuation during the irradiation, and background neutrons as described in [3].

Results

The results obtained in the present measurements are shown in Figs. 1 and 2.

^{174}Hf(n,2n)^{173}Hf reaction cross section.
The present data are in a good agreement with the data of Patrick et al. from 1990 [7]. There exist 25 % differences between the results from this experiment and the data of Qaim from 1974 [7], Lankasshmana Das et al. from 1981 [7] and Xianghzhong Kong et al. from 1998 [7]. However the γ-ray emission probabilities of the 296.974 keV γ-line employed in the present measurement is about 7% lower than those used by those authors and the cross section for the ^{27}Al(n,α)^{24}Na reaction used for the neutron flux determination reported in the work of Qaim is 10% higher than the current evaluations. The trend of the excitation function above 14 MeV

determined from the present experiment is the same as those proposed by JEFF-3.1 and JENDL-3.3 evaluations with about 25% difference in the absolute values as well.

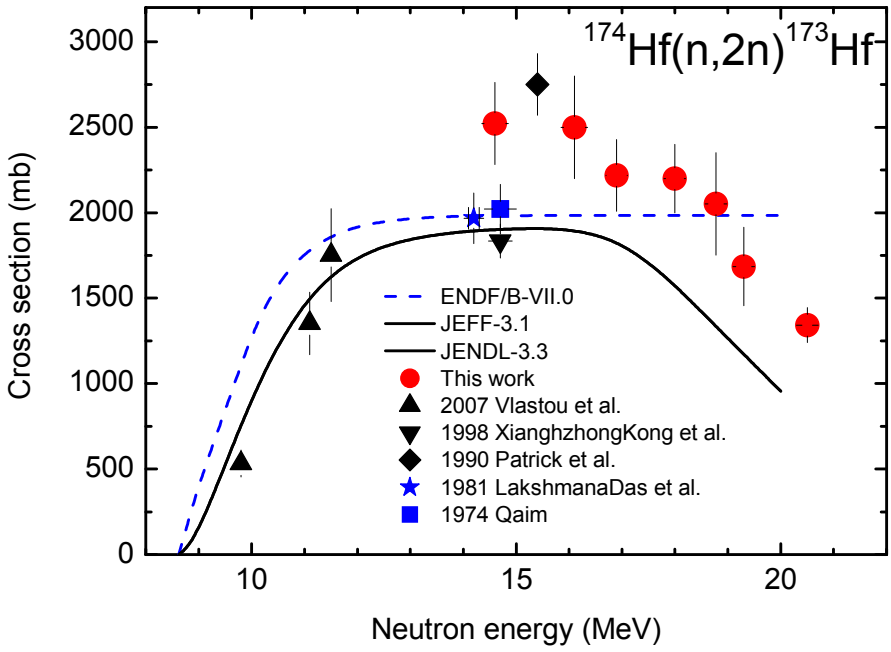

Figure 1. *Comparison between present results, experimental data from EXFOR and evaluated nuclear data for the ^{174}Hf(n,2n)^{173}Hf reaction cross section.*

^{176}Hf(n,2n)^{175}Hf and ^{177}Hf(n,3n)^{175}Hf reaction cross sections.

The EXFOR data base for the ^{176}Hf(n,2n)^{175}Hf reaction cross section is relatively consistent. Our results are in a very good agreement with the bulk of the data around 14 MeV and with JEFF-3.1 and JENDL-3.3 evaluations. Very good agreement with the evaluations was found for the ^{177}Hf(n,3n)^{175}Hf reaction cross section were no experimental data exist so far. The contribution of the ^{177}Hf(n,3n)^{175}Hf reaction to the ^{175}Hf production becomes appreciable above 16 MeV.

^{177}Hf(n,p)^{177g}Lu and ^{178}Hf(n,x) ^{177g}Lu reaction cross sections.

The ground and isomeric state information for ^{177}Lu is given in Table 3. The two most intensive γ-lines from the decay of the ground state ($T_{1/2}$ = 6.647 d) are present in the β^- decay of the 970 keV isomeric state (($T_{1/2}$ = 160.44 d) as well. However, the measurement of the complex decay curve shows that the contribution of the isomeric state to the 208 keV and 112.9 keV γ-line activities is negligible.

Table 3. *Ground and isomeric state information for ^{177}Lu ref. [2].*

E(level) (MeV)	Jπ	$T_{1/2}$	Decay Modes	E_γ (keV)	I_γ (%)
0.0	7/2+	6.647 d *4*	β^- : 100.00 %	208.4 112.9	10.36 *7* 6.17 *7*
0.9702	23/2-	160.44 d *6*	β^- : 78.60 % IT : 21.40 %	208.4 228.5 378.5 112.9	57.4 *24* 37.1 *16* 29.9 *17* 21.9 *9*

There are no experimental data found in EXFOR for both reaction cross sections. The results are shown on Fig. 2. The evaluated data for the total ^{177}Hf(n,p)^{177}Lu reaction cross section for comparison.

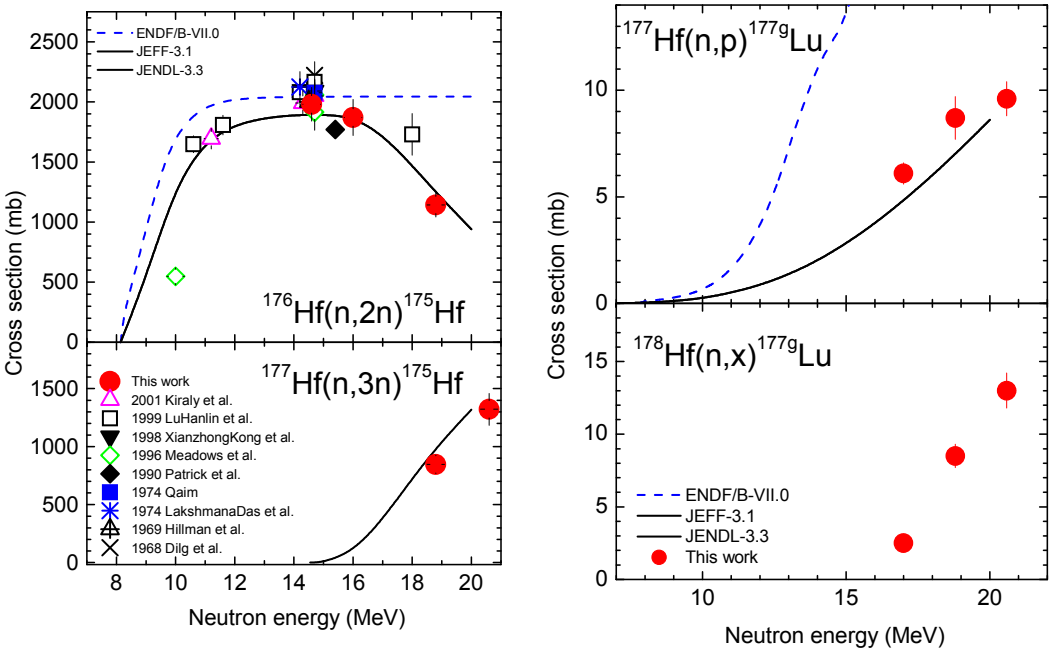

Figure 2. *Comparison between present results, experimental data from EXFOR and evaluated nuclear data for the indicated reaction cross section.*

Summary and conclusions

New experimental results were obtained for the ^{174}Hf(n,2n)^{173}Hf, ^{176}Hf(n,2n)^{175}Hf, ^{177}Hf(n,3n)^{175}Hf, ^{177}Hf(n,p)^{177g}Lu, ^{178}Hf(n,x)^{177g}Lu reaction cross sections in the energy range from 14 to 21 MeV. The induced activities were determined by gamma-spectrometry using a HPGe detector. The ^{27}Al(n,α)^{24}Na standard reaction was used for the neutron fluence determination. The use of enriched samples allowed resolving the interferences between ^{176}Hf(n,2n)^{175}Hf and ^{177}Hf(n,3n)^{175}Hf reactions as well as the interference between ^{177}Hf(n,p)^{177g}Lu and ^{178}Hf(n,x)^{177g}Lu reactions. Three of the studied reactions were measured for the first time. The new results improve the knowledge of the ^{176}Hf(n,2n)^{175}Hf and ^{174}Hf(n,2n)^{173}Hf reactions in the investigated energy range.

Acknowledgements
We want to acknowledge the IRMM Van de Graaff Laboratory personnel for providing as with the best possible experimental conditions. The work was carried out within the collaboration between EC/JRC/IRMM and INRNE.

References

[1] Alan B. Smith, The interaction of fast neutrons with hafnium, Annals of Nuclear Energy 29 (2002) 1241-1252.
[2] R. A. Forrest, Data requirements for neutron activation. Part I: Cross sections, Fusion Engineering and Design 81 (18), pp. 2143-2156.
[3] A. Fessler, A. J. M. Plompen, D. L. Smith, J. W. Meadows, Y. Ikeda, Nucl. Sci. Eng. 134, 171-200 (2000).
[4] P. Reimer, V. Avrigeanu, S. V. Chuvaev, A. A. Filatenkov, T. Glodariu, A. Koning, A. J. M. Plompen, S. M. Qaim, D. L. Smith, and H. Weigmann, Phys. Rev. C 71, 044617 (2005).
[5] D. Schlegel, TARGET User's manual, Laborbericht PTB-6.42-05-2, Braunschweig (2005).
[6] Nuclear Data Sheets: http://www-nds.iaea.org/ensdf/.
[7] EXFOR: http://www-nds.iaea.org/exfor/.

Target preparation and characterisation at IRMM

G. Sibbens, R. Eykens, A. Moens, M. Peeters, K. Luyckx, D. Sapundjiev, Y. Aregbe

European Commission, Joint Research Centre, Institute for Reference Materials and Measurements, Retieseweg 111, 2440 Geel, Belgium
goedele.sibbens@ec.europa.eu

Abstract: Since its establishment, IRMM has produced and characterised a wide variety of samples for neutron transmission and partial cross-section measurements. IRMM became a world-wide recognised supplier of targets for its own studies but also for external research groups. In the past several techniques were applied in house for preparing actinide targets of U, Pu, Np, Am and Th. However, in the late nineties priorities changed, denuclearisation started at IRMM and human and financial resources were gradually placed elsewhere. The target preparation activities were scaled down to cover the minimum requirements of the IRMM Neutron Physics unit. Today, in view of the nuclear renaissance, target preparation has been partly "revived" at IRMM. After decontamination and refurbishment of old equipment, the first custom-made ^{233}U and ^{235}U targets since 2003 were prepared by electrodeposition and by vacuum deposition. Several nuclear and non-nuclear targets have been prepared with mechanical reshaping techniques. The target preparation group at IRMM still has a reputation being one of the very few providers of active targets on a global scale. Therefore a crucial aspect for the future of target preparation, particularly at IRMM, is the knowledge transfer to the next generation of scientists and technicians working in the field.

Introduction

Target preparation has been carried out at IRMM (Institute for Reference Materials and Measurements, former Central Bureau of Nuclear Measurements) since 1961. A variety of foils, enriched stable isotope targets, actinide deposits and other samples which could not be obtained commercially, were fabricated. The target preparation facility was established to support the accelerators on site for cross section measurements and fission fragment studies and also to provide targets to outside customers. In addition, reactor dosimetry reference materials, flux monitor capsules and reactor temperature monitors were supplied to testing and power reactor facilities [1-8].
After a period of denuclearisation and reduction of human and financial resources, the production of nuclear and non-nuclear targets at IRMM started again. Part of the old equipment has been decontaminated and refurbished or replaced by new equipment. Today the target preparation group at IRMM exists of 4.2 persons among which 2.2 with a permanent position.
This paper gives an overview of the targets that can be prepared today at IRMM with a short description of their preparation and characterisation techniques.

Thin actinide targets

Spectroscopy study of charged particles and fission fragments requires thin homogeneous targets. The energy loss of the emitted particles has to be as small as possible and constant over the entire target area. Vacuum deposition in particular, but also electrodeposition is an excellent technique to prepare high-quality targets.

Vacuum deposition of $^{235}UF_4$

At IRMM, vacuum deposition of $^{235}UF_4$ is done by fluoride sublimation from a resistance-heated Ta crucible [9]. This fluoride is prepared by a "wet chemical precipitation" [10]. The original triuranium octoxide is first converted into uranylchloride by dissolving in hydrogen chloride (reaction 1). In the second step the uranium is reduced by adding tin chloride at a temperature of about 40°C (reaction 2). Finally the reduced uranium chloride is converted into a fluoride in reaction with hydrogen fluoride and a residue is formed that consists of uranium fluoride (reaction 3).

$$U_3O_8 + 6HCl \leftrightarrow {}^{6+}3UO_2Cl_2 + 2H_2O + H_2\uparrow \qquad (1)$$

$^{6+}UO_2Cl_2 + SnCl_2 \leftrightarrow {}^{4+}UCl_4 + SnO_2$ (2)

$UCl_4 + 4HF \rightarrow UF_4\downarrow + 4HCl$ (3)

Fluorides have the advantage that they sublimate between 1000°C and 1500°C, so that heat sensitive substrates can be used and there is no interaction with the resistance heated crucible. Oxide sublimation requires a temperature above 2500°C.
The vacuum deposition equipment is designed and constructed at IRMM (Fig. 1). It consists of a Ta-crucible connected to a power supply in a closed chamber that is connected to a pump system in order to work under vacuum conditions. The substrates and masks are mounted in a planetary rotating system, having six moving positions at the periphery and a fixed one in the middle at a distance of 22 cm from the crucible.

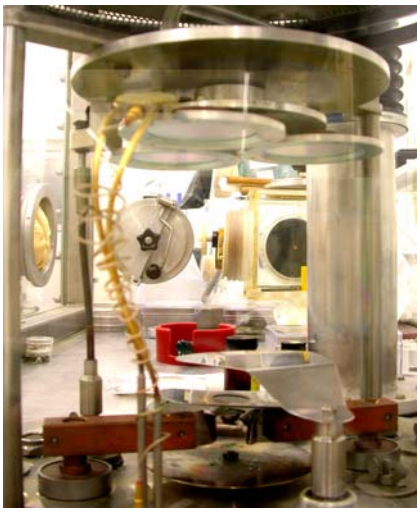

Figure 1. *Vacuum deposition equipment with three $^{235}UF_4$ targets.*

The area of the active layer on the substrates is defined by the masks. The crucible is loaded with $^{235}UF_4$ material and is heated for sublimation. A quartz crystal oscillator is used to monitor the thickness of the deposited layer during the vacuum deposition process. The whole setup is placed in a glove box.
The advantage of vacuum deposition is that the deposited layers are thin and homogeneous [11]. The disadvantage is the low yield because of high material losses during the deposition.

Electrodeposition
Electrodeposition is a relatively simple, fast and high-yielding method for producing thin actinide layers. The layers are formed due to the movement of charged particles in a solution when an electrical field is applied. At IRMM the method is based on cathodic deposition of ^{233}U, ^{234}U, ^{235}U, ^{236}U, ^{238}U, ^{237}Np or ^{239}Pu onto metallic backings from isopropanol and onto carbon-coated polyimide films from isobutanol [12].
The electrodeposition equipment is an electrolysis cell designed and constructed at IRMM from polyacetal which was chosen for its machinability and resistance to organic solvents (Fig.2). A stainless steel substrate holder provides the electrical connection between the substrate and the cathode. The substrate can be Al, Cu or Si and is sealed on the cell wall with a Teflon® PTFE (polytetrafluoroethylene) and thin alumunium ring to avoid leakage of the electrolyte. The anode is a rotating platinum grid to mix the electrolyte without disturbing the deposition. The electrolysis cell is placed in a glove box.
Mother solutions are prepared by dissolution of oxides of U, Pu, Np in 0.75 M HNO_3 at a concentration between 10 $g \cdot L^{-1}$ and 20 $g \cdot L^{-1}$ and added to isopropanol to make the electrolyte. An organic solvent as electrolyte, like isopropanol, has the advantage that the current density is between 1 $mA \cdot cm^{-2}$ and 3 $mA \cdot cm^{-2}$ compared to several $A \cdot cm^{-2}$ for the aqueous electrolytes. The material losses are very limited during electrodeposition and a yield approaching 100% can be reached. Because of the excellent adherence, targets with a thickness in the $mg \cdot cm^{-2}$ range can be prepared. Compared with deposits obtained by vacuum deposition, electrodeposited targets are less homogeneous, the target substrates need to be

conductive and the final composition of the deposit is unknown and assumed to be a hydroxide.

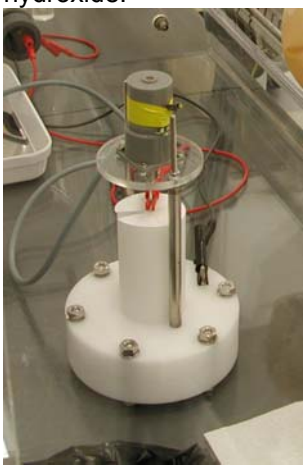

Figure 2. *Electrolysis cell designed and constructed at IRMM from polyacetal.*

Thin polyimide foils

For fission fragment spectroscopy the deposited material is often requested on very thin polyimide substrates to keep the absorption of fission fragments in the substrate as low as possible. At IRMM polyimide foils with a thickness between 25 $\mu g \cdot cm^{-2}$ and 100 $\mu g \cdot cm^{-2}$ are prepared by in-situ polymerisation on glass plates [13-15].

Figure 3. *Polyimide foils on ring.*

First stoichiometric quantities of the 1, 2, 4, 5 – benzenetetracarboxylicdianhydrid and 4, 4' – diaminodiphenylether powders are weighed and dissolved in a volumetric quantity of N,N' – dimethylformamide at room temperature. The concentration of this polycondensate solution is related to the relative humidity in the working area. The solution is spread on a glass plate by spinning in a centrifuge. It is important that the glass plate is clean, degreased and without scratches. The speed of the centrifuge and the concentration of the polycondensate solution determine the thickness of the polyimide layer. The last step in the process is the polymerisation. This is performed by heating the covered glass plate in the oven, first at 100°C to remove the solvent and then at 350°C for polymerisation.
With a fine sharp knife the foil, still on the glass plate, is cut into squares that can cover the support ring. The foil is than floated from the glass plate onto a surface of clean water and transferred onto a ring (Fig 3).

Mechanical transformation techniques

At IRMM targets can be re-shaped by different mechanical transformation techniques: rolling, wire drawing, punching and pressing.

Rolling
Thin metallic sheets with a thickness between 1.0 mm and 0.05 mm are prepared by rolling.
The installation consists of two highly polished hardened steel rollers. They can rotate in the forward or backward direction with an adjustable speed from 5 rpm to 40 rpm. The distance between the rollers can be changed by a turning wheel.
Before rolling, the metal foil is annealed to lower the chance of breaking. This is done by heating the material for several hours beneath the melting temperature under vacuum. Afterwards, it is oiled to fit more easily between the rollers.
During the rolling process, the rollers are brought closer to each other in small steps depending on the kind of foil material. During each step the foil is rolled several times and is positioned in different ways to increase the quality. To avoid contamination of the rollers the foil is placed between two 1 mm thick, polished, stainless steel plates, the so called "sandwich method".

Wire drawing
At IRMM the diameter of metallic wires can be reduced to 0.5 mm by wire drawing. Before starting the process, the metal piece is annealed to lower the chance of breaking.
The first reduction to a diameter of 3.5 mm is done in steps of 1 mm. The installation consists of two rollers with grooves of different depths. The wire is manually moved and transferred to the next groove. Further reduction to 1.1 mm is done with rolling mills in steps of 0.1 mm. This is another type of installation where the wire is moved by an engine and reduced by means of diamond dies. Finally the equipment designed at IRMM is used to reduce the diameter to 0.5 mm in steps of 0.01 mm. The wire is drawn through a diamond die by unrolling and rerolling two coils.

Punching
Metallic discs with a diameter ranging from 1 mm to 50 mm are made by punching.
The punching equipment that is designed at IRMM is used for larger discs from 50 mm to 100 mm. Metallic discs with a thickness up to 0.5 mm can be prepared.
With another punching device the depth that the punch moves into the die, can be adjusted. For each installation a set of punches and dies is available. The metallic discs are prepared by moving the punch arm downwards into the die. For hard metals (e.g. hafnium), the sheet is first annealed by heating the material for several hours beneath the melting temperature under vacuum.

Pressing
Homogeneous powder compacts are prepared by pressing. The installation can press pellets up to 400 kN and consists of a lab press, an external hand pump and a press load display. The press and the hydraulic hand pump are connected with the hydraulic tube and quick lock components. The required pressure depends on the diameter of the matrix and the die. For a diameter up to 9 mm a pressure of 0.8 $kN \cdot mm^{-2}$ is used. For bigger targets the pressure is 1 $kN \cdot mm^{-2}$.

Preparation of alloys by arc melting

Alloys are prepared by arc melting. The metals are melted by direct contact with an electric arc. The arc is produced by striking current from a charged tungsten electrode to the metals. The arc-melting apparatus is effective in melting and alloying high melting point and reactive substances under inert gas (argon) atmosphere.

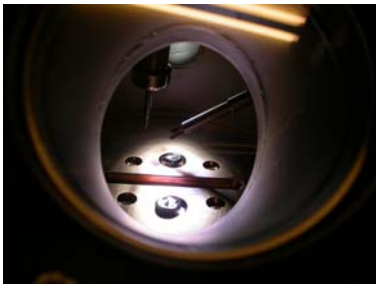

Figure 4. *Arc melter to melt and alloy metals with quantities up to 200 g in an Argon atmosphere at temperatures up to 3500°C.*

At IRMM, two arc melters are available. One is used to melt and alloy quantities up to 200 g in an Argon atmosphere at temperatures up to 3500°C (Fig. 4). The other one is a compact arc melter for melting and alloying samples between 10 g and 20 g in an Argon atmosphere at temperatures up to 3500°C. The latter is especially designed for a glove box and will be installed later.

Characterisation of thin foils and layers

Defined solid angle alpha-particle counting

The thickness of the actinide targets is calculated from its activity [11]. Activity measurements are done relative to a reference material with comparable characteristics. The solid angle is determined by the distance of the source to the diaphragm in front of the detector, the diameter of the diaphragm and the diameter of the deposited layer.
The low-geometry alpha-particle counting system in the target preparation group was designed and built at IRMM. The target chamber is the central part of the system and is connected to a pump system. In the chamber the targets are mounted on movable holders in order to be able to measure several targets without opening the chamber. The alpha-particles are detected by a surface barrier with a diaphragm in front of it. The distance between the detector and the targets can be changed by moving the detector.
If the targets are used for cross section measurements it is important to know the amount of particles on the target. Via the specific activity the mass of the active material is calculated. This specific activity is defined via isotopic analysis of the solution before preparation of the targets or via isotopic dilution mass spectrometry of a target prepared in the same conditions.
For larger sources it can be important to know the distribution of the active material on the source. Therefore a diaphragm is positioned on top of the target and measurements are performed for different horizontal positions of the target.

Spectrophotometry

The thickness of the polyimide foils is measured with a photospectrometer [16-18]. With this instrument the amount of light can be measured that is transmitted, absorbed or reflected. A calibration has been done with polyimide foils that have been measured before with other methods. This can be done in the light reflection or transmission mode. When the foil is still on the glass plate, the reflection mode is applied. In the transmission mode the foil has been transferred on a ring.

Dimensions and mass

The thickness and diameter of targets are measured with a calliper that has a readability of 10 µm and a micrometer with a readability of 1 µm. The mass is determined by weighing the target on a balance with a readability of 10 µg.

Future developments

The target preparation group will restart the preparation of thin deposited layers of ^{6}LiF by vacuum deposition and ^{10}B by electron beam physical vapour deposition.
The preparation of actinide deposited layers by vacuum deposition in a glove box will be expanded for ^{233}U and ^{238}U.
Research and tests are on-going for the preparation of reactor melt-wire temperature monitors by arc melting.
For the characterisation of high radioactive actinide targets, the low-geometry alpha counting in a glove box will be made operational.
A manual lab press up to 350 kN press force and a compact arc melter with temperature up to 3500°C for samples from 10 g to 20 g will be installed in glove boxes.
Investigation to improve the characterisation of targets like thickness, homogeneity and area measurements started.

Conclusion

As a response to the increased request for nuclear and non-nuclear targets, efforts are continuously made to restart target preparation techniques.
Today thin qualitative actinide targets can be produced with two different techniques. For highly enriched ^{235}U the sample is prepared by vacuum deposition and for ^{233}U, ^{234}U, ^{235}U,

^{236}U, ^{238}U, ^{237}Np and ^{239}Pu electrodeposition is applied. The actinide targets are characterised by low-geometry alpha counting.
When very tin substrates are required, thin polyimide foils are prepared by in situ polymerisation on glassplates. The thickness is between 25 $\mu g \cdot cm^{-2}$ and 100 $\mu g \cdot cm^{-2}$ and is determined by spectrophotometry.
Targets are reshaped applying mechanical transformation techniques like rolling, wire drawing and punching. By rolling, thin metallic foils with a thickness between 1.0 mm and 0.05 mm can be produced. Metallic wires with a diameter between 1.0 mm and 0.5 mm are made by wire drawing. And by punching metallic discs are produced with a diameter between 1 mm and 100 mm and a thickness below 0.5 mm.
Also homogeneous powder compacts can be produced. This is done by pressing. And finally alloys are made by melting and alloying metals with an arc melter.
The activities of the target preparation group at IRMM are mainly focused on the preparation of targets for the Neutron Physics unit at IRMM. Refurbishment or replacement of old equipment is ongoing. Besides equipment, the experience is an important factor in the preparation of targets. Therefore the know-how, still present at IRMM, is transferred to new permanent and temporary staff. Special emphasise is given to detailed documentation describing the different techniques of target preparation and characterisation.

References

[1] G. H. Debus, Sample preparation at the Central Bureau of Nuclear Measurement, Report AERE-R 5097 (1965) 1.
[2] J. Van Audenhove, J. Joyeux, Sample preparation by metallurgical methods, Nucl. Instr. and Meth. 102 (1972) 409.
[3] J. Van Audenhove, V. Verdingh, H. Eschbach, P. De Bievre, Sample preparation and definition at the Central Bureau for Nuclear Measurements, Proceedings of 3rd INTDS conf. (1974) 119.
[4] J. Van Audenhove, J. Pauwels, History of target and special sample preparation at CBNM, Book* (Ed. J. Jaklovsky, Plenum Press, NY) (1981) 79.
[5] J. Van Audenhove, Special nuclear target preparation at CBNM, Book* (Ed. J. Jaklovsky, Plenum Press, NY) (1981) 89.
[6] J. Pauwels, Specific nuclear target preparation and characterization techniques used at CBNM, Nucl. Instr. and Meth. B56/57 (1991) 938-941.
[7] C. Ingelbrecht, Metallurgical sample preparation at the Institute of Reference Materials and Measurements, Nucl. Inst. and Meth. B99 (1995) 790.
[8] A. Stolarz, R. Eykens, A. Moens, Y. Aregbe, Actinide targets preparation at IRMM – then and now, in press.
[9] J. Van Audenhove, P. De Bievre, J. Pauwels, F. Peetermans, M. Gallet, A. Verbruggen, The preparation and characterisation of reference fission foils, Nucl. Instr. and Meth. 167 (1979) 61.
[10] R. Eykens, J. Pauwels, J. Van Audenhove, The hydrofluorination of uranium and plutonium, Nucl. Instr. and Meth. A236 (1985) 497.
[11] B. Denecke, R. Eykens, J. Pauwels, P. Robouch, D. M. Gilliam, P. Hodge, J. M. R. Hutchinson, J. S. Nico, Characterization of actinide targets by low solid-angle alpha particle counting, Nucl. Instr. and Meth. A 438 (1999) 124.
[12] C. Ingelbrecht, A. Moens, R. Eykens, A. Dean, Improved electrodeposited actinide layers, Nucl. Instr. and Meth. A397 (1997) 34.
[13] J. Pauwels, J. Van Craen, J. Van Gestel, J. Van Audenhove, Polymide substrate foils for nuclear targets, Nucl. Instr. and Meth. 167 (1979) 109.
[14] J. Van Gestel, J. Pauwels, J. Van Audenhove, Improved polymide foils for nuclear targets, Book* (Ed. J. Jaklovsky, Plenum Press, NY) (1981) 117.
[15] R. Eykens, P. Maier-Komor, J. Van Gestel, J. Pauwels, New aspects of thin polyimide foils, Nucl. Inst. and Meth. A362 (1995) 175.
[16] J. Pauwels, Fast thickness measurements of thin foils and layers, Proceedings of the 10th INTDS conf. (1981) 208.
[17] J. Pauwels, J. Wesenbeek, M. Pauwels, J. Van Gestel, The use of a visible light spectrophotometer for nuclear target production control, EUR 7985 EN.
[18] H. Tagziria, Preparation and characterisation of reference deposits for the determination of the free neutron lifetime, GE/R/SP/002/90.

Measurement of (n,xnγ) reactions of interest for the new nuclear reactors

J.C. Thiry[1)], C. Borcea[3)], Ph. Dessagne[1)], J.C. Drohé[2)], E. Jericha[4)], H. Karam[1)], M. Kerveno[1)], A. L. Negret[3)], A. Pavlik[5)], A. Plompen[2)], P. Romain[6)], C. Rouki[2)], G. Rudolf[1)], M. Stanoiu[2)]

1) Institut Pluridisciplinaire Hubert Curien, Université de Strasbourg, CNRS/IN2P3, 23 rue du Loess, 67037 Strasbourg, France
2) Institute for Reference Materials and Measurements, Retieseweg 111, B-2440 Geel, Belgium
3) National Institute of Physics and Nuclear Engineering “Horia Hulubei”, IFIN-HH Str. Atomistilor no. 407, P.O.BOX MG-6, Bucharest – Magurele, Romania
4) Technische Universität Wien, Atominstitut der Österreichischen Universitäten, Austria
5) Universtität Wien, Fakultät für Physik, Währinger Str. 17, 1090 Wien, Austria
6) Commissariat à l'Energie Atomique, Centre DAM - Ile-de-France, Service de Physique Nucléaire, Bruyères-le-Châtel, 91297 Arpajon Cedex, France

jean-claude.thiry@ires.in2p3.fr

Abstract: The design of the Generation IV nuclear reactors requires knowledge of cross sections of different nuclear reactions. Our research is focused on measurement of data such as (n,xn) reaction cross sections occurring in these new reactors. The goal of our work is to measure unknown cross sections and to reduce uncertainty on present data of reactions and isotopes present in transmutation or regeneration processes.
The current work consists of ^{235}U(n,xnγ) measurements in the fast neutron energy domain (up to 20 MeV). The experiments are performed at GELINA, a pulsed, white neutron beam at IRMM, Belgium. The pulsed beam enables us to measure neutron energies with the time of flight (TOF) technique. The neutron induced reactions (in this case inelastic scattering and (n,2n) reactions) are determined by online prompt γ spectroscopy. The employed methods and an analysis of a preliminary data set will be presented.
This work is a first step in the preparation of the measurement of ^{233}U(n,xnγ) reactions, which are completely unknown today although of very high importance in the ^{232}Th regeneration process.

Introduction

Precise knowledge of (n,xnγ) reactions is a key issue in present day’s reactor development studies. The new Generation IV nuclear reactors explore new energy domains, and imply reaction rates unknown at this stage.
(n,xn) reactions are of crucial importance for the design of new reactors. They are an important energy loss mechanism which has to be taken into account in the calculations of new reactors as they lead to neutron multiplication and production of radioactive isotopes.
The presented work is performed using the (n,xnγ) technique, for which a high precision experimental setup was developed and is in the phase of optimization. The ultimate goal of developing these measurement techniques is to study (n,xn) reactions on ^{233}U, lacking experimental data, which is of upmost importance for the Thorium cycle. For example, the ^{233}U(n,2n)^{232}U reaction leads in its decay to ^{208}Pb, emitter of a 2.6 MeV γ ray. Presence of such energetic photons has a major impact for the reactor core temperature, and therefore needs to be studied precisely.

Experimental Setup

This section treats the applied measurement techniques as well as the experimental setup, shown in figure 1.

The (n,xnγ) technique
A sample enriched in ^{A}X isotopes is irradiated by a neutron beam, inducing (n,xn) reactions. This leads to production of $^{A-(x-1)n}X$ isotopes in excited states. Decay of these isotopes leads to emission of characteristic γ rays, witnessing a prior reaction. These γ rays yield the cross section of isotope production in a given excited state. The data can be used to validate theoretical codes, such as TALYS, which is able to predict (n,xnγ) reaction cross sections.

The TOF technique
The experiment is realized with neutrons produced by GELINA, a neutron facility at IRMM, Belgium. GELINA produces a white, pulsed neutron beam using the (γ,F) and (γ,xn) reactions on a ^{235}U target. This leads to an incident neutron flux spectrum from a few keV up to several MeV.
The pulsed beam enables energy separation of the incident neutrons using a time spectrum, which can be calibrated thanks to the presence of a γ-flash. The measurements are performed at a flight path located 30m behind neutron production. Using the relativistic energy-speed formulae, this gives a resolution of 1MeV/10ns in the 20 MeV domain and a 1MeV/500ns resolution in the 1 MeV domain. The data acquisition precision being 10ns, this flight distance is the best compromise between time resolution and neutron flux intensity.

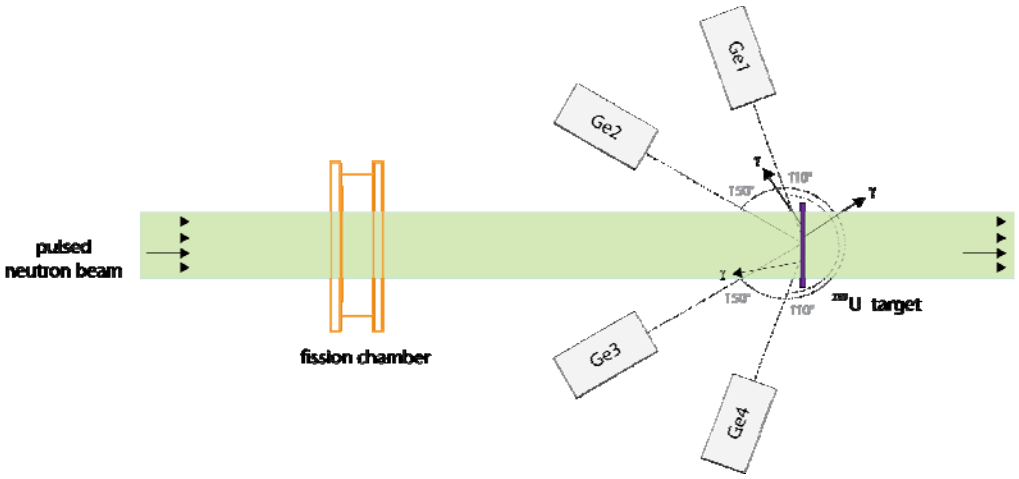

Figure 1. *Experimental setup used at GELINA, FP16/30m.*

Data acquisition
Data are treated online using TNT2 cards (Treatment for NTof) developed at IPHC. Signals are processed with the Jordanov [1] signal treatment method, which determines the energy and time of incident events. Those are stored in list mode files, where the energy is encoded on 14 bits, time resolution is 10ns.

Flux monitoring
Precision of cross section measurements depends very strongly on the uncertainties of the incident neutron flux (figure 2), thus it is of upmost importance to have very precise flux data.

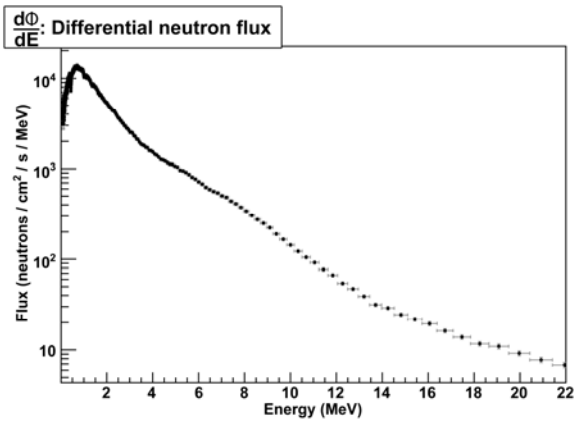

Figure 2. *Differential neutron flux measured at FP16/30m at GELINA.*

The flux is measured using a double layer ^{235}U fission chamber. The deposits, both highly enriched in ^{235}U (>99.5%) are very thin: 324μg/cm^2 for the vacuum evaporated $^{235}UF_4$ layer and 387μg/cm^2 for the spray painted $^{235}U_3O_8$ layer. The effective distance of the fission chamber was chosen between 6 and 7 mm, as this leads to the best ratio of fission fragment energy loss (signal) and radioactivity α particle energy loss (background noise).
The measurements show a combined evaporation and fission neutron spectrum, and present uncertainties ranging from 5 to 10% at this moment depending on the energy.

γ detection
The γ rays, witnessing the decay of created isotopes, are detected using four high purity Germanium (HPGe) detectors, made of planar crystals with depths ranging from 2 to 3 cm and surfaces dimensioned between 10 and 28 cm^2. The detectors are optimized for high resolution detection at low energies (resolution of 0.7 keV at 122 keV). They are placed at angles of 110° and 150° which allows the angular dependence to be taken into account. Backward angles were chosen to reduce dead time caused by the observation of events due to γ-flash scattering, arriving up to 25% of the detections.

Data analysis

The differential γ production cross section for a ray of interest at a given angle θ_i and energy E_i is expressed as:

$$\frac{\mathrm{d}\sigma}{\mathrm{d}\Omega}(\theta_i, E_i) = \frac{1}{4\pi}\frac{n_{GE}(\theta_i, E_i)}{n_{FC}(E_i)}\frac{\varepsilon_{FC}\sigma_{U,f}(E_i)}{\varepsilon_{GE}(E_i)}\frac{\varsigma_{FC}}{\varsigma_{sample}}\frac{s_{FC}}{s_{sample}} \quad (1)$$

where n_{GE} and n_{FC} represent the dead time corrected numbers of detections for a given ray in the Ge energy spectrum and for the fission chamber high energy spectrum respectively, ε_{GE} and ε_{FC} the Germanium detector's and the fission chamber's efficiency, $\sigma_{U,f}$ the ^{235}U fission cross section, ς_{FC} and ς_{sample} the areal densities of the Uranium layer in the fission chamber and the sample, s_{FC} and s_{sample} the surfaces of the Uranium layer in the fission chamber and the sample.

Angle integration
The quantity of interest is the total reaction cross section, which requires integration of equation (1). One can show that the differential cross section can be expressed as a finite sum over even degree Legendre polynomials [2], [3]:

$$\frac{\mathrm{d}\sigma}{\mathrm{d}\Omega}(\theta_i, E_i) = \frac{\sigma}{4\pi}\sum_{k=0}^{[j_i]} c_{2k}P_{2k}(\cos\theta_i) \quad (2)$$

where $[j_i]$ is the largest integer smaller than or equal to the spin of the decaying state j_i. Gaussian quadrature specialized to even degree polynomials [4] can be used: for a given number n of detectors, we need the best angles ($x_j = \cos\theta_j$) and weights w_i to verify:

$$\sigma = 2\pi\int_{-1}^{1}\frac{\mathrm{d}\sigma}{\mathrm{d}\Omega}(x)\,dx = 2\pi\sum_{i=1}^{n} w_i\frac{\mathrm{d}\sigma}{\mathrm{d}\Omega}(x_i) \quad (3)$$

This is achieved for x_i being the n positive zeroes of the Legendre polynomial P_{2n} and

$$w_i = \frac{1}{\sum_{m=0}^{n-1}((4m+1)/2)P_{2m}^2(x_i)} \quad (4)$$

For the two detector configuration, the following results are found:

Table 1. *Weights for integration of γ ray angular distributions.*

No.	Weight w_i	Angle θ_j
1	**0.69571**	**30.56 ; 149.44**
2	**1.30429**	**70.12 ; 109.88**

Results

In this paper the (preliminary) results for two different measurement sets are presented, which were part of the thesis work done by H. Karam [5]

The ^{206}Pb isotope

In order to validate the experimental procedures, inelastic scattering reactions on ^{206}Pb were measured. These have already been studied by different research groups and therefore present a large amount of experimental data. We examined the case of the $2^+ \rightarrow 0^+$ transition, characterized by emission of a 803.1 keV γ ray. The energy has been averaged on intervals of 620 ns for energies below one MeV and intervals of 120 ns for energies above one MeV. The results for both angles (110° and 150°) have been summed using Gauss quadrature. They are shown in figure 3. The same analysis procedure has been applied to the $3^+ \rightarrow 2^+$ transition of the same isotope, leading to a 537.4 keV γ emission. The results are shown in figure 4.

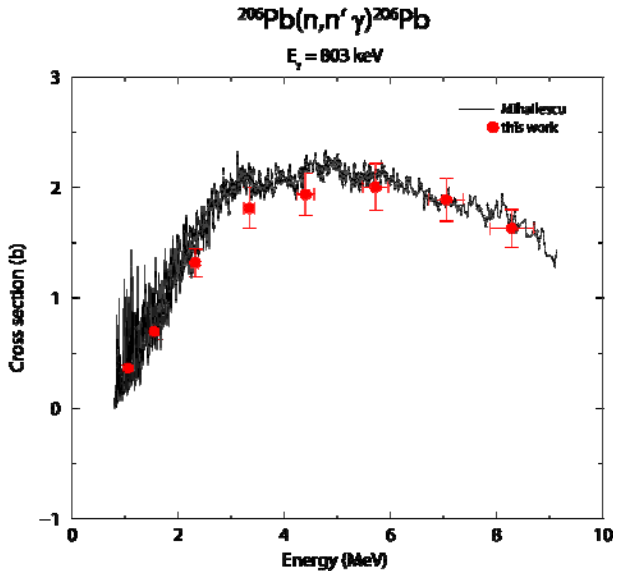

Figure 3. *γ ray production cross section for the 803.1 keV transition of ^{206}Pb.*

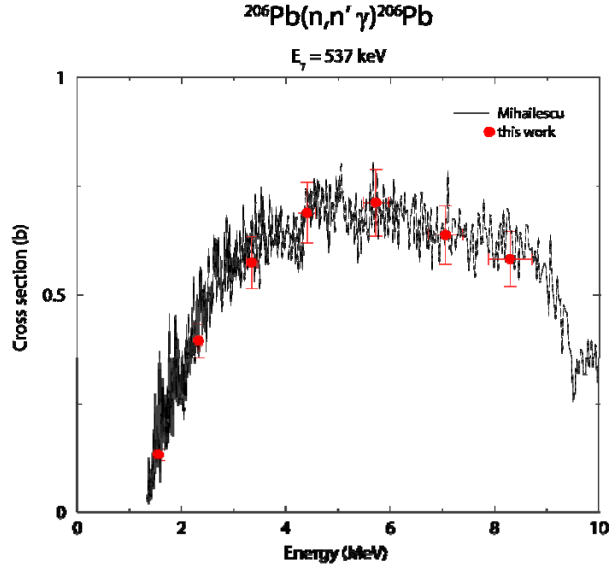

Figure 4. *γ ray production cross section for the 537.4 keV transition of ^{206}Pb.*

The obtained results are in very good agreement with those measured by L.C. Mihailescu [6], who used a similar experimental setup at a flight path located at 200m at GELINA. It is to remark that the statistics of his work are nearly 18 times higher than the ones acquired for this study.

The ^{235}U isotope

In this paper we present a preliminary data set of measurements of the $5/2^+ \rightarrow 7/2^-$ transition, observed through emission of a 129.3 keV γ ray. This γ ray transition due to an inelastic scattering reaction on ^{235}U has never been measured before. Energies have been averaged on different time intervals. The results for both angles (110° and 150°) have been summed using Gauss quadrature. Total beam time of this experiment was 1059 hours.

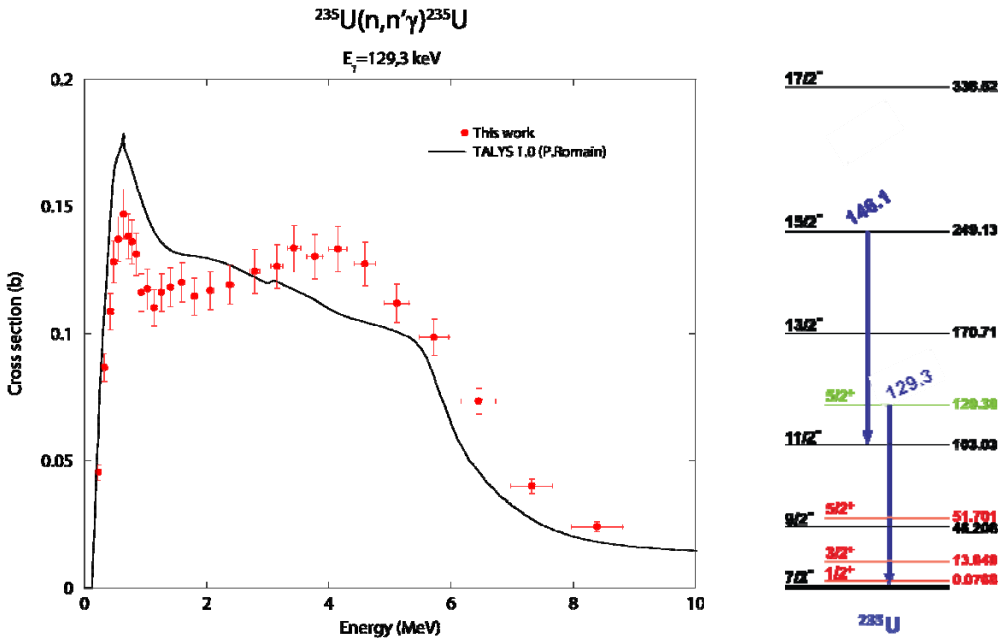

Figure 5. *γ ray production cross section for the 129.3 keV transition of ^{235}U with level scheme.*

Figure 5 shows that the measured data points are located below the simulated TALYS codes for energies below 3 MeV, and above the simulated ones for energies higher than 3 MeV. The used TALYS code was optimized for the fission cross section of the isotope of interest and its descendants. As its parameterisation is very delicate, one should only consider these data with caution. Nevertheless we can observe the same order of magnitude for the measured data, as well as a fairly good agreement in the shape of the curves.
Another γ ray transition of 152,7 keV issued from a $^{235}U(n,2n)^{234}U$ reaction has also been observed. It results from a $6^+ \rightarrow 4^+$ transition. The obtained results are shown in figure 6, including a partial ^{234}U level scheme.

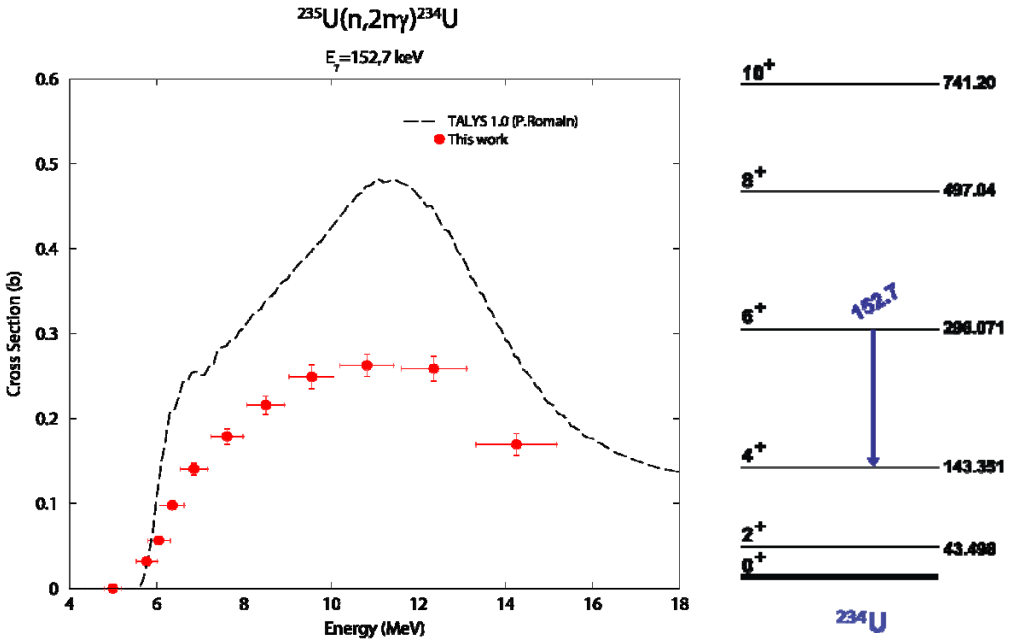

Figure 6. *γ ray production cross section for the 152.7 keV transition of ^{234}U with level scheme.*

For the observed $^{235}U(n,2n)^{234}U$ reaction, a good agreement of the shape, but a factor 2 in amplitude are noticed between our measurements and the TALYS simulations. More parameterization work will have to be made on TALYS, mainly for the descendants of ^{234}U.

Conclusions

The experimental setup that was developed allows to measure precise cross section values of unknown isotopes, as shows the comparison of the measured lead inelastic cross sections to existing data. The upcoming projects include finalizing the analysis of the $^{235}U(n,n'\gamma)^{235}U$ and $^{235}U(n,2n\gamma)^{234}U$ data and moving on to measuring unknown (n,xnγ) reactions on isotopes such as ^{232}Th, ^{nat}W and ^{238}U.
The presented results will be subject of further investigations from experimental as well as from theoretical point of view.
A closer look has to be taken to the uncertainties of these measurements. Currently ranging within 8 to 10%, the results need to be improved. Calibration experiments on the fission chamber, as well as precise efficiency measurements on the used detectors are being performed.

Acknowledgements
The authors thank the team of operators of the GELINA facility for the preparation of the neutron beam. This work was partially supported by the Integrated Project for European Transmutation (EUROTRANS).

References

[1] V. T. Jordanov, G. F. Knoll, Digital synthesis of pulse shapes in real time for high resolution radiation spectroscopy, Nuclear instruments and Methods in Physics Research A345 (1994) 337-345.
[2] H. J. Rose, D. M. Brink, Angular distributions of gamma rays in terms of phase-defined reduced matrix elements, Revs. Mod. Phys. 39 (1976) 306.
[3] H. Olliver, T. Glasmacher, and A. E. Stuchbery. Angular Distributions of Rays with Intermediate-Energy Beams, Physical Review C68, (2003), 044312.
[4] K. E. Atkinson, An Introduction to Numerical Analysis, 2nd Edition, Wiley, New York, USA, 1989.
[5] H. Karam, Mise au point de la mesure de sections efficaces de réactions (n,xn) par spectroscopie γ prompte sur des cibles très radioactives, PhD Thesis, University of Strasbourg (2009).
[6] L. C. Mihailescu, Neutron (n,xnγ) cross-section measurements for 52Cr, 209Bi and 206,207,208Pb from threshold up to 20 MeV, PhD Thesis, University of Bucharest (2006).

AMS measurements of long-lived radionuclides produced in fusion and fission environments

A. Wallner[1)], I. Dillmann[2,3)], T. Faestermann[3)], F. Käppeler[2)], A. Klix[4)], G. Korschinek[3)], C. Lederer[1)], G. Rugel[3)], P. Steier[1)]

1) VERA Laboratory, Isotope Research, Faculty of Physics, University of Vienna, Währinger Str. 17, 1090 Wien
2) Forschungszentrum Karlsruhe, Institut f¨ur Kernphysik, Postfach 3640, D-76021 Karlsruhe
3) Physik Department, TU Munich, James-Franck Strasse 2, D-85748 Garching
4) Institut für Kern- und Teilchenphysik, TU Dresden und Forschungszentrum Dresden-Rossendorf, Germany

anton.wallner@univie.ac.at

Abstract: Accelerator mass spectrometry (AMS) represents a complementary technique for the detection of long-lived radionuclides through ultra-low isotope ratio measurements. In many cases, counting atoms rather than measuring decay products yields much higher sensitivities. For a few cases the powerful combination of activation and subsequent AMS detection is exemplified; typical radionuclides of interest have half-lives between some years and up to hundred million years. Lack of information exists for a list of nuclides for quantifying production in fusion and fission environments as pointed out by nuclear data requests. A brief overview on detection limits at a typical AMS facility, the VERA facility, and some applications for selected long-lived radionuclides are given.

Accelerator Mass Spectrometry

Accelerator Mass Spectrometry (AMS) represents a mass spectrometric technique based on the used of a (tandem) accelerator. It deals with longer-lived radionuclides, which are also of some concern and importance in fusion and fission technology, mainly with respect to radioactive waste disposal. The advantage of AMS is that it does not suffer from molecular isobaric interferences due to the use of tandem accelerators and can even be used for separating specific atomic isobars. An advantage is also its flexibility for switching to different isotopes and elements because scaling is a function of the mass directly. It offers a powerful tool to measure cross sections of nuclear reactions leading to radioactive nuclides, independent of their decay times or schemes. The extra-ordinary sensitivity of AMS for detection of long-lived radionuclides leads to a million-times higher sensitivity than decay counting for the typical AMS nuclides -a consequence of their long half-lives.

The Vienna Environmental Research Accelerator (VERA) represents a state-of-the-art AMS facility based on a 3-MV tandem [1-4] which provides the ability for quantifying nuclides over the whole mass range. Among the measured radioisotopes are e.g. ^{10}Be, ^{14}C, ^{26}Al, ^{36}Cl, ^{41}Ca, ^{55}Fe ^{129}I, ^{182}Hf, ^{202}Pb, ^{210}Bi, ^{236}U and $^{239\text{-}244}$Pu, within a wide range of applications – from archaeology via climate research to astrophysics.

The detection of long-lived nuclides via AMS is not hampered by low counting rates or unfavorable decay characteristics as the produced atoms are detected directly rather than their decay. In general, those radioisotopes whose detection does not suffer from isobaric interferences allow ultra-sensitive measurements, e.g. ^{14}C, ^{26}Al, ^{55}Fe or $^{239\text{-}244}$Pu.

In combination with use of negative ions and the suppression of molecules by applying acceleration and charge exchange, AMS offers an excellent sensitivity. The actually measured parameters in AMS are isotope ratios, i.e. rare isotope versus stable isotope contents in a sample. Detection limits of 10^{-15} and below have been achieved for several nuclides which allow the detection of these isotopes at natural concentrations.

AMS uses negative ion sputter sources: Solid sample material is inserted into an ion source. It represents a “sample-destructive” technique. Typical samples masses in AMS are a few mg of material. In view of the very low sample masses needed, AMS offers a tremendously higher sensitivity compared to the decay counting method, which is a consequence of the long half-life of those radionuclides (see e.g. [5]).

In AMS the typical measurement procedure is the following (as exemplified by the setup of the VERA facility): In a cesium sputter source, negatively charged ions are produced, pre-accelerated and sent through a low-energy mass spectrometer, which analyzes a specific mass. The ions are further injected into a tandem accelerator. Any molecules that might contribute to a molecular interference are completely destroyed in the terminal stripper of the accelerator. Due to this stripping process, only atomic, positively charged ions leave the tandem accelerator. A specific charge state is selected by a second, high-energy 90° analyzing magnet and a 90° electrostatic analyzer for further transport to the detector. At the VERA 3-MV-tandem, the particles are accelerated to 10 and 25 MeV particle energy. Rejection of isotopic interferences can be achieved with additional filters, like a Wien-filter, an electrostatic analyzer, and a time-of-flight system. Further reduction of any isobaric and isotopic interference is also achieved by means of specific energy-loss techniques, used either in front of the detection system or as a part of the particle detector. A final particle detector measures the energy of the incoming ions, which are stopped in the detector. Typical parameters for the various nuclides measured at VERA are listed e.g. in [2,5,6].
AMS is a mass spectrometric technique. Basically, it measures isotope count rates for different isotopes. To this end, sequentially, stable ion currents are measured with Faraday cups, positioned at the low-energy and high-energy sides of the AMS beamline (Fig. 1). These current measurements are alternated with counting the rare isotope with the particle detector. With this raw data, i.e. countrate and particle current, an isotope ratio is calculated. For quality control, the transmission is regularly monitored by means of standards with well-known isotope ratios. In order to quantify or check the background level, blank samples are measured, too.

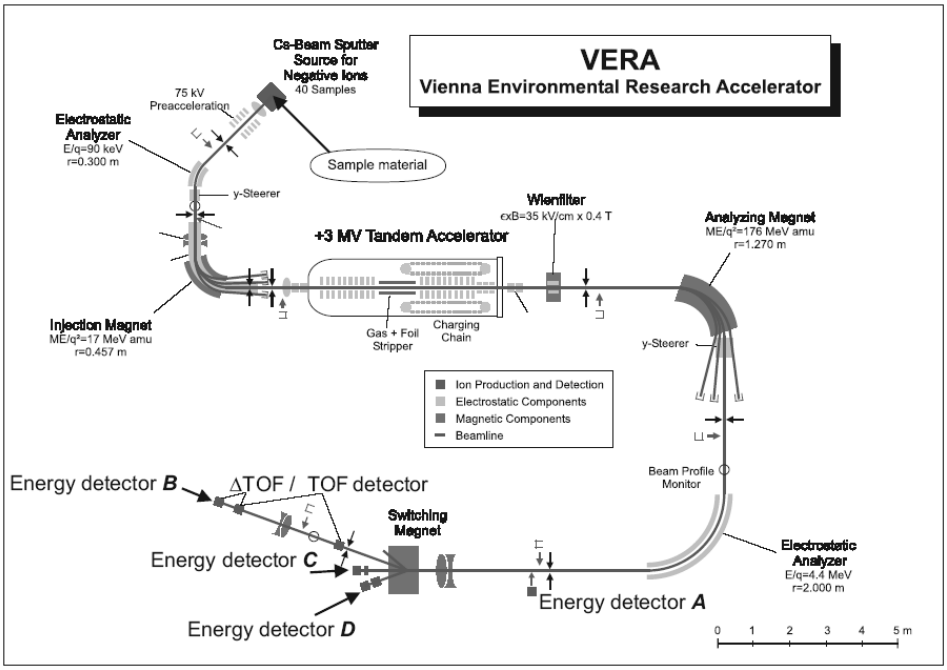

Figure 1. *Schematic layout of the VERA facility. Currents of stable ions are measured in sequential mode with Faraday cups positioned after the injection magnet (low-energy section, negative ions) and after the analyzing magnet (high-energy section, positive ions). Various detectors are available for counting rare isotopes (detectors A to D): The heavy-ion beamline (which is also used for ^{236}U and actinide detection) consists of time-of-flight (TOF) detectors and an ionization chamber (= detector B).*

Combining Activation and AMS

In general, cross section measurements can be classified into two complementary techniques: direct and indirect methods. The direct method makes use of the detection of the prompt and characteristic radiation associated with the production of a specific nuclide, or selectively detects the reaction product itself by means of the recoil separator technique. Typical examples of experimental facilities in "direct mode" are, -among many others- e.g. the DRAGON setup at TRIUMF (combined with recoil separator technique [7]) and LUNA at Gran Sasso [8] for charged particle induced reactions; and e.g. in Europe GELINA [9] and the n_TOF facility at CERN [10] for studying neutron-induced reactions.
A second and independent method makes use of the activation technique, with sample irradiation and subsequent measurement of the reaction product. After the irradiation the number of produced radioactive nuclei can be quantified either by decay counting or by mass spectrometric methods. This method is mostly restricted to radioactive products; however, it represents a very sensitive technique due to potential long irradiation periods. Contrary, direct methods have the advantage that, e.g. with the time-of-flight technique, an energy-dependent cross section over a wide energy range can be obtained. Direct methods can be applied to both radioactive and stable reaction products, and can be applied to radioactive beams. Nowadays, detection-setups are becoming state-of-the-art which offer higher detection efficiencies (e.g. in 4π geometry) compared to AMS.
It is important to support existing precise data with different and independent experimental methods to verify the accuracy of these cross sections. The main advantage of TOF measurements is that they cover a wide neutron energy range. However, the experimental design and also complex decay schemes of prompt reaction products require sophisticated methods to be taken into account in an appropriate way for deducing accurate cross sections. The determination of cross sections via the combination of the activation technique and AMS represents an important indirect method. It is complementary to these direct measurements, since this independent approach implies different systematic uncertainties. It is the combination of the TOF method and the independent activation technique using AMS, which will allow producing cross-section data as accurate as needed for various applications.
To be applicable, radionuclides to be studied for cross section measurements have to survive the irradiation campaign till the subsequent AMS measurement. For specific cases AMS allows measuring cross sections precisely, thus elucidating current open questions for technological applications.
Several neutron activations in combination with subsequent AMS measurements at VERA were performed recently: "keV neutrons" were produced at Forschungszentrum Karlsruhe (FZK) [11] via the ^{7}Li(p,n)^{7}Be reaction. By choosing a proper irradiation geometry, a quasi-stellar neutron spectrum is generated which approximates a Maxwellian distribution for kT = 25 keV [11]; increased proton energies allow also to produce higher neutron energies. Thermal neutrons and cold neutrons were produced at the Atominstitut of the Vienna University of Technology, and the Budapest Research Reactor (IKI, Institute of Isotopes, Hungarian Academy of Sciences). Cross section measurements via neutron activations in the fast neutron energy range are preformed in cooperation with TU Dresden (TUD), utilizing their neutron generator, i.e. producing 14-MeV neutrons via the (d,T) reactions; and higher energy neutrons were produced via the Van de Graaff facility at IRMM Geel with neutron energies up to 20 MeV. Depending on the cross-section value, isotope ratios between 10^{-11} and 10^{-15} were produced in such activations. After the neutron irradiation, the subsequent AMS measurements are performed at AMS facilities, like the VERA facility in Vienna or with the GAMS setup at Munich. Here, we report on samples activated at TUD with fast neutrons (14-MeV) and at FZK with keV neutrons.

Long-lived Radionuclides as Activation Products in a Fusion Environment

In a fusion environment particularly long-lived activation products may lead to significant long-term waste disposals and radiation damage. Many of these production cross sections are not well-known, making it difficult to calculate concentration limits [12]. With the high neutron flux, also impurities in structure materials may lead to significant or dominating activations. For such nuclides production cross-sections and induced activities are key parameters for safety and design analysis.

Also structural materials suffer from a continuous production: Prominent long-lived fusion products will be found in the medium-mass range, i.e. Cu, Fe and Ni containing materials will steadily accumulate e.g. the radionuclides ^{53}Mn, ^{55,60}Fe and ^{59,63}Ni.
The potential and power of AMS for detecting ^{55}Fe has been demonstrated recently in a first irradiation campaign [13,14]. ^{55}Fe detection benefits from the fact that no isobaric interference exists because ^{55}Mn does not form stable negative ions. At VERA AMS allows to perform measurements on the level of 1% reproducibility with a background level ^{55}Fe/^{56}Fe < 2×10^{-15} [14]. Precise measurements for ^{54}Fe(n,γ)^{55}Fe from thermal to several hundred keV neutron energies and for ^{56}Fe(n,2n)^{55}Fe are in progress at the VERA laboratory. The new data are expected to be accurate to a level of about 3%.
^{53}Mn will be produced either directly from ^{54}Fe via the (n,np+d) reaction. The respective neutron threshold energies are 9 and 6.8 MeV. It can also be produced to a lesser extent indirectly via the beta-decay of ^{53}Fe ($t_{1/2}$= 8.5 min). Besides its drawback as an activation product, ^{53}Mn may also be of interest in plasma diagnostics. Similar to the ^{27}Al(n,2n)^{26}Al reaction, the ^{54}Fe(n,2n)^{53}Fe excitation function has a threshold at 13.63 MeV, which makes it sensitive to temperature changes, too [4]. However, the knowledge of this excitation function is still very poor. The high production rate of ^{53}Mn ($t_{1/2}$ = 3.7Myr) is of some concern as an activation product since this activity will increase steadily during the lifetime of an operating reactor. In particular, Fe-containing materials are candidate materials for fusion reactor systems. Experimental information for the production of ^{53}Mn is scarce and discordant to calculations. Recent activation experiments in a fusion peak neutron field showed, that for materials like the favoured Eurofer, production of ^{26}Al and ^{53}Mn are the dominant long-term activities, with estimated contributions of 70% and 27% to the total dose rate, respectively, however, for ^{53}Mn with an uncertainty of 60% [15,6].

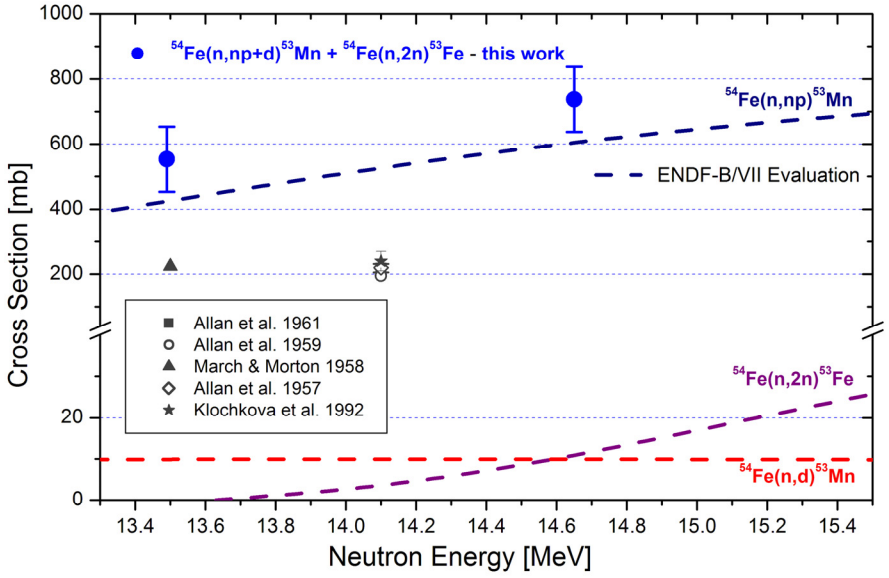

Figure 2. *Excitation function for the production of ^{53}Mn around 14 MeV. Experimental data are shown as symbols. A recent evaluation [16] disentangles the contribution of the three different reaction channels producing the long-lived ^{53}Mn (dashed lines). Filled circles depict the data obtained in this work.*

Fe metal samples, highly enriched in ^{54}Fe, were irradiated with quasi-monoenergetic neutrons at TU Dresden's 14-MeV neutron generator [17]. Via the T(d,n)^{4}He reaction, neutrons with energies between 13.4 and 14.9MeV were produced. Several Fe samples were exposed to neutrons with a total fluence of a few 10^{13} n cm^{-2}. In addition, short-term irradiations were performed to measure the production of short-lived ^{53}Fe. After the neutron activations the Fe samples were dissolved and a known amount of stable ^{55}Mn was added and Manganese was separated from the Fe bulk material. Long-lived ^{53}Mn was measured via AMS utilizing the 14-MV tandem accelerator of the Maier-Leibnitz-laboratory, Garching/ TU Munich [18]. Assuming a cross-section value of 600mbarn [16] and with the well-known neutron fluence (> 10^{13} n

cm^{-2}), an isotope ratio $^{53}Mn/^{55}Mn$ of at least $6 \cdot 10^{-12}$ can be produced- well above background. Previous measurements for the $^{54}Fe(n,np+d)^{53}Mn$ reaction [19] have been performed in the neutron energy range between 13.5 and 14.1MeV. These measurements are based on the detection of emitted protons and are sensitive to the np-channel only. Their results indicate a constant cross section of about 200mbarn. However, they disagree by a factor of 2–3 with recent evaluations (see e.g. [16]). The evaluations indicate an increasing excitation function with cross-section values of 400 and 650 mbarn between 13.4 and 15MeV. Preliminary experimental data obtained in this work are plotted in Fig. 2 (solid circles). Our data, for the first time based on AMS, are sensitive to the total production of ^{53}Mn in such a neutron environment. They indicate that previous data seem to strongly underestimate the production of ^{53}Mn in this energy range. The new data are also slightly higher than the ENDF evaluation.

Neutron-Capture Studies of ^{235}U and ^{238}U as examples for Studying Fission Products

Improved and highly accurate nuclear data are urgently required for the design of advanced reactor concepts (Gen IV, ADS). This demand holds for minor actinides but also for the main fuel materials. The capture to fission ratio of the fissile isotopes is one such quantity. Existing data for the capture channel have been measured by time-of-flight techniques via detection of the prompt capture γ-rays. A major difficulty in these experiments is the safe discrimination against the strong γ-background from the competing fission channel. Neutron activation with subsequent AMS measurement represents an independent measurement, where interference from the fission channel is completely excluded. Within EFNUDAT two transnational access projects are performed [20] with the goal to determine independently the neutron capture cross sections of ^{235}U and ^{238}U via neutron irradiations at thermal (cold) and keV-neutrons: ^{235}U and ^{238}U was activated in well defined, intense neutron fields at the Van de Graaff accelerator of FZK and at the Budapest Research Reactor and the produced ^{236}U and the decay product of ^{239}U, ^{239}Pu are subsequently counted by AMS at the Vienna Environmental Research Accelerator (VERA). The AMS facility VERA has been recently upgraded to reach high sensitivities also for actinide isotopes [2,3,5]. Accordingly, measurements could be performed with very small samples of natural uranium. This method for measuring the neutron capture cross section of $^{235,238}U$ has the advantages that any radiation hazards are avoided and that the involved systematic uncertainties are in no way correlated with the uncertainties inherent to the TOF technique. Therefore, this experiment provides important and independent information for this key reaction of reactor physics.

The accuracy of the AMS analysis is determined by the conversion ratio achieved in the irradiation. Neutron activations, performed at neutron energies from cold neutrons, thermal and of 30 and 350 keV, the latter with neutron energy distributions between 20 to 50 keV FWHM. At VERA, measurement methods were established which work for the detection of the long-lived radionuclides where suppression of isobars is not required. To suppress interference from neighboring masses, the resolution of VERA was increased, both by improving the ion optics of existing elements and by installing a new electrostatic analyzer after the analyzing magnet. Interfering ions which pass all beam filters are identified with a high-resolution time-of-flight (TOF) system, using a diamond-like carbon (DLC) foil in the start detector, which substantially reduces beam straggling [2]. VERA allows high precision measurements with low interfering background. To this end, a fast beam switching mode is used to sequentially measure both the count rate of the radionuclide of interest (i.e. ^{236}U) and the current of the quasi-stable ^{238}U and/or ^{235}U ions.

The neutron flux during sample irradiation is crucial because it determines the conversion ratio given. For these measurements, uranium samples of natural isotopic composition are used. AMS measurements of this material revealed a low ^{236}U and ^{239}Pu concentration. The extremely high sensitivity of the AMS technique requires only very small samples of typically some 10 mg natural U. Typical conversion ratios $^{236}U/^{235}U$ of better than 3×10^{-10} convert to an isotope ratio $^{236}U/^{238}U$ of higher than 3×10^{-12}. Fig. 3 shows some preliminary results from such samples for $^{235}U(n,\gamma)^{236}U$. The data from the keV activations for 25 and 500 keV fit to the expected values from ENDF evaluation. Detailed measurements are now in progress. Based on existing experience with previous AMS measurements of neutron cross sections in the keV range [4], we expect to achieve an overall uncertainty in the range between 5-10%.

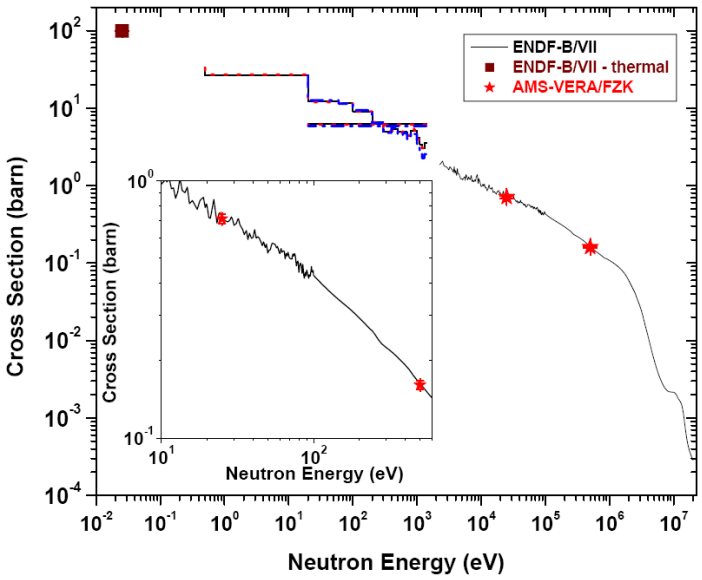

Figure 3. *Preliminary data for the $^{235}U(n,\gamma)^{236}U$ neutron capture cross section in the keV neutron energy range (FZK irradiations). The asterix depicts the AMS data, solid lines represent the ENDF-B/VII evaluation and the square symbol the thermal value.*

References

[1] W. Kutschera, Int. J. Mass Spectrom. 242 (2005)145.
[2] P. Steier, R. Golser, V. Liechtenstein, W. Kutschera, A. Priller, C. Vockenhuber, A. Wallner, Nucl. Instrum. Meth. B240 (2005) 445.
[3] C. Vockenhuber, I. Ahmad, R. Golser, W. Kutschera, V. Liechtenstein, A. Priller, P. Steier, S. Winkler. Int. J. Mass Spectrometry 223–224 (2003) 713.
[4] A. Wallner, R. Golser, W. Kutschera, A. Priller, P. Steier, C. Vockenhuber, The Europ. Phys. J. A 27 (2006) 337.
[5] A. Wallner, O. Forstner, R. Golser, W. Kutschera, A. Priller and P. Steier, Proc. NEMEA 05 (2009); see http://candide.nri.cz/nemea.php.
[6] A. Wallner et al., AIP Conf. Proc. Volume 769, Proc. Nuclear Data for Science and Technology 2004, Santa Fe, New Mexico (USA), pp. 621-624, 2005.
[7] D. Hutcheon, Nucl. Instr. and Meth. A498 (2003) 190.
[8] A. Formicola et al., Nucl. Instr. and Meth. A507 (2003).
[9] http://www.irmm.jrc.be/html/about_IRMM/laboratories/GELINA_neutron_time_of_flight_facility.htm.
[10] The n_TOF Collaboration, “CERN n_TOF Facility: Performance Report”, CERN/INTC-O-011 INTC-2002-037 CERN-SL-2002-053ECT, 2002 (unpublished).
[11] W. Ratynski, F. Käppeler, Phys. Rec. C37 (1988) 595.
[12] D.L. Bowers and L.R. Greenwood: J. Radioanal. Nucl. Chem. 123 (1988) 461.
[13] L. Coquard, F. Käppeler, I. Dillmann, A. Wallner, K. Knie and W. Kutschera, Proceedings of Science (2006), PoS(NIC-IX)274.
[14] A. Wallner, M. Bichler, I. Dillmann, R. Golser, F. Käppeler, W. Kutschera, M. Paul, A. Priller, P. Steier, and C. Vockenhuber, Nucl. Instr. and Meth. B259 (2007) 677.
[15] K. Seidel et al., Journal of Nuc. Mat. 307-311 (2002) 1037-1041.
[16] ENDF/B-VII.0 Evaluation, evaluated nuclear data library, IAEA, Vienna, see: http://www-nds.iaea.org/exfor/endf.htm.
[17] K. Seidel et al., Fusion Eng. Des. 81 (2006) 1211-1217.
[18] M. Poutivtsev, Ph.D. thesis, TU München, 2007.
[19] Experimental nuclear reaction data (EXFOR), IAEA, Vienna, see: http://www-nds.iaea.org/exfor/exfor.htm.
[20] A. Wallner et al., see http://www.efnudat.eu/.

DSP algorithms for fission fragment and prompt fission neutron spectroscopy

O. Zeynalova[1)], Sh. Zeynalov[1,2)], F.-J. Hambsch[2)], S. Oberstedt[2)], I. Fabry[2)]

1) Joint Institute for Nuclear Research, Joliot Curie 6, Dubna, Moscow region, Russia
2) European Commission, Joint Research Centre, Institute for Reference Materials and Measurements, Retieseweg 111, 2440 Geel, Belgium

shakir.zeynalov@ec.europa.eu

Abstract: Digital signal processing (DSP) algorithms for fission fragment (FF) and prompt fission neutron (PFN) spectroscopy are described in the present work. The twin Frisch-grid ionization chamber (GTIC) is used to measure the kinetic energy-, mass- and angular distributions of the FF in the ^{252}Cf(SF) reaction. Along with the neutron time-of-flight (TOF) measurement the correlation between neutron emission and FF mass and energy is investigated. The TOF is measured between common cathode of the GTIC and the neutron detector (ND) pulses. Waveform digitizers (WFD) having 12 bit amplitude resolution and 100 MHz sampling frequency are used for the detector pulse sampling. DSP algorithms are developed as recursive procedures to perform the signal processing, similar to those available in various nuclear electronics modules, such as constant fraction discriminator (CFD), pulse shape discriminator (PSD), peak-sensitive analogue-to-digital converter (pADC) and pulse shaping amplifier (PSA). To measure the angle between FF and the cathode plane normal to the GTIC a new algorithm is developed having advantage over the traditional analogue pulse processing schemes. Algorithms are tested by comparing the numerical simulation of the data analysis of the ^{252}Cf(SF) reaction with data available from literature.

Introduction

In recent decades the DSP technology gained dominance in respect to the traditional analogue signal processing technique in experimental nuclear physics due to the higher flexibility and an obvious economical reason. Hardware modules (usually made of WFD and the signal level adapting amplifier) provided diversity of signal analysis possibilities by modification of the signal processing software only. In this work we present algorithms developed for investigation of correlations between prompt neutron emission and the FF mass and energy distributions. The ^{252}Cf target was mounted in the centre of the common cathode of a twin Frisch-grid ionization chamber (GTIC) in such a way that each of the FF is stopped in the corresponding half of the GTIC. Anodes pulses caused by FF were used to obtain mass-, kinetic energy and the emission angle of the FF with respect to the cathode-plane normal. The anode current pulse after being integrated with a charge-sensitive pre-amplifier (CSA) was converted to the step-like pulse with the height proportional to the FF kinetic energy released during its deceleration in the TGIC working gas mixture. Since a portion of the FF kinetic energy is absorbed inside the target layer and the target backing, the angle between cathode normal and FF (Θ-angle) was needed for the correction of the measured FF kinetic energy. The GTIC cathode pulse was used as the time reference both for the neutron time-of-flight (TOF) measurement and for the Θ-angle measurement. The correlated anode pulses along with the corresponding cathode pulse and the neutron detector (ND) signal were sampled with four 100 MHz WFD having 12 bit amplitude resolution. The waveforms were analysed to obtain the following information about every fission event: kinetic energy values for both FF, their Θ-angles, prompt fission neutron (PFN) pulse shape and pulse height information along with the corresponding TOF value. These data eventually are converted to FF masses and kinetic energies, to PFN kinetic energy and the Ψ-angle between neutron and the FF.

Experimental setup

The TGIC was mounted inside a stainless steel cylindrical vessel having a diameter of 285 mm and a height of 200 mm. As counting gas a mixture made of 90%Ar+10%CH_4 (P-10) was used in the TGIC at a pressure of 1.05 bar. The continuous regeneration of the counting gas was kept at a constant flow rate of 30-50 ml/min. The cathode was made of stainless steel

having the diameter of 178 mm and a thickness of 2 mm. The circular hole in the cathode centre was used to mount the ^{252}Cf target with a source strength of about 500 fissions/s. Anodes were made from an aluminium foil (0.1 mm thickness) glued onto the stainless steel ring with an external diameter of 178 mm, a width of 20 mm and a thickness of 1 mm. Grids were made of stainless steel wires with a diameter of 0.1 mm and a pitch of 2 mm stretched over the stainless steel disks, similar to those used for the anodes. The spot of the ^{252}Cf target of ~10 mm is made by depositing ^{252}Cf nuclei on a nickel foil with a thickness of 100 μg/cm^2 and a diameter of 50 mm.

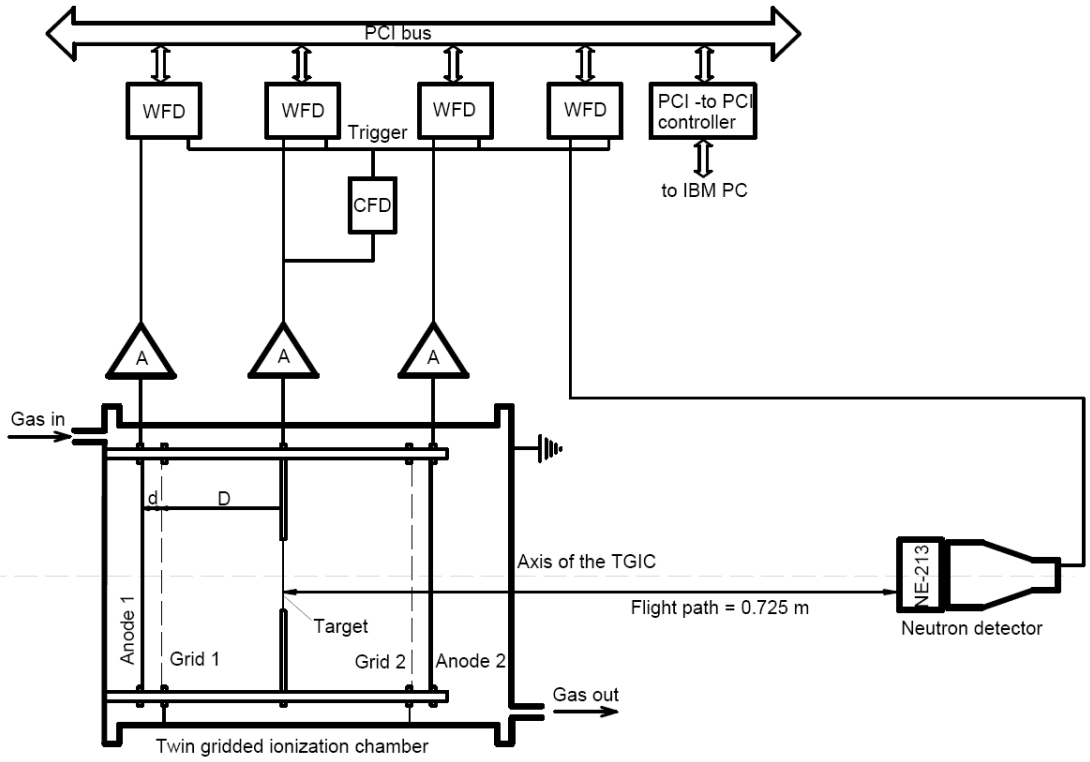

Figure 1. *Simplified block diagram of the experimental setup(D =30 mm, d=6 mm).*

A simplified block diagram of the TGIC and the data acquisition system consisting of four WFD is presented in Fig. 1. Sampling of the detector pulses was performed with 12 bit pulse height resolution and 100 MHz sampling frequency. Sampling was triggered when the common cathode pulse passes the selection criteria of the CFD. Four simultaneously sampled waveforms were acquired for each fission event in the local random access memory of the PC. Each of the waveforms consisted of L samples taken before and of M samples taken after the triggering. The L and M values were programmatically configured before the data acquisition is started. Union of L+M samples composed the sampled pulse of the corresponding detector output. *It would be convenient to name the four waveforms measured for every fission event as A_1, A_2 – for two anode pulses, as K- for the cathode pulse and as N – for the neutron detector*. Sequential unions were combined in blocks containing 10000 fission events that were recorded to the PC hard disk.

Fission fragment analysis

Main data analysis was performed off-line by retrieving waveforms from the hard disk. Each fission event was fully represented by the set of four waveforms A_1, A_2, K and N. The K-waveform was used as a time reference. The FF fragment kinetic energy consumed during the ionization of the working gas of TGIC was proportional to the height of the corresponding A_1-, A_2- waveform. Determination of the height of the step-like pulse performed using the following signal processing described in more detail in ref. [1]. Anode pulse (*V(t)*-continuous form, *V(kΔ)* – sampled form) passed through the following differentiating filter:

$$Q(t) = V(t)W(0) - \int_0^t V(t)\frac{dW(t-\tau)}{d\tau}d\tau \Rightarrow \text{for } W(t) = \exp(-\lambda t)$$
$$Q(k\Delta) = V(k\Delta) - \frac{1}{\lambda}\sum_{i=0}^{k} V(i\Delta)\exp(-\lambda\Delta(k-i)) \quad (1)$$

The main aims of the differentiating filter were: 1) subtract the non-zero basement from the waveforms; 2) to localise the peak value of the pulse. Then the pulse *Q(kΔ)* was integrated in order to improve the signal-to-noise ratio. In this work the following simple integration formula was implemented:

$$P_i = \sum_{j=Tg}^{Tg+100} Q(k\Delta) \quad (2),$$

where Tg is time reference of fission event and P_i stand for two (i=1,2) anode pulse height values. Determination of the Θ_1- and Θ_2-angles as schematically illustrated in Fig. 2 was done using anode waveforms *V(kΔ)*. Free electrons drifting towards the corresponding anodes with the constant velocity *W* approached the anodes at different time depending on the FF angle. Time *T* between the fission

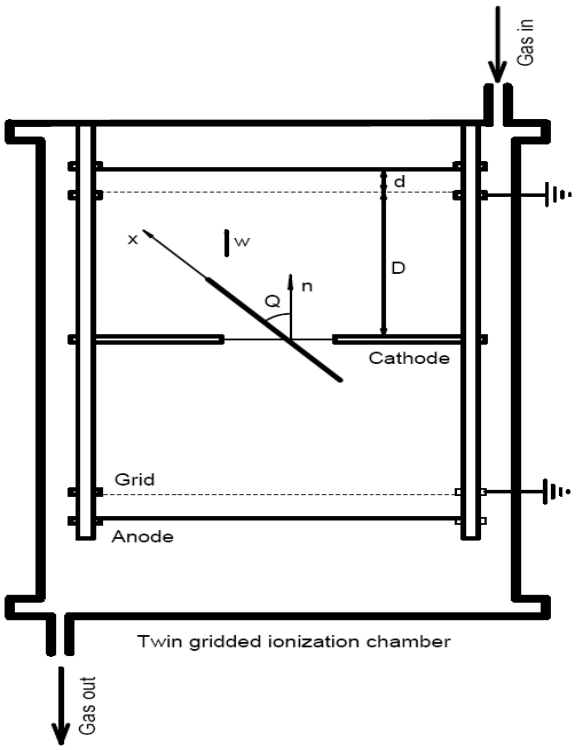

Figure 2. *Illustration of the fission-fragment angle determination: free electrons are drifting towards the anode on electrostatic field created between cathode-grid-anode.*

reference Tg and the time instant, when the anode pulse raised to the half of its full height could be found using the following formula:

$$T_{90} - T = (T_{90} - T_0(\mathrm{E})) * \cos(\Theta) \quad (3),$$

where $T = \sum_{k=Tg}^{Tg+100} k\Delta I_i[k\Delta] - Tg$, $T_{90} = \frac{D + 0.5 * d}{W}$. *D and d* – are the cathode-grid and grid-anode distances respectively and $I_i(k\Delta)$, *i=1,2* were the current waveforms obtained from the corresponding waveforms $V_i(k\Delta)$ as was explained in ref. [1] Function $T_0(E)$ can be determined experimentally in calibration measurement by preselecting the FF emitted with angle $\Theta=0$. The measured FF pulse height first was corrected taking into account grid inefficiency factor, characterizing incompleteness of anode shielding by the grid from the current, created by moving charges in the cathode-grid space of the TGIC:

$$P^C = \frac{P^O * T_{90}}{T_{90} + \sigma * T} \qquad (4),$$

where P^C, P^O - are corrected and measured pulse height values respectively and σ-is a grid inefficiency factor as defined in ref. [2]. Two dimensional function $R(P^C, T)$ was constructed using the pairs of P^C, T values are presented in Fig. 3. Considering $R(P^C = const, T)$ as function of argument T one got equation (1) with the fixed value of P^C, which provided the possibility to evaluate the values T, corresponding to $\cos(\Theta) = 1$. The procedure was repeated for different values of P^C in order to obtain pairs of (P^C,T), represented the samples of function $T_0(P^C)$. These samples were fitted with parabola, represented analytically the $T_0(P^C)$ - function. After the described calibration procedure was implemented the equation (1) was used to determine the $\cos(\Theta)$ using the measured value of T. For each fission event the two cosine values were determined in each chamber and a distribution function $n(\cos(\Theta_1), \cos(\Theta_2))$ was plotted as shown on the left hand side of Fig. 4. The right side graph of Fig. 4 illustrates the precision of cosine measurement in the range $0.5<\cos(\Theta)<1.0$ obtained as the differences distribution of $n(\cos(\Theta_1)-\cos(\Theta_2))$. The cosine value used in the data analysis was evaluated as:

$$\cos(\Theta) = 0.5 * (\cos(\Theta_1) + \cos(\Theta_2) \qquad (5)$$

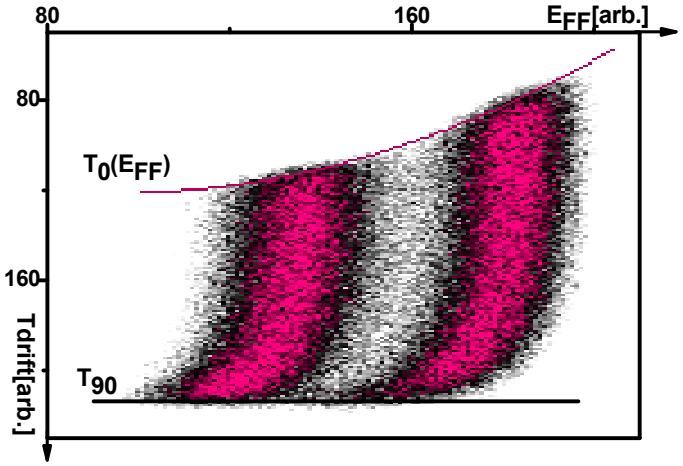

Figure 3. *Illustration of the cos(Q) determination.*

The cosine value used for correction of the FF pulse height due to the energy lose in the target and the backing layers using the procedure developed in refs [3,4]. Final pulse height and mass distribution were plotted in fig. 5.

Prompt fission neutron time-of-flight spectroscopy

The flight path for PFN chosen to be 0.725m and the signals K and N were used for the TOF measurement. The time marks were obtained using constant fraction time marking algorithm (CFTM), which widely used in commercially available nuclear electronics module – constant fraction discriminator (CFD). This algorithm produced accurate time mark independent on the signal pulse height provided the signal rise time did not depend on the signal pulse height. In programmatic realization of the CFTM method one needed the signal interpolation between sampling points. The Shannon interpolation polynomial is the natural interpolation approach in this case, providing most accurate result.

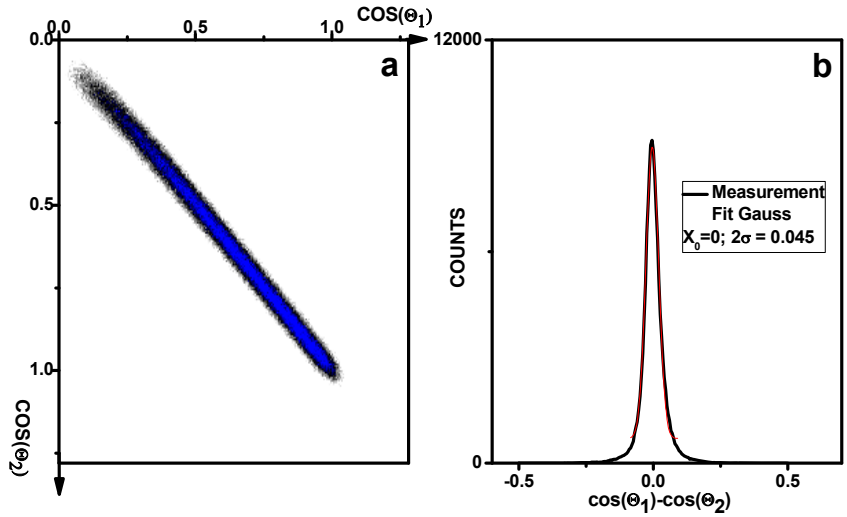

Figure 4. *a) Two dimensional plot of measured n(cos(Θ_1),cos(Θ_2)) distribution; b) One dimensional distribution n(cos(Θ_1)-cos(Θ_2)) illustrating the accuracy of the cosine measurement.*

In practical implementations Shannon interpolation suffered from sampling noise due to the finite resolution of the sampling ADC, therefore, linear, parabola or cubic interpolation schemes are frequently used instead due MORE sampling noises immunity. To improve the sampling noises influence the waveforms passed through the low pass the finite impulse response (FIR) - 4-th order Butterworth filter:

$$B_4(t,\tau) = \frac{1}{\tau * 3!}\left(\frac{t}{\tau}\right)^3 * \exp(-\frac{t}{\tau}) \text{ or in the sampled form}$$

$$V[i] = a_0 U[i] + b_1 U[i-1] + b_2 U[i-2] + b_3 U[i-3] + b_4 U[i-4] + b_5 U[i-5]$$

$$x = \exp(-1/\tau),\ a_0 = (1-x)^4 \qquad (6),$$

$$b_1 = 5x,\ b_2 = -10x^2,\ b3 = 10x^3,\ b_4 = -5x^4,\ b_5 = x^5$$

where V[i] is the filter output, U[i] is input waveform and τ is the shaping parameter. It should be noticed that filtering improved significantly the differential nonlinearity of the pulse height measurement, making it even better than one of the analogue signal processing module. The PFN spectroscopy was done using parabola interpolation formula. Below the formulas for different interpolation polynomials are presented:

$f(t_k + \Delta) = f(t_k) + \Delta * (f(t_{k+1}) - f(t_k))$ - linear interpolation

$$f(t_k + \Delta) = a(t_k + \Delta)^2 + b(t_k + \Delta) + c$$

$$a = \frac{f(t_{k+2}) - 2f(t_k) + f(t_k)}{2},$$ - parabola

$$b = f(t_{k+1}) - f(t_k) - a(2k+1),$$

$$c = f(t_k) - bk - ak^2.$$

$$f(t_k+\Delta)=a(t_k+\Delta)^3+b(t_k+\Delta)^2+c(t_k+\Delta)+d$$

$$a=\frac{f(t_{k+2})-3f(t_{k+1})+3f(t_k)-f(t_{k-1})}{(k+2)^3-3(k+1)^3+3k^3+(k-1)^3},$$

$$b=\frac{f(t_{k+2})-2f(t_{k+1})+f(t_k)-a((k+1)^3-2(k+1)^3+k^3)}{2},\ \text{-cubic parabola}$$

$$c=f(t_{k+2})-f(t_{k+1})-b(2k+3)-a((k+2)^3-(k+1)^3),$$

$$d=f(t_{k+2})-c(k+2)-b(k+2)^2-a(k+2)^3.$$

Because of high sensitivity of ND to the prompt fission gamma radiation a pulse shape discrimination procedure was implemented to suppress the gamma background. The pulse shape discrimination method utilised a difference between the falling edges of the pulses caused by neutrons and photons. One of the popular analogue methods performed the integration of the ND pulse inside two intervals - the narrow window of ~25 nsec width and the wide window of ~250 nsec width refs. [5, 6]. The beginning of both windows were adjusted to the beginning of the ND pulse. In the present report we implemented the similar method and the pulse shape separation is illustrated in Fig. 6a where for each pulse two dimensional distribution was plotted in coordinates x and y calculated using the following calculation:

$$x=\int_0^T I(t)dt,\quad y=\int_0^{10*T} I(t)dt,\ \text{where } I(t)\text{ - is interpolated signal} \qquad (7)$$

After the photons were suppressed by pulse shape analysis in the range of pulse heights from 0.05 to 5.0 V the TOF distribution was created and plotted in fig. 6b. The reference shift and the width of the reference distribution broadening are shown in Fig. 7. A similar effect was observed and reported in ref [7].

Conclusions

Digital signal processing (DSP) algorithms for FF and PFN spectroscopy were developed in our work. The algorithms were implemented in the measurement of the ^{252}Cf(SF) reaction using a complete digitization approach with four 12 bit/100 MHz WFD. DSP algorithms were developed as recursive procedures performing signal processing similar to those available in various analogue nuclear electronics modules such as CFD, pulse shape discriminator (PSD), peak-sensitive analogue-to-digital converter (pADC), pulse shaping amplifier (PSA) or timing filter amplifier (TFA). To measure the angle between FF and the cathode plane normal of the GTIC a new algorithm was developed having advantage over the traditional analogue pulse processing schemes. Algorithms were tested by comparing our results of DSP data analysis of the ^{252}Cf(SF) reaction with data available from literature [9] demonstrating the better quality of DSP over traditional analogue signal processing.

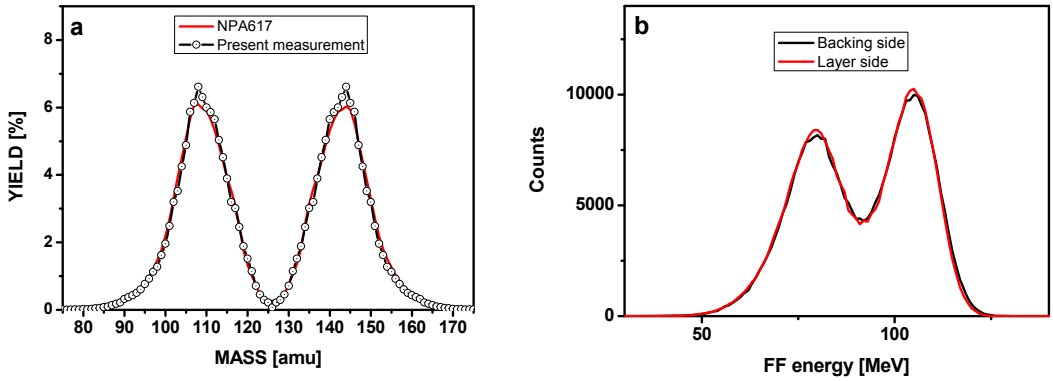

Figure 5. *a) Comparison of the mass distribution measured in this measurement with literature data available for a measurement with analogue electronics in [9] b) Energy distributions of the FF after all corrections were applied.*

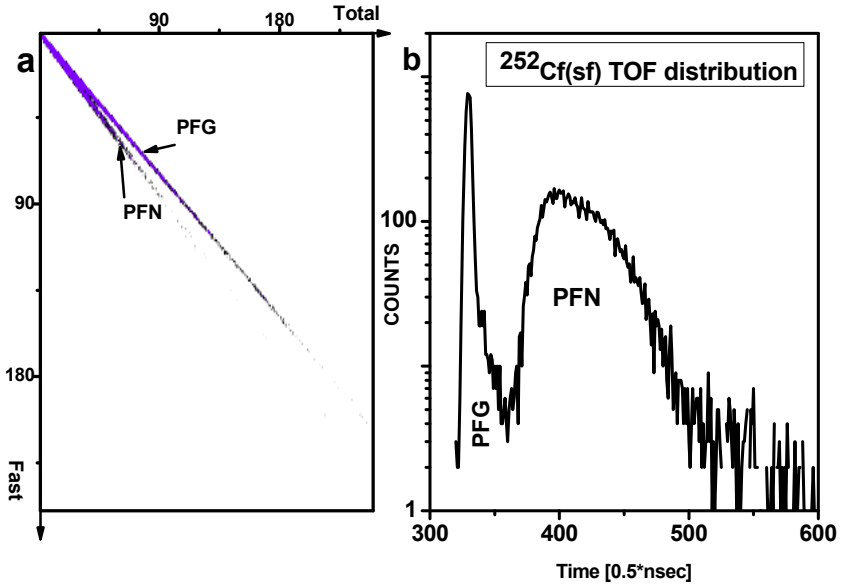

Figure 6. *a) PFN from PFG pulse shape separation principle illustrated in a two dimensional representation of total light output versus fast component light output b)TOF distribution acquired in ^{252}Cf(SF) after pulse shape separation was applied.*

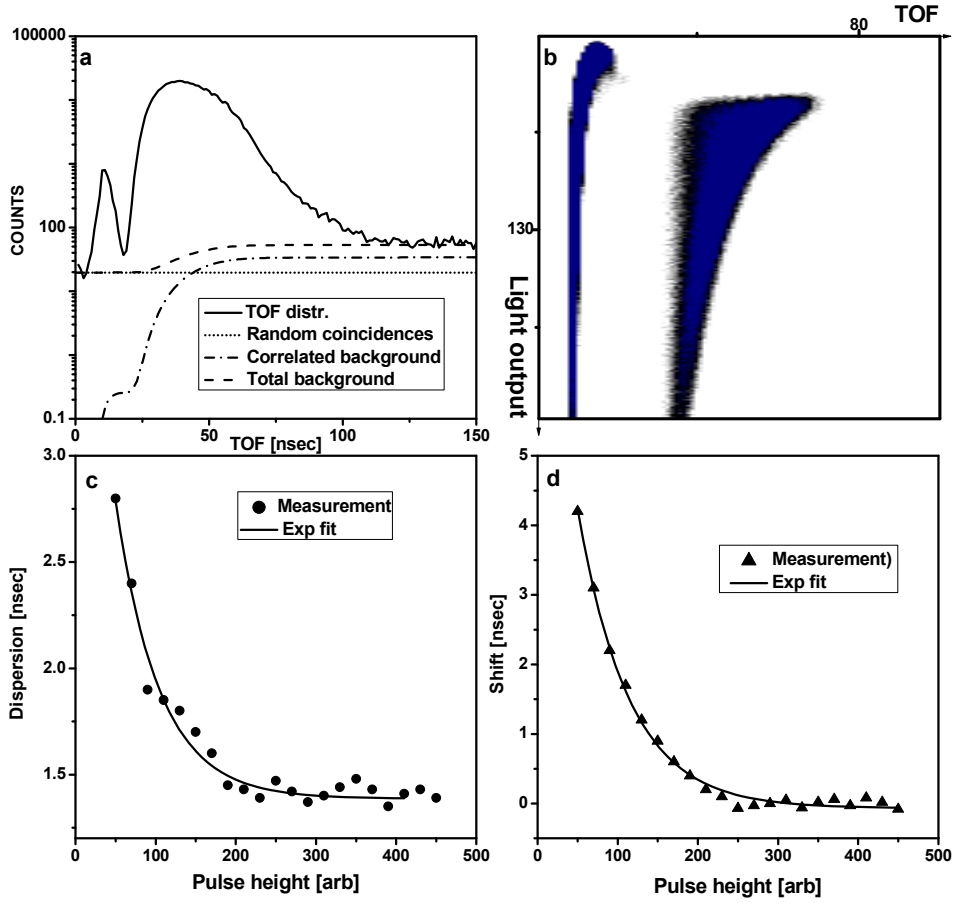

Figure 7. *a) PFN TOF distribution illustrating the n-γ separation and background subtraction; b) PFN TOF versus total light output plot demonstrates reference shift and widening; c)Dependence of the reference width on the light output; d) dependence of the reference shift on the light output.*

References

[1] O.V. Zeynalova, Sh.S. Zeynalov, F.-J. Hambsch, S. Oberstedt, Bulletin of the Russian Academy of Sciences: Physics, 2009, Vol. 73, No. 4, pp. 506–511. © Allerton Press, Inc., 2009.
[2] O. Bunemann, T.E. Granshaw and J.A. Harvey, Can. Jour. Res. A 27 (1949) 19.
[3] C. Budz-Jørgenson, H.-H. Knitter, Ch. Streade, F.-J. Hambsch and R. Vogt, Nucl. Instr. and Meth. A 258 (1987) 209.
[4] Sh.S. Zeinalov, M. Florek, W.I. Furman, V.A. Kriatchkov, Yu.S. Zamyatnin, Proc. VII Int. Seminar on Interaction of Neutrons with Nuclei (ISINN-7), Dubna, Russia, May 25-28, 1999, p.258. Nucl. Instr. and Meth. A 274 (1989) 217.
[5] M. Moszynski, G.J. Costa, G. Guillaume, B. Heusch, A. Huck and S. Mouatassim Nucl. Instr. and Meth. A 350 (1994) 226.
[6] G.F. Knoll, Radiation detection and measurements (Wiley, New York, 2000).
[7] J. Cub, E. Finckh, K. Gebhardt, K. Geissdorfer, R. Lin, J. Strate and H. Klein.
[8] R. Bottger, H. Klein, A. Chalupka, Strohmaier, Nuclear Science and Engineering 106 (1990) 377.
[9] F.-J. Hambsch, S. Oberstedt, Nucl. Phys. A 617 (1997) 347.

AUTHOR INDEX

European Commission

EUR 23883 EN – Joint Research Centre – Institute for Reference Materials and Measurements
Title: EFNUDAT Fast Neutrons - Proceedings of the Scientific Workshop on Neutron Measurements, Theory and Applications - Nuclear Data for sustainable nuclear energy. 28 – 30 April, 2009. Geel, Belgium
Editor: Franz-Josef Hambsch
Luxembourg: Publications Office of the European Union
2010 – viii, 190 pp. – 21.0 x 29.7 cm
EUR – Scientific and Technical Research series – ISSN 1018-5593
ISBN 978-92-79-11705-3
DOI 10.2787/23116

Abstract
The EFNUDAT (European Facilities for Nuclear Data Measurements) project workshop was held from April, 28 – 30, 2009 at EC-JRC-IRMM, Geel, Belgium. These proceedings collect the full papers summarising the contributions to this workshop.

The mission of the JRC is to provide customer-driven scientific and technical support for the conception, development, implementation and monitoring of EU policies. As a service of the European Commission, the JRC functions as a reference centre of science and technology for the Union. Close to the policy-making process, it serves the common interest of the Member States, while being independent of special interests, whether private or national.

JRC
EUROPEAN COMMISSION

LA-NA-23883-EN-C

ISBN 978-92-79-11705-3

Publications Office
Publications.europa.eu